Synthesis and Reactivity of Bio-Inspired Copper Complexes Supported by Non-Traditional Ligands

A DISSERTATION
SUBMITTED TO THE FACULTY OF THE GRADUATE SCHOOL
OF THE UNIVERSITY OF MINNESOTA
BY

Aalo Kumar Gupta

IN PARTIAL FULFILLMENT OF THE REQUIREMENTS
FOR THE DEGREE OF
DOCTOR OF PHILOSOPHY

William B. Tolman, Advisor

August 2011

Acknowledgements

A number of individuals of contributed greatly to my academic and scientific career and all deserve a greater thank you than what can be put into an acknowledgement. First I would like to thank and acknowledge my thesis advisor Professor William B. Tolman. His mentorship has helped shape all aspects of my research career and for that I am forever grateful. Additionally I would like to thank and acknowledge Prof. Larry Que for being an unofficial co-advisor during my graduate education and always showing interest and enthusiasm in my graduate work.

I would like to acknowledge both Tolman and Que groups because without the support and help of strong co-workers, none of the research presented in this thesis would have been possible. Of particular importance to my graduate work were Drs. Lyndal Hill and Sungjun Hong. Their advice and friendship was critical in my success as a graduate student. I would also like to thank Drs. Itsik Bar-Nahum, Patrick Donaghue, John York, Agostino Pietrangelo, Jonathan Frisch, Matt Cranswick, and Aidan MacDonald for countless discussions and advice given over the years. Additionally I would like to acknowledge Joseph Kumka and Christopher McGuirk, two talented undergraduates that made significant contributions to the work presented in Chapter 4 of this thesis.

Finally I would like to thank my friends and family for all the years of support. The greatest thank you goes to my parents, whose love and support over the years has without a doubt been the most important influence in my scientific career and life.

Thank you all.

Dedication

Dedicated to my parents, Dr. Arjun K. Gupta and Indrani Gupta

Table of Contents

List of Tables

List of Figures

CHAPTER 1. Towards New Cu/O_2 Species Capable of Challenging Oxidative Transformations:

A Review of Elusive $[CuO]^+$ Species

1.1 Introduction

Oxidations of organic molecules by transition metal-O_2 (M/O_2) species in biology and synthetic chemistry have been of interest to researchers for a number of years. To better understand the fundamental chemistry of these reactions, synthetic inorganic chemists have targeted the syntheses of discrete M/O_2 species. The isolation, characterization, and reactivity of such species can lead to mechanistic insight into how oxidation reactions occur. Better mechanistic understanding of these oxidation reactions may lead to the design of new, more effective catalysts, expansion of the scope of reactivity and substrates, and new fundamental understanding of the breaking and formation of C–H and C–O bonds, among others, with activated M/O_2 species.

This chapter will focus on the activation of molecular dioxygen (O_2) by a metal center, specifically copper, and the structural, electronic, and reactivity characteristics of a specific copper-oxygen species, namely a $[CuO]^+$ species. Important both to biological systems and industry, O_2 is a relatively inexpensive, plentiful, and "green" reagent. These characteristics make its activation and use in organic transformations highly desirable. The 4-electron reduction of O_2 to H_2O has an E^0 = 1.23 V (25 °C, pH = 0),[1] so it is thermodynamically favorable. However, the reaction has a significant kinetic barrier (> 58 kJ/mol).[2] The kinetic barrier of O_2 reduction is generally attributed to its triplet ground

state that requires either electron transfer or pairing with an additional unpaired electron.[3] Biological systems that activate O_2 use first-row transition metals to control the redox chemistry and substrate activation/modification, including, but not limited to, copper, iron, and manganese.[4]

In both synthetic and biological systems, a number of M/O_2 species with varying nuclearities have been observed and characterized. Dioxygen has been found to bind metal centers in different coordination geometries and oxidation states, and can be fully cleaved to form oxo ligands. This flexibility leads to a variety of metal complexes with differing oxidation states of both the metal and O-atoms. For example, metal bound hydroperoxo species (M-OOH) have been synthesized and characterized with manganese,[5] iron,[6] and copper[7] whereas high valent metal-oxo species ($[MO]^{n+}$) are common in manganese[8] and iron[9] chemistry but experimentally unobserved in copper chemistry (except for in the gas phase).

Research in the Tolman laboratory has focused on the activation of O_2 using copper ions ligated by bio-inspired ligand sets. Recent synthetic efforts have targeted $[CuO]^+$ species. The subsequent sections will discuss the motivation for attempting the synthesis of a $[CuO]^+$ species along with a critical review of the literature detailing both theoretical and experimental work aimed at understanding the properties of $[CuO]^+$ species and how it might be synthesized.

1.2 Cu(II)-Oxyl and Cu(III)-Oxo

1.2.1 Postulated $[CuO]^+$ Species in Biological Systems

Copper-containing metalloenzymes have been reported to catalyze a number of oxidation reactions found in Nature using active site copper atoms and O_2, including C–H bond activation and hydroxylation.[10] An ongoing debate involving a number of copper-containing monooxygenases is concerned with the identity of the active oxidant responsible for H-atom abstraction and substrate oxidation. One particular motif that has been suggested but never experimentally observed in solution is a $[CuO]^+$ species.

The involvement of a $[CuO]^+$ species as the active oxidant in a copper-containing monooxygenase was reported by Tian *et al.*[11] This report focused on the metalloenzyme dopamine β-monooxygenase (DβM) that catalyzes the stereospecific hydroxylation of a C–H bond in dopamine to form norepinephrine. DβM uses an active site copper atom and O_2 in its activity. At the time of the Tian study, it was believed that a Cu(II)-hydroperoxo species was responsible for the H-atom abstraction step. Tian *et al*. sought to gain insight into the mechanistic steps involved in the enzyme's activity, particularly if a Cu(II)-hydroperoxo or $[CuO]^+$ species is the active species that performs H-atom abstraction. Two energy diagrams depicting H-atom abstractions from substrates by a Cu(II)-hydroperoxo and $[CuO]^+$, drawn as a Cu(II)-oxyl radical, are shown in Figure 1.1.[11] To experimentally probe the reaction mechanism, a number of substrates that ranged from those that demonstrated very rapid reaction rates to those that were oxidized slowly by DβM were used. Using the Hammond postulate, the authors reasoned that substrates that demonstrated slower kinetics would have a transition state more closely resembling the

final products (Figure 1.1, *late t.s.*). This relationship was used to differentiate between a mechanism involving a Cu(II)-hydroperoxo versus one involving a Cu(II)-oxyl radical. In a mechanism involving a Cu(II)-hydroperoxo, the O-atom bound to the Cu-atom experiences a decrease in bond order upon H-atom abstraction and O–O bond cleavage (Figure 1.1, *a*). In a mechanism involving a Cu(II)-oxyl radical species as the active oxidant, the O-atom bound to the Cu-atom experiences an increase in bond order upon H-atom abstraction (Figure 1.1, *b*). The authors experimentally determined the ^{18}O-isotope effect using $^{18}O_2$ and five substrates with known rate constants in oxidations catalyzed by DβM. Based on the hypothesis presented above and the transition state models shown in Figure 1.1, it would be expected that if a Cu(II)-hydroperoxo species was the active oxidant, the slowest reaction, i.e. latest transition state, should demonstrate the greatest decrease in O–O bond order. This would result in a trend of increasing ^{18}O-isotope effect with decreasing reaction rates. However, the authors observed the opposite trend, suggesting that a Cu(II)-hydroperoxo could not be the active oxidant in DβM.[11] The alternative proposed mechanism involving a Cu(II)-oxyl radical species would demonstrate an increase in bond order for H-atom transfer to a copper-bound O-atom with a late transition state (Figure 1.1, *b*). This would result in a decrease in ^{18}O-isotope effect with decreasing reaction rate, consistent with the experimental evidence presented.[11] This led to the assignment of a $[CuO]^+$ species as the active oxidant responsible for H-atom abstraction. The authors then proposed a new reaction mechanism for the formation of a Cu(II)-oxyl radical in DβM involving several conserved active site tyrosine residues (Figure 1.2). In the proposed mechanism, O_2 first reacts with a reduced

Cu(I) ion to form a Cu(II)-superoxo species. Proton coupled electron transfer to this species forms a Cu(II)-hydroperoxo. The Cu(II)-hydroperoxo species then abstracts a H-atom from an active site tyrosine residue to form a tyrosine radical, one molecule of water, and a Cu(II)-oxyl radical (Figure 1.2). This $[CuO]^+$ species then abstracts an H-atom from the substrate followed by radical rebound to form a copper-bound alkoxide that dissociates to yield the final hydroxylated product.[11]

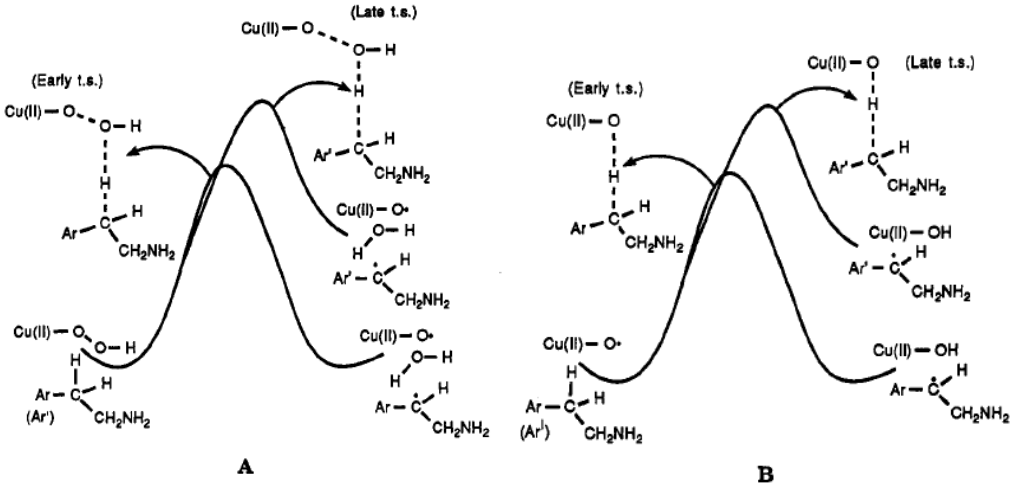

Figure 1.1. Proposed transition state models based on the Hammond postulate for H-atom abstraction by a Cu(II)-hydroperoxo (A) and Cu(II)-oxyl radical (B). Figure reproduced from Ref [11].

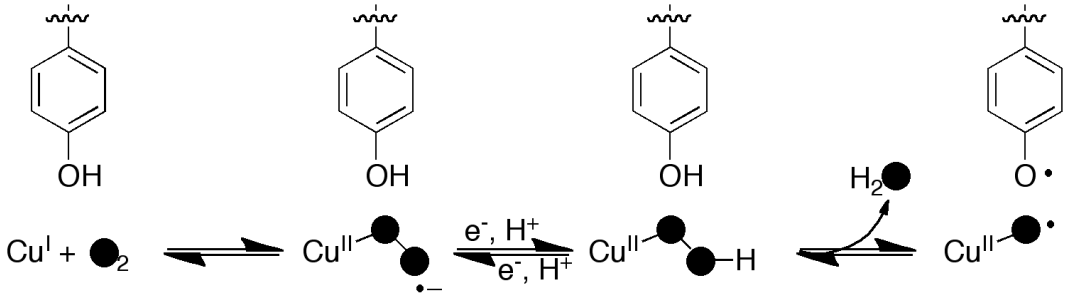

Figure 1.2. Proposed reaction mechanism for the formation of a Cu(II)-oxyl radical by H-atom abstraction from a active-site tyrosine residue. Adapted from Ref [11].

A mechanism similar to that postulated by Tian *et al*.[11] involving a $[CuO]^+$ species was proposed by Wimalasena and May.[12] Their report focused on *N*-dealkylations of *N*-phenylethylenediamine (PEDA) and *N*-methyl-*N*-phenylethylenediamine (*N*-MePEDA) catalyzed by DβM. It was found during this study that both PEDA and *N*-MePEDA act as inhibitors to DβM under turnover conditions. Additionally, it was found that the introduction of a variety of *N*-alkylamines that were not oxidized by DβM acted as potent inhibitors. Based on their experimental observations and drawing parallels to cytochrome P-450 catalyzed *N*-dealkylation reactions,[13] the authors proposed a mechanism that involves a one electron transfer from the substrate/inhibitor to a Cu(II)-hydroperoxo species inducing O–O bond cleavage to yield a $[CuO]^+$ species, hydroxide, and a nitrogen cation radical (Figure 1.3).[12] The nitrogen cation radical acts as an inhibitor or can undergo C–H bond cleavage at the α-carbon leading to *N*-dealkylation. From the cationic amine radical, two potential mechanistic routes were envisioned. In one path, H-atom abstraction by the Cu(II)-oxyl radical leads to the formation of an iminium cation that can undergo O-atom rebound with the formed Cu(II)-OH (Figure 1.3, *top*). This path would yield a hydroxylated product that undergoes *N*-dealkylation. In an alternative route, proton transfer from the α-carbon and radical rearrangement leads to the formation of a carbon-based radical (Figure 1.3, *bottom*). This species then transfers an electron to the $[CuO]^+$ species followed by O-atom rebound to form the hydroxylated species and final *N*-dealkylated products. The second route could potentially be described as a proton coupled electron transfer, although the authors do not explicitly state this.[12] Experimental support for the proposed inhibitor versus *N*-dealkylation pathway came

from the use of substrates that acted as inhibitors to DβM but did not contain H-atoms on the α-carbons, particularly aniline and 5-hydroxyindole. Additionally, fluorination of the α-carbon and kinetic isotope effect studies of deuterated substrate were consistent with the proposed pathways starting with a one electron transfer to a Cu(II)-hydroperoxo complex to form a $[CuO]^+$ species and a nitrogen-based radical inhibitor. The authors made no assumptions about the electronic nature of a $[CuO]^+$ species and such a species was not directly observed.[12]

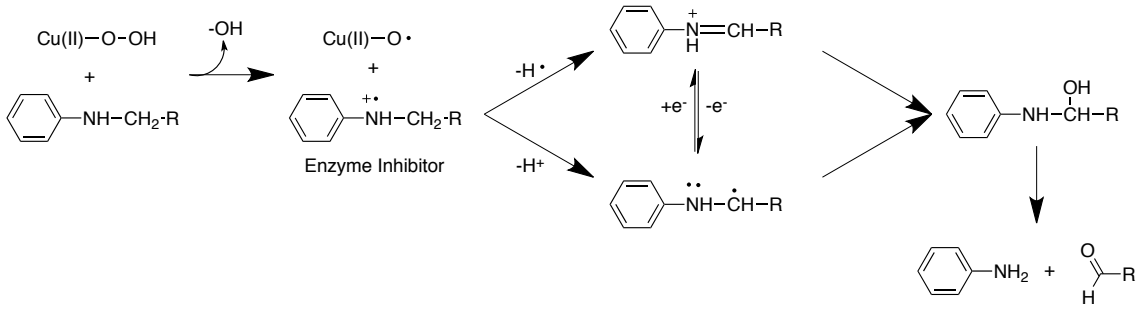

Figure 1.3. Reaction pathway proposed by Wimalasena and May to explain the *N*-dealkylation of benzylic-nitrogen substrates catalyzed by DβM. Adapted from Ref [12].

A mechanism for DβM involving a $[CuO]^+$ species, particularly that proposed by Tian *et al*,[11] was challenged several years later by Francisco *et al.* in a report that examined mutant forms of peptidylglycine α-hydroxylating monooxygenase (PHM).[14] PHM and DβM are generally considered to follow similar mechanisms because both enzymes use similar active site copper ions and O_2 in the hydroxylation of C−H bonds and both enzymes share a high degree of peptide homology, particularly in the residues comprising the active site.[10] The mechanism proposed by Tian *et al*. relies on a conserved active site tyrosine residue in the formation of the $[CuO]^+$ species from a Cu(II)-hydroperoxo intermediate.[11] Francisco *et al*. examined mutant forms of PHM that

replaced two highly conserved tyrosine residues in both PHM and DβM with phenylalanine residues. Kinetic analysis of the reactivity of these mutant PHM enzymes suggested the C-H bond scission has a significant contribution from tunneling. This conclusion was based on a kinetic isotope effect (KIE) for the C–H bond cleavage step that was larger than a value of 7 for a primary deuterium intrinsic isotope effect. The contribution of tunneling in PHM activity suggests the original interpretation of experimental results by Tian *et al*. may be incorrect because they were based on the Hammond postulate and did not consider a contribution from tunneling.

Although a mechanism for PHM and DβM may not use a $[CuO]^+$ species as an active oxidizing species, a number of alternate mechanisms for PHM and DβM include a $[CuO]^+$ species *after* H-atom abstraction on the route to a final hydroxylated product.[10,15,16] One such mechanism proposed for DβM activity by Miller *et al*. is shown in Figure 1.4.[17] In this mechanism, a Cu(II)-hydroperoxo species is formed by the two electron reduction of O_2 and protonation. This species then abstracts a hydrogen atom from a substrate C–H bond to yield a water molecule, a substrate carbon radical, and a Cu(II)-oxyl radical species (Figure 1.4). Radical rebound results in the formation of a copper-bound alkoxide that dissociates to yield the final hydroxylated substrate. This mechanism does not implicate a $[CuO]^+$ species as the active oxidant for enzymatic activity, although such a species is nonetheless formed.

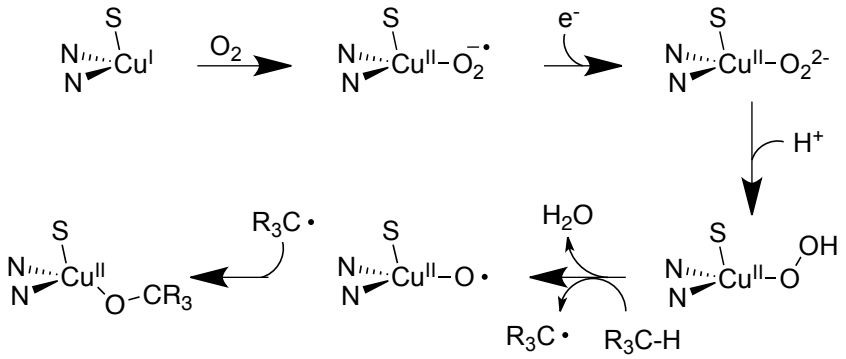

Figure 1.4. Mechanism proposed by Miller *et al*. for the activity of DβM using a Cu(II)-hydroperoxo as the active oxidant. Adapted from Ref. [17].

1.2.2. Electronic Character, Mechanistic Routes, and Reactivity of a $[CuO]^+$ Species: Theory

A $[CuO]^+$ species has been described in the literature either as a Cu(III)-oxo or Cu(II)-oxyl radical species.[18] The two possible electronic ground states for a $[CuO]^+$ species are either S = 0 or 1, with the S = 0 state corresponding to a singlet Cu(III)-oxo species and S = 1 to the triplet Cu(II)-oxyl radical species. The S = 0 species has the Cu-atom in a +3 oxidation state (d^8) along with an oxo ligand ($O(p)^6$). The triplet Cu(II)-oxyl radical species contains a d^9 Cu(II) metal ion with an oxyl radical ligand ($O(p)^5$).[18] Recent computational work examining a $[CuO]^+$ species in the active site of PHM found the Cu(II)-oxyl radical species in a trigonal bipyramidal coordination geometry to be the electronically favored state by approximately 5 kcal/mol (Figure 1.5.).[15,19] This species contains a half-occupied non-bonding oxygen p-orbital giving rise to the oxyl radical assignment. A second half-occupied copper orbital (d_{z2}) displays overlap with the O-atom p_z orbital forming a half σ-bond. This weak half bond is the only bonding interaction in the Cu(II)-oxyl radical species. This weak bonding description is different than that

proposed for the analogous $[FeO]^{2+}$ species that is best described as having a strong Fe–O σ-bond supplemented with two partial π-bonds resulting in an overall double bond (Figure 1.5). Strong Fe–O bonds have been experimentally observed as short Fe–O bond distances of approximately 1.65 Å [Fe(IV)=O].[20] The differences in electronic structures of high valent $[CuO]^{+}$ species compared to $[FeO]^{2+}$ species are likely contributing factors to the difficulty in observing the former.

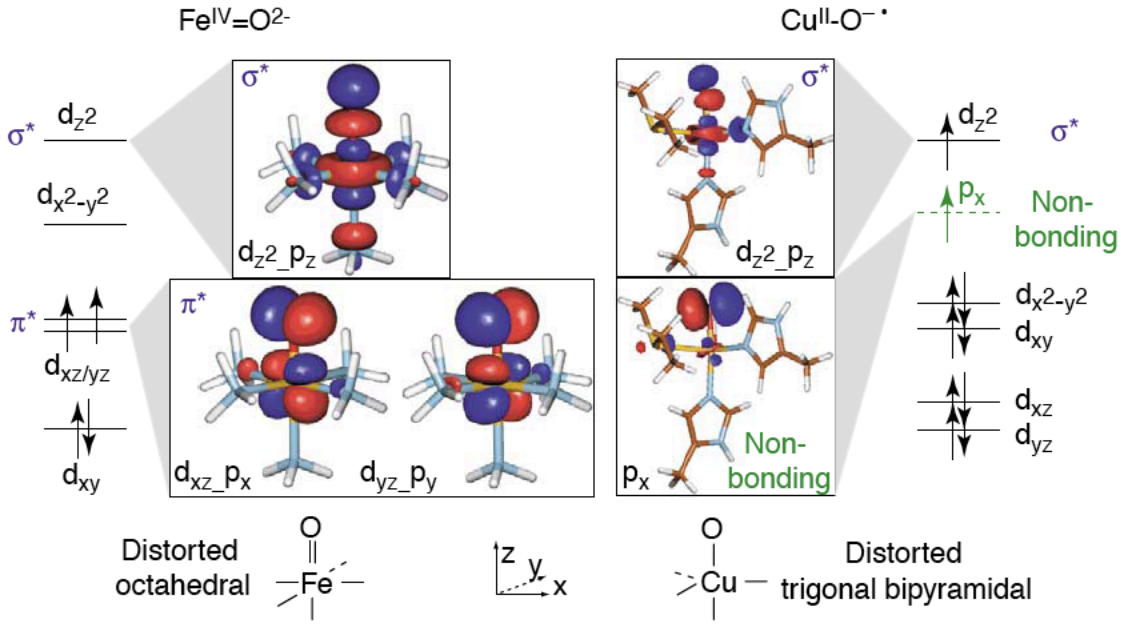

Figure 1.5 Energy diagram and calculated orbitals for S = 1 $[FeO]^{2+}$ (*left*) and $[CuO]^{+}$ (*right*) species. Figure reproduced from Ref. [18].

Shiota *et al*. recently reported a computational study examining the electronic structures of a number of $[MO]^{+}$ species (M = Sc, Ti, V, Mn, Fe, Co, Ni, and Cu) and their reactivities in converting methane to methanol.[21] The electronic states, M–O bond distances, M–O vibrational frequencies, and bond dissociation energies (BDE) were calculated for a number of MO^{+} species (Table 1.1). The general trend observed in the data is that the M–O bonds become weaker with increasing d-electron count as observed

by lengthened M–O bonds, decreased vibrational frequencies, and decreased BDEs, with CuO^+ containing the weakest M–O interaction.[21] This trend was justified by examining the bonding and anti-bonding molecular orbitals involved in the metal-oxo interaction, with the cases of FeO^+ and CuO^+ shown in Figure 1.6. Based on the data presented in Table 1.1, the bonding interaction in FeO^+ (BDE = 69 kcal/mol) is more significant than that calculated and observed for CuO^+ (BDE = 38 kcal/mol). In examining the MO diagram shown in Figure 1.6 we see that both FeO^+ and CuO^+ have filled bonding (2σ and 1π) and non-bonding (1σ) orbitals. Differences in the electronic structure become evident when examining the higher energy non-bonding (1δ) and anti-bonding orbitals (2π and 3σ) in both species. The FeO^+ species has partially filled 1δ, 2π and 3σ orbitals giving rise to a bond order of 1.5. The CuO^+ species has three additional electrons that are found in the non-bonding 1δ orbital and anti-bonding 2π orbital giving rise to an overall bond order of 1. The MO diagrams presented below explain the overall trend observed in Table 1.1 because lower electron counts result in less population of anti-bonding orbitals leading to higher overall bond orders.[21]

The capacity of these MO^+ species to convert methane to methanol was computationally examined and the results for three $[MO]^+$ species are shown in Table 1.2. The CuO^+ species, which was found to have the weakest metal-oxo bonding interaction, was found to have the most favorable energetics for methane oxidation (ΔE_{calc} = –50 kcal/mol). This is consistent with a weaker metal-oxo interaction leading to a more reactive MO^+ species towards substrate oxidation. As the M–O interaction is strengthened, oxidation of methane becomes less favorable as indicated by the more

positive ΔE_{calc} values for FeO^+ and ScO^+ for the conversion of methane to methanol (Table 1.2).[23] These results suggest that if a $[CuO]^+$ species can be synthesized, it would be a very potent oxidant, and that the synthesis and isolation of a $[CuO]^+$ species would be difficult due to the very weak Cu–O interaction and high reactivity.

Table 1.1. Calculated and experimental parameters for MO^+ species reported in Ref [21].

MO^+	**Electronic State**	***r*(M–O) (Å)**	**Vib Freq (cm^{-1})**	**BDE (kcal/mol)**	**BDE_{exp}[22] (kcal/mol)**
ScO^+	$^1\Sigma^+$	1.603	1095	156.1	165.1
TiO^+	$^2\Delta$	1.563	1146	155.1	159.8
VO^+	$^3\Sigma^-$	1.532	1160	137.2	138.1
CrO^+	$^4\Sigma^-$	1.573	830	81.3	85.3 ± 1.3
MnO^+	$^5\Sigma^+$	1.715	640	56.4	68 ± 2
FeO^+	$^6\Sigma^+$	1.632	850	75.2	81 ± 2
	$^4\Delta$	1.683	675	69.4	
CoO^+	$^5\Delta$	1.625	816	73.3	77 ± 2
	$^3\Pi$	1.719	644	49.9	
NiO^+	$^2\Sigma^-$	1.646	642	69.3	63 ± 3
	$^4\Sigma^-$	1.618	783	57.9	
CuO^+	$^3\Pi$	1.758	569	37.6	37

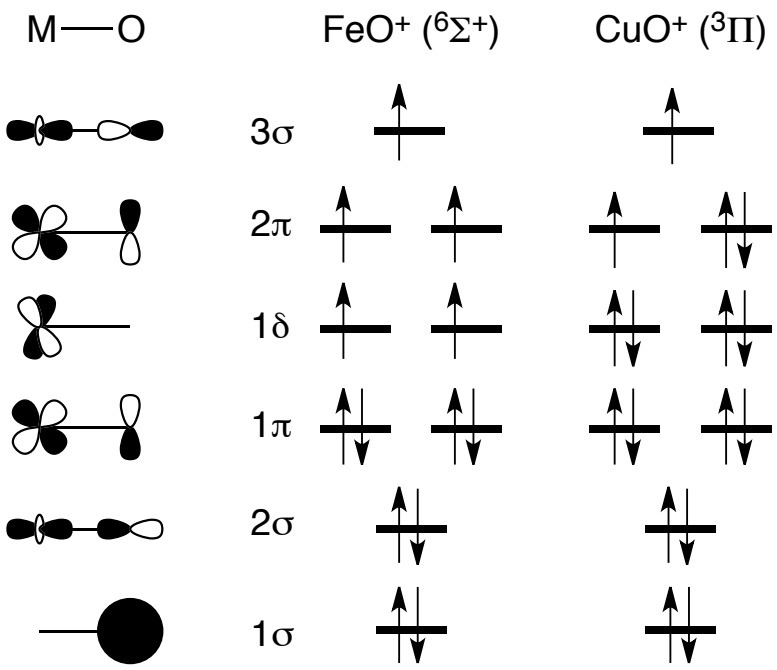

Figure 1.6. Molecular orbital diagrams for both FeO^+ and CuO^+ species with pictorial representations of the involved orbitals shown to the left. Figure was adapted from Ref [21].

Table 1.2. Overall energies for the oxidation of methane to methanol by a MO^+ species as calculated in Ref [21].

Overall Energies for the Reactions:

$MO^+ + CH_4 \rightarrow M^+ + CH_3OH$

MO^+	ΔE_{calc} (kcal/mol)	ΔE_{exp}[23] (kcal/mol)
ScO^+	73.5	90.1 ± 1.6
FeO^+	–12.6	–8.2 ± 1.6
CuO^+	–50.0	–60.1 ± 4.1

The oxidizing potential of a $[CuO]^+$ species in the active sites of DβM[24,25] and particulate methane monooxygenase (pMMO)[26] has been examined by computational methods. In these studies, the geometry optimized structures of $[CuO]^+$ species included

two histidine nitrogen and one methionine sulfur donor atoms for DβM[24,25] or two histidine nitrogen and one glutamate oxygen atom for pMMO.[26] All reports found the triplet $[CuO]^+$ species to be more stable than the corresponding singlet ground state by 3.9–6.5 kcal/mol, consistent with previously reported electronic descriptions.[15,19] In the two cases examining DβM reactivity, benzylic C–H hydroxylation by a $[CuO]^+$ species was more energetically favorable compared to other examined copper-oxygen species including Cu(II)-superoxo and Cu(II)-hydroperoxo complexes. [25,25] The Cu(II)-hydroperoxo species was found to be the least potent oxidant leading the authors to focus on the H-atom abstractions performed by $[CuO]^+$ and Cu(II)-superoxo species. In both reports a $[CuO]^+$ species was found to have a very low energy barrier for rate-determining H-atom abstraction (3.8–5.4 kcal/mol) compared to a Cu(II)-superoxo species (16.9–23.1 kcal/mol).[24,25] Additionally, the final oxidized products were found to be 46.6 kcal/mol lower in energy with respect to the starting $[CuO]^+$ species (18.9 kcal/mol lower in energy for the Cu(II)-superoxo reaction).[24] The extremely low energy barrier and overall favorable thermodynamics seen in $[CuO]^+$ mediated H-atom abstraction and subsequent substrate hydroxylation suggests that such a species would be a more potent oxidant in the active site of DβM relative to other copper-oxygen species examined. This finding is consistent with the previously discussed study by Shiota *et al*. that found a $[CuO]^+$ species to be a potent oxidizer of strong C–H bonds.[21] Neither studies that examined an enzyme-supported $[CuO]^+$ species addressed the energy differences between the starting $[CuO]^+$ and Cu(II)-superoxo species. This energy

difference likely contributes to the favorable energetics calculated by Shiota *et al*. for the oxidations carried out by a $[CuO]^+$ compared to a Cu(II)-superoxo species.[21]

Yoshizawa *et al*. recently examined a $[CuO]^+$ species in the active site of pMMO by theory and addressed the energetics for the formation of the $[CuO]^+$ species from Cu(I) and O_2.[26] The calculated structure of $[CuO]^+$ was found to be significantly higher in energy with respect to a Cu(II)-hydroperoxo (7.8 kcal/mol) and Cu(II)-superoxo (24.4 kcal/mol) species. The 24.4 kcal/mol energy difference found between the $[CuO]^+$ and Cu(II)-superoxo species in this work is likely the source of the overall thermodynamic difference (43.3 kcal/mol) in the hydroxylation reactions catalyzed by similar species discussed above in the active site of DβM.[24] The oxidation of methane to methanol by a $[CuO]^+$ species in the active site of pMMO was calculated to be exothermic by 59.3 kcal/mol with respect to the starting $[CuO]^+$ species, showing that, if formed, a $[CuO]^+$ species would be a very potent oxidant.[26]

We turn next to a more detailed discussion of the energetics of the formation of a $[CuO]^+$ species. Most proposed mechanisms, including the mechanism described above for DβM (Section 1.2.1),[11] involve homolytic cleavage of an O–O bond of a Cu(II)-OOH species to form a Cu(III)-O^{2-} (S = 0 or 1) species.[18] A DFT study on this bond cleavage using a tridentate tris(pyrazolyl)hydroborate supporting ligand to form an S = 0 species revealed the reaction to be energetically unfavorable (ΔE = +75 kcal/mol, $\Delta G \sim 60$ kcal/mol).[27] Use of a 5-coordinate model complex containing a methionine ligand resulted in slightly less unfavorable energetics (ΔE = +59 kcal/mol, $\Delta G \sim 47$ kcal/mol) compared to the system supported by a tris(pyrazolyl)hydroborate ligand.[10] The more

favorable energies were attributed to an axial methionine along with a higher coordination number stabilizing the high-valent Cu(III) ion. Additionally, formation of the 5-coordinate triplet (S = 1) $[CuO]^+$ species was found to be the most favorable (ΔE = +33 kcal/mol, $\Delta G \sim 42$ kcal/mol).[10] These reactions were compared to the analogous O–O bond cleavage in a low-spin Fe(II)-OOH complex to yield an Fe(IV)=O (S = 1) species.[28] This latter reaction has been experimentally observed and studied by calculations and found to have ΔG = 10–13 kcal/mol, nearly 20 kcal/mol lower in energy than the most favorable copper model system.[20] Two factors that contribute to the difference in reactivities between a low-spin Fe(II)-hydroperoxo and Cu(II)-hydroperoxo to form the corresponding $[MO]^{n+}$ species have been proposed.[27] First, the starting Cu(II)-hydroperoxo species has strong O–O and weak Cu–O bonds compared to the iron analog making it less activated for O–O bond cleavage. Second, the relative instability of the $[CuO]^+$ product relative to the $[FeO]^{2+}$ species contributes to the overall unfavorable energetics of the reactions. The majority of the results presented above suggest that the formation of a $[CuO]^+$ species from a Cu(II)-hydroperoxo precursor has a significant thermodynamic barrier (+33–75 kcal/mol) and overall unfavorable energetics (ΔG = 42–60 kcal/mol). If these calculations are an accurate representation of the energetic cost to form a $[CuO]^+$ species, it seems synthetic chemists must find an alternative route to such an intermediate.

A report by Crespo *et al*. examined the reactivity of a number of different copper-oxygen species in the active site of PHM by theoretical calculations using a whole enzyme model.[29] The key aspects of this work relevant to this discussion involved the

barriers of H-atom abstraction by a number of copper-oxygen species. It was found that a Cu(II)-superoxo species would have barriers of 25 kcal/mol (triplet) or 20 kcal/mol (singlet) in abstracting a hydrogen atom from a substrate. The authors reasoned barriers of this magnitude to be too high to realistically overcome, making a Cu(II)-superoxo species an unlikely oxidant. The next logical species, a Cu(II)-peroxo species, was examined and found to have a similarly high thermodynamic barrier for H-atom abstraction of 25 kcal/mol, ruling out its involvement in the oxidation reaction. Protonation of this species forms a Cu(II)-hydroperoxo adduct. This species was found to be the least potent oxidant relative to other copper-oxygen species examined with an energetic barrier in excess of 40 kcal/mol for abstracting an H-atom. The authors claimed that addition of a proton to a Cu(II)-hydroperoxo species would cause release of a water molecule via homolytic O–O bond cleavage and formation of a $[CuO]^{2+}$ species.[29] This species is distinct from the previously discussed $[CuO]^{+}$ species as it is a dication. A $[CuO]^{2+}$ species, based on the MO diagram presented in Figures 1.5 and 1.6, would have a stronger Cu–O interaction compared to a $[CuO]^{+}$ species because it has one less electron in the anti-bonding 3σ orbital. Examination of the Mulliken charges and spin populations of the metal and coordinated ligands showed significant radical character on the ligating enzyme histidine and methionine ligands. This finding led the authors to reassign this species as a $[CuO]^{+}$ species with a delocalized ligand based radical cation ($L_3^{+\cdot}$). This species is analogous to the high-valent Fe(IV)-oxo/delocalized porphyrin radical found in cytochrome P-450 enzymes.[30] Additionally, the $[(L_3^{+\cdot})(CuO)]^{2+}$ species

was found to have a negligible barrier for H-atom abstraction from a substrate molecule.[29]

The review of the literature in this section has led to the identification of several common conclusions concerning the electronic description of a $[CuO]^+$ species, its oxidative reactivity, and the thermodynamics for its formation. First, it seems universally accepted based on calculated structures that the electronic ground state is best described as a triplet Cu(II)-oxyl radical rather than a singlet Cu(III)-oxo species.[10,18,19,20,22,24,25,26,29] It was also universally found in all discussed reports that if formed, a $[CuO]^+$ species would be a potent oxidant and more reactive towards C–H bond activation compared to other examined copper-oxygen species. This heightened reactivity is no doubt related to the evidence that the formation of a $[CuO]^+$ species is generally thermodynamically unfavorable in an enzyme environment. The overall thermodynamic barrier for the formation of a $[CuO]^+$ species varies in the literature, with reported barriers in excess of 40 kcal/mol. The high reactivity and high energetic barrier for formation of a $[CuO]^+$ species are likely contributors to the fact that it has not been observed experimentally in enzymes. The following sections will present the rare examples of experimentally observed $[CuO]^+$ species along with synthetic systems for which the intermediacy of a discrete $[CuO]^+$ species has been proposed.

1.2.3. Experimental Observation of $[CuO]^+$ Species in the Gas Phase

The experimental observation of a $[CuO]^+$ species has not been achieved to date outside of the gas phase. Sülzle *et al*. first reported the experimental observation of such a species using mass spectrometry techniques.[31] Formation and observation of the $[CuO]^+$

fragment was accomplished by two separate means. Electron impact ionization of anhydrous $Cu(II)(NO_3)_2$ followed by collision-induced dissociation with helium yielded the $[CuO]^+$ fragment along with peak envelopes assigned to $[CuN]^+$, $[CuO_2]^+$, and $[CuNO]^+$ ions. In an MS-MS experiment, the $[CuO_2]^+$ ion was mass selected and further examined by neutralization-reionization mass spectrometry (NR-MS) that revealed further fragmentation of the parent ion to yield a $[CuO]^+$ fragment. A more recent study by Rodgers *et al.* used guided ion beam mass spectrometry to react Cu(I) ions with a number of neutral reagent gases, including O_2, CO, CO_2, NO, NO_2, and N_2O.[32] These experiments involved accelerating Cu^+ ions into a reaction cell containing a neutral reactant followed by mass analysis. In all reactions involving a reagent gas with an O-atom, $[CuO]^+$ fragments were detected. No experimental evidence was reported for the ground electronic state of a $[CuO]^+$ species so the authors extrapolated spectroscopic results for the known CuO fragment in order to propose an electronic structure assignment.[32,33] CuO has a $^2\prod$ (doublet) ground state. Ionization of this species to yield a $[CuO]^+$ species would yield a $^3\sum$ (triplet) species that was described by the association of a Cu(I) (^{1}S, $3d^{10}$) atom with an O(^3P, $2p^4$) atom with a lone pair of electrons on the O-atom directed at the Cu-atom.[32] This species is related to the Cu(II)-oxyl radical discussed in Section 1.2.2 by an electron transfer between the metal center and O-atom ligand, although this relationship was not presented in this work.

The third experimental report of a $[CuO]^+$ species in the gas phase differs from the examples described above by the fact that the $[CuO]^+$ species is ligated by a bidentate *N*-donor ligand, 1,10-phenanthroline (phen).[34] Schröder *et al*. reported the collision

induced dissociation of a starting $[(phen)Cu(NO_3)]^+$ ion which resulted in the formation of both $[(phen)Cu]^+$ and $[(phen)CuO]^+$ in the gas phase. The reactivity of $[(phen)CuO]^+$ towards a number of alkanes was studied. $[(phen)CuO]^+$ was mass selected and reacted with neutral substrates; no reactions occurred with methane or ethane, but reaction with propane resulted in the observation of both the propyl radical cation and propanol. The selectivity of the observed C–H bond activation was probed with deuterium labeled propane. Four propane derivatives were examined: (i) $CH_3CH_2CH_3$, (ii) $CH_3CD_2CH_3$, (iii) $CD_3CH_2CD_3$, and (iv) $CD_3CD_2CD_3$. From the relative peak intensities of the observed oxidized products, the authors drew two conclusions: (i) $[(phen)CuO]^+$ could activate C–H bonds at both the primary and secondary carbon positions and (ii) with increased deuteration, the O-atom transfer products became more favorable. Similar reactivity was observed with other alkanes, including *n*-butane and *i*-butane, and O-atom transfer reactions occurred almost exclusively with unsaturated hydrocarbons.

The most recent gas phase observation of a $[CuO]^+$ ion was reported by Dietl *et al*.[35] This work examined the oxidation of methane to methanol by $[CuO]^+$ in the gas phase both experimentally and by theoretical calculations. The $[CuO]^+$ cation was generated by laser desorption/ionization of a copper target in the presence of He/N_2O plasma, presumably by oxo-transfer from N_2O. It was found that the $[CuO]^+$ species was capable of reacting with methane at room temperature to abstract a hydrogen atom to form the methyl radical and $[CuOH]^{\cdot+}$ in 40% yield. The oxygen transfer product, methanol, and Cu(I) were also detected in 60% yield. It was also found that the $[CuOH]^{\cdot+}$ species could abstract an H-atom from methane to form the $[Cu(OH_2)]^+$ cation. Theory

demonstrated that it is likely a triplet ($^3\Sigma^-$) ground state $[CuO]^+$ species that is responsible for H-atom abstraction, an assignment consistent with what was postulated by Rodgers *et al.* previously.[32,35] Dietl *et al.* suggests that the weak Cu–O bond strength of 130 kJ/mol (~31 kcal/mol) is sufficiently activated to perform the oxidation of methane to methanol.[36]

The work described in this section has demonstrated that the formation of a $[CuO]^+$ species by O-atom transfer in the gas phase can not only form the desired $[CuO]^+$ species, but that such a species is capable of C–H bond activation and oxidation. These results suggest that oxo-transfer rather than O_2-reduction may be a preferable synthetic route towards a $[CuO]^+$ species not only in the gas phase, but in the solution state.

1.2.4. $[CuO]^+$ Species as Postulated Intermediates in Synthetic Systems

Reactions with O_2. $[CuO]^+$ species have been proposed as potential intermediates and active oxidizing species in a number of synthetic systems.[37,38,39,40,41] The Maumy group reported reactions of Cu(I) or Cu(II) salts with O_2 and suggested the intermediacy of a $[CuO]^+$ species.[37,39,42,43,44] Several of these reports described the copper-mediated oxidations of phenols,[37] alcohols,[42,43] and carboxylic acids.[44] The active oxidant in all cases was proposed to be an unobserved Cu(III)-oxo species derived from the heterolytic cleavage of an O–O bond in a μ-peroxodicopper(II) precursor (Figure 1.7). In all of the examples reported by the Maumy group, the copper center was ligated by a bound substrate that contained strong electron donating groups, typically phenoxides,[43] alkoxides,[42,43] or carboxylates.[44] The presence of strongly donating ligands may facilitate

the O-O bond cleavage and stabilization of the high-valent $[CuO]^+$ species although this was not further explored in these works.

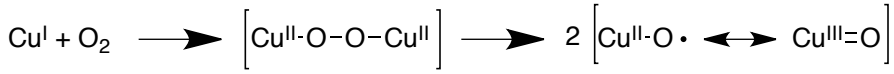

Figure 1.7. Proposed formation of two Cu(II)-oxyl radical species from the heterolytic O–O bond cleavage in a dicopper(II)-peroxide species.

Hong *et al*. described the O_2 reactivity of a series of Cu(I) complexes supported by bidentate pyridyl-imine ligands and α-ketocarboxylate co-ligands in a recent report.[45] The aim was to introduce α-ketocarboxylates as ligands to a Cu(I) complex to access a $[CuO]^+$ species in a route analogous to one that yields related Fe(IV)=O moieties in α-ketogluterate dependent enzymes (Figure 1.8).[46] The mechanism shown in Figure 1.8 depicts the accepted catalytic cycle for α-ketoglutarate dependent enzymes. The mechanism begins with the binding of an α-ketocarboxylate to the metal center (Figure 1.8, a → b) followed by displacement of a metal-bound water molecule by introduction of a substrate (SH) into the active site (Figure 1.8, b → c). Coordination of O_2 to the metal site and a one electron reduction by the metal results in the formation of an Fe(III)-superoxo species (Figure 1.8, c → d). The distal O-atom of the Fe(III)-superoxo species then attacks the α-keto carbon position of the α-ketocarboxylate ligand (Figure 1.8, d → e) inducing C–C bond cleavage and the formation of an Fe(II)-peracid species and CO_2 (Figure 1.8, e → f). Heterolytic O–O bond cleavage results in the formation of a bound carboxylate and an $[Fe(IV)O]^{2+}$ species (Figure 1.8, f → g) that is responsible for attacking a C–H bond in the substrate and forming the final hydroxylated species (S–OH) (Figure 1.8, g → h). Ligand exchange reforms the starting Fe(II) complex ready for a new

catalytic cycle (Figure, 1.8, h → a). In this mechanism, the $[MO]^{n+}$ species is formed by O–O bond heterolysis in the metal-peracid species. This pathway differs from the unfavorable reactions discussed in Section 1.2.2 involving the cleavage of an O–O bond in a Cu(II)-hydroperoxo to form a $[CuO]^{+}$ species. It was envisioned that an analogous mechanism involving the oxygenation of a Cu-α-ketocarboxylate complex rather then the O–O bond cleavage in a Cu(II)-hydroperoxo may circumvent the high thermodynamic barrier found in the latter case and result in the formation of a $[CuO]^{+}$ species.

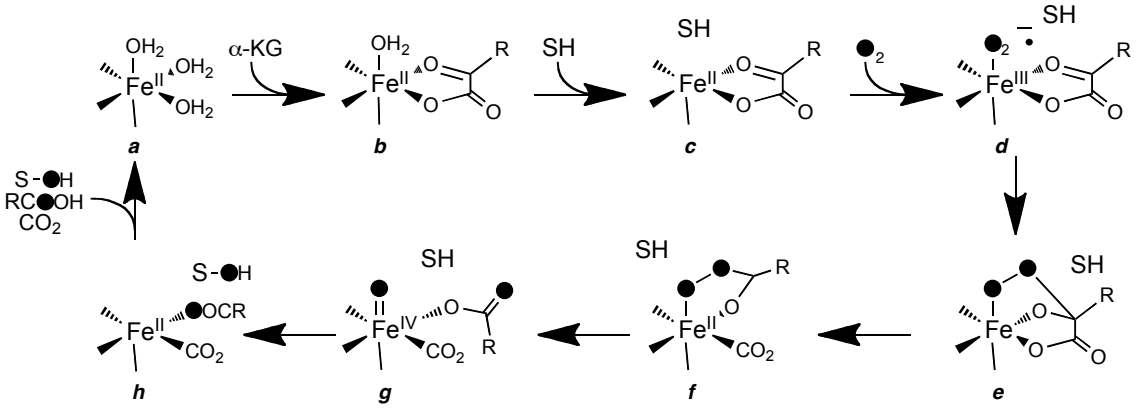

Figure 1.8. Proposed reaction mechanism for α-ketogluterate dependent iron metalloenzymes.

Hong *et al.* reported the syntheses of a number of Cu(I) complexes supported by both a bulky pyridyl-imine ligand and α-ketocarboxylate, two of which are shown in Figure 1.9.[45] Both $(PyrIm^{H,H})Cu(O_2CC(O)Ph)$ and $(PyrIm^{H,OMe})Cu(O_2CC(O)Ph)$ reacted with O_2 at –80 °C over several hours (2 to 4 h). Aryl hydroxylated ligands were observed in yields up to 40% after the reactions reached completion. Additionally, benzoic acid, the expected oxidative decarboxylation product, was observed by ^1H NMR spectroscopy in yields up to 60%. ESI-MS data were obtained on the crude reaction solutions of $(PyrIm^{H,OMe})Cu(O_2CC(O)Ph)$ with O_2 and peak envelopes that contained the oxidized

$PyrIm^{H,OMe}$ ligand were identified and found to shift by two mass units when ^{18}O-labeled O_2 was used. This result indicated that the incorporated O-atom originated from added O_2 and suggested that the observed O_2-reaction of both $(PyrIm^{H,H})Cu(O_2CC(O)Ph)$ and $(PyrIm^{H,OMe})Cu(O_2CC(O)Ph)$ might involve a similar mechanistic route to that followed by Fe-α-ketocarboxylate complexes (Figure 1.8).[45] A mechanistic route involving a $[CuO]^+$ species was supported by a theoretical study (Figure 1.10). Starting from the Cu(I) complex (Figure 1.10, 2') an oxygen adduct was found to have approximately 8–9 kcal/mol higher free energy. The following steps leading to the peracid intermediate were found to be thermodynamically favorable with decarboxylation being exergonic by 34 kcal/mol overall (Figure 1.10, 2'→ Peracid). From the peracid intermediate, O–O bond cleavage either results in the formation of a discrete $[CuO]^+$ species (Figure 1.10, Oxo) that then oxidizes the aryl C–H bond, or a concerted O–O bond cleavage and O–C bond formation with no discrete $[CuO]^+$ species (Figure 1.10, TS-Peracid). The formation of TS-Oxo was found to be more energetically favorable with activation energies of 10.4 versus 17.8 kcal/mol for TS-peracid.[45] Consistent with previously reported computational studies,[10,18,19] the discrete $[CuO]^+$ species was found to be best described as a Cu(II)-oxyl radical in a triplet ground state.[45]

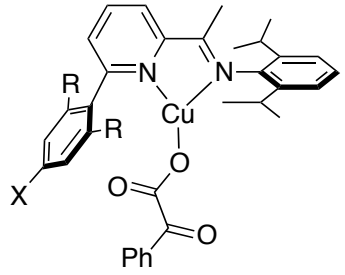

$(PyrIm^{H,H})Cu(O_2CC(O)Ph)$ (R=X=H)
$(PyrIm^{H,OMe})Cu(O_2CC(O)Ph)$ (R = H, X=OMe)

Figure 1.9. Cu(I) complexes supported by pyridyl-imine ligands reported in Ref [45].

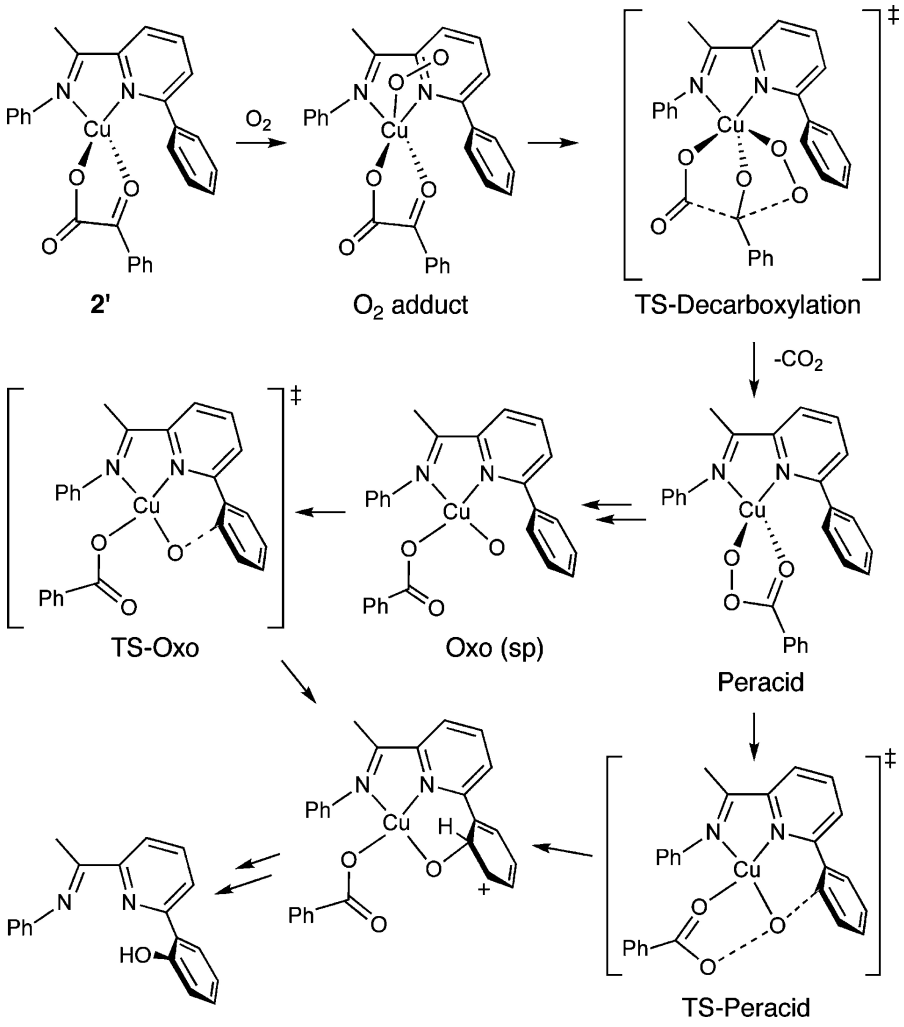

Figure 1.10. Proposed reaction mechanism for the intramolecular aryl-oxidation observed by the oxygenation of a pyridyl-amine supported Cu(I)-complex ligated by an α-ketocarboxylate. Reproduced from Ref. [45].

The mechanism proposed in Figure 1.10. by Hong *et al*. was studied in further detail by Huber *et al*.[47] Starting from a truncated ligand set containing both pyridyl-imine and α-ketocarboxylate ligands similar to the complexes reported by Hong *et al.*[45] (Figure 1.11), the energetics of the various oxygenated intermediates were examined via computation. Three positions on the pyridyl-imine and α-ketocarboxylate ligands (R_1, R_2, and R_3) were substituted with various electronically differing substituents to examine the effect on the relative stabilities of intermediate species. Identical to what was previously proposed and presented in Figure 1.10,[45] this work reported that the oxygenation, decarboxylation, and subsequent aryl-hydroxylation likely follows a path involving the formation of a discrete $[CuO]^+$ species.[47] It was reported that addition of either an electron donating (Figure 1.11, L^1) or withdrawing (Figure 1.11, L^2) substituent at the R_3 position has little aeffect on the stability of the $[CuO]^+$ species. Introduction of an electron withdrawing group (Figure 1.11, L^2) decreased the energetic barrier of decarboxylation by 3 kcal/mol and addition of an electron donating group (Figure 1.11, L^1) increased the energy barrier by 3 kcal/mol with respect to the non-substituted ligand (L^0). This result suggests the attack of the α-ketocarbonyl by a copper-oxygen species is a nucleophillic attack at the electron deficient carbonyl group.

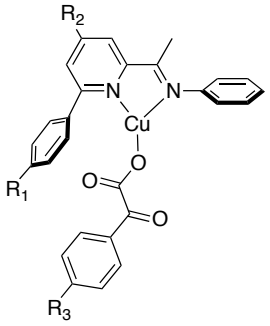

	R_1	R_2	R_3
L^0	H	H	H
L^1	H	H	NH_2
L^2	H	H	NO_2
L^3	H	NME_2	H
L^4	H	NO_2	H
L^5	OMe	H	H
L^6	NO_2	H	H

Figure 1.11. Cu(I) complexes used by Huber *et al.* in theoretical study examining the formation of a reactive $[CuO]^+$ species. Adapted from Ref [47].

Addition of an electron-donating group at R_2 led to increased stabilization of species that contained copper at higher oxidation states, including the $[CuO]^+$ species. Electron-donating groups at R_2 also led to the destabilization of species with lower copper oxidation states including the Cu(I)-peracid intermediate. Complete replacement of the pyridyl-imine ligand with strongly electron donating diamine and tridentate amine–bis(pyridine) ligands also led to the increased stabilization of high-valent intermediates with respect to poor electron-donating ligands. The authors conclude that oxygenation of a Cu(I)-α-ketocarboxylate complex likely proceeds via the formation of a $[CuO]^+$ species, although isolation of such a reactive species is difficult. This is consistent with the experimental and theoretical results reported by Hong *et al*.[45,47]

Reactions with Iodosobenzene. Iodosobenzene (PhIO) is known to react with metal complexes to form discrete metal-oxo species through oxo-transfer.[48] It has also been used as a reagent in metal-mediated oxidation reactions.[49] A number of reactions of PhIO with copper complexes have been reported in the literature, but strong evidence for the formation of discrete copper-oxygen intermediates remains absent.[50,51] Kitajima *et al.*

reported the reaction of $(HB(3,5\text{-}Me_2pz)_3)Cu(I)(PPh_3)$ ($HB(3,5\text{-}Me_2pz)_3$ = (hydrotris(3,5-dimethyl-l-pyrazolyl)borate)) with PhIO.[50d] The reaction of the Cu(I) complex with excess PhIO resulted in a color change from colorless to dark green over 6 h at room temperature. It was suggested that one equivalent of PhIO first oxidizes the coordinated PPh_3 to form and displace $O{=}PPh_3$ and expose a coordination site on the copper atom. A second PhIO reacts with the Cu(I) complex forming either a Cu(I)-PhIO adduct or a $[CuO]^+$ species that immediately reacts with an additional Cu(I) complex to form a $Cu(II)_2$-(μ-oxo) species.[50d] The $Cu(II)_2$-(μ-oxo) species was identified using field desorption mass spectrometry (FD-MS); experimental spectra for both ^{16}O-labeled and ^{18}O-labeled species are shown in Figure 1.12 (*solid*) along with simulated spectra (*dashed*). Unfortunately, the entire spectra for the ^{16}O-labeled or ^{18}O-labeled samples were not presented so the presence of additional copper-containing species cannot be evaluated. Also, there are significant deviations from the expected isotope patterns for a species containing two copper and two boron atoms. Deviations in the ^{18}O-labeled spectrum (Figure 1.12, *right*) could potentially be attributed to a certain degree of ^{16}O-contamination, but this was not addressed. Kitajima *et al*. claimed that these spectra are "reasonably consistent" with their postulated $Cu(II)_2$-(μ-oxo) species.[50d] This species was reported to be EPR silent as a result of antiferromagnetic coupling between the Cu(II) centers. ^1H NMR spectra obtained at both 25 °C and –30 °C exhibited shifted features relative to the starting Cu(I) complex. The smaller shifts in the –30 °C spectrum were attributed to a decrease in the magnetic moment caused by antiferromagnetism at lower temperatures.[50d] Attempts to obtain a crystal structure of this complex did not yield a

structure for the proposed intermediate. Only disproportionated Cu(II) product ((HB(3,5-$Me_2pz)_3)_2Cu$) or a dicopper(II)-bis(μ-hydroxo) complex were isolated and characterized by X-ray crystallography. It was postulated that a water contaminant in the benzene used for crystallization reacted with the $Cu(II)_2$-(μ-oxo) species leading to the formation of the isolated a dicopper(II)-bis(μ-hydroxo) species.[50d] Elemental analysis and FTIR spectroscopy were reported for the $Cu(II)_2$-(μ-oxo) species, although titration data or further evidence for the proposed nuclearity were not presented.

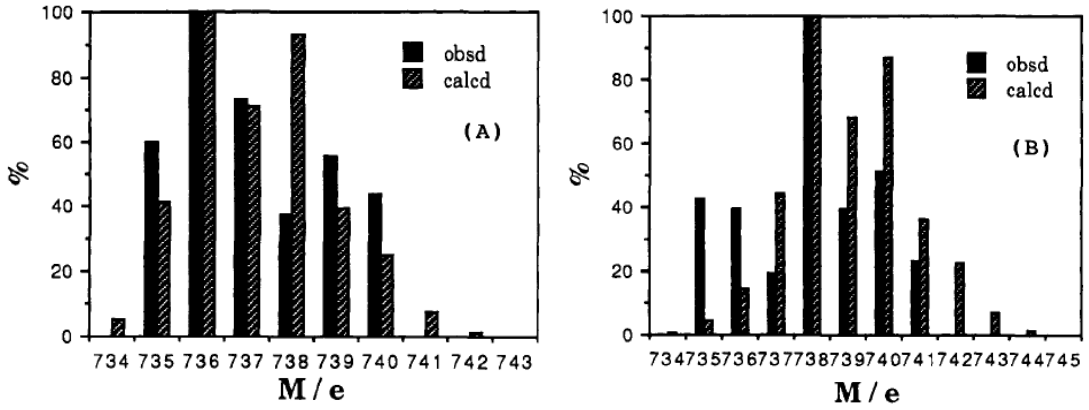

Figure 1.12. FD-MS spectra of the reactions between (HB(3,5-$Me_2pz)_3$)Cu(I)(PPh_3) and $PhI^{16}O$ (*left*) and $PhI^{18}O$ (*right*). Experimental spectra are shown in solid lines with simulated spectra shown in diagonally dashed lines. Reproduced from Ref [50d].

Reactions of Cu(I) complexes with PhIO typically result in oxo-transfer and ligand or substrate oxidation without the observation of a discrete copper-oxygen species.[40,41,51] A recent report by Hong *et al*. included a reaction between a Cu(I) complex supported by a pyridyl-amine ligand and PhIO (Figure 1.13.). The product of this reaction, which was characterized by elemental analysis, ESI-MS, and X-ray crystallography, was determined to be a tricopper(II) cluster bound to ligands that had been hydroxylated (Figure 1.13).[51] Similar intramolecular ligand oxidations were

reported by Maiti *et al*. with two different Cu(I) complexes (Figure 1.14).[40,41] In one example, treatment of a Cu(I) complex supported by a tripodal tetradentate TMPA ligand having a pendant -$N(CH_2Ph)_2$ group with PhIO resulted in hydroxylation of the C–H bond α to the nitrogen atom (Figure 1.14, *top*).[40] No intermediates were isolated from this reaction but ESI-MS was used to examine the reaction mixture over time. Shortly after reaction initiation (~1 min) a peak envelope displaying an isotope pattern consistent with a mononuclear copper species was observed at *m/z* = 564.25 that was assigned as a $[LCu(II)–O•]^+$ cation. The final product alkoxo complex was also observed as an overlapping peak envelope (*m/z* = 563.18), which dominated the spectra at longer reaction times.[40] The observation of a peak envelope assignable to a $[CuO]^+$ species in the ESI-MS spectrum led the authors to speculate that it may be involved in the observed ligand hydroxylation chemistry. In a related work, reacting a tetradentate tris(guanidine)amine supported Cu(I) complex with PhIO resulted in the hydroxylation of an *N*-bound methyl group (Figure 1.14, *bottom*).[41] This later work did not report any ESI-MS data on a transient $[CuO]^+$ species although it was postulated that such a species may play a role in the observed oxidation chemistry.

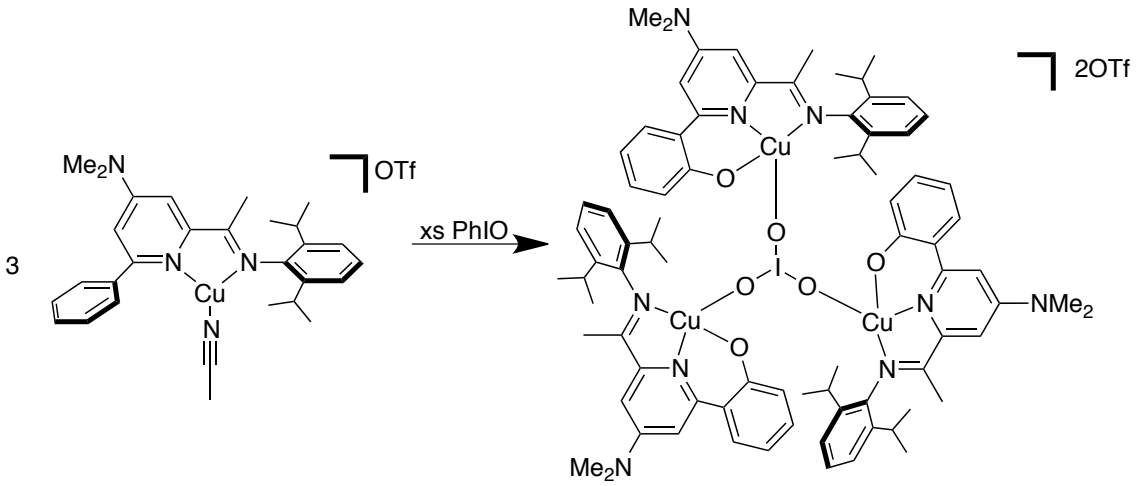

Figure 1.13. Reaction of a pyridyl-imine supported Cu(I) complex with PhIO to form a trinuclear Cu(II) cluster with aryl hydroxylated ligands.

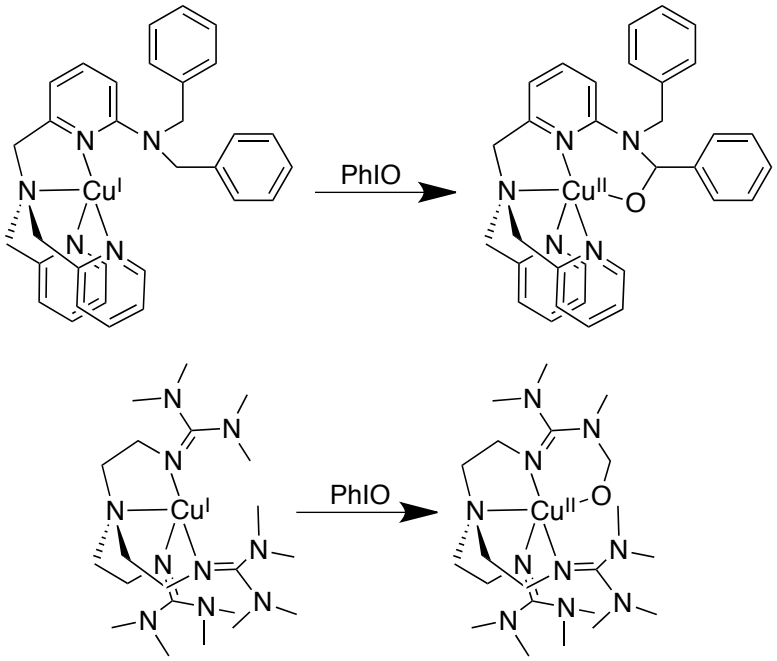

Figure 1.14. Reactions of Cu(I) complexes supported by tripodal tetradentate *N*-donor ligands with PhIO to form hydroxylated ligand Cu(II) complexes. Reactions described in Refs [40,41]

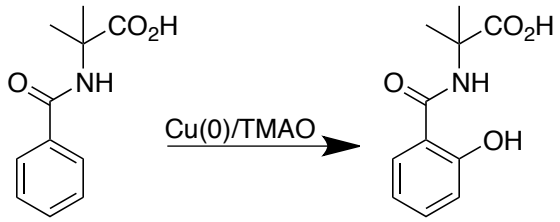

Figure 1.15. Reaction reported by Reinaud *et al.* for the ortho-aryl hydroxylation catalyzed by Cu(0) and TMAO.

Reactions with N-Oxides. Reinaud *et al.* and Capdevielle *et al*. examined the reactivities of both Cu(I) and Cu(II) salts with trimethylamine *N*-oxide (TMAO) in a variety of oxidation reactions.[38,39] Reinaud *et al.* reported a reaction that used metallic copper [Cu(0)] and TMAO in the aromatic hydroxylation of *N*-benzoyl-2-methylalanine to *N*-(2-hydroxybenzoyl)-2-methylalanine (Figure 1.15).[39] This reaction was proposed to occur through a $[CuO]^+$ species that was generated through O-atom transfer from TMAO (Figure 1.16). In the proposed mechanism, copper metal is oxidized by TMAO to form the starting Cu(II) complex that then reacts with additional TMAO to form a $[CuO]^+$ species (Figure 1.16). Ionization of the amide group results in the formation of a Cu(III)-OH species that is stabilized by amide coordination. Homolytic cleavage of the Cu(III)-OH bond, transfer of the •OH group to the aryl ring, and an intramolecular redox reaction results in the formation of a Cu(I) metal center and oxidized ligand. The Cu(I) complex is reoxidized by the aminium radical, formed in the initial O-atom transfer reaction from TMAO, to reform a stable Cu(II) complex.[39] A related report by Capdevielle *et al.* found that reactions of either Cu(I) or Cu(II) salts with TMAO resulted in the oxidation of either alcohols or carboxylates leading the authors to postulate a similar $[CuO]^+$ species as the active oxidant.[38] In none of these reports was any direct evidence for the intermediacy of the $[CuO]^+$ species provided.

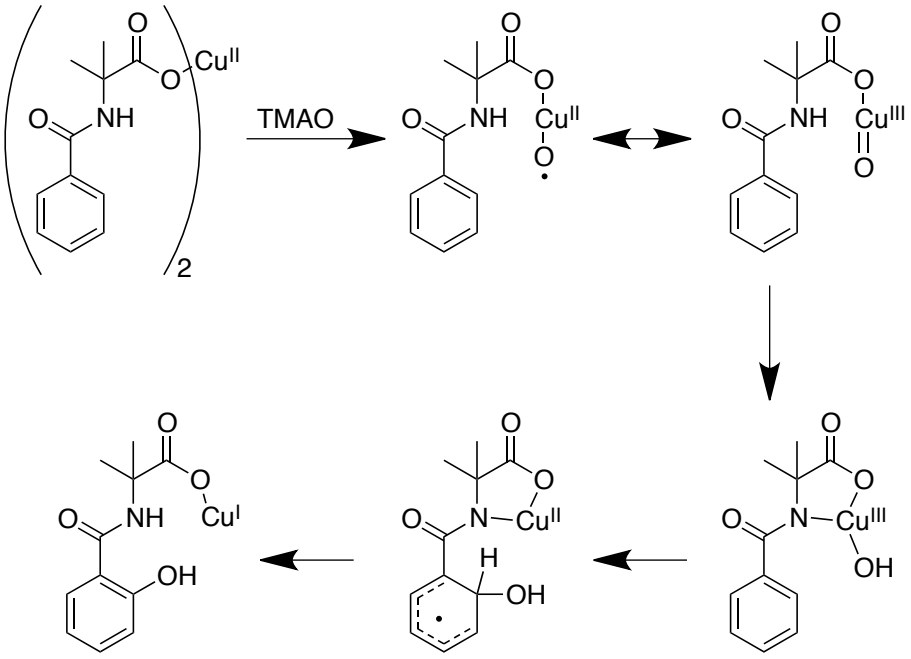

Figure 1.16. Reaction mechanism for the *ortho*-aryl hydroxylation involving a $[CuO]^+$ species proposed by Reinaud *et al.* Figure adapted from Ref [39].

In recent work from the Tolman laboratory, a discrete $[CuO]^+$ species was targeted via reactions of Cu(I) complexes with amine *N*-oxides.[51] A series of supporting ligands with varying electronic donating properties were selected and the corresponding Cu(I) complexes synthesized (Figure 1.17). Reactions of these Cu(I) complexes with a number of *N*-oxides were then examined. It was found that with less electron donating ligands stable Cu(I)-*N*-oxide adducts were isolated. In these cases, the coordinated *N*-oxide displayed little N–O bond activation; N–O bond lengths were similar to either free *N*-oxides or previously reported stable Cu(II)-*N*-oxide complexes.[51] When a Cu(I) complex supported by a β-diketiminate ligand, $^{H,Me}Dk^{Me}$ (Figure 1.17, *top right*), was reacted with TMAO at low temperature (–80 °C), features due to a dicopper(III)-bis(μ-oxo) species were observed by UV-vis spectroscopy, a notable one being a peak with λ_{max} = 423 nm (Figure 1.18, *left*). Resonance Raman spectroscopy was used to

characterize this species and a feature at 608 cm^{-1} was observed (Figure 1.18, *right bottom*).[51] An identical dicopper(III)-bis(μ-oxo) species derived via O_2-reduction was previously reported and displayed a spectral feature at 423 nm in the UV-Vis spectrum and a feature at 608 cm^{-1} in the resonance Raman spectrum (Figure 1.18, *right top*).[52] Thus, the dicopper(III)-bis(μ-oxo) species derived via oxo-transfer from TMAO displayed identical features to those previously reported. This is the first, and currently only, definitive example of the formation of a discrete copper-oxygen species derived from oxo-transfer (Figure 1.19). Two potential reaction pathways are shown for the formation of the dicopper(III)-bis(μ-oxo) species from Cu(I) and TMAO in Figure 1.20. The top pathway involves oxo-transfer from TMAO to Cu(I) resulting in the formation of a discrete $[CuO]^+$ species (Figure 1.20, *top*). Two $[CuO]^+$ species then dimerize to form the observed dicopper(III)-bis(μ-oxo) species. An alternative reaction pathway is shown involving the formation of a Cu(I)-*N*-oxide adduct that dimerizes to form a $Cu(I)_2$(*N*-oxide)$_2$ species (Figure 1.20, *bottom*). N–O bond cleavage in this species yields the observed dicopper(III)-bis(μ-oxo) complex. This alternate reaction pathway does not involve a discrete $[CuO]^+$ species.

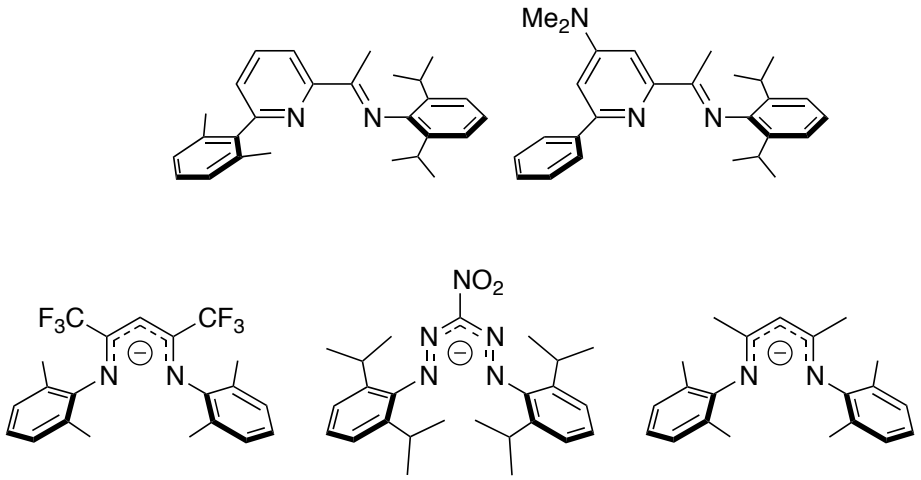

Figure 1.17. Ligands used in the study reported by Hong *et al* in Ref [51].

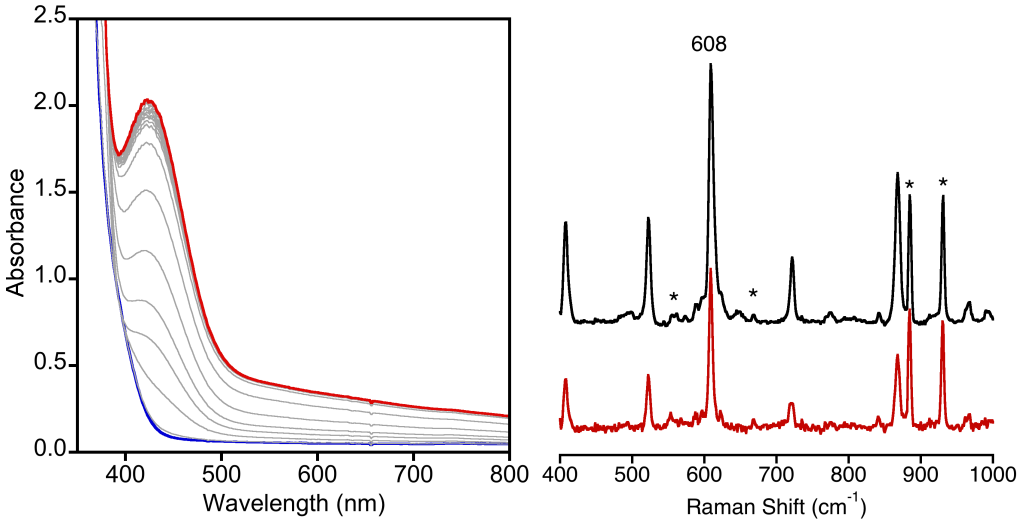

Figure 1.18. (left) UV-vis spectra obtained during the reaction of (^{H,Me}Dk^{Me})Cu(CH$_3$CN) (0.25 mM) with TMAO (10 equiv) in THF at –80 °C over 1 h (starting spectrum in blue, final spectrum in red). (right) Resonance Raman spectra obtained on samples obtained from the reaction of (^{H,Me}Dk^{Me})Cu(CH$_3$CN) in THF at –80 °C with TMAO (red) or O_2 (black). The spectra were obtained using λ_{ex} = 457.9 nm at –196 °C; solvent peaks are marked with asterisks and the peak assigned as the Cu_2O_2 core vibration is indicated at 608 cm^{-1}. Figure reproduced from Ref. [51].

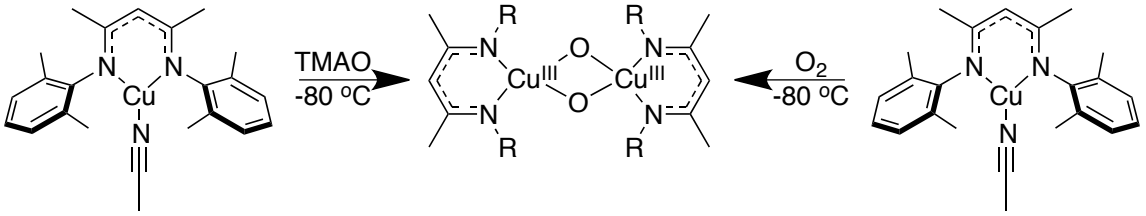

Figure 1.19. Formation of a dicopper(III)-bis(μ-oxo) from either oxo-transfer from TMAO (*left*) or from the four electron reduction of O_2 (*right*).

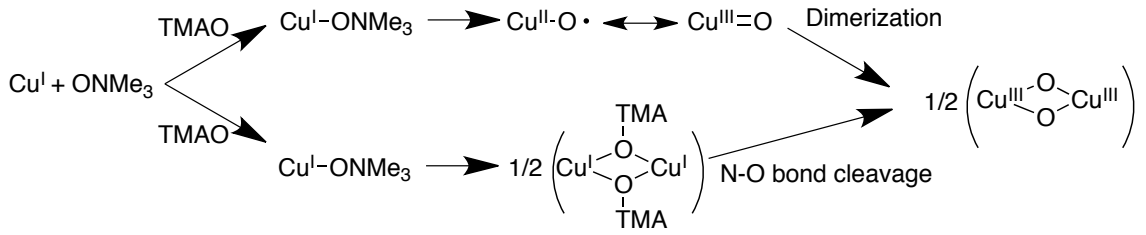

Figure 1.20. Two potential reaction pathways for the formation of a dicopper(III)-bis(μ-oxo) derived from a reaction between Cu(I) and TMAO.

1.3. Conclusions and Perspectives

Metal-catalyzed reactions of organic molecules are relevant both in synthetic chemistry and biological systems. As has been discussed in this chapter, oxidations involving copper and O_2 in the functionalization of C–H bonds are found in a number of biological systems including those catalyzed by DβM and pMMO. Attempts to further understand these biological systems to develop bio-inspired catalysts has led synthetic chemists to target the syntheses of discrete copper-oxygen species. The synthesis, isolation, and characterization of such species can lead to fundamental information about the reactivities of individual copper-oxygen species and further mechanistic understanding of the biological systems.

One proposed intermediate that was discussed at length in this chapter is a $[CuO]^{+}$ species. This species has been proposed to be the active oxidant involved in C–H bond functionalization in DβM and has been implicated in a number of synthetic systems.

Although this species has been postulated to be involved in a number of reactions, experimental observation has been limited to gas phase formation and detection. Nonetheless, theoretical calculations of the electronic description, formation, and reactivity of $[CuO]^+$ species in the gas phase, model compounds, and in whole-enzyme systems have become more common in the literature.

A $[CuO]^+$ species has been consistently calculated to be best described as a S = 1 triplet Cu(II)-oxyl radical species. This electronic ground state has generally been found to be approximately 5 kcal/mol lower in energy than the corresponding S = 0 singlet Cu(III)=oxo species. The formation of a Cu(II)-oxyl radical in enzymatic systems has been proposed to occur via proton coupled electron transfer to a Cu(II)-hydroperoxo species resulting in heterolytic O–O bond cleavage. In most theoretical studies, the O–O bond cleavage to form a Cu(II)-oxyl species has a large thermodynamic barrier (+33–75 kcal/mol) and overall unfavorable energetics (ΔG = 42–60 kcal/mol), suggesting that this reaction pathway is an unlikely route to a $[CuO]^+$ species.

The overall unfavorable thermodynamics for the formation of a $[CuO]^+$ species were attributed to the instability of a Cu(II)-oxyl radical, which only contains a partial Cu–O bond (Figure 1.5 and 1.6). The instability of a Cu(II)-oxyl species was reflected by high reactivity towards exogenous substrates in theoretical calculations. In theoretical models, Cu(II)-oxyl species were found to be a more potent oxidants of C–H bonds, specifically in H-atom abstraction reactions, relative to other copper-oxygen species, including Cu(II)-superoxo, Cu(II)-peroxo, and Cu(II)-hydroperoxo units.

The high reactivities that were postulated and calculated for Cu(II)-oxyl radical species were observed in the limited examples of gas phase formation of $[CuO]^+$ species and subsequent reaction with hydrocarbon substrates. It was found that $[CuO]^+$ species can be generated in the gas phase by reactions not only of high energy Cu^+ ions with O_2, but also via O-atom transfer to Cu(I) or Cu(II) salts from various reagents such as PhIO, N_2O, and nitrate. This provides an alternative strategy towards the synthetic isolation of a Cu(II)-oxyl species that may circumvent the poor energetics for the calculated formation of a $[CuO]^+$ species via O_2 reduction. Additionally, gas phase reactivity studies of $[CuO]^+$ ions revealed that such a species is capable of oxidizing a number of hydrocarbons, including methane. This reactivity is consistent with the high oxidizing potential predicted by a number of theoretical reports of Cu(II)-oxyl species.

Synthetic attempts to form and isolate a Cu(II)-oxyl radical have yet to successfully lead to the isolation of such a species in solution. A number of reports, including those from our group, have examined alternative pathways involving either oxo-transfer reagents or oxidizable α-ketocarboxylate co-ligands. These reactions did not yield an isolable Cu(II)-oxyl species, although such an intermediate may be implicated to explain the observed reactivities.

Further efforts to isolate a Cu(II)-oxyl radical species will no doubt focus on novel reaction pathways, new copper complexes, and nontraditional reagents. As has been presented in this chapter, a Cu(II)-oxyl radical species is a highly reactive species capable of substrate oxidation. The properties that make a Cu(II)-oxyl radical such a potent oxidant are due to its instability and high thermodynamic cost of formation, a cost

that synthetic chemists must overcome in order to synthesize, isolate, and characterize such a species.

1.4. Research Goals

Synthetic bioinorganic chemists aim to synthesize copper complexes inspired by biological systems, like DβM, to further understand the structures and reactivities of biologically relevant metalloenzymes. In the cases of copper-containing metalloenzymes that activate and use O_2 as an oxidant, the isolation and characterization of copper-oxygen species that may be relevant to the activity and mechanism of the enzyme system are of particular interest. Further understanding of copper-oxygen species may aid in assigning intermediate species that act as oxidants and provide a better understanding of the enzyme systems and further development of bio-inspired catalysts that use inexpensive transition metals like copper.

The work described in this thesis was aimed at synthesizing and characterizing bio-inspired Cu(I) complexes that could be reacted with O_2 or oxo-transfer reagents to form discrete copper-oxygen species. The work described in Chapter 2 sought to expand on the chemistry previously reported in our laboratory by Dr. Sungjun Hong that was discussed in Section 1.2.4. of this chapter. Cu(I)-α-ketocarboxylate complexes supported by neutral diamine ligands were synthesized and reacted with O_2 in attempts to access a reaction pathway analogous to Fe-α-ketogluterate dependent enzymes involving the intermediacy of a $[CuO]^+$ species (Figure 1.10). Chapter 3 introduces new Cu(I) complexes supported by β-diketiminate ligands derived from asymmetrically substituted bis(alkyl)hydrazines. These complexes were synthesized to examine the reactivity of

highly electron rich and sterically unhindered Cu(I)-complexes towards O_2 and oxo-transfer reagents and examine the reactivity of corresponding copper-oxygen complexes towards substrate oxidation. Chapter 4 examines the syntheses of Cu(I) complexes supported by the strongly electron donating *N*-heterocyclic carbene (NHC) ligands. As was described in Section 1.2.4, a computational study by Huber *et al.* found that more strongly electron-donating ligands stabilized high-valent copper-oxygen intermediates. We reasoned that NHC ligands, which are known to be strong electron donors, would be an interesting supporting ligand in copper-oxygen chemistry. The syntheses of Cu(I) complexes supported by monodentate, bidentate, and mixed donor ligands that contain NHC donors or NHC with amine or pyridine functionalities are presented.

Finally, co-authored works that highlight experiments performed by myself including resonance Raman spectroscopy and single crystal X-ray crystallography are presented in the Appendices following the main body of this thesis. These reports include work relevant to copper-oxygen chemistry along with projects focused on N_2O activation by Cu/S species and the formation of biorenewable polymers via metal catalysis.

CHAPTER 2. α-KETOCARBOXYLATES AS LIGANDS AND EXOGENOUS SUBSTRATES IN CU/O_2 CHEMSITRY

2.1 Introduction

As discussed in Chapter 1, a $[CuO]^+$ species has been postulated to play a role in a number of biological[11,53,54] and synthetic systems[40,41,45,51,55,56] although it has never been experimentally observed outside of the gas phase.[57,58] On the basis of theoretical studies that were discussed at length in Section 1.2.2, a $[CuO]^+$ species derived from the cleavage of the O–O bond in a Cu(II)-hydroperoxo species is energetically unfavorable. This result has led our group to explore alternative mechanistic routes for the synthesis of a $[CuO]^+$ species, some of which differ from those proposed for Cu-containing metalloenzymes. For inspiration we examined other $[MO]^{n+}$ species and routes by which they form. For example, $[FeO]^{2+}$ species have been observed both in biological and synthetic systems.[59] One way they can be derived from O_2 involves decarboxylation of an organic cofactor, specifically an α-ketocarboxylate.

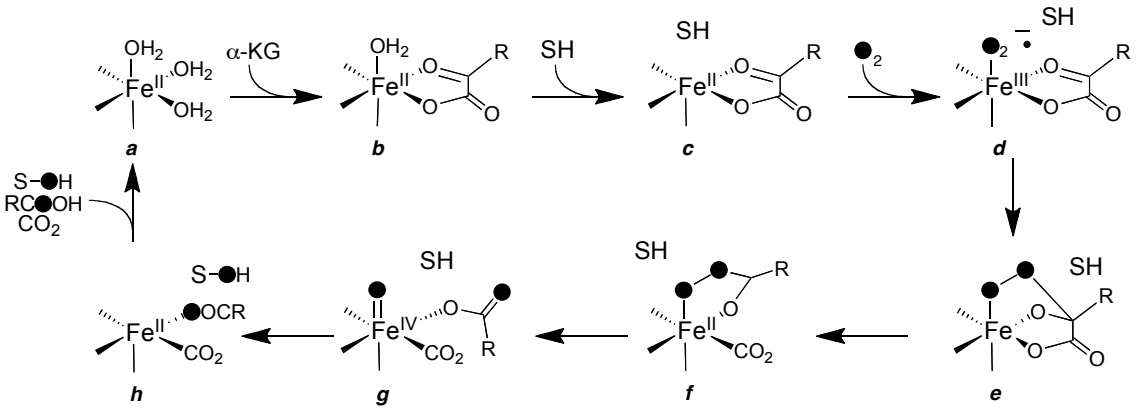

Figure 2.1. Proposed mechanism for α-ketogluterate-dependent non-heme iron enzymes adapted from Ref [12].

α-Ketoglutarate-dependent non-heme iron enzymes require an α-ketocarboxylate co-substrate that acts as a ligand coordinated to a non-heme iron center. During catalytic turnover, the oxidation of the enzyme's substrate occurs via a mechanism that is coupled to the oxidation of the α-ketocarboxylate (Figure 2.1). The final reaction products are CO_2 and a carboxylate, both derived from the α-ketocarboxylate, and the oxidized substrate. Through a number of reported studies both on model and biological systems, the mechanism shown (Figure 2.1) is generally accepted.[60] Steps leading to the formation of the reactive $[FeO]^{2+}$ intermediate involve the binding of O_2 to a reduced metal center (Figure 2.1, *c* → *d*), the nucleophilic attack of the bound O_2 species (superoxo) onto the keto-carbon of the α-ketocarboxylate (Figure 2.1, *d* → *e*), followed by the loss of CO_2 and the formation of a metal-bound peracid species (Figure 2.1, *e* → *f*). This peracid species then undergoes an O–O bond cleavage to form an $[FeO]^{2+}$ species and a metal bound carboxylate (Figure 2.1, *f* → *g*). It is this species (*g*) that oxidizes the substrate (Figure 2.1, *g* → *h*) and after ligand exchange reforms the resting enzyme (Figure 2.1, *h* → *a*). We hypothesized that a Cu(I)-α-ketocarboxylate complex would react with O_2 to form a $[CuO]^{+}$ species through a related pathway (Figure 2.2). In this related mechanism, a Cu(I)-α-ketocarboxylate complex reacts with O_2 to form a Cu(II)-superoxo species (Figure 2.2, *a* → *b*). A nucleophilic attack of the Cu(II)-superoxo on the α-ketocarbonyl carbon would result in the loss of CO_2 and the formation of a Cu(I)-peracid species (Figure 2.2, *b* → *c* → *d*). O–O bond cleavage of the peracid ligand results in the formation of a $[CuO]^{+}$ species and a carboxylate ligand (Figure 2.2, *d* → *e*).

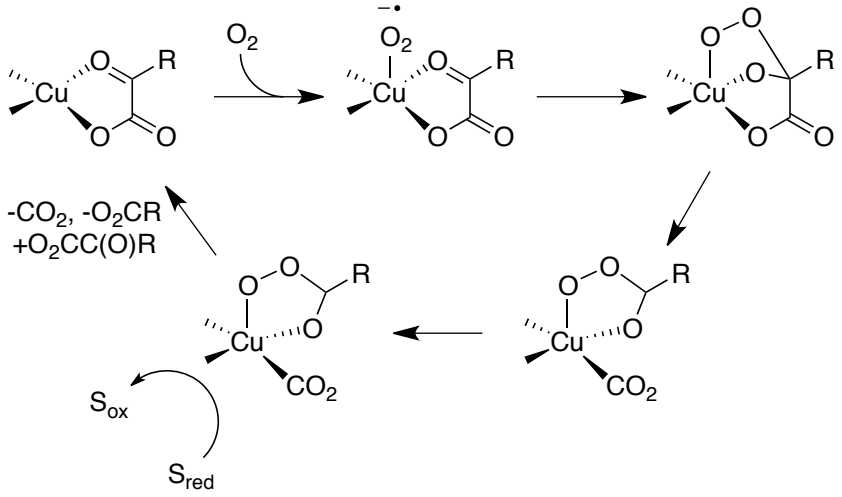

Figure 2.2. Reaction pathway proposed by Hong *et al*. for the oxygenation of a Cu(I)-α-ketocarboxylate complex leading to the formation of a Cu(II)-oxyl radical.[45]

Previous work from the Tolman group using α-ketocarboxylates as ligands in model Cu(I) complexes was reported by Hong *et al.* and is described in greater detail in Section 1.2.4.[45] Cu(I) complexes supported by relatively poor electron donating pyridyl-imine ligands (L) were synthesized with either a triflate counteranion or anionic α-ketocarboxylate co-ligands. It was reported that the coordination of an α-ketocarboxylate to the metal center increased the reactivity of the complex towards dioxygen, as the complex $LCu(O_3SCF_3)$ lacking an α-ketocarboxylate did not react with O_2. Hong *et al.* did not report any observable intermediates that could be assigned as copper-oxygen species. Upon oxygenation of the Cu(I)-α-ketocarboxylate complex, intramolecular oxidation of the supporting ligand's aryl group along with the decarboxylation of the initially coordinated α-ketocarboxylate were found. It was postulated using the experimental evidence and a thorough computational study that a $[CuO]^+$ species could be involved, however without direct experimental observation of such an intermediate, more effort in this project was warranted. Additionally, while interesting, the

intramolecular oxidation of a supporting ligand is a synthetic dead end. The expansion of this chemistry toward the oxidation of exogenous substrates could be useful and at the inception of my work had yet to be reported.

The original aim of the work described in this chapter was to explore and expand upon the work reported previously in this laboratory by Hong *et al.*[45] Key goals included observing and characterizing intermediates derived from Cu(I)-α-ketocarboxylate complexes and examining the capability of any observed intermediates to effect exogenous substrate oxidation. With these goals in mind, we focused on using a new supporting nitrogen-donor ligand set, peralkylated diamine ligands that are generally commercially available or easily accessible through short syntheses.[61] These diamine ligands are stronger σ-donors and have smaller steric profiles compared to the ligands previously used to support Cu(I)-α-ketocarboxylate complexes. Peralkylated diamines were reported to support copper-oxygen chemistry and form thermally sensitive $[Cu_2O_2]^{2+}$ species.[61,62] These properties led us to target peralkylated diamine supported Cu-(I)-α-ketocarboxylate complexes to generate an isolable $[CuO]^+$ intermediate and/or oxidize exogenous substrates (Figure 2.3, *route a*).

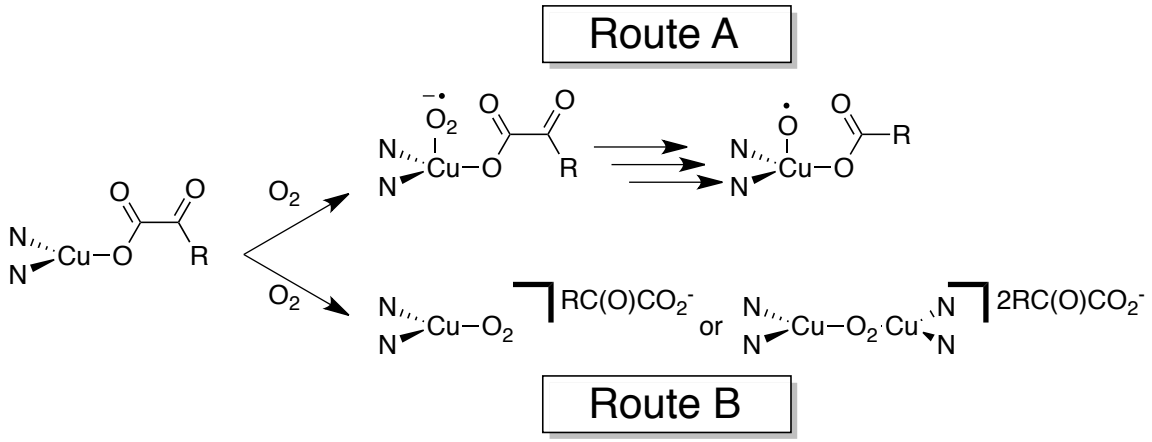

Figure 2.3. Two potential reaction routes of oxygenation for a discrete Cu-α-ketocarboxylate complex. Path A displays the formation of a discrete $[CuO]^+$ species and Path B displays the displacement of the α-ketocarboxylate upon oxygenation.

We also wished to examine the validity of a mechanistic route starting from a discrete Cu-(I)-α-ketocarboxylate complex that does not include a $[CuO]^+$ species but rather known mononuclear or dinuclear copper-oxygen species (Figure 2.3, *route b*). To accomplish this we performed experiments to examine the oxidative capabilities of species with dinuclear $[Cu_2O_2]^{2+}$ cores towards exogenous α-ketocarboxylates. These experiments were undertaken with the prior knowledge that peralkylated diamine supported Cu(I) complexes are known to react with O_2 to form $[Cu_2O_2]^{2+}$ species. This chapter will examine these two potential mechanistic routes. During the course of this study we identified a carboxylate bridged $[Cu_2O_2]^{2+}$ species and revealed a new oxidative reaction by a $[Cu_2O_2]^{2+}$ core. Portions of this work were previously reported.[63]

2.2 Synthesis and Characterization of Diamine Supported Cu(I)-α-Ketocarboxylate Complexes

2.2.1 Syntheses of Complexes

Two synthetic routes were explored with the aim of isolating O_2-reactive Cu(I) complexes supported by both a peralkylated diamine ligand and an α-ketocarboxylate (Figure 2.4). Initial attempts to isolate the desired complex began with the synthesis and isolation of (TMPDA)CuCl (TMPDA = *N,N,N′,N′*-tetra(methyl)-1,3-propanediamine), which was previously reported.[64] The α-ketocarboxylate benzoylformate (BF) was introduced to solutions of (TMPDA)CuCl as a sodium salt in what was envisioned as a metathesis reaction that would lead to the formation of a discrete (TMPDA)Cu(BF) complex and an insoluble chloride salt. This salt would be removed via filtration leaving the presumably soluble complex in solution. Reactions of (TMPDA)CuCl in either THF or CH_2Cl_2 with NaBF did not result in BF incorporation, however. Instead, filtration of cloudy solutions of (TMPDA)CuCl and NaBF resulted in the re-isolation of the starting Cu(I) complex.

We postulated that this result was due to the insolubility of the BF starting material or the poor thermodynamic driving force of NaCl formation and precipitation. With the latter idea in mind, the thallium salt of BF was synthesized according to a literature procedure as an alternative reagent to NaBF.[65] The precipitation of TlCl proved thermodynamically favorable, as we observed a fine off-white powder upon addition of TlBF to CH_2Cl_2 or THF solutions of (TMPDA)CuCl. The precipitate was removed via filtration to yield a clear gold colored solution. However, over 20 min this solution turned

green and a copper mirror deposit formed on the inner vial surface indicative of a disproportionation reaction [Cu(I) → ½Cu(0) + ½Cu(II)]. Disproportionation occurred regardless of solvents used (THF or CH_2Cl_2) or temperature (RT to –20 °C) and became more rapid when reaction solutions were concentrated *in vacuo*. Nonetheless, the decomposition of the product of (TMPDA)CuCl and TlBF was slow enough to obtain a ^{1}H NMR spectrum of the initial product complex in d_8-THF. Signals for aryl protons at 7.85 (doublet), 7.41 (triplet), and 7.33 (doublet) ppm were observed, although they were broad. A large peak with no discernible splitting was observed at 2.24 ppm and is likely due to a combination of *N*-methyl (12 H) and TMPDA backbone methylene (6 H) protons as it integrates to approximately 18 protons with respect to the five aryl protons. Similar features were observed when samples were made and ^{1}H NMR spectra recorded in CD_2Cl_2. The ^{1}H NMR spectrum of the reaction of (TMPDA)CuCl and TlBF recorded when the solution displayed a green color and orange solid was observed did not contain any features other than solvent. The intermediate spectrum that contains broad features, described above, is consistent with a solution that contains a paramagnetic species causing line broadening en route to the decomposed species containing only insoluble Cu(0) and paramagnetic Cu(II) species.

After samples fully decomposed in the glove box, a deep green crystalline solid was obtained after the mother liquor was allowed to stand overnight at –20 °C. Analysis of this solid by EPR and FTIR spectroscopies, elemental analysis, and X-ray crystallography (Section 2.2.2) led to its identification as the Cu(II) complex (TMPDA)Cu$(BF)_2$. To corroborate this finding, this Cu(II) compound was synthesized

independently and isolated by first making the Cu(II) complex (TMPDA)$CuCl_2$,[66] adding two equivalents of TlBF, removing TlCl by filtration, and removing the solvent *in vacuo*, to yield a green solid.

Additionally, a minor product with the formula $(TMPDA)_2Cu_3(BF)_4O$ was isolated from reaction mixtures of (TMPDA)CuCl and TlBF, although this compound could not be reproducibly synthesized in significant yield. In the X-ray structure, described below in Section 2.2.2, one BF ligand is found with an additional O-atom bound to the α-ketocarbonyl carbon, consistent with it being a hydrated, fully deprotonated form of benzoylformic acid.

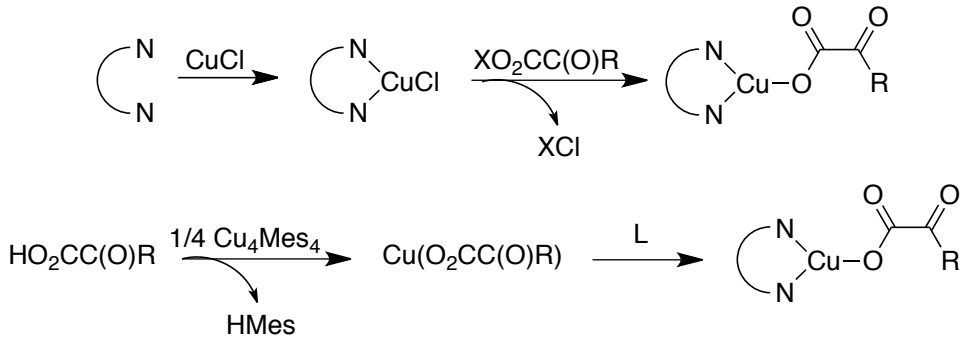

Figure 2.4. Two proposed synthetic routes to an LCu(I)-α-ketocarboxylate complex.

No (TMPDA)Cu-α-ketocarboxylate complexes with copper in the Cu(I) oxidation state have been reported in the literature, suggesting that the isolation of such a compound may be difficult. Therefore, we attempted to synthesize a (TMPDA)Cu-carboxylate species as a model system to determine if a stable (TMPDA)Cu(I)-(α-keto)carboxylate complex might be accessed. Reactions of (TMPDA)CuCl with Li(2,4,6-Me-BA) (BA = benzoate) in THF generated a dark precipitate that upon filtering yielded gold colored solutions. From these solutions, an air sensitive yellow-brown solid was

precipitated with the addition of pentanes. The solid was recrystallized and characterized by X-ray crystallography as (TMPDA)Cu_2(2,4,6-Me-BA)$_2$. The structure of this complex is discussed below in Section 2.2.2. The ^{1}H NMR spectrum of this compound displayed sharp singlets at 8.56, 4.15, 4.07, and 4.05 ppm that integrated to 4, 12, 12, and 6 protons each, respectively. These peaks were assigned to the aryl protons for the two (2,4,6-Me-BA) ligands, four *ortho*-methyl groups on the (2,4,6-Me-BA) ligands, four methyl groups on the TMPDA ligand, and two *para*-methyl groups on the (2,4,6-Me-BA) ligands. A clear multiplet is also observed between 3.4 and 3.5 ppm that is assigned to the central methylene protons on the TMPDA ligand backbone. A number of broad features were observed in this region and are likely due to the methylene groups adjacent to the nitrogen heteroatoms in the TMPDA backbone. This complex contains a Cu(I) center ligated by both TMPDA and a carboxylate but does not have the desired mononuclear structure. We hypothesized that an alternate ligand and possibly an alternative synthetic route to a mononuclear peralkylated diamine ligated Cu(I)-α-ketocarboxylate was necessary.

A new target complex supported by a less electron donating peralkylated diamine ligand along with a new synthetic route was examined to overcome the disproportionation problems observed when attempting to isolate (TMPDA)Cu(BF). The ligand, *N,N'*-dimethyl-*N,N'*-di-*tert*-butylethylenediamine (^{t}Bu2Me2EN), was chosen because of its ability to form a 5-membered chelate ring upon coordination to a metal[61] in addition to the crystallinity of several previously reported metal complexes.[65] The alternative synthetic route involved using the organometallic reagent Cu_4Mes_4 (Mes =

mesityl) (Figure 2.4, *bottom*). Cu_4Mes_4 is a bifunctional reagent acting as both a metal source and a base with the only byproduct of reaction, mesitylene, being easily removed under vacuum.

Benzoylformic acid or 4-nitrobenzoylformic acid (nitro-BF) was reacted with a ¼ equivalent of Cu_4Mes_4 to form a cloudy yellow solution. Addition of $^{t\text{Bu2Me2}}$EN to this cloudy mixture yielded a golden, clear, homogeneous solution. Removal of solvent *in vacuo* from the gold solution left a pale yellow solid. Recrystallization from CH_2Cl_2 yielded pure samples of either ($^{t\text{Bu2Me2}}$EN)Cu(nitro-BF) or ($^{t\text{Bu2Me2}}$EN)Cu(BF). The structural characterizations of ($^{t\text{Bu2Me2}}$EN)Cu(BF) and ($^{t\text{Bu2Me2}}$EN)Cu(nitro-BF) were accomplished by X-ray crystallography and will be discussed in Section 2.2.2. It should be noted that this synthetic method was unsuccessful when TMPDA was used instead of $^{t\text{Bu2Me2}}$EN. The addition of TMPDA to a mixture of benzoylformic acid and Cu_4Mes_4 resulted in disproportionation, similar to the results of the previously described metathesis reactions.

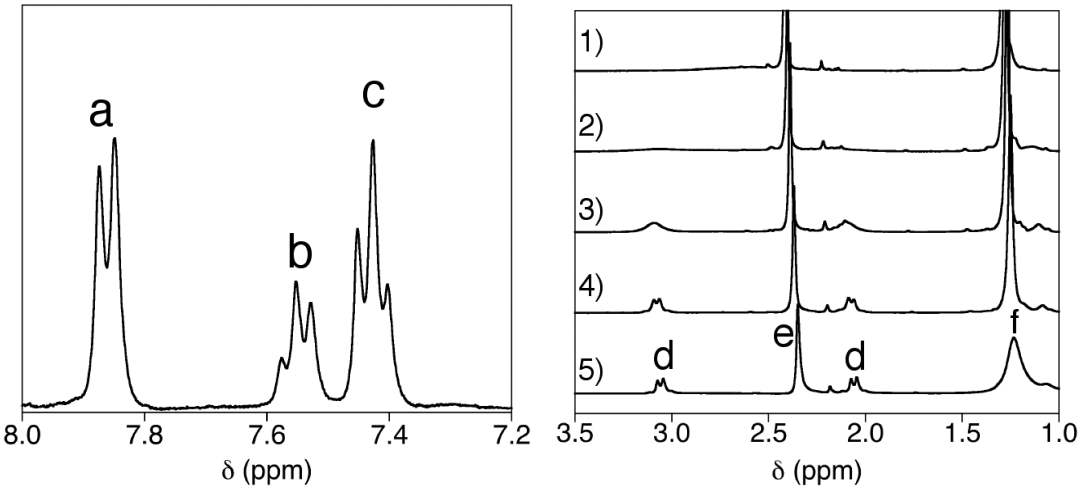

Figure 2.5. Room temperature ^{1}H NMR spectrum of the aryl protons for (^{t}Bu2Me2EN)Cu(BF) in CD_2Cl_2 (*left*). Variable temperature ^{1}H NMR spectra of (^{t}Bu2Me2EN)Cu(BF) in CD_2Cl_2 at Room temperature (1); 0 °C (2); –20 °C (3); –40 °C; (4) and –60 °C (5) (*right*).

^{1}H NMR spectra of both (^{t}Bu2Me2EN)Cu(BF) and (^{t}Bu2Me2EN)Cu(nitro-BF) display one sharp set of peaks for the α-ketocarboxylate ligand. For example, the spectrum for (^{t}Bu2Me2EN)Cu(BF) displays a doublet and two triplets, assignable to the BF *ortho*- (Figure 2.5, *left, a*), *para*- (Figure 2.5, *left*, *b*), and *meta*-aryl protons (Figure 2.5, *left, c*) between 7 and 8 ppm. Additional features appear upfield with a peak at 2.4 ppm integrating to 6 protons (Figure 2.5, *right,* e) and a peak at 1.3 ppm integrating to 12 protons (Figure 2.5, *right,* f) assignable to the *N*-methyl and *N*-*tert*-butyl protons, respectively. At room temperature, peaks assignable to the ethylene backbone (–CH_2–) protons are not observed but a broad feature centered at 2.64 ppm is apparent (Figure 2.5, RT). Low temperature ^{1}H NMR spectra were recorded of (^{t}Bu2Me2EN)Cu(BF) at 0 °C, –20 °C, –40 °C, and –60 °C (Figure 2.5). As the sample was cooled, the broad feature at 2.64 ppm converted to two features at 3.06 and 2.07 ppm (Figure 2.5, *right, d*) each integrating to two protons. These features were modeled as an A_2X_2 spin system and were assigned

to the diastereotopic protons of the ^{t}Bu2Me2EN ethylene backbone (Figure 2.6). We hypothesize that these peaks were not observed at room temperature due to fluxionality of the backbone, and that upon cooling, this ring movement is slowed and the peaks are resolved.[67] Identical features at 2.07 and 3.06 ppm are observed in the ^{1}H NMR spectrum of (^{t}Bu2Me2EN)Cu(nitro-BF) at –60 °C, confirming that these peaks are from the supporting ^{t}Bu2Me2EN ligand and not from the α-ketocarboxylate ligand.

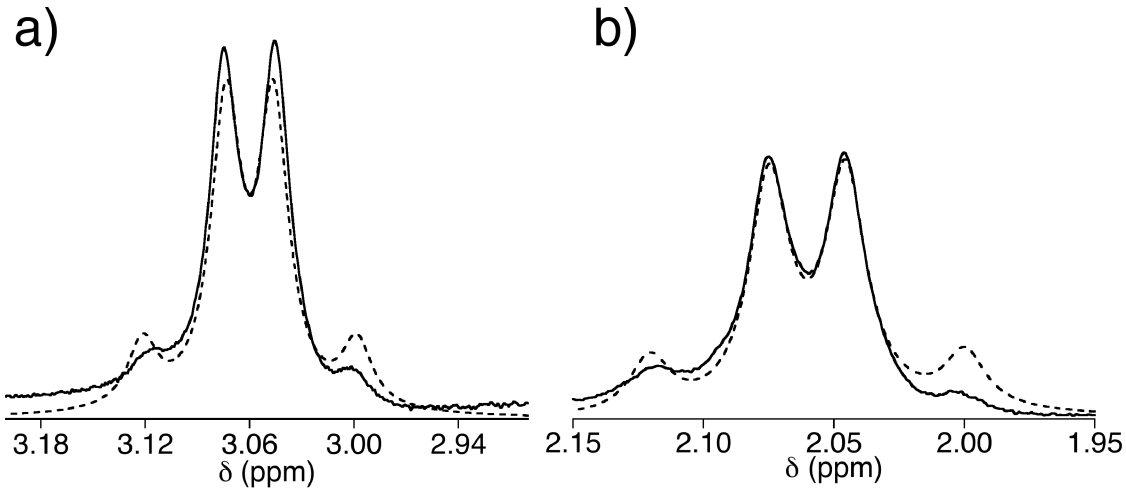

Figure 2.6. Variable temperature ^{1}H NMR spectra of (^{t}Bu2Me2EN)Cu(BF) in CD_2Cl_2 at –60 °C (*solid*) overlaid with simulated features for an A_2X_2 spin system (*dotted*) The feature shown in (a) was simulated with spin A at 3.09 ppm, spin B at 3.03 ppm, and a coupling constant of 23 Hz using MestReNova v6.0.2 NMR processing software. The feature in (b) was simulated with a spin A at 2.09 ppm, spin B at 2.03ppm, and a coupling constant of 24 Hz.

Further characterization of both (^{t}Bu2Me2EN)Cu(BF) and (^{t}Bu2Me2EN)Cu(nitro-BF) in the solution state was accomplished by UV-vis spectroscopy. UV-vis spectra for the complexes are relatively featureless with only a weak feature at λ_{max} = 362 nm (ε ~ 465 $M^{-1}cm^{-1}$) for (^{t}Bu2Me2EN)Cu(BF) and λ_{max} = 470 nm (ε ~ 162 $M^{-1}cm^{-1}$) for

(^{t}Bu2Me2EN)Cu(nitro-BF) (Figure 2.7). Previously reported Fe(II)-α-ketocarboxylate complexes with an η^2-ketocarb ligation (Figure 2.8) displayed absorption features between 500-700 nm that were assigned to Fe(II) to BF charge transfer (CT) bands.[59,68] This coordination forces a coplanarity and π-conjugation between the carboxylate, the α-ketocarboxylate, and the aryl ring that leads to the observed low energy CT bands. Extending these observations to the visible spectra of (^{t}Bu2Me2EN)Cu(BF) and (^{t}Bu2Me2EN)Cu(nitro-BF), the absence of observable absorptions are consistent with η^1- and/or η^2-ketocarb coordination of the α-ketocarboxylate ligands to the Cu(I) centers and no π-conjugation throughout the α-ketocarboxylate ligands (η^2-ketocarb ligation).

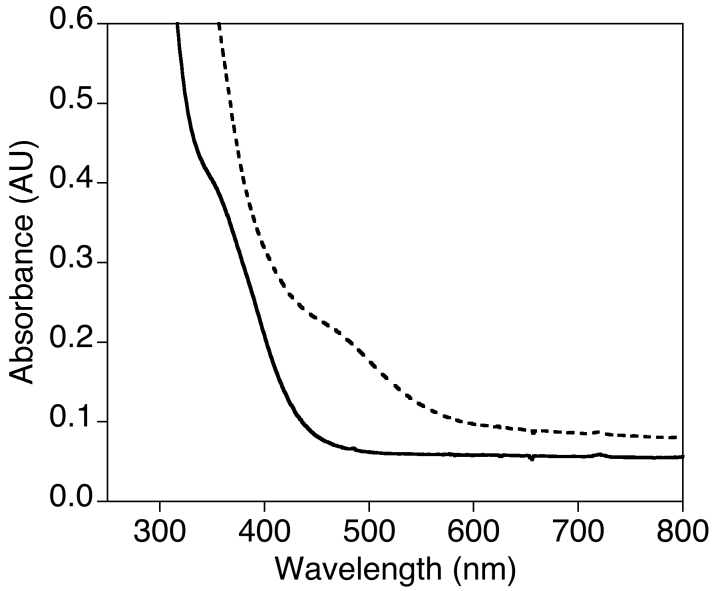

Figure 2.7. UV-vis spectra of (^{t}Bu2Me2EN)Cu(BF) (*solid*) and (^{t}Bu2Me2EN)Cu(nitro-BF) (*dotted*) 1 mM in CH_2Cl_2 at –80 °C.

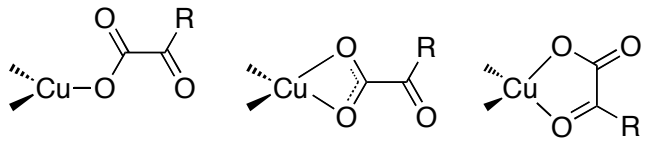

η^1-carb η^2-carb η^2-ketocarb

Figure 2.8. Potential binding modes for an α-ketocarboxylate ligand to a Cu(I) metal center.

Fourier transform infrared spectroscopy (FTIR) spectra of all synthesized Cu(I) and Cu(II) complexes were collected in both the solid and solution states (Figure 2.9). All samples displayed two peaks between 1600 and 1700 cm^{-1} that can be assigned to carboxylate and/or ketone C-O vibrations (e.g. ν_{asym}) in addition to a number of peaks between 1300 and 1500 cm^{-1} that resemble features generally assigned to ν_{sym} vibrations of a carboxylate group.[69] A sharp feature at approximately 1530 cm^{-1} was only observed in FTIR spectra of (^{t}Bu2Me2EN)Cu(nitro-BF). This feature is most likely due to a N-O vibration from the nitro functionality.[70] Assigning the coordination mode of the α-ketocarboxylate from the FTIR spectra is difficult as the literature contains many seemingly contradictory assignments. A comprehensive review by Deacon *et al*. provides the most convincing and widely accepted method for the interpretation of data.[69] The proposed method uses the difference in observed $\nu(CO_2)$ frequencies relative to the free carboxylate ion rather than making assignments based on discrete vibrational features. For the complexes discussed in this chapter this method could easily lead to overinterpretation of the spectra as there are numerous peaks in the regions of interest. Without isotope labeling to definitively assign observed features to specific $\nu(CO_2)$ modes, the peaks chosen for this analysis and the differences between them would be arbitrary. Therefore, the conclusion drawn from the FTIR spectra is that α-

ketocarboxylate introduction and coordination to the metal center was accomplished, but that these data are not sufficient for assigning the specific binding mode(s).

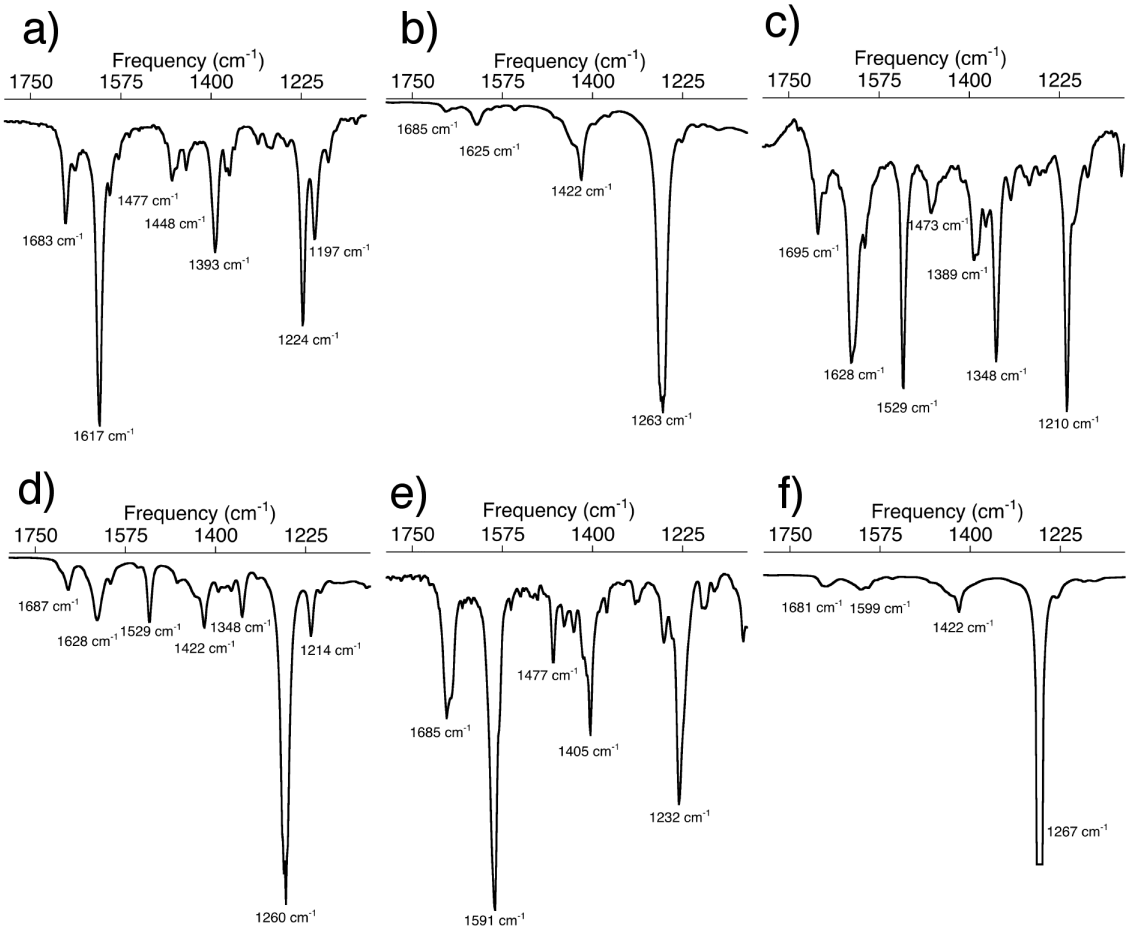

Figure 2.9. FTIR spectra of (^{t}Bu2Me2EN)Cu(BF) (solid, *a*; solution *b*); (^{t}Bu2Me2EN)Cu(nitro-BF) (solid, *c*; solution *d*); and (TMPDA)Cu(BF)$_2$ (solid, *e*; solution *f*) with all solution samples being 10 mM in CH_2Cl_2.

To explore the possibility of dissociation of the α-ketocarboxylate ligand from the metal center in solution, conductivity data were obtained for (^{t}Bu2Me2EN)Cu(BF). All conductivity measurements in this study were performed at –78 °C in CH_2Cl_2 to match the experimental conditions of oxygenation reactions, which will be discussed in Section

2.3.1. Specific conductance (κ) of samples of varied concentrations (c) were experimentally determined and used to calculate the equivalent conductance (Λ_e) (Equation 1). Λ_e was plotted against $c^{1/2}$ and the linear portion of the data extrapolated to zero concentration. The y-intercept yielded the equivalent conductance at infinite dilution (Λ_0), and $\Lambda_0 - \Lambda_e$ was plotted against $c^{1/2}$ to obtain an Onsager plot.[71,72]

$$(1)\ \Lambda_e = \kappa/c$$

$$(2)\ \Lambda_0 - \Lambda_e = (A + B\Lambda_0)c^{1/2}$$

The linear fit of the data yields the slope that is equal to the $(A + B\Lambda_0)$ term in the Onsager Law (Equation 2). Both A and B are empirical constants with $A = 82.4/(\varepsilon T)^{1/2}\eta$ and $B = 8.20 \times 10^5/(\varepsilon T)^{3/2}$ where η is the viscosity, ε is the dielectric constant, and T is the temperature. The term $(A + B\Lambda_0)$ is dependent on a number of factors, including the charges of the ions being examined, thus allowing for the direct comparison of various electrolytes based on the slopes observed in the Onsager plot. A model 1:1 electrolyte, $[N(Bu)_4PF_6]$, was first examined and the slope of the data plotted in the Onsager plot was found to be 8.31 (Figure 2.10, *left*). Solutions of (^{t}Bu2Me2EN)Cu(BF) demonstrated a slope of 0.91, significantly less than that of an ideal 1:1 electrolytic species. Additionally, a 5-fold excess of various coordinating additives were premixed with (^{t}Bu2Me2EN)Cu(BF) and conductivity measurements performed to attempt to encourage the dissociation of the α-ketocarboxylate ligand. The data show no appreciable difference in the slopes of the lines with additives present. Cyclohexene, cyclooctene, and acetonitrile doped samples of (^{t}Bu2Me2EN)Cu(BF) displayed slopes of 0.87, 0.99, and 0.88, respectively, that were nearly identical to the pure (^{t}Bu2Me2EN)Cu(BF) sample (Figure 2.10, *right*). Additionally, low

temperature ^{1}H NMR spectra were obtained of ($^{t\text{Bu2Me2}}$EN)Cu(BF) in the presence of cyclohexene as a complementary experiment to attempt to observe an alkene coordinated Cu(I) species. The data do not support the presence of such a species. An unobserved equilibrium concentration of dissociated [($^{t\text{Bu2Me2}}$EN)Cu]$^+$[BF]$^-$ may exist but based on the experimental evidence presented it seems unlikely.

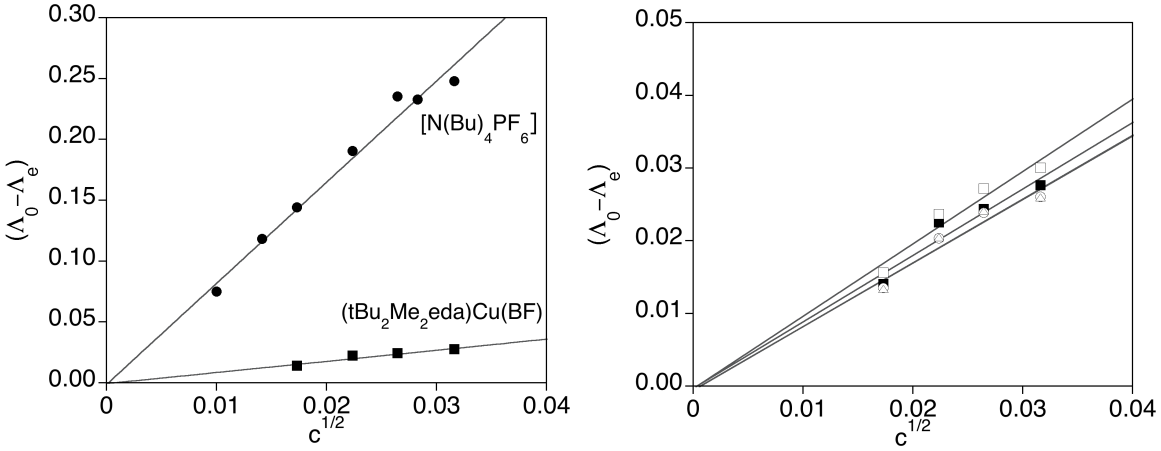

Figure 2.10. Onsager plot of [N(Bu)$_4$PF$_6$] compared to ($^{t\text{Bu2Me2}}$EN)Cu(BF) (*left*). The best fit line for [N(Bu)$_4$PF$_6$] data (*circles*) has a slope of 8.31 versus that for ($^{t\text{Bu2Me2}}$EN)Cu(BF) (*squares*) with a slope of 0.91. Overlay of conductivity data for ($^{t\text{Bu2Me2}}$EN)Cu(BF) + S. (*right*) Slopes for ($^{t\text{Bu2Me2}}$EN)Cu(BF) + 5 eq. S (S = Additive): cyclohexene = 0.87 (*open circles*); cyclooctene = 0.99 (*open squares*); acetonitrile = 0.88 (*open triangles*).

2.2.2. X-Ray Crystallography

Both ($^{t\text{Bu2Me2}}$EN)Cu(BF) and ($^{t\text{Bu2Me2}}$EN)Cu(nitro-BF) were characterized by X-ray crystallography to elucidate the binding modes of the α-ketocarboxylate ligand in the solid state (See Table 2.1 for complete refinement details). The structure of ($^{t\text{Bu2Me2}}$EN)Cu(BF) is shown in Figure 2.11. The Cu-atom is trigonal planar (sum of donor-Cu-donor angles = 359.9°) and is ligated by the bidentate diamine ligand and BF. The α-ketocarboxylate is bound as a monodentate ligand through O1 with a Cu-O1 distance of 1.9341(17) Å. A weak but insignificant interaction is seen between the Cu-

atom and O2 with a Cu-O2 distance of 2.8096(17) Å. The keto-carboxylate torsion angle, defined by O1-C-C-O3 or O2-C-C-O3, is 104°. A value of 90° would indicate that the keto-functionality is perpendicular to the carboxylate group, while a value of 180° signifies co-planar carboxylate and keto-carbonyl functionalities. The observed value of 104° is consistent with previously reported torsion angles of η^1-carb bound α-ketocarboxylate ligands (102–120°) and indicates that no conjugation between the carboxylate and α-ketocarbonyl exists.[45]

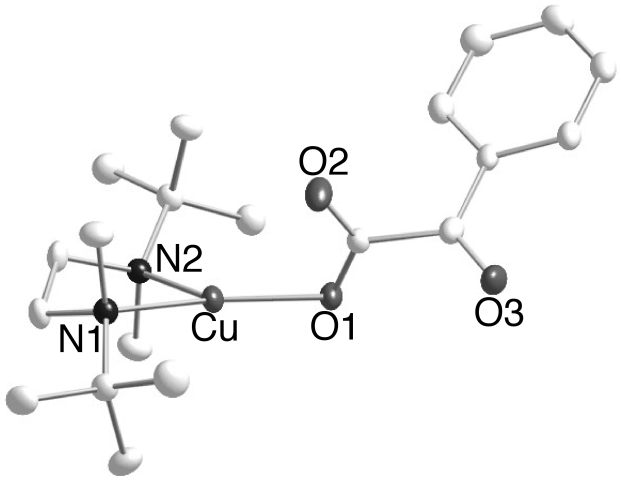

Figure 2.11. Representation of the X-ray structure of (^{t}Bu2Me2EN)Cu(BF) with all nonhydrogen atoms shown as 50% thermal ellipsoids. Selected interatomic distances (Å) and angles (deg): Cu1-O1, 1.9341(17); Cu1-O2, 2.8096(17); Cu1-N1, 2.0455(19); Cu1-N2, 2.1615(19); N1-Cu1-N2, 87.75(8); O1-Cu1-N1, 150.72(7); O1-Cu1-N2, 121.38(7).

The initial solution to the X-ray structure of (^{t}Bu2Me2EN)Cu-(nitro-BF) displayed a highly disordered O2 atom with an elongated thermal ellipsoid directed towards the copper atom. Simply modeling O2 over two positions resulted in an unstable refinement. This problem was overcome by modeling the entire α-ketocarboxylate ligand over two positions while holding the (^{t}Bu2Me2EN)Cu fragment constant. The structural solution contained two different species with distinctive coordination geometries at the metal

center in the same crystal (Figure 2.12). In one complex the α-ketocarboxylate ligand is coordinated in a monodentate geometry (minor, 25% occupancy), while in the other (major, 75% occupancy) the α-ketocarboxylate is bidentate. The monodentate complex (Figure 2.12, *a*) displays a coordination geometry and ligand-metal bond distances similar to those found in (^{t}Bu2Me2EN)Cu(BF). The Cu atom is trigonal planar (sum of donor-Cu angles = 356.2°) and has Cu-O1 and Cu-O2 distances of 1.942(5) and 2.981(6) Å, respectively. The bidentate complex displays similar Cu-O distances (Cu1-O1, 2.028(18) and Cu1-O2, 2.322(16) Å) with the copper atom in a distorted tetrahedral geometry (τ_4 = 0.63, where τ_4 = 0 corresponds to a square planar and τ_4 = 1 corresponds to a tetrahedral geometry).[73] Bidentate coordination by a carboxylate was reported in a number of metal complexes but to the best of our knowledge, this is the first reported bidentate coordination of an α-ketocarboxylate to a metal through both carboxylate O-atoms.[65,68,74,75] The existence of both a trigonal planar and tetrahedral copper ligated by a monodentate and bidentate α-ketocarboxylate suggests similar thermodynamic stabilities for these two structures. Computations on related complexes provide precedence for this observation.[45]

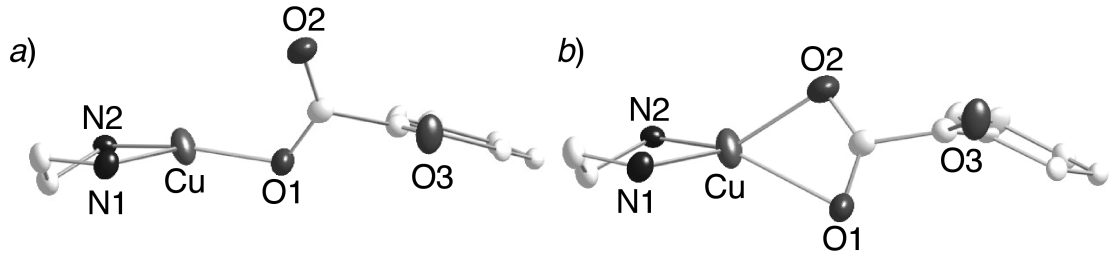

Figure 2.12. Representation of the X-ray structures of (^{t}Bu2Me2EN)Cu-(nitro-BF) with nonhydrogen atoms shown as 50% thermal ellipsoids and ^{t}Bu2Me2EN methyl and *t*-butyl groups omitted for clarity. The monodentate (*a*) and bidentate (*b*) α-ketocarboxylate bound forms are shown. Selected interatomic distances (Å) and angles (deg): [Monodentate, (*a*)]: Cu-O1, 1.942(5); Cu-O2, 2.981(6); Cu-N1, 2.094(4); Cu-N2, 2.087(4); O1-Cu-N1, 138.30(19); O1-Cu-N2, 119.1(5); N1-Cu-N2, 88.07(14); [Bidentate, (*b*)]: Cu-O1, 2.028(18); Cu-O2, 2.344(16); Cu-N1, 2.094(4); Cu-N2, 2.087(4); N1-Cu-N2, 88.07(14); O1-Cu-N1, 139.1(5); O1-Cu-N2, 119.1(5); O2-Cu-N1, 124.9(5); O2-Cu-N2, 132.6(5).

As stated in Section 2.2.1, the synthesis of a Cu(I)-α-ketocarboxylate complex supported by TMPDA was hindered by disproportionation and the formation of Cu(0) and Cu(II) products. Two Cu(II) compounds were isolated from these mixtures as crystalline materials and characterized by X-ray crystallography. (TMPDA)Cu(BF)$_2$ was isolated from either the disproportionation of reaction mixtures of (TMPDA)CuCl and TlBF or from reactions of (TMPDA)CuCl$_2$ and 2TlBF (Figure 2.13; see Table 2.1 for complete refinement details). (TMPDA)Cu(BF)$_2$ displayed a distorted square planar geometry (τ_4 = 0.36)[73] with the Cu ion ligated by two N-donors and two O-donors. The ligating α-ketocarboxylates displayed longer Cu-O distances, 2.014(2) and 1.997(19) Å, than those observed in a previously reported Cu(II)-α-ketocarboxylate complex (1.932(2) Å).[74f] The previously reported Cu(II)-α-ketocarboxylate complex was ligated by the neutral tripodal ligand, TMPA, and contained one α-ketocarboxylate ligand with the

copper atom in a 5-coordinate geometry. The different coordination number and geometry of the copper atom along with a different number of anionic ligands directly bound to the metal center all likely contribute to the slight elongation of the observed Cu–O distances in (TMPDA)Cu(II)BF_2. In addition, O2 and O5 both showed an elongated distance to but nonetheless a significant interaction with the copper center (~2.5 Å). The torsion angles of the bound α-ketocarboxylates (107.12° and 93.25°) indicate large deviations from coplanarity of the carboxylates and α-ketocarbonyls. The deviation from coplanarity of the ketocarbonyl group from the carboxylate and aryl groups is generally observed for all metal complexes displaying η^1-carb bound α-ketocarboxylates[45,68] and the complexes discussed in this work remain consistent with the literature.

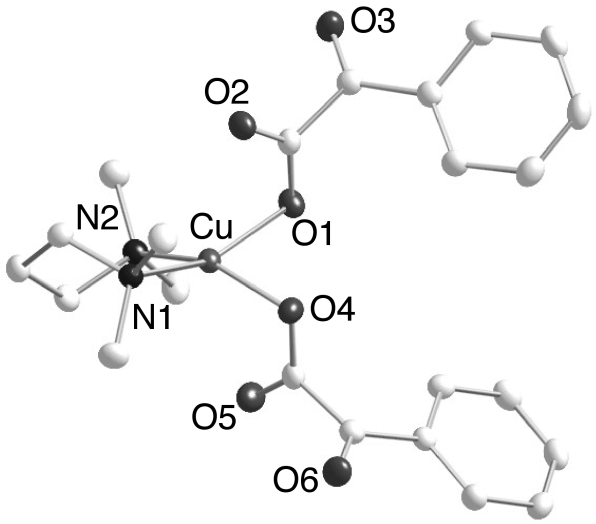

Figure 2.13. Representation of the X-ray structure of (TMPDA)Cu$(BF)_2$ with all nonhydrogen atoms shown as 50% thermal ellipsoids. Selected interatomic distances (Å) and angles (deg): Cu(1)-N(1), 2.035(2); Cu(1)-N(2), 2.031(2); Cu(1)-O(1), 2.014(2) Cu(1)-O(4), 1.997(19); N(2)-Cu(1)-N(1), 97.47(8); O(4)-Cu(1)-O(1), 88.50(7).

A second isolated product from the reaction between (TMPDA)CuCl and TlBF

was found to be a cluster, $(TMPDA)_2Cu_3BF_4O$ (Figure 2.14, See Table 2.1 for complete refinement details). The compound was isolated as several discrete crystals from the wall of the reaction flask and were not isolated in appreciable quantity. The quality of the X-ray structure is somewhat poor due to several highly disordered THF solvent molecules found within the crystal lattice (not shown). Based on charge balance, the copper atoms in this cluster are all formally Cu(II). All three copper ions are five-coordinate with τ_5 values of 0.12 (Cu1), 0.27 (Cu2), and 0.67 (Cu3). The τ_5 values indicate that Cu1 and Cu2 are described as being in a distorted square pyramidal geometry with Cu3 in a distorted trigonal bipyramidal geometry. An interesting feature of this cluster is the presence of the $[O_2CO_2C(C_6H_5)]^{3-}$ ligand that includes O4, O5, O6, and O7. The O7 atom displays similar O–C (1.43 and 1.39 Å) and O–Cu (1.96 and 1.93 Å) bond distances compared to O6 suggesting that this atom is indeed an oxygen. This ligand is possibly derived from the O-atom insertion product of benzoylformate or potentially, and more likely, this is the hydrate product of benzyolformate from adventitious water. The hydrated forms of α-ketocarboxylates exist as diols at the α-carbon.[76] The diol character of this ligand is also seen in an elongated C–O (~1.4 Å) bond compared to C=O (~1.2 Å) bonds found in carbonyl groups in the same structure. Due to the low yield of this product, ^{18}O-labeling studies to determine the source of this O-atom were not pursued. The other α-ketocaboxylate ligands resemble those already described in related complexes with dihedral angles between 95.1° and 109.2°, indicating a lack of conjugation between the α-ketocarbonyl and the carboxylate.

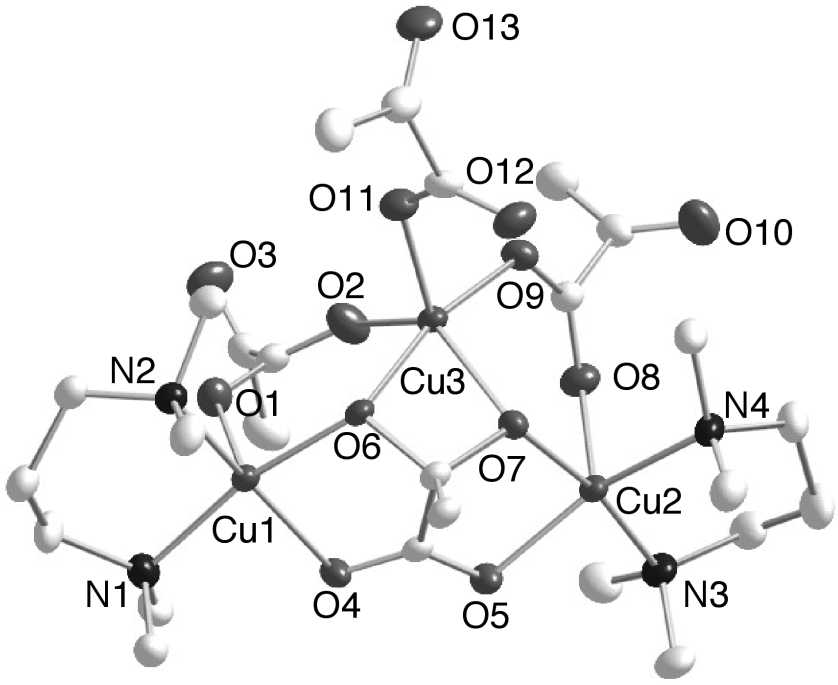

Figure 2.14. Representation of the X-ray structure of $(TMPDA)_2Cu_3(BF)_4O$ with all nonhydrogen atoms shown as 50% thermal ellipsoids and aryl rings from BF and hydrogen atoms omitted for clarity. Selected interatomic distances (Å) and angles (deg): Cu1-N1, 2.046(5); Cu1-N2, 2.066(5); Cu1-O1, 2.184(4); Cu1-O4, 2.022(4); Cu1-O6, 1.965(4); Cu2-N3, 2.080(5); Cu2-N4, 2.013(5); Cu2-O5, 2.030(4); Cu2-O7, 1.925(4); Cu2-O8, 2.244(4); Cu3-O2, 2.085(4); Cu3-O6, 1.974(4); Cu3-O7, 2.028(4); Cu3-O9, 1.944(4), Cu3-O11, 2.025(4); N1-Cu1-N2, 97.9(2); N1-Cu1-O1, 91.54(19); N2-Cu1-O1, 97.00(17); N1-Cu-O6, 167.79(17); N2-Cu1-O4, 160.46(18), O4-Cu1-O6, 82.84(14); O4-Cu1-N1, 86.62(18); N2-Cu1-O6, 90.10(16); O1-Cu1-O6, 96.63(15); O1-Cu1-O4, 101.89(17); N3-Cu2-N4, 98.5(2); O5-Cu2-N4, 87.16(18); N3-Cu2-O5, 153.7(2); N3-Cu2-O7, 90.80(18); O5-Cu2-O7, 82.95(15); N4-Cu2-O7, 170.06(18); O7-Cu2-O8, 93.58(15); N4-Cu2-O8, 88.94(19); O5-Cu2-O8, 110.24(17); N3-Cu2-O8, 95.59(18); O6-Cu3-O9, 165.83(16); O9-Cu3-O11, 93.87(17); O6-Cu3-O11, 99.68(16); O9-Cu3-O7, 100.36(16); O6-Cu3-O7, 68.35(14); O11-Cu3-O7, 125.38(18); O9-Cu3-O2, 85.24(17); O6-Cu3-O2, 94.46(16); O11-Cu3-O2, 107.8(2); O7-Cu3-O2, 125.69(18).

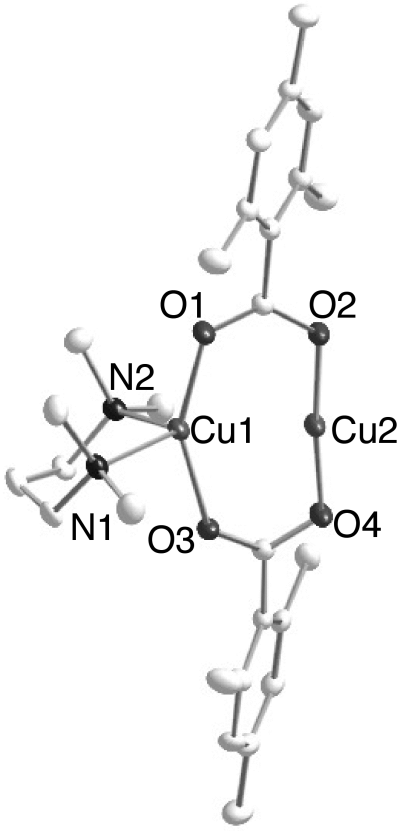

Figure 2.15. Representation of the X-ray structure of (TMPDA)Cu_2(2,4,6-Me-BA)$_2$ with all nonhydrogen atoms shown as 50% thermal ellipsoids and hydrogen atoms omitted for clarity. Selected interatomic distances (Å) and angles (deg): N1-Cu1, 2.147(2); N2-Cu1, 2.163(2); Cu1-O1, 1.9945(18); Cu1-O3, 2.0713(18); Cu1-Cu2, 2.6199(15); Cu2-O2, 1.8477(18); Cu2-O4, 1.8565(18); O1-Cu1-O3, 150.22(7); O1-Cu1-N1, 106.04(8); O1-Cu1-N2, 104.28(8); O3-Cu1-N1, 94.57(7); O3-Cu1-N2, 93.70(7); N1-Cu1-N2, 97.78(8); O1-Cu1-Cu2, 77.69(5); O3-Cu1-Cu2, 73.12(5); N1-Cu1-Cu2, 144.53(6), N2-Cu1-Cu2, 115.78(5); O2-Cu2-O4, 173.12(8); O2-Cu2-Cu1, 90.75(6); O4-Cu2-Cu1, 95.59(6).

In attempts to determine the viability of obtaining a Cu(I) complex supported by both the TMPDA ligand and an anionic carboxylate co-ligand, we explored the reaction of (TMPDA)CuCl with Li(2,4,6-Me-BA) in THF. This reaction yielded a complex of the formula (TMPDA)Cu_2(2,4,6-Me-BA)$_2$ that was characterized by X-ray crystallography (Figure 2.15; see Table 2.1 for complete refinement details). This complex displays two Cu-atoms in different environments. Cu1 is four coordinate and is ligated by two

nitrogens from the TMPDA ligand and two carboxylate O-atoms in a distorted tetrahedral geometry (τ_4 = 0.74). Cu2 is ligated by two carboxylate O-atoms in a near linear geometry (O2-Cu-O4 = 173.1°) with a short Cu1–Cu2 distance of 2.62 Å. A number of carboxylate bridged dicopper species have been reported in the literature, including mixed valent species.[77] The shortest reported Cu–Cu distance within these complexes is that of a dicopper(I,II) species synthesized by Hagadorn *et al.* that was supported by two carboxylate and two solvent THF molecules.[77a] The dicopper(I,I) species displayed a Cu–Cu bond of 2.524 Å that was shortened to 2.3947 Å upon conversion to the dicopper (I,II) species. The longer Cu1–Cu2 distance of 2.62 Å in (TMPDA)Cu_2(2,4,6-Me-BA)$_2$ suggests that there is little bonding between the two copper centers.

2.3. O_2-Reactivity of Diamine Supported Cu(I)-α-Ketocarboxylate Complexes and α-Ketocarboxylates as Exogenous Substrates in Cu/O_2 Chemistry

2.3.1 Low Temperature Oxygenation of Cu(I) Complexes

Oxygenation of solutions of ($^{t\text{Bu2Me2}}$EN)Cu(BF) in THF or CH_2Cl_2 at room temperature caused a rapid color change from yellow to bright green. ESI-MS analysis of solutions of ($^{t\text{Bu2Me2}}$EN)Cu(BF) after oxygenation displayed a strong peak envelope that was assigned to [$^{t\text{Bu2Me2}}$EN + H^+]$^+$, plus other non-identifiable peaks at higher m/z. Attempts to crystallize any species from these mixtures for X-ray analysis were unsuccessful. After a mild acidic workup to remove paramagnetic species the samples were found to contain <1% benzoic acid, the expected product of decarboxylation, by ^{1}H NMR spectroscopy. The major isolated product was benozylformic acid. This result was

an early indication that this complex was not following the expected reaction mechanism proposed for Fe(II)-α-ketocarboxylate complexes (Figure 2.1).

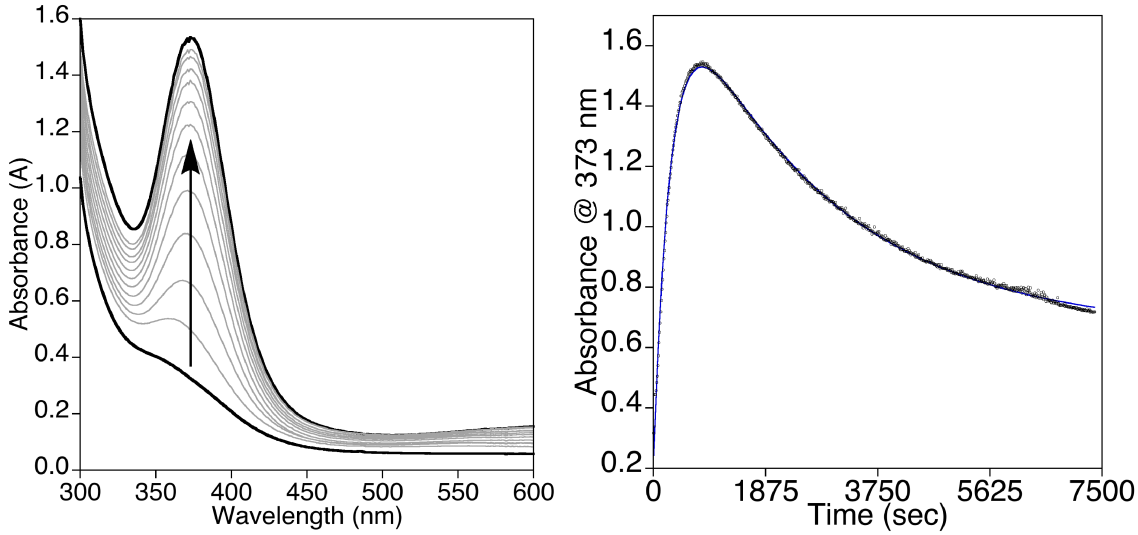

Figure 2.16. (*left*) UV-vis spectroscopic data for the reaction of (^{tBu2Me2}EN)Cu(BF) in CH_2Cl_2 (0.67 mM) with O_2 at –80 °C. (*right*) Time trace for the formation and decay of the intermediate with data monitored at 373 nm and fit to a bi-exponential equation [A_t = A1 + A2*exp(–k_2t) – A3*exp(–k_1t), k_1 = 0.0034 s^{-1} and k_2 = 0.00039 s^{-1}; R = 0.999].

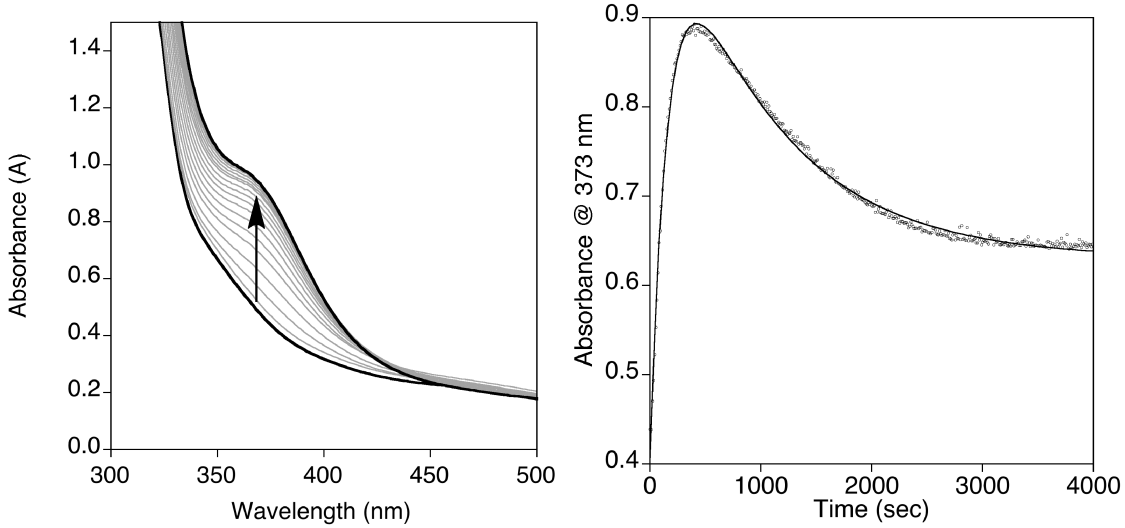

Figure 2.17. (*left*) UV-vis spectral data for the reaction of (^{tBu2Me2}EN)Cu(nitro-BF) in CH_2Cl_2 (0.67 mM) with O_2 at –80 °C with spectra shown every 20 sec. (*right*) Time trace for the formation and decay of the intermediate data monitored at 375 nm (*dots*) and fit to a bi-exponential equation [A_t = A1 – A2*exp(–k_1t) + A3*exp(–k_2t), k_1 = 0.0062 s^{-1} and k_2 = 0.0010 s^{-1}; R = 0.998].

Oxygenation of (^{t}Bu2Me2EN)Cu(BF) –80 °C in CH_2Cl_2 increased the yield of decarboxylation (conversion of BF to BA) to approximately 5%. This reaction was monitored using low temperature UV-vis spectroscopy and a transient feature at λ_{max} = 373 nm was observed (Figure 2.16, *left*). This species was not stable at –80 °C, as revealed by the decay of the UV-vis feature. The kinetic trace showing the absorbance at 373 nm is shown in Figure 2.16 (*right*). These data were fit by a simple bi-exponential A_t = A1 + A2*exp(–k_2*t) – A3*exp(–k_1*t) with k_1 representing the rate constant for formation, k_2 the rate constant for decay, t representing time, A_t the absorbance at time t, and other A values representing absorption correction factors. The fit yielded k_1 = 0.0034 s^{-1} and k_2 = 0.00039 s^{-1} (R = 0.999).

Solutions of (^{t}Bu2Me2EN)Cu(nitro-BF) in CH_2Cl_2 were oxygenated under identical conditions to those described above and monitored via UV-vis spectroscopy. It was observed that a slightly different intermediate and more rapid kinetics were found compared to the oxygenation of (^{t}Bu2Me2EN)Cu(BF). When the sample of (^{t}Bu2Me2EN)Cu(nitro-BF) was oxygenated the transient species displayed a feature at λ_{max} = 371 nm (Figure 2.17, *left*). The formation and decay of this spectral feature was modeled with a simple bi-exponential as described above with k_1 =0.0062 s^{-1} and k_2 = 0.0010 s^{-1} with R = 0.998 (Figure 2.17, *right*). The yield of decarboxylation, as determined by ^{1}H NMR spectroscopy, for (^{t}Bu2Me2EN)Cu(nitro-BF) (< 5%) was comparable to that observed for (^{t}Bu2Me2EN)Cu(BF).

Efforts to increase the yield of decarboxylation or trap the observed intermediate involved the addition of easily oxidizable substrates including cyclohexene and

cyclooctene to the reaction mixtures of (^{t}Bu2Me2EN)Cu(BF). This methodology had precedence in the work reported by Hong *et al*. involving the isolation and characterization of a oxidized ligand species derived from the oxygenation of a Cu(I)-α-ketocarboxylate complex.[45]

Samples of (^{t}Bu2Me2EN)Cu(BF) in CH_2Cl_2 were preloaded with 1 to 5 equivalents of cyclohexene or cyclooctene. After cooling to –78 °C, samples were oxygenated and stirred for 2 h to ensure complete decomposition of the intermediate. Samples were then warmed to room temperature and subjected to a mild acidic workup to remove copper and enable product analysis by GC-MS. In the cases of cyclohexene and cyclooctene, no oxidized products (epoxides, alcohols, coupled products, and enones) were observed above trace amounts. Interestingly, the yields of decarboxylation increased significantly to 11.5% and 16% when cyclohexene or cyclooctene were present, respectively, as determined by ^{1}H NMR spectroscopy. These results showed that the presence of these additives/substrates influenced the reactivity of the α-ketocarboxylate complex, despite the fact that they were not oxidized. Moreover, addition of 1 to 5 equivalents of acetonitrile with respect to the copper complex gave an increase of decarboxylation yield to 12%. Taken together, the data suggest that the additives are most likely acting as coordinating ligands rather than oxidizable substrates, and that such coordination somehow increases the efficiency of α-ketocarboxylate decarboxylation.

The role of cyclohexene as a ligand to (^{t}Bu2Me2EN)Cu(BF) was examined by ^{1}H NMR spectroscopy both at room temperature and –60 °C. No bound alkene was observed at either temperature. Attempts to isolate crystals of (^{t}Bu2Me2EN)Cu(BF) with bound

alkene were not successful. Concentrated solutions of ($^{t\text{Bu2Me2}}$EN)Cu(BF) in CH_2Cl_2 with excess cyclohexene yielded crystals that were found to be ($^{t\text{Bu2Me2}}$EN)Cu(BF) based on unit cell determination and comparison to the complete structure presented in Figure 2.11.

Given the experimental evidence presented thus far on the reactivity of ($^{t\text{Bu2Me2}}$EN)Cu(BF) and ($^{t\text{Bu2Me2}}$EN)Cu(nitro-BF) we cannot determine the identity of the observed intermediate nor draw a definitive conclusion about the reaction pathway that results in the minimal yield of observed decarboxylation. The transient natures of the observed intermediates along with the high energy of the UV-vis spectral features do not allow for further structural identification by X-ray crystallography or resonance enhanced Raman spectroscopy. The increase in decarboxylation yields for ($^{t\text{Bu2Me2}}$EN)Cu(BF) when coordinating compounds are present suggests the possible displacement of the α-ketocarboxylate ligand may be necessary for reactivity. This observation would be consistent with Path B of the originally proposed reaction pathways (Figure 2.3). Path B includes a reaction of an α-ketocarboxylate with a copper-oxygen species as a substrate. This idea was experimentally examined and the results are discussed in the following sections.

2.3.2. Reactivity of μ-η²:η²-Peroxo-Dicopper(II)/Bis(μ-oxo)dicopper(III) Species Towards Exogenous α-Ketocarboxylates

As a complementary set of experiments to the oxygenations of discrete Cu(I)-α-ketocarboxylate complexes, isolable $[Cu_2O_2]^{2+}$ intermediates supported by the same diamine ligands used in the previously described experiments were synthesized and

reacted with exogenous α-ketocarboxylates. These experiments were conducted to determine the viability of a $[Cu_2O_2]^{2+}$ species in the observed decarboxylation chemistry in the oxygenation of discrete Cu(I)-α-ketocarboxylate complexes.

Copper complexes that form dinuclear copper-oxygen species of the general formula $[Cu_2O_2]^{2+}$ are known to form from Cu(I) complexes supported by the peralkylated diamines used in the current study.[61,62] For example, (^{t}Bu2Me2EN)Cu(NCCH$_3$)OTf was reported by Stack *et al.* to yield an equilibrium mixture of μ-η^2:η^2-peroxo-dicopper(II) and bis(μ-oxo)dicopper(III) species upon oxygenation at low temperature.[61] The reactivity of these species towards various exogenous substrates was reported, although O-atom insertion/oxidation of α-ketocarboxylates was not examined in that work.[63]

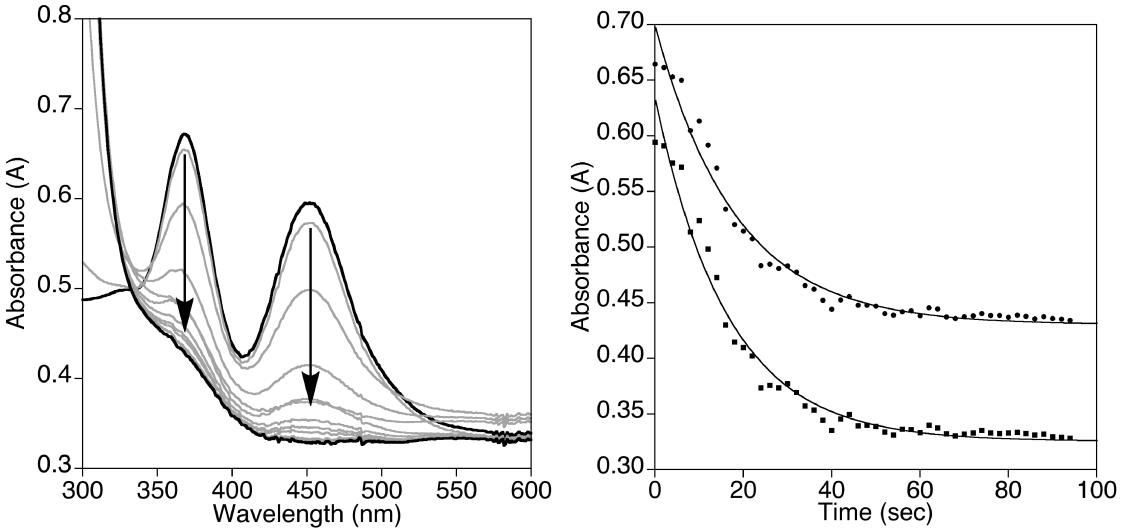

Figure 2.18. (*left*) UV-vis spectra of the reaction of the mixture of bis(μ-oxo)dicopper(III) and μ-η^2:η^2-peroxodicopper(II) complexes resulting from oxygenation of [(^{tBu2Me2}EN)Cu(NCCH3)]OTf (0.1 mM) with N(Bu)$_4$BF (10 equiv) at –80 °C in CH_2Cl_2, with intermediate spectra shown every 6 s. (*right*) The plot shows the time trace for the decay of the μ-η^2:η^2-peroxodicopper(II) (*top, circles*) and bis(μ-oxo)dicopper(III) (*bottom, squares*) cores at 369 and 455nm, respectively. The data were fit to exponential equations [$A_t = A_1 - A_2*\exp(-kt)$] (see text for *k* values).

As per the previously reported procedure, oxygenations of (^{t}Bu2Me2EN)Cu(NCCH$_3$)OTf in CH_2Cl_2 at –80 °C resulted in the formation of an equilibrium mixture of μ-η^2:η^2-peroxo-dicopper(II) and bis(μ-oxo)dicopper(III) species distinguishable by UV-vis spectroscopy (Figure 2.18, *left*). The μ-η^2:η^2-peroxo-dicopper(II) species displays a feature at λ_{max} = 369 nm and the bis(μ-oxo)dicopper(III) species displays a feature at λ_{max} = 455 nm, consistent with the values reported in the literature.[61,62] The observed features remain unperturbed indefinitely at –80 °C and only decay when the sample is warmed. A solution of tetrabutylammonium benzoylformate (TBABF) in CH_2Cl_2 (3 mM) was added to this mixture via syringe and the reaction monitored by UV-vis spectroscopy (Figure 2.18, *left*). The features assigned to the μ-η^2:η^2-peroxo-dicopper(II) (λ_{max} = 369 nm) and bis(μ-oxo)dicopper(III) (λ_{max} = 455 nm) species rapidly decayed upon addition of TBABF (Figure 2.18, *left*). The kinetic traces of the decay of both features were obtained (Figure 2.18, *right*), with the data on top (*circles*) representing the decay of the μ-η^2:η^2-peroxo-dicopper(II) species and on the bottom (*squares*) for the bis(μ-oxo)dicopper(III) species. The decay data were fit to a simple exponential to give rate constants k = 0.055 s^{-1} and 0.066 s^{-1} for the μ-η^2:η^2-peroxo-dicopper(II) and bis(μ-oxo)dicopper(III) cores, respectively. It is difficult to discern from these results which species is reacting with the α-ketocarboxylate, or if one or both species are independently reacting with the substrate due to a rapid preexisting equilibrium between both cores.

The yields of decarboxylation of these reactions were determined by GC-MS. Attempts to use ^{1}H NMR spectroscopy were complicated by poor resolution between the

aryl peaks of the product benzoic acid and starting benzoylformic acid in the presence of TBA^+. Samples were warmed to room temperature after the complete decay of the intermediate $[Cu_2O_2]^{2+}$ species, treated by HCl (aq) to extract the copper ion, and MeI/K_2CO_3 added to the organic fraction to methylate any carboxylic acids. Subsequently, the fraction was passed through a silica plug to remove TBA salts and the products were quantified by GC-MS using a standard curve for methylbenzoate. A 19% yield of decarboxylation with respect to starting $[Cu_2O_2]^{2+}$ species was found. This result comprises strong evidence that a $[Cu_2O_2]^{2+}$ core is capable of reacting with an α-ketocarboxylate and inducing decarboxylation. However, because isomerization between the μ-η^2:η^2-peroxo-dicopper(II) and bis(μ-oxo)dicopper(III) cores makes assigning the active oxidant impossible, we turned to a slightly different supporting ligand that supports only one of these two possible oxidants.

2.3.3. Reactivity of a Bis(μ-oxo)dicopper(III) Species Towards Exogenous Carboxylates and α-Ketocarboxylates

Copper(I) complexes supported by TMPDA have been reported to react with O_2 at low temperatures to form a bis(μ-oxo)dicopper(III) species, with no evidence for the concomitant formation of a peroxodicopper isomer.[41] As reported, the bis(μ-oxo)dicopper(III) species supported by TMPDA was generated by the oxygenation of $(TMPDA)Cu(NCCH_3)OTf$ in CH_2Cl_2 (0.1 mM) at –80 °C as indicated by an intense feature at λ_{max} = 397 nm in the UV-visible spectrum (Figure 2.19). Upon addition of 60 equivalents of TBABF to the preformed and argon purged solution of $[(TMPDA)_2$bis(μ-

oxo)dicopper(III)]OTf$_2$, the feature at 397 nm rapidly decayed and a transient species with λ_{max} = 352 nm and a weak shoulder at ~420 nm was observed, followed by eventual decomposition (Figure 2.19). The final spectrum displayed a weak feature at λ_{max} = 364 nm that persisted after warming of the reaction mixtures and is presumed to be from a final decomposition product.

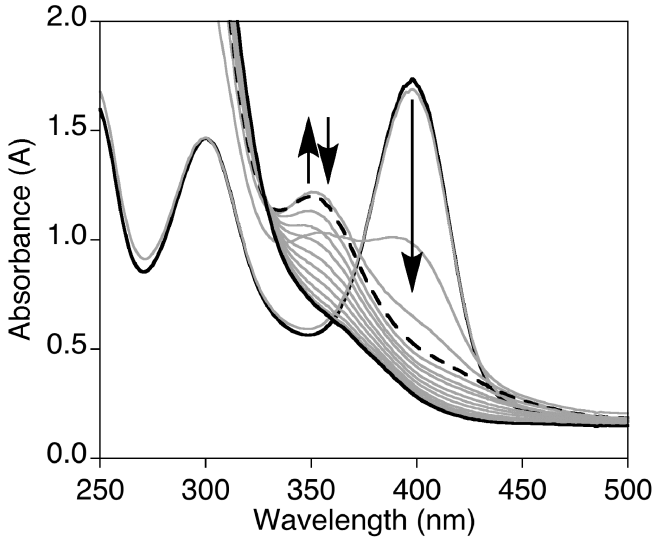

Figure 2.19. UV-Vis spectra of the reaction of [(TMPDA)$_2$Cu$_2$(O)$_2$](OTf)$_2$ in CH_2Cl_2 (0.1 mM) at –80 °C with 60 equivalents of TBABF to form a transient species (*dotted*) in route to the final product, with intermediate spectra at 0.5 s intervals shown in gray.

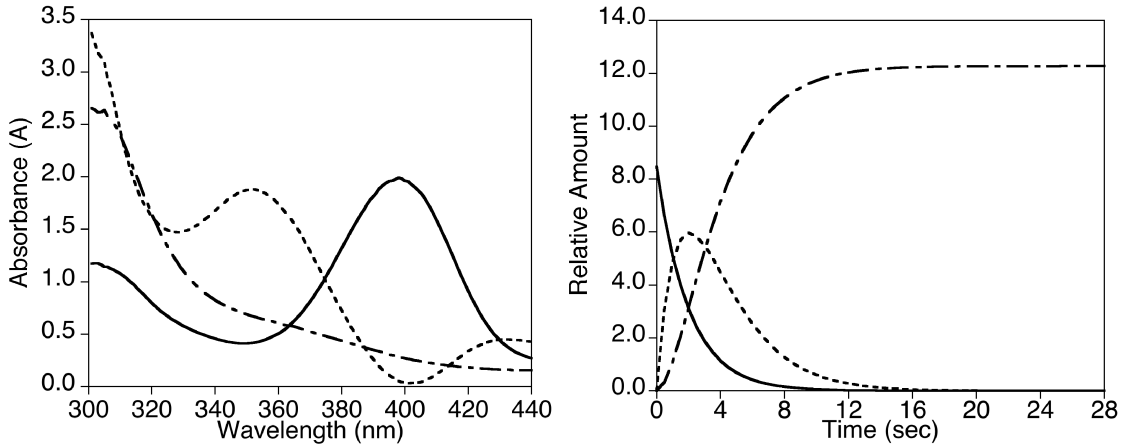

Figure 2.20 Results from the global fitting analysis of the UV-vis spectra obtained during the reaction of $[(TMPDA)_2Cu_2O_2]OTf_2$ in CH_2Cl_2 (0.1 mM) at –80 ºC (*left, solid*) with 60 equivalents TBABF. Data were truncated to a region between 300-440 nm to only include areas of significant spectral change followed by singular value decomposition (SVD) factor analysis using Olis GlobalWorks™. Three kinetic species were chosen from the significant eigenvectors resulting from the SVD process and are shown (*left*). The data were fit to an A(solid)→B(dotted)→C(dot-dash) model with the relative amounts of intermediate species with respect to time shown (*right*). Each step was treated as a first order reaction with the following rate constants k_1 = 5-7 x 10^{-1} s^{-1} and k_2 = 4-7 x 10^{-1} s^{-1}.

Approximate rate constants for the formation and decay of the transient species were obtained by global fitting of the UV-vis data using the Olis GlobalWorks™ software package. The UV-vis data were truncated to focus on a region between 300-440 nm, the only areas of significant spectral change. Singular value decomposition (SVD) factor analysis was performed. From the SVD analysis, three significant kinetic species were identified (Figure 2.20, *left*) and the data fit to an A→B→C model. The relative amounts of each species with respect to time are plotted in Figure 2.20 (*right*). The fits yielded the rate constants for the formation and decay of the transient of k_1 = 5-7 x 10^{-1} s^{-1} and k_2 = 4-7 x 10^{-1} s^{-1}, respectively.

The yield of decarboxylation for the reaction of [(TMPDA)$_2$bis(μ-oxo)dicopper(III)]OTf$_2$ with TBABF was examined next. After the reactions were warmed to room temperature they were treated to a mild acidic workup, methylation of organic products as described above, and GC-MS quantification of the benzoate ester. The yields of decarboxylation as a function of equivalents of TBABF are plotted in Figure 2.21, with the maximum yield of approximately 30% achieved near 5 equivalents of added TBABF (Figure 2.21). This suggests the bis(μ-oxo)dicopper(III) core is capable of inducing the decarboxylation of exogenous α-ketocarboxylate.

To gain a better understanding of the structural nature of the observed transient species with λ_{max} = 352 nm, resonance enhanced Raman spectroscopy was performed. Samples of [(TMPDA)$_2$bis(μ-oxo)dicopper(III)]OTf$_2$ were reacted with TBABF and then frozen in liquid N_2 within a few seconds of reaction initiation. Samples were excited with λ_{ex} = 406.7 nm radiation and resonance Raman spectra were obtained; a representative spectrum is shown in Figure 2.22 (*left*). Strong non-solvent peaks at λ_{max} = 609 (not shown) and 764 cm^{-1} were observed. The feature at 609 cm^{-1} is assigned to an a_1 symmetric core breathing mode of the bis(μ-oxo)dicopper(III) starting material.[78] The peak at 764 cm^{-1} falls in an energy region that is typically assigned to ν(O–O) of a metal-peroxide species.[79] An unambiguous assignment requires the preparation of ^{18}O-labeled samples and determination of the isotope sensitivity of the spectral features. Unfortunately, because of the transient nature of this particular species, forming and trapping an ^{18}O-labeled sample was impractical. Nonetheless, we postulate that the peroxo-like feature derives from a bridged/butterflied μ-η^2:η^2-peroxo-dicopper(II) core

that results from the coordination of the α-ketocarboxylate substrate to the bis(μ-oxo)dicopper(III) core. There is precedent for such an isomerization of a bis(μ-oxo) core to a peroxo core upon addition of basic anions or other substrates.[80,81]

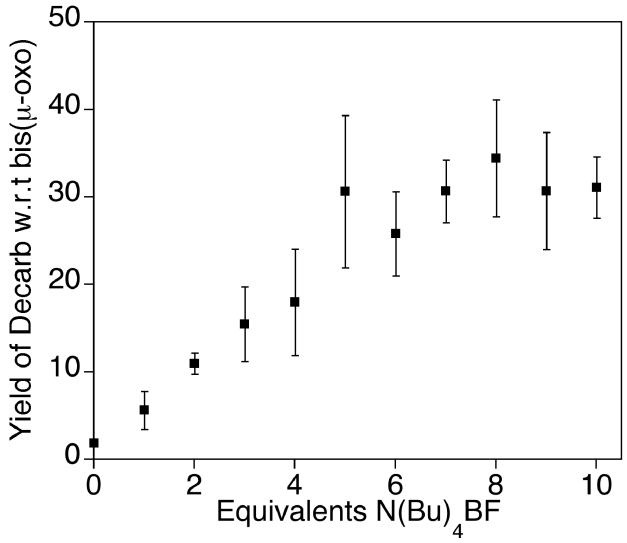

Figure 2.21 Yields of decarboxylation for the reaction of $[(TMPDA)_2Cu_2(O)_2](OTf)_2$ with various amounts of TBABF. The data are plotted as averages of 3 replicate determinations with standard deviation indicated as error bars. The yields were determined by GC-MS analysis of methylbenzoate (see Experimental Section) and are reported relative to the amount of starting complex, $[(TMPDA)_2Cu_2(O)_2](OTf)_2$.

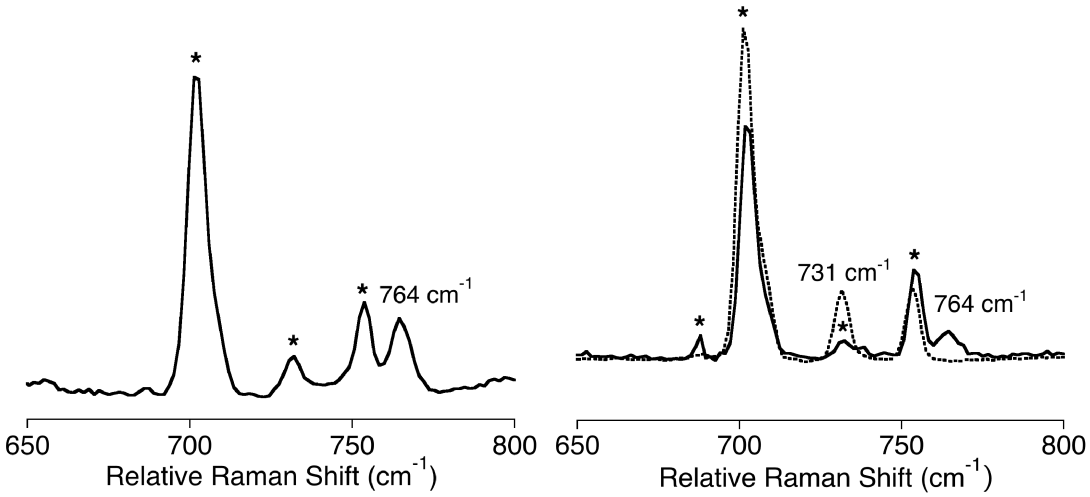

Figure 2.22. Resonance Raman spectra of $[(TMPDA)_2Cu_2(O)_2](OTf)_2$ (20 mM in CH_2Cl_2) after addition of (a) TBABF (60 eq.) or (b) TBABA (10 eq.), for samples prepared from $^{16}O_2$ (*solid*) or $^{18}O_2$ (*dotted*). Conditions: λ_{ex} = 406.7 nm, –196 °C. Solvent peaks are marked with asterisks (*).

To test this hypothesis experimentally, an alternative transient intermediate that could be stabilized and properly ^{18}O-labeled for a definitive resonance Raman experiment had to be found. We turned to TBABA (BA = Benzoate), which mimics the carboxylate binding mode of BF but lacks the keto-carbonyl functionality. We reasoned that the more robust BA species would be less susceptible to oxidation and would better stabilize the hypothesized carboxylate bridged μ-η^2:η^2-peroxo-dicopper(II) core. Addition of 10 equivalents of TBABA to the preformed and argon purged solution of $[(TMPDA)_2$bis(μ-oxo)dicopper(III)$]OTf_2$ in CH_2Cl_2 at –80 °C caused rapid spectral changes displayed in Figure 2.23. The initial features at λ_{max} = 397 and 300 nm assigned to the $[(TMPDA)_2$bis(μ-oxo)dicopper(III)$]OTf_2$ rapidly give way to a new species with spectral features at λ_{max} = 352, 413, and 587 nm, with clear isosbestic points. This spectrum contains features similar to those observed when TBABF was added to $[(TMPDA)_2$bis(μ-

oxo)dicopper(III)]OTf_2 although the species derived from TBABA is more stable, facilitating acquisition of a well resolved UV-vis spectrum. These spectroscopic features are comparable to reported butterflied or distorted μ-η^2:η^2-peroxo-dicopper(II) complexes synthesized by hindered directing ligands[82] or the addition of anionic bridging ligands, discussed below.[80]

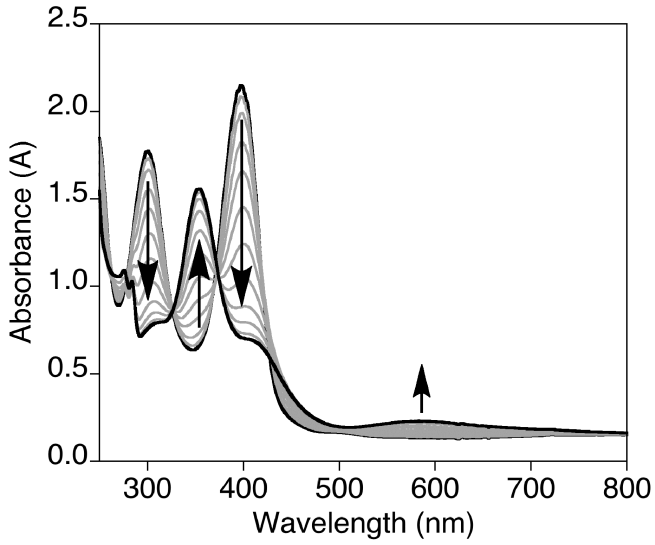

Figure 2.23. UV-vis spectroscopic changes for the reaction of $[(TMPDA)_2Cu_2O_2]OTf_2$ in CH_2Cl_2 (0.1 mM; *blue*) at –80 ºC with TBABA (10 equiv.), with spectra displayed every 4 s.

The species formed from [(TMPDA)$_2$bis(μ-oxo)dicopper(III)]OTf_2 and TBABA was stable for several minutes that allowed for the preparation of resonance Raman samples both with $^{16}O_2$ and $^{18}O_2$. The sample prepared from $^{16}O_2$ displayed a resonance-enhanced feature at 764 cm^{-1} (Figure 2.22, *right,* solid), identical to the feature observed from samples prepared from TBABF. When the benzoate samples were synthesized with $^{18}O_2$, the feature shifted to 731 cm^{-1} (Figure 2.22, *right,* dotted). The shift of 33 cm^{-1} upon ^{18}O-labeling is consistent with the assignment of this feature to an ν(O–O) of a peroxide O–O stretch in a μ-η^2:η^2-peroxo-dicopper(II) species.[79]

Taking into account both the UV-vis and resonance Raman spectroscopic results, parallels to previously reported $[Cu_2O_2]^{2+}$ cores can be made. It is helpful to briefly address the assignments of the electronic transitions that lead to the features in the visible spectra. The simplest case relevant to the assignment of the intermediate described in this chapter is a planar μ-η^2:η^2-peroxo-dicopper(II). Upon coordination of a peroxide ligand to the first Cu(II) center, the degenerative peroxide π^* orbitals split into two non-degenerative orbitals that by generally accepted nomenclature are referred to as π^*_σ and π^*_v. The π^*_σ orbital lies along the Cu-O-O plane and has significant orbital overlap with the Cu d_{x2-y2} orbitals. A LMCT transition from this peroxide orbital to the copper d-orbital leads to the more intense high-energy feature in the UV-region of the UV-vis spectrum. The π^*_v orbital lies orthogonal to the Cu-O-O plane and interacts weakly with the out-of-plane copper d-orbitals, giving rise to a less intense lower energy feature between 500-600 nm.[78,83] Addition of a second copper splits these two transitions into symmetric and antisymmetric combinations to each of the copper d-orbitals. In a planar μ-η^2:η^2-peroxo-dicopper(II) core (C_{2h} symmetry), the LMCT transitions involving one component of the respective π^* levels are electric dipole allowed so only two features are seen in the visible spectra.[82] This description does not accurately describe the experimental UV-vis spectrum observed in the current work, which has three distinct features (Figure 2.23).

More applicable to the work described in this chapter is when the symmetry of the planar μ-η^2:η^2-peroxo-dicopper(II) core is broken, either by a bridging ligand

coordinated to the $[Cu_2O_2]^{2+}$ or by a tethered binucleating ligand. A tethered or bridged $[Cu_2O_2]^{2+}$ core falls under C_{2v} symmetry and in a number of reports adopts a butterflied shape, with the Cu-O_2-Cu plane being somewhat distorted or puckered.[80] In this symmetry, the ligand π^*_σ and π^*_v transform as A_2 and B_2, which is the same as the positive and negative combinations of the copper d_{x2-y2} orbitals. This results in both contributions for each of the π^*_σ and π^*_v charge transfer transitions having the proper symmetry for all four LMCT transitions to be electric dipole allowed.[82] In reality, only three features are observed because one of the weaker features from the π^*_v to Cu(II) transition is obscured by a stronger π^*_σ to Cu(II) transition feature. Based on the previously assigned visible spectra that have three characteristic features, the visible spectra observed by the addition of $N(Bu)_4X$ (X = BF or BA) to $[(TMPDA)_2Cu_2O_2]OTf_2$ are consistent with the formation of a bridged, nonplanar μ-η^2:η^2-peroxo-dicopper(II) core.[80,82,83]

The resonance Raman spectra of tethered and bridging μ-η^2:η^2-peroxo-dicopper(II) cores have been previously reported and are consistent with the current assignment of a TMPDA supported μ-η^2:η^2-peroxo-dicopper(II) core with a bridging BA or BF ligand. In cases involving complexes supported by tethered binucleating ligands reported by Pidcock *et al,* the observed O–O vibration moved to higher energy, from 741 to 764 cm^{-1}, as the alkyl linker was shortened; i.e. a more distorted $[Cu_2O_2]^{2+}$ core.[82] The strengthening of the O–O bond was explained by a change in orbital overlap between the

metal d-orbitals and the peroxide bonding and anti-bonding orbitals as the peroxide ligand is lifted out of the plane. The authors found that the π-bonding contribution of the peroxide ligand has overlap with and donates into the empty Cu-atom $4p_x$ orbital in a planar $[Cu_2O_2]^{2+}$ core. This orbital interaction is diminished as the peroxide ligand moves out of plane, thus leaving more electron density in an O–O bonding orbital. Additionally, the π^*_v orbital has an *increased* interaction with the empty Cu $4p_y$ orbital in a butterflied geometry compared to the planer geometry. This leads to a diminished occupancy in an anti-bonding orbital and further strengthening of the O–O bond. The O–O stretching frequencies of reported butterflied peroxo-like species reported by Pidcock *et al.* (741-764 cm^{-1})[82] and Funahashi *et al.* (756 cm^{-1})[80] are comparable to the resonance Raman spectrum for the products of $[(TMPDA)_2bis(\mu\text{-oxo})dicopper(III)]OTf_2$ with TBAX (X = BF or BA), both of which displayed features at 764 cm^{-1}. Considering both the resonance Raman data along with the previously described UV-vis spectroscopy experiments, the species formed from the reaction of $[(TMPDA)_2bis(\mu\text{-oxo})dicopper(III)]OTf_2$ with TBAX (X = BF or BA) are most likely butterflied $\mu\text{-}\eta^2\text{:}\eta^2$-peroxo-dicopper(II) complexes with bridging (α-keto)carboxylate ligands.

2.4. Conclusions and Perspectives

The work described within this chapter aimed to examine the affect of α-ketocarboxylates as oxidizable co-ligands on copper-oxygen chemistry supported by peralkylated diamines and expand on work developed in our laboratory by Hong *et al.*[45] A number of Cu-α-ketocarboxylate complexes were synthesized and characterized by

several techniques including ^{1}H and ^{13}C NMR, FTIR, and UV-vis spectroscopies along with elemental analysis and X-ray crystallography.

Two Cu(I)-α-ketocarboxylate complexes, (^{tBu2Me2}EN)Cu(BF) and (^{tBu2Me2}EN)Cu(nitro-BF), were isolated and fully characterized and their reactivity towards O_2 was examined. Oxygenations of these compounds at low temperature (–80 °C) led to the formation and observation of transient species via UV-vis spectroscopy, although poor yields of decarboxylation (< 5%) were observed compared to previous work conducted in our laboratory with Cu(I)-α-ketocarboxylate complexes.[45] The identity of the transient species were not determined based on their short lifetimes and the high energy of visible features that prevented use of resonance enhanced Raman spectroscopy. It was also found that the yields of decarboxylation were modestly increased (~10-15%) with the introduction of coordinating solvents or alkenes. This finding led to the hypothesis that a $[Cu_2O_2]^{2+}$ species supported by peralkylated diamines may be formed and that this species then reacts with either a coordinated or exogenous α-ketocarboxylate.

To test this hypothesis, preformed solutions of $[Cu_2O_2]^{2+}$ species supported by either ^{tBu2Me2}EN or TMPDA were reacted with exogenous TBABF. It was found that both systems demonstrated reactivity towards α-ketocarboxylates with a maximum yield of decarboxylation occurring with an excess of BF added to a solution of $[(TMPDA)_2Cu_2(\mu\text{-}O)_2](OTf)_2$ (~30%). During this reaction an additional transient species was observed by UV-vis spectroscopy. This transient species was examined by resonance Raman

spectroscopy and on the basis of the results we hypothesized it was a bridged μ-η^2:η^2-peroxo-dicopper(II) species. More extensive UV-vis and resonance Raman spectroscopic experiments with additional $^{18}O_2$ labeling studies were conducted with the more stable benzoate substrate that generated a nearly identical species when reacted with $[(TMPDA)_2Cu_2(\mu\text{-}O)_2](OTf)_2$. These experiments confirmed the assignment of a carboxylate bridged μ-η^2:η^2-peroxo-dicopper(II) species. This bridged species displayed spectroscopic features very similar to other butterflied, nonplanar μ-η^2:η^2-peroxo-dicopper(II) complexes in the literature.[80,82]

With the experimental evidence described above, an updated mechanistic route for reactivity that does not imply the intermediacy of a $[CuO]^+$ species can be drawn for these systems and is shown in Figure 2.24. In this updated mechanism, the active oxidizing species is a bridged μ-η^2:η^2-peroxo-dicopper(II) species that can be accessed both from discrete Cu(I)-α-ketocarboxylate complexes (Figure 2.24, *left*) or by the addition of a carboxylate or α-ketocarboxylate to a $[Cu_2O_2]^{2+}$ species (Figure 2.24, *bottom*).

The reactivity described in this section is the first reported example of the decarboxylation of an α-ketocarboxylate by a $[Cu_2O_2]^{2+}$ core. This reactivity is surprising because the bulk of reported $[Cu_2O_2]^{2+}$ reactions can be best described by the copper-oxygen species acting as an electrophile.[84] A detailed mechanism for decarboxylation for the current system was not proposed and was beyond the scope of this work, but some support for a nucleophilic attack of the α-ketocarboxylate is available. It was presented in Section 2.3.1 that the kinetics for the formation and decay of the transient species were

more rapid for (^{t}Bu2Me2EN)Cu(nitro-BF) relative to (^{t}Bu2Me2EN)Cu(BF). Nitro-BF has an electron withdrawing substituent at the *para* position on the aryl ring making the α-ketocarbonyl carbon more electron deficient. This characteristic should make nitro-BF more susceptible to nucleophilic attack and this was seen in the more rapid kinetics for formation and decay of the transient. The nucleophilic character demonstrated by the $[Cu_2O_2]^{2+}$ species described within this section contrasts the known aryl hydroxylations, *N*-dealkylations, benzylic oxidations and other oxidations reported previously for similar species that were shown to be electrophilic in nature. This report shows that the range of reactivity of known copper-oxygen species remains to be fully understood and explored.[84]

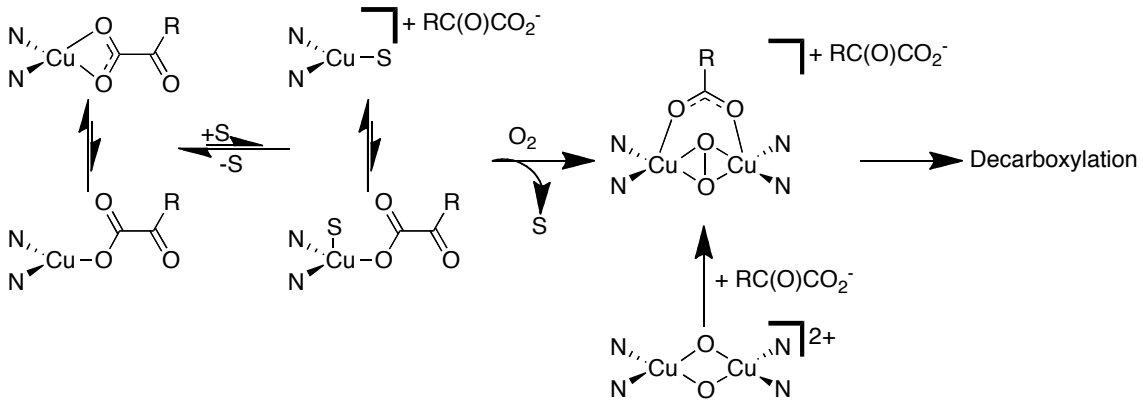

Figure 2.24. Proposed formation of a (α-keto)carboxylate bridged μ-η^2:η^2-peroxo-dicopper(II) species from either a discrete Cu(I)-α-ketocarboxylate or from the isomerization of a bis(μ-oxo)dicopper(III) unit to a μ-η^2:η^2-peroxodicopper(II) core upon binding of BF or BA.

2.5. Experimental

General Considerations. All solvents and reagents were obtained from commercial sources unless otherwise noted. Solvents were thoroughly degassed via three cycles of freezing, evacuating, and thawing. THF was dried over Na/benzophenone and distilled

under vacuum. CH_2Cl_2 and CD_2Cl_2 were dried over CaH_2 and distilled under vacuum. Et_2O and pentanes were passed through solvent purification columns and stored over CaH_2 (Glass Contour, Laguna, CA). All metal complexes were prepared and stored in a Vacuum Atmospheres inert atmosphere glove box under dry nitrogen or were manipulated under argon or dry nitrogen using standard Schlenk techniques. [LCu(CH_3CN)]OTf (L = TMPDA[62a] or ^{tBu2Me2}EN[61]), Cu_4Mes_4,[85] TBABF (BF = benzoylformate),[86] and TlBF[65] were prepared by literature methods and TBABA (BA = benzoate) was purchased from Aldrich.

Physical Methods. NMR spectra were recorded on either Varian VI-300, VXR-300, or VI-500 spectrometers at room temperature. Chemical shifts (δ) for ^{1}H and ^{13}C NMR spectra were referenced to residual protium in the deuterated solvent (^{1}H NMR experiments) or the characteristic solvent resonances of the solvent nuclei (^{13}C NMR experiments). Variable temperature ^{1}H NMR spectra were obtained on a Varian VI-300 spectrometer fitted with a liquid nitrogen cryostat. UV-vis spectra were collected on a HP8453 (190-1000 nm) diode array spectrophotometer. Low temperature UV-vis spectroscopy experiments were performed using an Unisoku low temperature UV-vis cell holder. UV-vis spectra that had drifting baselines due to minor frosting caused by the low-temperature device were corrected when necessary by subtracting the average of a region with no absorbance from the entire spectrum. Resonance Raman spectra were recorded on an Acton 506 spectrometer using a Princeton Instruments LN/CCD-11100-4 PB/UBAR detector and ST-1385 controller interfaced with Winspec software. The spectra were obtained at –196 °C using backscattering geometry. Excitation at 406.7 nm

was provided by a Spectra-Physics BeamLok 2060-KR-V Krypton ion laser. Raman shifts were externally referenced to liquid indene and internally referenced to solvent (CH_2Cl_2). Elemental analysis was performed by Robertson Microlit Lab (Madison, NJ). Electrospray ionization mass spectrometry (ESI-MS) was performed on a Bruker BioTOF II instrument. All GC-MS experiments were conducted on an Agilent Technologies 7890A GC system and 5975C VL MSD. The GC column was a HP-5ms with dimensions 30 m x 0.250 mm. The standard method used for all runs involved an initial oven temperature of 60 °C (held for 4 min) followed by a 20 °C/min ramp to 230 °C that was held for 15 min. Infrared spectra were collected on a Nicolet Avatar 370 FT-IR equipped with an attenuated total reflectance attachment, using a CaF_2 solution cell (International Crystal Laboratories) or a Smart OMNI-Sampler for solid samples. Electrical conductivity measurements were performed in CH_2Cl_2 using a Fischer Scientific Accumet Portable AP65 model conductivity bridge with a cell constant of 1.0 cm^{-1}. Anaerobically prepared solutions of (^{tBu2Me2}EN)Cu(BF) in CH_2Cl_2 (5 mL, 0.1-0.6 mM) were loaded into a 10 mL Schlenk flask, sealed with a glass stopper, and cooled to –78 °C in a dry ice/acetone bath under positive argon pressure. Measurements were taken by removal of the glass stopper under an argon purge and insertion of the probe. Values were acquired after ~ 5-10 sec to compensate for solution warming from the probe. Samples involving additives were prepared in an identical manner with additives added to stock solutions of the Cu(I) complex followed by serial dilutions. The equivalent conductance Λ_e was calculated from the conductance measurement and plotted vs. the square root of the concentration. Extrapolation of the linear portion of the plot allowed

determination of the equivalent conductance at infinite dilution, Λ_0. A plot of (Λ_o–Λ_e) vs. the square root of the concentration (Onsager plot) was then constructed.[71,72] Global fitting of UV-vis data was performed using Olis GlobalWorks™ software.

(^{tBu2Me2}EN)Cu(X) (X = BF or nitro-BF). In a typical procedure, Cu_4Mes_4 (41.5 mg, 0.055 mmol) and benzoylformic acid (34.1 mg, 0.22 mmol) were combined in CH_2Cl_2 (5 mL) and stirred for 20 min to give a cloudy yellow solution. ^{tBu2Me2}EN (45.5 mg, 0.22 mmol) in CH_2Cl_2 (1 mL) was added to afford a pale yellow solution. The solvent was removed under vacuum to yield a yellow oil, which was redissolved in a small amount of CH_2Cl_2 (~ 0.5 mL). Pentanes (~ 5 mL) was added to precipitate a bright yellow solid, which was collected by filtration and washed with pentanes (3 x 5 mL) (77.4 mg, 82% for X = BF; 56 mg, 65% for X = nitro-BF). Crystals suitable for X-ray crystallography were obtained by slow diffusion of pentanes into a concentrated CH_2Cl_2 solution. For X = BF: ^{1}H NMR ($CDCl_3$, 300 MHz): δ 7.92 (d, *J* = 9 Hz, 2H), 7.53 (t, *J* = 9 Hz, 1H), 7.42 (t, *J* = 6.9 Hz, 2H), 2.42 (s, 6H), 2.64 (b), 1.29 (s, 18H) ppm. ^{13}C{^{1}H} NMR (75.0 MHz, CH_2Cl_2): δ 195.23, 170.94, 134.76, 133.64, 130.02, 58.02, 49.28, 36.46, 26.62 ppm. Anal. Calc. for $C_{20}H_{33}CuN_2O_3$: C, 58.16; H, 8.05; N, 6.78. Found: C, 58.21; H, 8.24; N, 6.58. IR (Neat): 1197, 1224, 1393, 1448, 1477, 1617, 1683 cm^{-1}. UV-vis [λ_{max}, nm (ε, M^{-1} cm^{-1}) in CH_2Cl_2]: 362 (465). For X = nitro-BF: ^{1}H NMR (CD_2Cl_2, 300 MHz): δ 8.19 (dd, *J* = 8.1, 30.3 Hz, 4H), 2.44 (s, 6H), 2.64 (b), 1.29 (s, 18H) ppm. ^{13}C{^{1}H} NMR (75.0 MHz, CD_2Cl_2): δ 193.19, 169.53, 150.79, 139.64, 131.13, 124.12, 58.09, 49.23, 36.51, 26.64 ppm. Anal. Calc. for $C_{20}H_{33}CuN_2O_3$: C, 52.44; H, 7.04; N, 9.17. Found: C, 51.85; H, 6.75; N, 8.79. IR (Neat): 1210, 1348, 1348, 1389, 1473, 1529, 1628, 1695 cm^{-1}. UV-

vis [λ_{max}, nm (ε, M^{-1} cm^{-1}) in CH_2Cl_2]: 470 (162).

Attempted synthesis of (TMDA)Cu(BF). Cu_4Mes_4 (25 mg, 0.56 mmol) and benzoylformic acid (20 mg, 0.14 mmol) were combined in THF (10 mL). The solution was stirred for 20 min to give a cloudy yellow solution. TMPDA (0.022 mL, 0.14 mM) was added via syringe resulting in a golden clear solution. Upon standing (~10-15 min) or reduction in volume, the solution changed to a bright green supernatant with an orange solid deposit typical of a disproportionation reaction. Crystals suitable for X-ray crystallography were obtained by allowing the filtered supernatant to sit at room temperature for several days, and were found to be (TMPDA)Cu(BF)2. Complete characterization of this complex was performed for an independently synthesized sample (see below).

(TMPDA)Cu(BF)2. $CuCl_2$ (124 mg, 0.9 mmol) was suspended in CH_2Cl_2 (5 mL) and TMPDA (0.128 mL, 0.77 mmol) was added via syringe. After stirring for 2 h, the solution was filtered and TlBF (541.6 mg, 1.5 mmol) was added and the mixture was stirred overnight. The mixture was filtered and solvent was removed under vacuum from the bright blue-green filtrate to leave the product as a blue-green solid (328 mg, 87%). Crystals suitable for X-ray crystallography were obtained allowing a concentrated CH_2Cl_2 solution to stand at –20 °C. Anal. Calc. for $C_{23}H_{28}CuN_2O_6$•0.25CH_2Cl_2: C, 54.41; H, 5.12; N, 5.46. Found: C, 54.58; H, 5.12; N, 5.31. IR (Neat): 1232, 1405, 1477, 1591, 1685 cm^{-1}. UV-vis [λ_{max}, nm (ε, M^{-1} cm^{-1}) in CH_2Cl_2]: 740 (141).

Low Temperature Oxygenations of (^{tBu2Me2}EN)Cu(X) (X = BF or nitro-BF). Anaerobically prepared CH_2Cl_2 solutions (0.7 mM) of (^{tBu2Me2}eda)Cu(X) (X = BF or

nitro-BF) were cooled to –80 °C under argon in a septum sealed quartz cuvette. Dry O_2 was bubbled through the solution with monitoring by UV-vis spectroscopy (data for X= BF shown in Figure 2.16; X = nitro-BF shown in Figure 2.17). In some experiments, 1-5 equivalents of cyclooctene or cyclohexene were preloaded into the cuvette prior to cooling and oxygenation. Samples preloaded with substrates were subjected to GC-MS analysis. These solutions were gradually warmed to room temperature, solvent was removed under vacuum, and the resulting residues were washed with 0.1 M HCl (~5 mL). The aqueous layers were extracted with CH_2Cl_2 (3 x 5 mL) and the extracts dried with Na_2SO_4, filtered through Celite, and analyzed by GC-MS. Observed peaks were compared to commercially available oxidized variants of the original alkene (cyclohexene oxide, 2-cyclohexene-1-one, 2-cyclohexene-1-ol, and cyclooctene oxide).

Reaction of $[(^{tBu2Me2}EN)_2Cu_2(\mu\text{-}\eta^2\text{:}\eta^2\text{-}O_2)](OTf)_2$/$[(^{tBu2Me2}EN)_2Cu_2(\mu\text{-}O)_2](OTf)_2$ Mixture with TBABF. An anaerobically prepared CH_2Cl_2 solution (0.1 mM) of $[(^{tBu2Me2}EN)Cu(CH_3CN)]OTf$ was cooled to –80 °C under argon in a septum sealed quartz cuvette. Dry O_2 was bubbled through the solution, and monitoring by UV-vis spectroscopy revealed the growth of absorption bands (λ_{max} = 365 and 450 nm) indicative of the formation of a mixture of $[(^{tBu2Me2}EN)_2Cu_2(\mu\text{-}\eta^2\text{:}\eta^2\text{-}O_2)](OTf)_2$/$[(^{tBu2Me2}EN)_2Cu_2(\mu\text{-}O)_2](OTf)_2$[27] Once growth of the bands ceased, the solution was purged with Ar (10 min) and a degassed solution of TBABF in dry CH_2Cl_2 (3 mM, prepared in a glove box) was added via syringe to the stirred reaction solution, which was monitored by UV-vis spectroscopy. For subsequent GC-MS quantification, samples were warmed to room temperature. Solvent was removed *in vacuo* and the residue washed with 0.1 M HCl (~5

mL). The aqueous layer was extracted with CH_2Cl_2 (3 x 5 mL) to isolate the Cu-free organic products. The solvent was again removed *in vacuo* and the residue redissolved in acetone. K_2CO_3 (5 equivs. per added TBABF) and MeI (5 equivs. per added TBABF) were added and the solution was stirred for 2 h under reflux. The acetone was removed *in vacuo*, the residue was extracted with toluene (~ 2 mL), and the solution was filtered through a silica plug. The filtrate was diluted to a known volume and analyzed by GC-MS, using a standard curve prepared with commercially available methylbenzoate for comparison.

Reactions of $[(TPMDA)_2Cu_2(\mu\text{-}O)_2](OTf)_2$ with TBAX (X = BF or BA). These reactions were performed using the same procedure as described above, except using a 0.2 mM solution of [(TMPDA)Cu(CH_3CN)]OTf and involving the intermediacy of $[(TMPDA)_2Cu_2(\mu\text{-}O)_2](OTf)_2$, as indicated by an intense absorption feature with λ_{max} = 397 nm. Samples for analysis by resonance Raman spectroscopy were prepared using a 20 mM solution (0.8 mL) of [(TMPDA)Cu(CH_3CN)]OTf. The solutions were cooled under an argon purge to –78 °C by submerging the flask in a dry ice/acetone bath. Dry O_2 was bubbled through the solution forming the characteristic yellow brown color of the bis(μ-oxo)dicopper(III) core. After 30 min, O_2 flow was discontinued and the flask was purged for 20 min with argon to remove excess O_2. The solution was transferred via a precooled pipette to a NMR tube charged with 60 equivalents of TBABF under an argon purge in a dry ice/acetone bath. This reaction sat at –78 °C for 5 s and then rapidly frozen in liquid nitrogen for resonance Raman spectroscopic analysis. For the reaction with TBABA, a portion (58 mg, 1.6 mmol) was dissolved in 0.1 mL of CH_2Cl_2 and loaded into

a syringe in the glove box. This solution was injected into the Schlenk flask containing the solution of the bis(oxo)dicopper(III) complex and mixed for 5 min before transferring to a precooled (–78 °C) NMR tube. The mixture was then subsequently frozen in liquid N_2 for resonance Raman spectroscopic analysis.

Table 2.1. Summary of X-Ray Crystallographic Data

	(^{tBu2Me2}EN)Cu(BF)	(^{tBu2Me2}EN)Cu(*p-nitro*-BF)	(TMPDA)Cu(BF$_2$)	(TMPDA)$_2$Cu$_3$(BF)$_4$O	(TMPDA)Cu$_2$(2,4,6-BA)$_2$
Empirical formula	$C_{20}H_{33}CuN_2O_3$	$C_{20}H_{32}CuN_3O_5$	$C_{23}H_{28}CuN_2O_6$	$C_{42}H_{56}O_{13}Cu_3$•3(C_4H_8O)	$C_{27}H_{40}Cu_2N_2O_4$
Formula weight	413.02	458.03	492.01	1175.84	583.72
Crystal system	Monoclinic	Monoclinic	Triclinic	Monoclinic	Triclinic
Space group	$P2_1$	$P2_1/c$	$P\bar{1}$	$P2_1/n$	$P\bar{1}$
a (Å)	9.7882(6)	19.2670(13)	8.076(5)	16.1906(12)	8.684(5)
b (Å)	10.3914(6)	8.9816(6)	11.998(5)	20.0592(14)	12.914(5)
c (Å)	10.3951(7)	13.6990(9)	12.092(5)	20.1539(14)	13.045(5)
α (deg)	90	90	86.948(5)	90	104.099(5)
β (deg)	97.540(2)	107.274(2)	81.838(5)	112.081(2)	95.644(5)
γ (deg)	90	90	76.588(5)	90	98.174(5)
Volume (Å^3)	1048.18(11)	2263.7(3)	1127.9(10)	6065.3(7)	1390.9(11)
Z	2	4	2	4	2
T(K)	173(2)	173(2)	173(2)	173(2)	173(2)
ρ (calculated) (Mg/m^3)	1.309	1.347	1.449	1.292	1.504
θ range (deg)	1.98 to 25.06	1.11 to 25.07	1.7 to 25.06	1.39 to 25.06	1.63 to 25.09
μ (mm^{-1})	1.062	0.999	1.010	1.147	1.570
Reflections collected	10469	21392	10940	55529	14016
Independent reflections	3708	4019	4007	10746	4940
parameters	244	313	293	851	326
R1, wR2 (for $I > 2\sigma(I)$)	0.0249, 0.0598	0.0660, 0.1425	0.0355, 0.0844	0.1139, 0.1894	0.0287, 0.0683
GOF	1.006	1.037	0.985	0.942	0.952
Largest Peak, Hole (e.Å^{-3})	0.307 and -0.181	1.917 and -1.754	0.424 and -0.382	1.438 and -1.130	0.297 and -0.270
F(000)	440	972	514	2372	664
Crystal color, morphology	yellow, plate	gold, plate	green, block	Green, block	colorless, needle
Crystal size mm^3	0.50 x 0.40 x 0.10	0.50 x 0.40 x 0.10	0.4 x 0.3 x 0.2	0.5 x 0.4 x 0.4	0.30 x 0.10 x 0.10
Index ranges	$-11 \le h \le 11$, $-12 \le k \le 12$, $-12 \le l \le 12$	$-22 \le h \le 22$, $-10 \le k \le 10$, $-16 \le l \le 16$	$-9 \le h \le 9$, $-14 \le k \le 14$, $-14 \le l \le 14$	$-19 \le h \le 19$, $-23 \le k \le 23$, $-24 \le l \le 24$	$-10 \le h \le 10$, $-15 \le k \le 15$, $-15 \le l \le 15$

CHAPTER 3. THE SYNTHESIS AND REACTIVITY OF BIOISPIRED CU(I)-COMPLEXES SUPPORTED BY *N,N*-DIALKYL-HYDRAZINE DERIVED β-DIKETIMINATES

3.1 Introduction

The synthesis of O_2-reactive copper complexes is relevant for modeling and understanding biologically significant metalloenzymes and developing bio-inspired oxidation catalysts.[10,87] To better understand the mechanistic details of the reactions involved in both biological and synthetic systems, significant effort has gone towards isolating and identifying reactive copper-oxygen species that play key roles in the reactions of interest.[79,84,88] Over the years, a number of copper-oxygen species have been synthesized and characterized (Figure 3.1).[79,87] The copper-oxygen species shown in Figure 3.1 are generally thermally unstable and must be isolated at low temperatures (–80 °C) from reactions between Cu(I) complexes and O_2. The supporting ligand (L) plays a significant role in determining the electronic nature, nuclearity, and reactivity of an isolated copper-oxygen species. Isolation of mononuclear copper-oxygen species (Figure 3.1, *top row*) generally requires the use of bulky ligands to protect the reactive species.[79,84,88,90] In the absence of a ligand scaffold that can effectively protect the mononuclear species, dimerization or trimerization occurs to form higher nuclearity species (Figure 3.1, *second and third rows*).

A direction of growth in the field of synthetic copper-oxygen bioinorganic chemistry has been the use of well-characterized intermediates in the oxidation of robust

substrates, particularly the oxidation of unactivated C–H bonds.[84] Oxidation of exogenous substrates by copper-oxygen species are generally limited to those that contain weak C–H or O–H bonds.[79,88,90] Commonly, when copper-oxygen species decay intramolecular oxidation of supporting ligands is observed,[40,79,88] with relatively few exceptions.[88,89] Continued effort in this field has focused on synthesizing copper-oxygen species supported by new ligands that may lead to novel electronic character and/or reactivities.

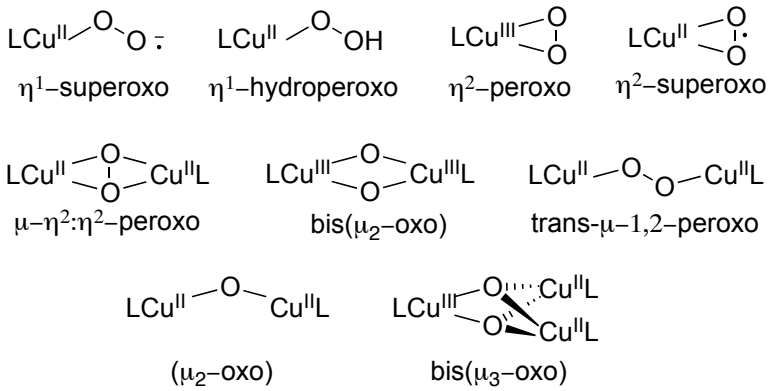

Figure 3.1. Experimentally observed and characterized copper-oxygen intermediates. L refers to a multidentate supporting ligand.

The aim of the work described in this chapter was to synthesize and characterize a new O_2-reactive Cu(I) complex, react it with O_2 and/or oxo-transfer reagents, characterize any intermediates that form, and examine the reactivity of the isolated intermediate towards substrates. To accomplish this goal, we turned to a class of ligands known as β-diketiminates. These ligands are strong electron donating anionic bidentate ligands with two ligating nitrogen atoms. β-Diketiminate ligands have been reported to support copper-oxygen chemistry.[90] Tuning of both steric and electronic properties in β-diketiminate ligands is possible because they may be prepared via a modular synthesis

starting from a β-diketone, typically 2,4-pentanedione, and a primary amine, typically an aniline derivative. When the steric profile of a β-diketiminate is small, i.e. derived from an unhindered amine or aniline, the resulting Cu(I) complexes generally react with O_2 or, in one case, oxo-transfer reagents to form bis(μ-oxo)-dicopper(III) species.[51,91] We chose to expand on this chemistry by synthesizing β-diketiminate ligands that would have small steric profiles but with different electronic character relative to β-diketiminate ligands previously used in copper-oxygen chemistry. We hypothesized that a Cu(I) complex supported by a small β-diketiminate with a particularly high electron donating capability would be highly reactive towards O_2 and oxo-transfer reagents such as iodosobenzene. The small steric profile would allow for the formation of multinuclear copper-oxygen species that could potentially be structurally or electronically distinct from species previously supported by β-diketiminate ligands.

The work described in the subsequent sections focuses on the synthesis of a new class of β-diketiminates used in the synthesis of electron rich Cu(I) complexes. Their full characterization both in the solid and solution state will be described using X-ray crystallography, cyclic voltammetry, ^{1}H NMR spectroscopy, and FTIR spectroscopy. The reactivities of the Cu(I) complexes towards a variety of substrates, including O_2 and aryl-nitrosyls, and the characterization of a thermally unstable $[Cu_3O_2]^{3+}$ species derived from either O_2 or oxo-transfer will be presented.

3.2. Synthesis and Characterization of Ligands and Complexes.

3.2.1 Synthesis of N,N-Dialkyl-Hydrazine Derived β-Diketiminate Ligands

The majority of reported syntheses of β-diketiminates involve the condensation reaction of two equivalents of a primary amine with a β-diketone, leading to the loss of water and the formation of the desired ligand.[91] We wished to incorporate an amine with a small steric profile that was electronically distinct from previously used aniline derivatives. *N,N*-dialkyl-substituted hydrazines offer both small steric profiles and the potential to yield an electronically distinct β-diketiminate upon reaction with a β-diketone (Figure 3.2). A hydrazine-derived β-diketiminate contains two sp^3-hybridized nitrogens bound directly to the ligating nitrogen atoms. We hypothesized that the peripheral nitrogen groups would act as electron donating groups bound to the ligating nitrogen atoms and would increase the reactivity of the Cu(I) center towards O_2 and oxo-transfer reagents.

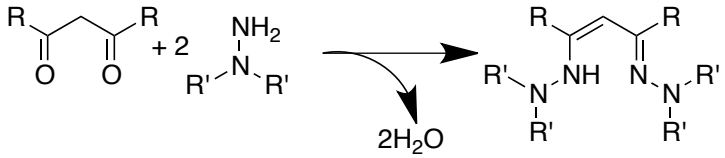

Figure 3.2. General synthetic route towards asymmetric hydrazine derived β-diketiminates.

A general scheme was followed to synthesize four hydrazine-derived β-diketiminate derivatives (Figure 3.2 and Figure 3.3). Condensation of *N,N*-dimethylhydrazine or *N,N*-diethylhydrazine with 2,4-pentanedione formed ^{Me2Hyd}NacH or ^{Et4Hyd}NacH, respectively.[92] Condensation of *N,N*-dimethylhydrazine with 3,5-heptanedione formed ^{Et2Hyd}NacH (Figure 3.3). ^{Me2Hyd}NacH was further functionalized at

the central backbone position of the β-diketiminate by reacting it with *n*-BuLi in THF at low temperature (–78 °C) and quenching the reaction with benzylbromide to form ^{Me2BzHyd}NacH (Figure 3.3). ^{1}H NMR spectroscopy and GC-MS analysis were used to confirm the identities of ^{Me2Hyd}NacH, ^{Et4Hyd}NacH, ^{Et2Hyd}NacH, and ^{Me2BzHyd}NacH on the basis of comparison to literature data.[92]

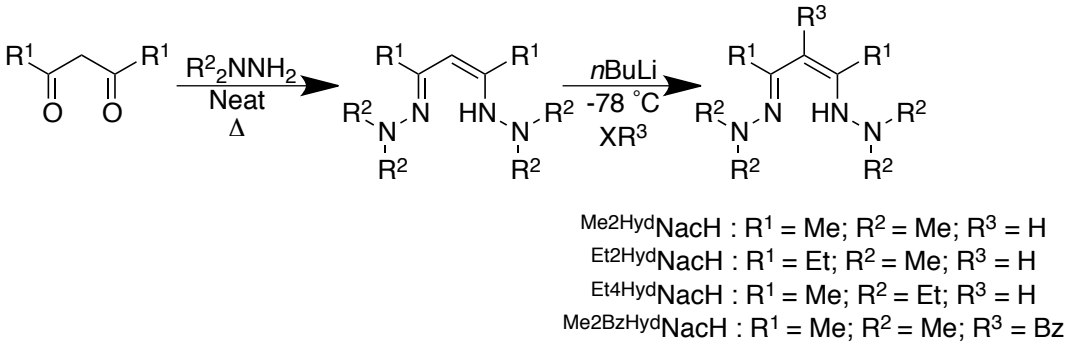

Figure 3.3. The synthetic route to asymmetrically substituted hydrazine derived β-diketiminate ligands.

The ^{1}H NMR spectrum of ^{Me2BzHyd}NacH is distinct from those of the other β-diketiminate ligands examined in this work. The data show that ^{Me2BzHyd}NacH exists as the diimine tautomer of the expected imine-amine structure (Figure 3.4). The assignment is based on observation of a doublet at 3.02 ppm (J = 7.8 Hz) integrating to 2 protons for the methylene group on the benzyl group and a triplet at 3.35 ppm (J = 7.8 Hz) integrating to 1 proton on the backbone position.

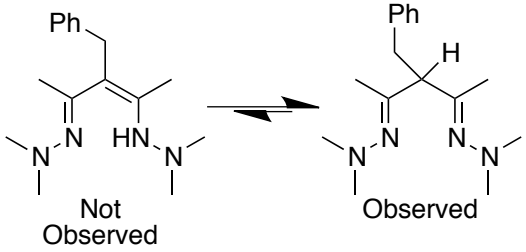

Figure 3.4. Tautomers of ^{Me2BzHyd}Nac.

3.2.2 Synthesis of Cu(I) Complexes

The complex (^{Me2Hyd}Nac)Cu(NCCH$_3$) was synthesized by reacting ^{Me2Hyd}NacH with ¼ equivalent of Cu_4Mes_4 in a THF/acetonitrile (50/50) mixture at room temperature for two hours. Removal of a yellow insoluble solid by filtration left a gold solution that upon concentration and addition of pentanes yielded a pale yellow microcrystalline material. The crystalline solid was isolated by filtration and characterized. The room temperature ^{1}H NMR spectrum of (^{Me2Hyd}Nac)Cu(NCCH$_3$) in d_8-THF displays features at 2.86, 2.32, and 1.97 ppm (Figure 3.5, a, c, d) integrating to 1, 15, and 6 protons, respectively. The features at 2.86 (a, ligand backbone position, -CH=) and 1.97 ppm (d, ligand backbone methyl positions, -CH$_3$) are observed as resolved singlets. The peak at 2.32 ppm (c) is assigned to the 4 nitrogen bound methyl groups (12 H) but consistently integrated for 15 protons, suggesting an underlying feature. Variable temperature ^{1}H NMR spectroscopy revealed the resolution of this feature into two distinct peaks at 2.46 and 2.29 ppm upon cooling samples to –80 °C (Figure 3.5, c → b and c). At –80 °C peaks b and c integrated to 3 and 12 protons, respectively, and are assigned to a metal-bound acetonitrile (Figure 3.5, b) and the *N*-methyl protons (Figure 3.5, c). We hypothesize that the coordinated acetonitrile observed as peak b at –80 °C is likely fluxional or labile at room temperature, resulting in the coalescence of this feature with the neighboring peak (c). The fluxionality of the acetonitrile ligand is further suggested by the elemental analysis results that yielded C, H, and N percentages for (^{Me2Hyd}Nac)Cu(NCCH$_3$) to be (C, 44.30%; H, 6.82%; N, 22.70%), closer to the calculated values for (^{Me2Hyd}Nac)Cu (C, 44.80%; H, 7.76%; N, 22.70%) than for

(^{Me2Hyd}Nac)Cu(NCCH$_3$) (C, 45.89%; H, 7.70.%; N, 24.33%). These results suggest the acetonitrile can be displaced from the Cu(I) center.

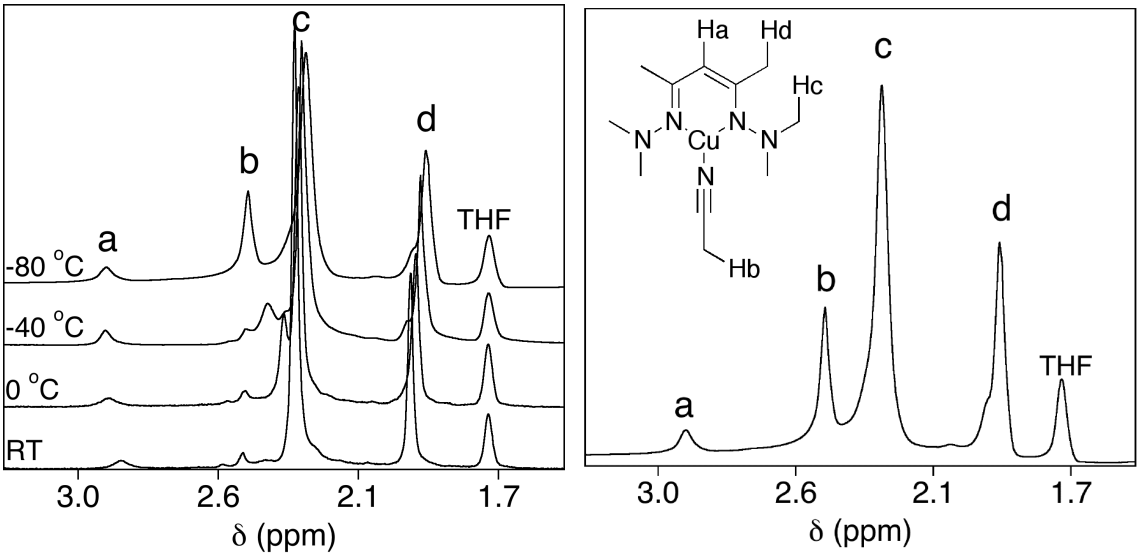

Figure 3.5. Variable temperature ^{1}H NMR spectra of (^{Me2Hyd}Nac)Cu(NCCH$_3$) in d_8-THF. Stacked spectra of (^{Me2Hyd}Nac)Cu(NCCH$_3$) (*left*) and the spectrum of (^{Me2Hyd}Nac)Cu(NCCH$_3$) measured at –80 °C shown with proton assignments (*right*).

3.2.3 X-Ray Crystallography of β-Diketiminate Cu(I) Complexes

Air-sensitive crystals of (^{Me2Hyd}Nac)Cu(NCCH$_3$) suitable for X-ray diffraction analysis were obtained from THF/pentanes solutions kept either at –20 °C (**A**) (Figure 3.6, left) or –80 °C (**B**) (Figure 3.6, *right*) and analyzed (See Table 3.1 for refinement details). Crystals grown at the two temperatures were found to be structurally similar despite being in different crystal lattices. Structure **A** solved in the P2$_1$/c space group compared to P2$_1$/n for structure **B**, with the structures displaying significantly different unit cell parameters (Table 3.1). Both crystal forms contain (^{Me2Hyd}Nac)Cu(NCCH$_3$) in a trigonal planar geometry (sum of donor angles = 360°) with the Cu ion ligated by two nitrogen atoms from the ^{Me2Hyd}Nac$^-$ ligand and one nitrogen from bound acetonitrile.

Structure **A** contains a canted acetonitrile coordinated to the metal center characterized by different N(5)-Cu(1)-N(1) and N(5)-Cu(1)-N(2) angles of 137.76(8)° and 124.67(8)°, respectively. Structure **B** has a more symmetrically bound acetonitrile with similar N(5)-Cu(1)-N(1) and N(5)-Cu(1)-N(2) angles of 129.23(12)° and 132.54(12)°. A significant distinction between the two structures is observed in the N–N bond lengths of the supporting $^{Me2Hyd}Nac^-$ ligand. Structure **A** displays N–N distances of 1.32 and 1.46 Å with the shorter bond (N3–N1) showing some degree of double bond character lying between an N–N single bond (1.45 Å) and N=N double bond (1.24 Å).[93] Structure **B** displays similar N–N distances of 1.45 and 1.46 Å. These differences may be a result of crystal packing interactions, as both **A** and **B** contain the same complex and there is no evidence for two distinct species in solution as determined by ^{1}H NMR spectroscopy. Sedai *et al*. reported several crystal structures of complexes supported by $^{Me2Hyd}Nac^-$ with calcium, strontium, barium, and magnesium.[92b,c] All of the reported structures display N–N bond distances of approximately 1.45-1.46 Å, making the short N–N distance (1.32 Å) found in the structure **A** of (^{Me2Hyd}Nac)Cu(NCCH$_3$) unique.

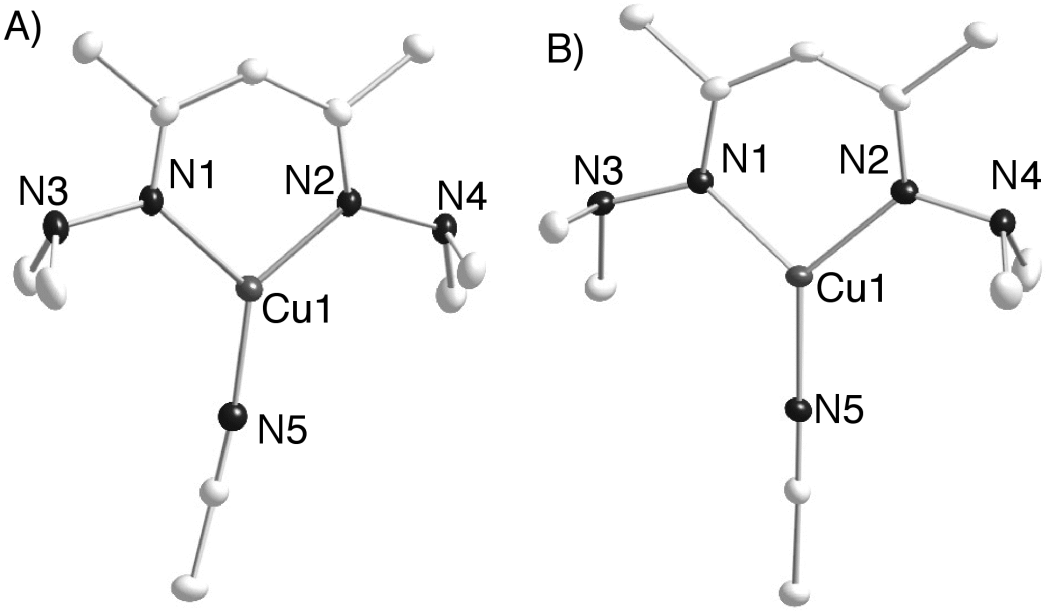

Figure 3.6. Representation of the X-ray structure of (^{Me2Hyd}Nac)Cu(NCCH$_3$) grown at –20 °C (*left,* **A**) and –80 °C (*right,* **B**) with nonhydrogen atoms shown as 50% thermal ellipsoids. Selected interatomic distances (Å) and angles (deg): Structure **A** grown at –20 °C: Cu(1)-N(1), 1.9305(19); Cu(1)-N(2), 1.9548(19); Cu(1)-N(5), 1.890(2); N(1)-N(3), 1.457(2); N(2)-N(4), 1.321(3); N(1)-Cu(1)-N(2), 97.56(8); N(5)-Cu(1)-N(1), 137.76(8); N(5)-Cu(1)-N(2), 124.67(8). Structure **B** grown at –80 °C: Cu(1)-N(1), 1.937(3); Cu(1)-N(2), 1.941(3); Cu(1)-N(5), 1.884(3); N(1)-N(3), 1.454(4); N(2)-N(4), 1.462(4); N(1)-Cu(1)-N(2), 98.23(12); N(5)-Cu(1)-N(1), 129.23(12); N(5)-Cu(1)-N(2), 132.54(12).

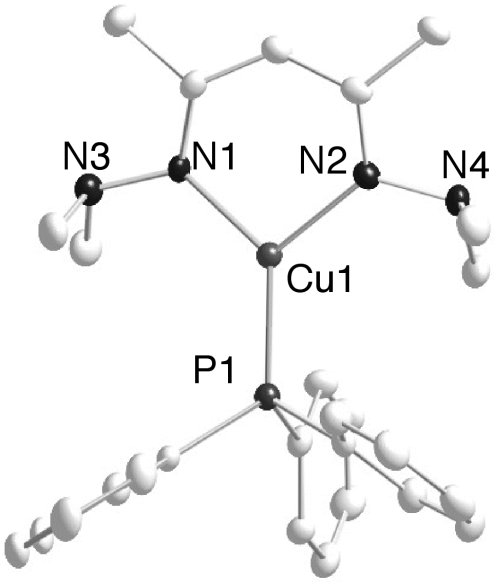

Figure 3.7. Representation of the X-ray structure of (^{Me2Hyd}Nac)Cu(NCCH$_3$) with nonhydrogen atoms shown as 50% thermal ellipsoids. Selected interatomic distances (Å) and angles (deg): Cu(1)-N(1), 1.9305(19); Cu(1)-N(2), 1.9548(19); Cu(1)-P(1), 1.890(2); N(1)-N(3), 1.457(2); N(2)-N(4), 1.321(3); N(1)-Cu(1)-N(2), 97.56(8); P(1)-Cu(1)-N(1), 137.76(8); P(1)-Cu(1)-N(2), 124.67(8).

Reactions of concentrated THF solutions of (^{Me2Hyd}Nac)Cu(NCCH$_3$) (40 mM) with one equivalent of PPh$_3$ yielded pale yellow crystals of (^{Me2Hyd}Nac)Cu(PPh$_3$) that were analyzed by X-ray crystallography (Figure 3.7). The structure shows the copper center in a trigonal planar geometry (sum of donor angles = 359.94°) ligated by two nitrogen donors from the ^{Me2Hyd}Nac$^-$ ligand and a phosphorus atom from the triphenylphosphine ligand. The structure of (^{Me2Hyd}Nac)Cu(PPh$_3$) is similar to that of structure **A** of (^{Me2Hyd}Nac)Cu(NCCH$_3$) insofar as it has two different N–N distances, one resembling a single bond (1.46 Å) and one (N2–N4) showing partial N–N double bond character (1.32 Å). For full refinement details see Table 3.1.

Table 3.1. Summary of X-Ray Crystallographic Data

	(^{Me2Hyd}Nac)Cu(NCCH$_3$) Grown at −20 °C **A**	(^{Me2Hyd}Nac)Cu(NCCH$_3$) Grown at −80 °C **B**	(^{Me2Hyd}Nac)Cu(PPh$_3$) •THF
Empirical formula	$C_{11}H_{23}CuN_5$	$C_{11}H_{23}CuN_5$	$C_{27}H_{34}CuN_4OP$
Formula weight	273.87	273.87	525.09
Crystal system	Monoclinic	Monoclinic	Triclinic
Space group	$P2_1/c$	$P2_1/n$	$P\bar{1}$
a (Å)	6.758(2)	10.4444(18)	10.031(4)
b (Å)	11.412(4)	10.0690(17)	11.418(4)
c (Å)	18.971(6)	13.659(2)	14.461(6)
α (deg)	90	90	79.751(5)
β (deg)	96.256(4)	94.531(2)	81.181(5)
γ (deg)	90	90	70.479(5)
Volume (Å^3)	1048.18(11)	1431.9(4)	1528.2(10)
Z	4	4	2
T(K)	173(2)	173(2)	173(2)
ρ (calculated) (Mg/m^3)	1.490	1.588	1.141
θ range (deg)	2.09 to 27.50	2.37 to 25.02	1.44 to 25.13
μ (mm^{-1})	1.062	1.885	0.789
Reflections collected	16229	13856	5399
Independent reflections	3318	2514	5399
Parameters	161	161	365
R1, wR2 (for $I > 2\sigma(I)$)	0.0354, 0.0745	0.0380, 0.0961	0.0606, 0.1324
GOF	1.127	1.044	0.963
Largest Peak, Hole (e.Å^{-3})	0.583 and -0.375	0.653 and -0.543	0.486 and -0.423
F(000)	612	725	552
Crystal color, morphology	yellow, block	yellow, block	colorless, plate
Crystal size	0.50 x 0.40 x 0.40	0.30 x 0.20 x 0.20	0.30 x 0.20 x 0.10
Index ranges	$-8 \le h \le 8$, $-14 \le k \le 14$, $-24 \le l \le 24$	$-12 \le h \le 12$, $-11 \le k \le 11$, $-16 \le l \le 16$	$-11 \le h \le 11$, $-13 \le k \le 13$, $0 \le l \le 17$

3.2.4 Cyclic Voltammetry of (^{Me2Hyd}Nac) and (^{Me2Hyd}Nac)Cu(NCCH$_3$)

Cyclic voltammetry (CV) measurements were performed on both the free ligand and (^{Me2Hyd}Nac)Cu(NCCH$_3$) to better understand their redox properties. The experiments were performed using acetonitrile as the solvent and TBAPF$_6$ (0.3 M) (TBA = tetrabutyl ammonium) as the electrolyte. The CV of ^{Me2Hyd}NacH (1 mM in acetonitrile, 0.3 M

$TBAPF_6$) is shown in Figure 3.8 (*left*). The voltammogram displays a number of features with the most significant being two oxidation peaks at –0.083 V and 0.458 V vs. Fc/Fc^+ (external). The feature at –0.083 V is irreversible while the feature at 0.458 V is pseudoreversible with a minor reduction peak at 0.347 V. A broad oxidation peak at 1.5 V and reduction peak at approximately 0.9 V also are present. The assignments of the individual redox events associated with each feature were not made based on the complexity of the spectra but it is clear that the free ligand in this study is redox active.

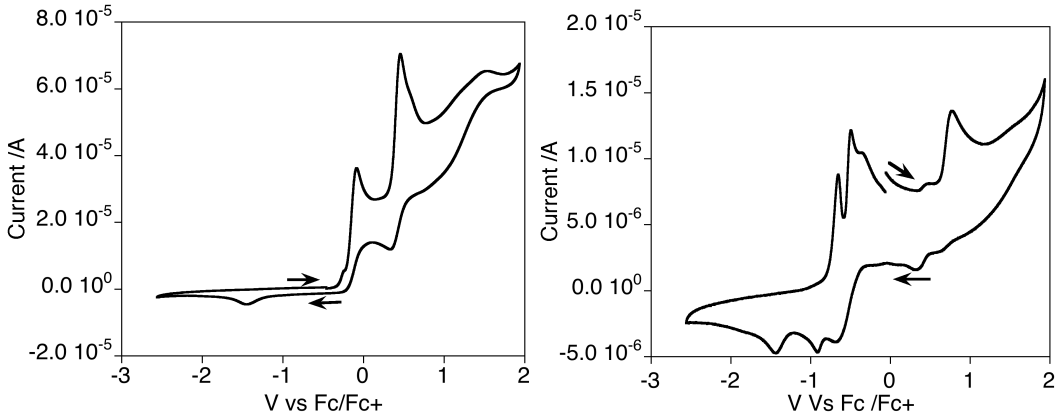

Figure 3.8. (*right*) The full CV of (^{Me2Hyd}Nac) (1 mM in acetonitrile, 0.3 M $TBAPF_6$) with a scan rate of 100 mV/s. (left) The full CV of (^{Me2Hyd}Nac)Cu($NCCH_3$) (1 mM in acetonitrile, 0.3 M $TBAPF_6$) with a scan rate of 100 mV/s.

The voltammogram for (^{Me2Hyd}Nac)Cu($NCCH_3$) is shown in Figure 3.8 (*right*). A number of features are observed that differ from those of the free ligand. A large irreversible oxidation peak is observed at 0.76 V with a number of small reduction features observed upon current switching. Two features at –0.666 and –0.930 V were observed from the sample, along with a feature at –1.45 V that was observed in an acetonitrile blank as well and thus is not due to (^{Me2Hyd}Nac)Cu($NCCH_3$). Upon current switching two more oxidation peaks were observed at –0.650 and –0.500 V. Definitive assignments of these features were not made as the spectrum is significantly complicated

and over interpretation of the data was a concern. The difficulty in assigning redox potentials to similar copper complexes that demonstrate complex CV spectra has led to additional experimental efforts and methods to comparing the electronic properties of Cu(I) complexes. One such method is the vibrational spectroscopy of Cu(I)-CO adducts (Described in the following section).[91]

3.2.5 FTIR Analysis of the CO Adduct of (^{Me2Hyd}Nac)Cu(NCCH$_3$)

The previous section described the difficulty of assigning the redox potentials and electronic character of (^{Me2Hyd}Nac)Cu(NCCH$_3$) by CV so an alternative more clear and definitive method was sought. A common method for examining electronic character of Cu(I) complexes, and of other metals, involves the syntheses of CO adducts of the starting metal complexes followed by vibrational spectroscopic characterization by FTIR spectroscopy.[94,95,96] This method takes advantage of the π-backbonding capability between a CO ligand and a metal. Electron rich metals, such as Cu(I), donate electron density into the π^* orbital of the CO ligand. This electron donation weakens the CO bond resulting in a detectable shift in the ν(CO) observable by FTIR spectroscopy relative to free CO (ν(CO) = 2143 cm^{-1}). Numerous Cu(I)-CO adducts have been synthesized, examined by FTIR spectroscopy, and reported in the literature to date.[97] FTIR spectroscopic characterization of (^{Me2Hyd}Nac)Cu(CO) would allow for direct comparison with other reported Cu(I)-CO complexes and enable evaluation of its electronic character.

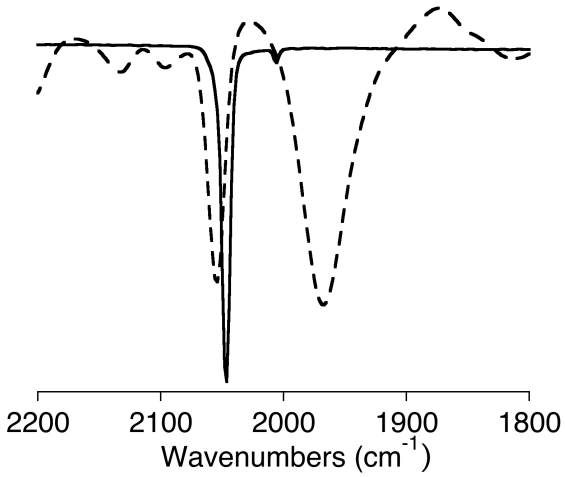

Figure 3.9. FTIR spectra of (^{Me2Hyd}Nac)Cu(CO) in the solid (*solid*) and solution (40 mM in THF) (*dotted*).

Solutions of (^{Me2Hyd}Nac)Cu(NCCH$_3$) in THF were reacted with gaseous CO (1 atm) and examined by FTIR spectroscopy in the solution and solid state. Both the solution (Figure 3.9, *dotted*) and solid state (Figure 3.9, *solid*) spectra of (^{Me2Hyd}Nac)Cu(CO) are shown. The FTIR spectrum for the solid-state sample displays a single sharp peak at 2047 cm^{-1} and the solution state spectrum displays two peaks of equal intensity at 2056 and 1968 cm^{-1}. The single feature at 2047 cm^{-1} in the solid sample is assignable to a C–O vibration and indicates a significant degree of C–O bond weakening relative to free CO. The ν(CO) values observed for (^{Me2Hyd}Nac)Cu(CO) in both the solid and solution state are significantly lower than those for previously reported β-diketiminate supported Cu(I)-CO adducts, suggesting a high degree of electron donating ability for the supporting ligand and increased electron density at the Cu(I) center.[97] The observed feature in the solid state resembles the features reported for Cu(I)-CO adducts supported by higher denticity ligands such as tris(pyrazolyl)hydroborate

(ν(CO) = 2056 cm^{-1})[98] or tris(pyridylalkyl)amine (ν(CO) = 2055 cm^{-1})[97b] ligands.

The two features observed in the solution FTIR spectrum for (^{Me2Hyd}Nac)Cu(CO) are more difficult to interpret compared to the solitary feature in the solid state spectrum. Three binding motifs for Cu(I)-CO complexes have been reported in the literature that give rise to two spectral features in a FTIR spectrum: (i) Multiple CO molecules bound to one copper center;[99,100,101,102,103,104] (ii) an individual CO molecule bridging two copper centers in equilibrium with a terminal Cu-CO species and a free Cu(I) complex;[97c] or (iii) one carbonyl bound to the metal center with an equilibrium that involves the dissociation of one of the ligating arms of the supporting ligand, resulting in two distinct Cu(I)-CO species in solution.[97b]

The small steric profile of $^{Me2Hyd}Nac^-$ makes scenarios (i) and (ii) easily envisioned. A number of studies have examined $[Cu(CO)_2]^+$ species by FTIR spectroscopy and report two features at higher ν(CO) frequencies than free CO.[105,106,107,108,109,110] All reports used either superacids or "superweak" coordinating counteranions to isolate Cu(I) complexes with multiple CO ligands, in stark contrast to the basic ligand system used in the current study. One example of a superweak coordinating counteranion comes from Ivanova *et al.*[105] The $[Cu(CO)_2]^+$ species was supported by a phenyl substituted undecaflourocarborane anion. Two features were observed in the FTIR spectrum at ν(CO) = 2166 and 2184 cm^{-1}, both higher than the ν(CO) frequency for free CO. The positive shift in ν(CO) frequency was attributed to less π back-bonding in this species than for other metal-CO complexes. In fact, all recently reported and fully characterized $[Cu(CO)_2]^+$ species display ν(CO) frequencies higher in

energy than for free CO. Polykov *et al*. adds that the more stabilized C–O bond indicated by the higher ν(CO) values may be due to competition between two CO ligands for the dπ electron density at the metal center.[100]

The second hypothesis (ii) could result from the small steric profile of $^{Me2Hyd}Nac^-$ that makes it easier to bring an additional Cu(I) center close to a Cu(I)-CO species, thus facilitating dimerization. An extensive report by Pasquali *et al*. examined the properties of bridging CO ligands in *N,N,N',N'*-tetra(methyl)ethylenediamine (TMEN) and TMPDA supported Cu(I) complexes.[97c] Several Cu(I)-CO adducts and reaction conditions were reported that lead to terminal CO binding, a bridging CO between two metals, or an equilibrium containing both bridging and terminally bound Cu-CO species. Two $[Cu_2(CO)]^{2+}$ species of particular interest were supported by either TMEN or TMPDA and a bridging benzoate. In the solid state a single bridging CO ligand displayed a feature at 1926 or 1925 cm^{-1} assignable to a ν(CO) vibration for the TMEN or TMPDA supported species, respectively. When these compounds were dissolved in THF, two features were observed at 2060 and 1930 cm^{-1} for the TMEN supported species and at 2065 and 1925 cm^{-1} for the TMPDA supported species.[97c] Observation of both features in solution FTIR spectra were indicative of equilibria involving both bridging and terminally bound CO ligands to the metal centers (Figure 3.10). These spectral features are remarkably similar to what is observed for the solution spectrum for (^{Me2Hyd}Nac)Cu(CO), suggesting that a similar equilibrium may be present.

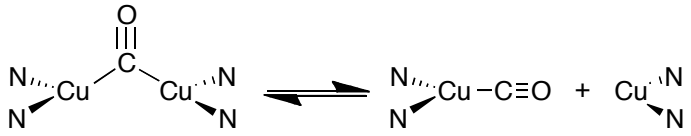

Figure 3.10. Proposed equilibrium for Cu(I)-CO adducts observed in the solution FTIR spectrum for (^{Me2Hyd}Nac)Cu(CO) as described in Ref [97c].

The third hypothesis for explaining the solution FTIR spectrum of (^{Me2Hyd}Nac)Cu(CO) originates from a recent report from Fry *et al*.[97b] In this work Cu-CO adducts were synthesized and supported by functionalized tris(methylpyridyl)amine (TMPA) ligands. The FTIR spectra for a number of the reported complexes contain two features in either the solution or solid state (Nujol mull) (ν(CO) ~ 2050 and 2077 cm^{-1}). The authors reasoned that in these cases, an equilibrium existed that involved the dissociation of one of the pendant pyridyl arms. The two features were assigned as the 5-coordinate (coordinatively saturated) and 4-coordinate (one pyridyl dissociated) Cu–CO adducts.[97c] This explanation likely does not apply to the solution FTIR spectrum of (^{Me2Hyd}Nac)Cu(CO) as there are no reports of a β-diketiminate dissociating one nitrogen donor in solution. In addition, the two observed features for all TMPA supported equilibria were higher in energy than the features observed for (^{Me2Hyd}Nac)Cu(CO).

Taking into account the experimental evidence and the literature precedent, it seems that the two features in the solution FTIR spectrum of (^{Me2Hyd}Nac)Cu(CO) are most consistent with the equilibrium as described in (ii) (Figure 3.10). Hypothesis (i) is unlikely because the current case would be in contrast with all reports that required a weakly basic ligand/anion to isolate a $[Cu(CO_2)]^+$ species, but the possibility of such a species cannot be unequivocally eliminated. Hypothesis (iii) is unlikely because of the difficulty envisioned in dissociating an arm of the bidentate ^{Me2Hyd}Nac$^-$ ligand.

3.2.6 Reactivity of (^{Me2Hyd}Nac)Cu(NCCH$_3$) with Aryl-Nitrosyl Compounds

The reactivity of (^{Me2Hyd}Nac)Cu(NCCH$_3$) towards aryl-nitrosyl compounds was examined in order to draw electronic and reactivity parallels with previously reported β-diketiminate supported Cu(I) complexes and adducts.[111] Solutions of (^{Me2Hyd}Nac)Cu(NCCH$_3$) in THF were reacted with 2,6-dimethylnitrosobenzene, resulting in a rapid color change from pale yellow to dark green. The reactions were run at room temperature in the glove box under an atmosphere of N_2 and the solutions retained their intense green color indefinitely when stored at –20 °C. The reactions were monitored by UV-vis spectroscopy and a chromophore with features at λ_{max} (ε, $M^{-1}cm^{-1}$) = 410 (3500) and 610 (1500) nm was observed (Figure 3.11, *left*). 2,6-Dimethylnitrosobenzene was titrated into THF solutions of (^{Me2Hyd}Nac)Cu(NCCH$_3$) (1 mM) and the photometric titration data are shown in Figure 3.11 (*right*). The growth and plateau regions of the data were each fit to a linear equation, the two best-fit lines set equal, and solved to determine the x-axis intercept. The features at 410 and 610 nm reach their maximums at 2,6-dimethylnitrosbenzene/(^{Me2Hyd}Nac)Cu(NCCH$_3$) ratios of 1.0(1) and 1.0(1), respectively, clearly indicating the formation of a 1:1 Cu-nitrosoaryl adduct. This species is spectroscopically distinct from a 1:1 Cu/nitrosoaryl compound supported by a β-diketiminate reported by Wiese *et al.*[111] The previously reported Cu-nitrosoaryl compound contains an η^2-bound ON-Ar group (Ar = 3,5-dimethylaryl) and displays a single spectral feature at λ_{max} (ε, $M^{-1}cm^{-1}$) = 582 nm (550) that is less intense than the species derived from (^{Me2Hyd}Nac)Cu(NCCH$_3$). This suggests that the Cu-nitrosoaryl species derived from (^{Me2Hyd}Nac)Cu(NCCH$_3$) has a higher degree of covalency in the

bonding interaction between the copper ion and the bound nitrosoaryl group compared to the species reported by Wiese *et al*.[111]

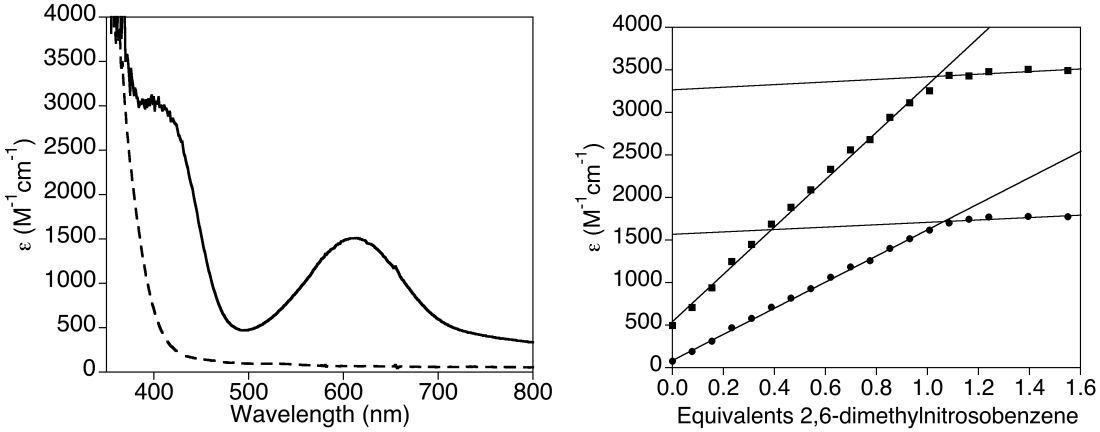

Figure 3.11. (left) UV-vis of reaction of (^{Me2Hyd}Nac)Cu(NCCH$_3$) (*dashed*) with 2,6-dimethylnitrosobenzene in THF (1 mM) to form a green species (*solid*). (*right*) Photometric titration of the features at 410 (*squares*) and 610 (*circles*) nm by addition of 2,6-dimethylnitrosobenzene to a solution of (^{Me2Hyd}Nac)Cu(NCCH$_3$) (1 mM, THF, RT). Fits for the linear portions of the data are shown. Linear fit equations for feature at 410 nm: y = 2780.5x + 556.31 (R = 0.99); y = 152.10x + 3273.3 (R = 0.83). Linear fit equations for feature at 610 nm: y = 1534.9x + 94.212 (R = 0.99); y = 140.37x + 1574.5 (R = .80).

Further evidence for the formation of a Cu-nitrosobenzene adduct came from ^{1}H NMR spectroscopy. (^{Me2Hyd}Nac)Cu(NCCH$_3$) and 2,6-dimethylnitrosobenzene were combined in d_8-THF in the glove box and the resulting solution was analyzed by ^{1}H NMR spectroscopy. The ^{1}H NMR spectrum displays resonances in the aryl region that integrate to 3 protons assignable to the aryl group in 2,6-dimethylnitrosobenzene (Figure 3.12, *left*). Four singlets of similar peak heights are found between 2.77 and 2.52 ppm that integrate to 12 protons total (Figure 3.12, a). These peaks are assigned to the 12 *N*-bound methyl protons that are all equivalent and appear as one singlet in the ^{1}H NMR spectrum of (^{Me2Hyd}Nac)Cu(NCCH$_3$) (Figure 3.12, *right*). Upon nitroso-adduct formation, these four methyl groups become inequivalent and appear as separate singlets. A singlet

appears at 2.29 ppm (Figure 3.12, b) that integrates to 6 protons and is assigned to the two aryl-bound methyl groups (Figure 3.12, b). Two equally intense singlets that integrate to a total of 6 protons are found between 2.08 and 2.03 ppm (Figure 3.12, c). These singlets are assigned to the inequivalent backbone methyl protons in the (^{Me2Hyd}Nac) ligand (Figure 3.12, c). The last non-solvent peak appears at 1.94 ppm (Figure 3.12, d) and is assigned to free acetonitrile[112] that is displaced from the Cu(I) complex upon reaction with 2,6-dimethylnitrosobenzene. The ^{1}H NMR data suggest that the bound 2,6-nitrosobenzene does not have free rotation around the metal-ligand bond resulting in an overall asymmetry in the complex. This asymmetry is observed in inequivalent *N*-bound and backbone methyl protons in the ^{1}H NMR spectrum.

EPR spectroscopy was used to examine the electronic properties of the reaction product between (^{Me2Hyd}Nac)Cu($NCCH_3$) and 2,6-dimethylnitrosobenzene (Figure 3.13). A very weak signal is observed near the g ~ 2 region that was modeled with the parameters $g_x = 2.0140$, $g_y = 2.0012$, $g_z = 1.98750$, and $A_x = 15$ G. In addition to this free radical-like species, a very weak signal that resembles a Cu(II) compound was observed between 2700–3400 G (Figure 3.13, *inset*). All the features in the EPR spectrum integrated to 2.4% of those in a 1 mM Cu(II) standard, indicating that the species associated with the signals are a minor component or impurity and that the 2,6-dimethylnitrosobenzene adduct is EPR silent and diamagnetic.

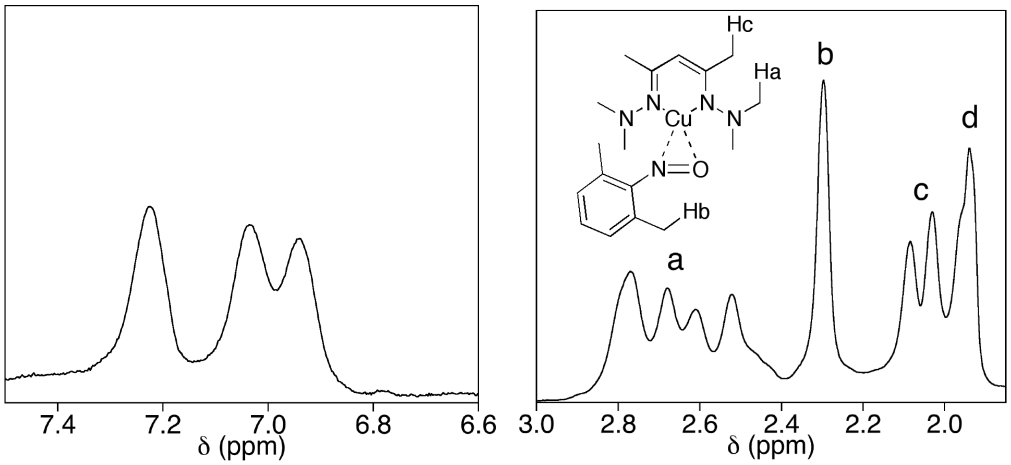

Figure 3.12. ^{1}H NMR spectra of the reaction products of (^{Me2Hyd}Nac)Cu(NCCH$_3$) with 2,6-dimethylnitrosobenzene in d_8-THF.

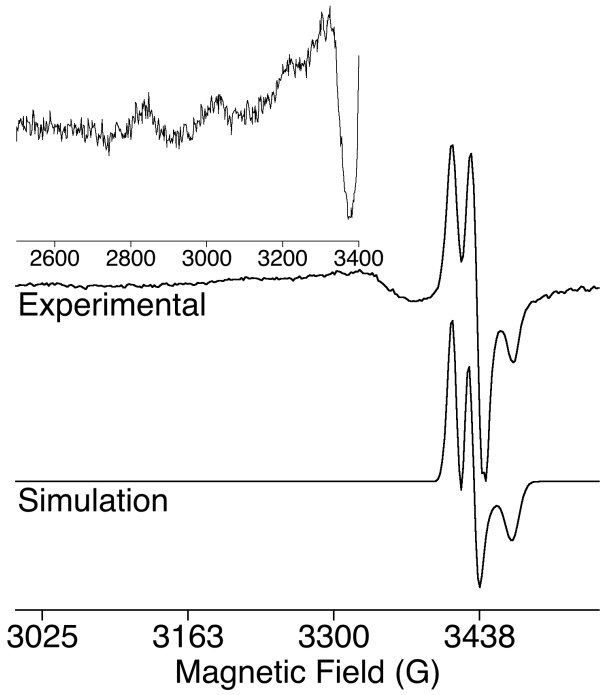

Figure 3.13. Perpendicular mode EPR spectra of the product between (^{Me2Hyd}Nac)Cu(NCCH$_3$) with 2,6-dimethylnitrosobenzene in THF (1 mM) (*top*) with the inset displaying an expanded view of the regions between 2700-3400 G at 4 K. Simulation of the EPR spectrum (*bottom*) with the parameters: g_x = 2.0140, g_y = 2.0012, g_z = 1.98750; A_x = 15 G; Line widths : x = 10 G, y = 0.1 G, z = 13 G.

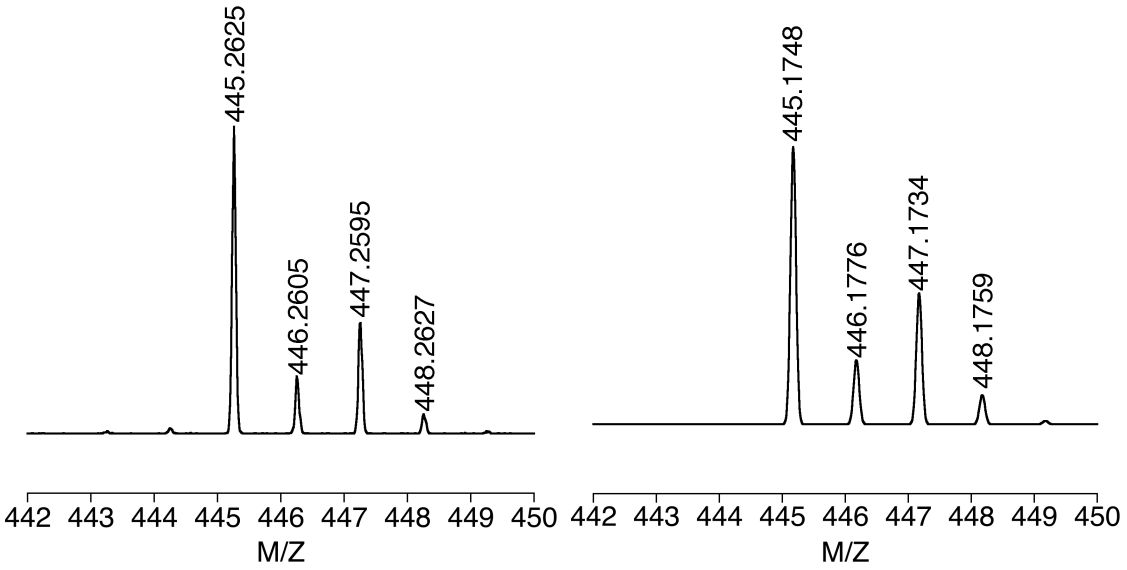

Figure 3.14. Experimental (*left*) and simulated (*right*) ESI-MS spectra of a $[(^{Me2Hyd}Nac)Cu(NCCH_3)(ONAr)Na]^+$ species.

ESI-MS analysis of the reaction of $(^{Me2Hyd}Nac)Cu(NCCH_3)$ with 2,6-dimethylnitrosobenzene was performed. Three significant peak envelopes were observed and all display the characteristic isotope pattern for one copper atom. The most intense feature was observed at m/z = 445.2625 (Figure 3.14, *left*). This species was simulated with a molecular formula of $[(^{Me2Hyd}Nac)Cu(NCCH_3)(ONAr)Na]^+$ with Ar = 2,6-dimethylnitrosobenzene (Figure 3.14, *right*). These data support the formation of a 1:1 Cu/nitrosyl species upon reaction of $(^{Me2Hyd}Nac)Cu(NCCH_3)$ with 2,6-dimethylnitrosobenzene, consistent with the photometric titration data and the ^1H NMR spectrum. A second significant peak envelope was observed at m/z = 429.2640 (Figure 3.15, *left*). This peak envelope was simulated as $[(^{Me2Hyd}Nac)Cu(NCCH_3)(NAr)Na]^+$ (Figure 3.15, *right*) which may result from the loss of an O-atom from $(^{Me2Hyd}Nac)Cu(NCCH_3)(ONAr)$. There was no evidence of this species upon workup of reaction mixtures so it was most likely formed within the ESI-MS instrument as a result

of the high temperatures required for ionization. A final copper containing peak envelope was observed at m/z = 564.3408 (Figure 3.16, *left*). This feature was modeled with the formula $[(^{Me2Hyd}Nac)Cu(NCCH_3)(NAr)(ONAr)Na]^+$ containing both the ONAr group and a species with an abstracted O-atom (Figure 3.16, *right*). Like the previously described species, this compound likely was formed from the extreme conditions of ionization as there is no other experimental evidence of its formation and the species is inconsistent with the photometric titration data presented above.

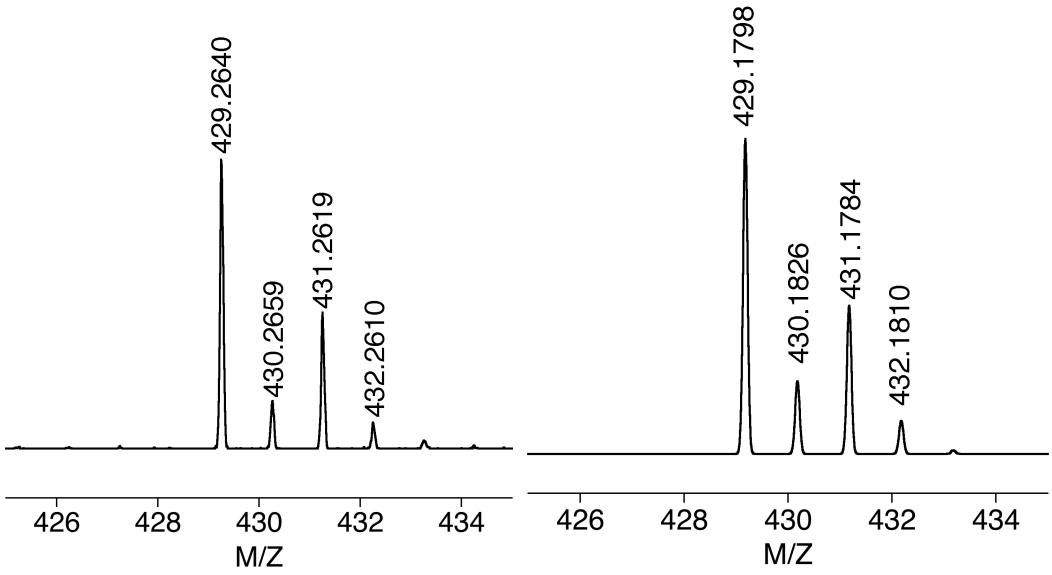

Figure 3.15. Experimental (*left*) and simulated (*right*) ESI-MS spectra of a $[(^{Me2Hyd}Nac)Cu(NCCH_3)(NAr)Na]^+$ species.

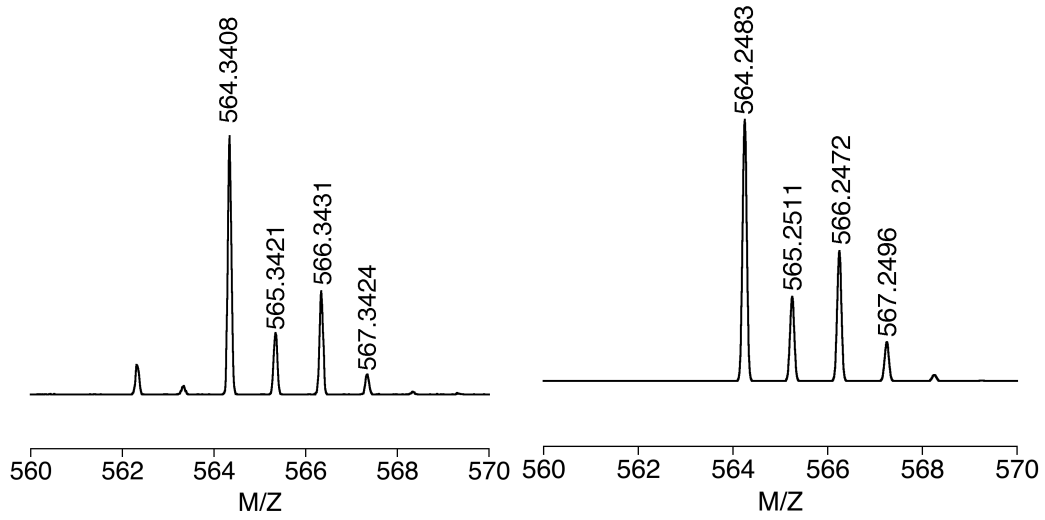

Figure 3.16. Experimental (*left*) and simulated (*right*) ESI-MS spectra of a $[(^{Me2Hyd}Nac)Cu(NCCH_3)(NAr)(ONAr)Na]^+$ species.

FTIR and resonance enhanced Raman spectroscopies were used to attempt to evaluate the nature of the N–O bond in the 1:1 adduct. The spectra shown below (Figure 3.17) include the solid state FTIR spectrum and the resonance Raman spectrum of the adduct. The FTIR spectrum of the adduct displays several features not present in the starting $(^{Me2Hyd}Nac)Cu(NCCH_3)$ complex, the most significant of which are seen at 1101 and 774 cm^{-1} (Figure 3.17, *left*). The resonance Raman spectrum of the adduct in THF was obtained using an excitation wavelength of λ_{ex} = 568.1 nm (Figure 3.17, *right*). Three non-solvent features are observed at 1090, 852, and 751 cm^{-1} (Figure 3.17, *right*). The previously reported β-diketiminate supported Cu-(η^2-ONAr) (Ar = 3,5-dimethylbenzene) complex displayed a ν(NO) = 1113 cm^{-1} by FTIR spectroscopy that was assigned to a reduced nitrosyl functionality.[111] Both the FTIR and resonance Raman spectra of the adduct we prepared contain features near the reported vibration at 1090 and 1101 cm^{-1}, respectively, but also contain lower energy features (< 900 cm^{-1}). The ^{15}N-

labeled nitrosyl compound has yet to be synthesized in order to identify the features that are isotope sensitive and definitively assign the vibrations of the N–O bond. The presence of lower energy features in both the FTIR and resonance Raman spectra seen in the current study suggest a further degree of N–O bond activation/reduction compared to previous reports but this assignment is beyond the scope of the present work.

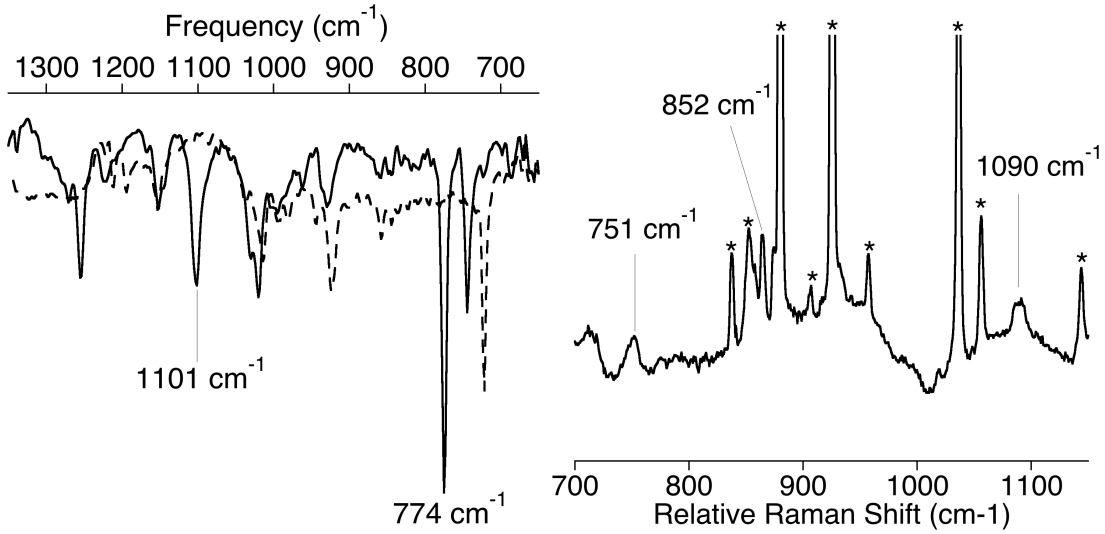

Figure 3.17. Solid state FTIR spectra of (^{Me2Hyd}Nac)Cu(2,6-dimethylnitrosobenzene) (*solid*) and (^{Me2Hyd}Nac)Cu(NCCH$_3$) (*dashed*) (*left)*. Resonance Raman spectrum of (^{Me2Hyd}Nac)Cu(2,6-dimethylnitrosobenzene) in THF (10 mM) with λ_{ex} = 568.1 nm. Peaks originating from THF are marked (*) (*right*).

In sum, the reactivity of (^{Me2Hyd}Nac)Cu(NCCH$_3$) towards 2,6-dimethylnitrosobenzene was examined and determined to yield a 1:1 adduct by a UV-vis spectrophotometric titration. The formation of this species was corroborated by ESI-MS and ^{1}H NMR spectroscopy. It was found to be diamagnetic and the ^{1}H NMR spectrum suggests the coordination of 2,6-dimethylnitrosobenzene to the copper-center. The ^{1}H NMR spectrum revealed an asymmetry in the nitroso-adduct as a result of a bound nitrosoaryl ligand without free rotation along the copper-ligand bond as observed by

inequivalent methyl groups in the ^{Me2Hyd}Nac ligand^{-}. Further characterization by resonance Raman and FTIR spectroscopies suggests the presence of a partially reduced 2,6-dimethylnitrosobenzene ligand with the N–O bond intact. Further vibrational studies with isotope labeling will be needed to confirm this along with structural analysis by X-ray crystallography. The X-ray structure of a copper-nitrosoaryl complex reported by Wiese *et al*. contained an η^2-bound nitrosoaryl metal bound ligand.[111] The ligand was bound to the copper ion by both oxygen and nitrogen atoms. This type of ligation is consistent with the ^{1}H NMR spectrum obtained for the reaction product of (^{Me2Hyd}Nac)Cu(NCCH$_3$) with 2,6-dimethylnitrosobenzene because such coordination would not allow for free rotation of the ligand resulting in a break in symmetry for the starting (^{Me2Hyd}Nac)Cu(NCCH$_3$) complex

3.3. Synthesis and Characterization of a Thermally Sensitive Cu/O$_2$ Species Supported by ^{Me2Hyd}Nac^{-}.

UV-vis spectroscopy. Oxygenation of (^{Me2Hyd}Nac)Cu(NCCH$_3$) in THF or acetone at –80 °C resulted in a rapid color change from pale yellow to a deep blue/green solution that was stable indefinitely at low temperature. The UV-vis spectra measured for the oxygenation (1 mM Cu(I), THF, –80 °C) are shown in Figure 3.18 with the starting complex (*dashed*), a transient species (*dotted*), and the final oxygenation product shown (*solid*). The transient species (Figure 3.18, *dotted*) forms instantaneously and gives way to the final species (Figure 3.18, *solid*) in seconds. The transient species has broad spectral features, with the most intense feature at λ_{max} = 740 nm but with additional significant spectral intensity near 630 nm. This species displays significant spectral

overlap with the stable product making it difficult to obtain relevant kinetic parameters for the product formation even using global analysis software. The stable intermediate displays two features with λ_{max} = 420 and 590 nm. Oxygenation of (^{Me2Hyd}Nac)Cu(NCCH$_3$) (1 mM, THF, –80 °C) in a short-path cuvette (0.2 cm) allowed for observation of more intense features below 400 nm (Figure 3.18, *right*). The starting Cu(I) complex has an intense absorption feature at λ_{max} = 345 nm that upon oxygenation gave way to an intense feature at λ_{max} = 328 nm and the two previously described features at 420 and 590 nm. The thermally stable intermediate nonetheless decayed completely at 10 °C over 2 h yielding a final spectrum that has a feature at λ_{max} = 310 nm (Figure 3.19, *left*). The decay of the feature at 328 nm did not follow first or second order kinetics suggesting the species decays by a complex pathway. ESI-MS analysis of the decayed product solution displayed only a peak assignable to the free unmodified ligand, ^{Me2Hyd}NacH.

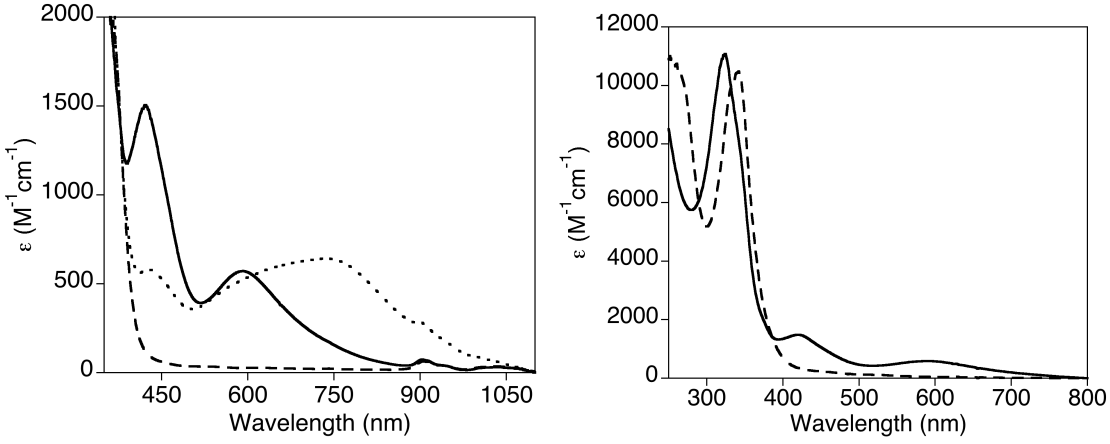

Figure 3.18. Oxygenation of (^{Me2Hyd}Nac)Cu(NCCH$_3$) (*dashed*) at –80 °C in THF (1 mM) in a 1 cm path length cuvette (*left*) and a 0.2 cm path length cuvette (*right*) with the final oxygenated product shown (*solid*).

Table 3.2. Summary of UV-Vis Spectroscopic Features of Reported $[Cu_3O_2]^{3+}$ Species.

Ligand	Species	Solvent	UV-vis, λ, nm (ε, M^{-1} cm^{-1}) per Cu	Ref
^{Me2Hyd}Nac	–	THF or Acetone	328(10700), 420(1500), 590(835)	This work
TMCD	$[Cu_3O_2]^{3+}$	CH_2Cl_2	290(4200), 355(5000), 480(470), 620(270)	113
TMEN	$[Cu_3O_2]^{3+}$	Acetone	345(4200), 500(440), 620(300)	115
^{H}Pyl^{Me,Me}	$[Cu_3O_2]^{3+}$	Acetone	342(4000), 515(333), 685(270)	114

A Beer's Law analysis of the intermediate species was conducted to determine accurate absorptivity (ε) values. A stock solution of (^{Me2Hyd}Nac)Cu($NCCH_3$) made in the glove box was serially diluted to known concentrations and oxygenated under the conditions described above. The absorptions at λ_{max} = 328, 420, and 590 nm were plotted against the concentrations to yield the data shown in Figure 3.19 (*right*). The ε values for each feature per copper were found to be 10700 $M^{-1}cm^{-1}$ (328 nm), 1500 $M^{-1}cm^{-1}$ (420 nm), and 835 $M^{-1}cm^{-1}$ (590 nm). The energies of the observed absorption features are similar to spectral features assigned to reported $[Cu_3O_2]^{3+}$ species although the ε values are more intense (Table 3.2).[113,114,115]

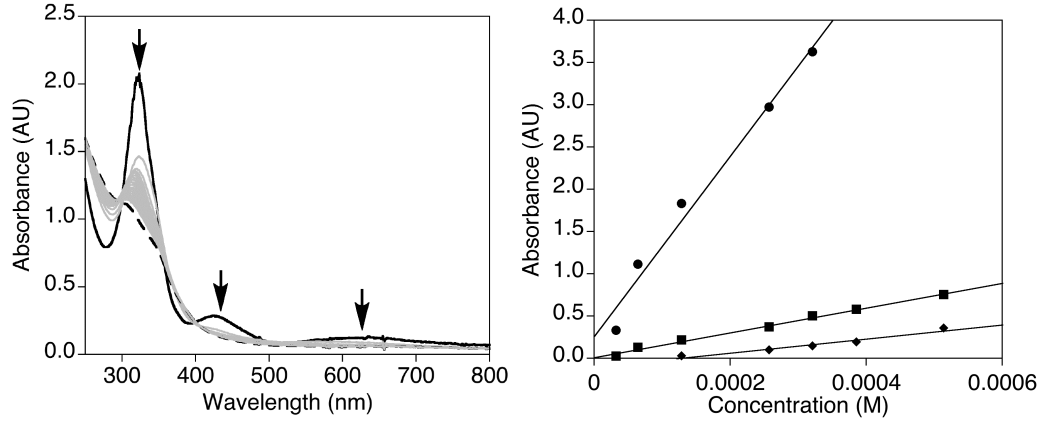

Figure 3.19. (left) Decay of (^{Me2Hyd}Nac)Cu(NCCH$_3$) at 10 °C in THF (1 mM) in a 0.2 cm path length cuvette (*right*)with intermediate spectra shown every 5 min. (*right*) Beers law plot of the oxygenation product of (^{Me2Hyd}Nac)Cu(NCCH$_3$) in THF at −80 °C. Features at 328 (*circles*), 420 (*squares*), and 590 nm (*diamonds*) are plotted.

A photometric titration was performed to determine the nuclearity (Cu:O ratio) of the intermediate. THF saturated with O_2 (10 mM)[116] was titrated into a known concentration of (^{Me2Hyd}Nac)Cu(NCCH$_3$) in THF at –80 °C (Figure 3.20). The spectral feature at 590 nm was monitored because it was the most resolved feature in the visible spectrum (Figure 3.20, *left*). The feature reaches a maximum intensity near 0.3 equivalents of O_2 per copper atom. The titration data suggests the intermediate is a multinuclear species with a higher nuclearity than in the typically observed $[Cu_2O_2]^{2+}$ species as described in Chapter 2, which contain 0.5 equivalents of O_2 per copper complex. The complete formation of the intermediate species by addition of approximately 0.3 equivalents of O_2 per copper is most consistent with a $[Cu_3O_2]^{3+}$ core (0.33 equivalents of O_2 per copper). $[Cu_3O_2]^{3+}$ species have been previously reported but are more rare than $[Cu_2O_2]^{2+}$ species in the literature.[88,113,114,115]

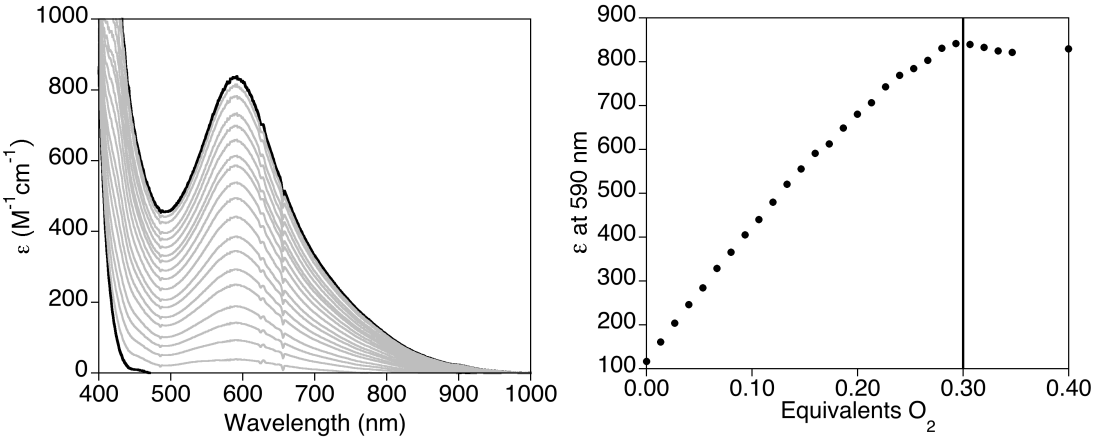

Figure 3.20. Photometric titration of O_2-saturated THF (10 mM) into a 10 mM solution of (^{Me2Hyd}Nac)Cu(NCCH$_3$) in THF at –80 °C (0.2 mm path length cell) (*left*). The growth of the spectral feature at λ_{max} = 590 nm is plotted against the number of equivalents of O_2 per Cu-atom (*right*).

^{1}H NMR Spectroscopy. The ^{1}H NMR spectrum for the oxygenated product of (^{Me2Hyd}Nac)Cu(NCCH$_3$) was obtained (Figure 3.21, *solid*) and is shown overlaid with the spectrum for the starting (^{Me2Hyd}Nac)Cu(NCCH$_3$) complex at –80 °C in THF (Figure 3.21, *dashed*). Upon oxygenation the features previously assigned to (^{Me2Hyd}Nac)Cu(NCCH$_3$) (Figure 3.21, a, b, c, and d) all gave way to one non-solvent feature at 2.32 ppm (Figure 3.21, b'). This peak integrated to three protons with respect to an internal standard of 1,3,5-trimethoxybenzene and was assigned to the displaced acetonitrile ligand.[112] The sweep width was expanded revealing the presence of broad peaks above 10 ppm (Figure 3.21, *right*) that are likely due to the presence of a paramagnetic species. This result prompted us to explore magnetic susceptibility experiments to determine the electronic character of this species.

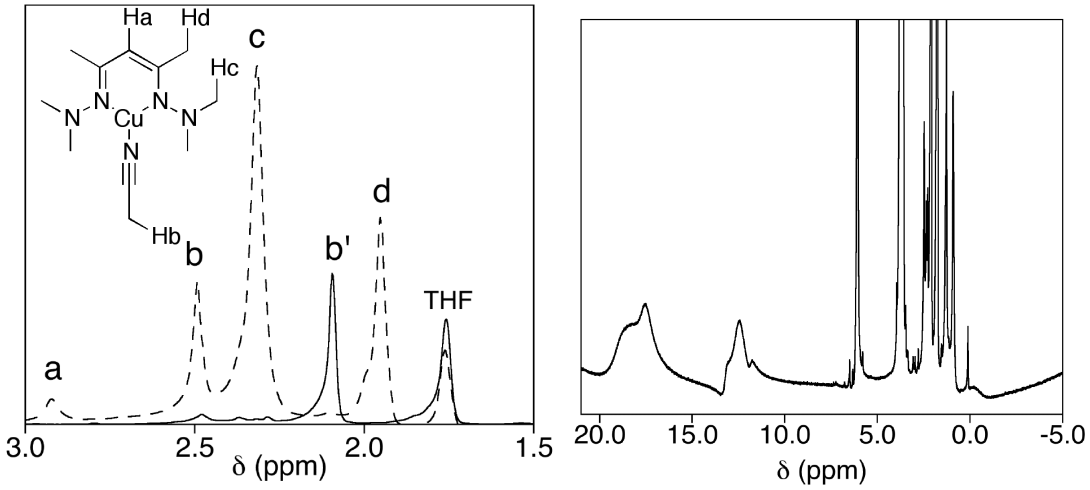

Figure 3.21. (left) The ^{1}H NMR spectrum for the oxygenated product of (^{Me2Hyd}Nac)Cu(NCCH$_3$) (*solid*) shown overlaid with the spectrum for the starting (^{Me2Hyd}Nac)Cu(NCCH$_3$) at –80°C in THF(*dotted*). (*right*) Expanded ^{1}H NMR spectrum of the oxygenated product of (^{Me2Hyd}Nac)Cu(NCCH$_3$) displaying peaks originating from a paramagnetic species.

The spin state of the observed intermediate derived from oxygenation of (^{Me2Hyd}Nac)Cu(NCCH$_3$) was determined using the Evans method.[117,118,119,120] A 54 mM solution of (^{Me2Hyd}Nac)Cu(NCCH$_3$) was oxygenated in d_8-THF at –80 °C along with an internal standard 1,3,5-trimethoxybenzene to yield a final concentration of 18 mM for (^{Me2Hyd}Nac)$_3$Cu$_3$(O)$_2$. A coaxial ^{1}H NMR spectroscopy insert was loaded with d_8-THF and 1,3,5-trimethoxybenzene and placed within the tube containing the oxygenated species and 1,3,5-trimethoxybenzene in d_8-THF. The region between 5-7 ppm for the ^{1}H NMR spectrum acquired at –80 °C with the coaxial ^{1}H NMR tube is shown (Figure 3.22). The two observed peaks, H_a and H_a', are both from the aryl proton of 1,3,5-trimethoxybenzene with the H_a originating from the sample chamber containing the paramagnetic species. From the peak positions, the shift in frequency ($\delta\nu$) is determined to be 114.3 Hz. Using equation (1) where ν_0 is the operating frequency of the NMR

spectrometer, C is the concentration of the complex (mol cm^{-3}), M_w is the molecular weight of the complex, and χ_0 is the mass susceptibility of the solvent we can determine the mass susceptibility of the complex (χ_p).[120] The mass susceptibility of the intermediate was determined to be 7 x 10^{-5} cm^3 g^{-1}. Equation (2) was used to determine the effective magnetic moment (μ_{eff}) from χ_p where T is the temperature in Kelvin. From this equation we find μ_{eff} = 2.8(1) T J^{-1} and using equation (3) where g is the magnetic moment of an electron[121] and S is the total spin we find this is consistent with two unpaired electrons or a triplet ground state, which ideally has a μ_{eff} of 2.83 T J^{-1}.[122] A triplet ground state is consistent with the assignment of the intermediate species as the trinuclear complex, $(^{Me2Hyd}Nac)_3Cu_3(O)_2$. A previously reported trinuclear $[Cu_3O_2]^{3+}$ core was assigned as a localized mixed valent Cu(III)Cu(II)Cu(II) cluster bridged by two μ_3-oxo ligands with a triplet S = 1 ground state.[113,123,124] A $[Cu_3O_2]^{3+}$ complex reported by Cole *et al*. was studied by the Evans method and determined to have a μ_{eff} = 2.9 T J^{-1}, similar to the value obtained with our system.[113] Our ^{1}H NMR spectroscopy data are consistent with our photometric titration data that suggest a Cu_3/O_2 species and our assignment of the intermediate species as $(^{Me2Hyd}Nac)_3Cu_3(O)_2$.

$$(1)\ \chi_p = -3\delta\nu/4\pi\nu_0 C M_w + \chi_0$$

$$(2)\ \mu_{eff}^2 = 8\chi_p M_w T$$

$$(3)\ \mu_{eff}^2 = g^2 S(S+1)$$

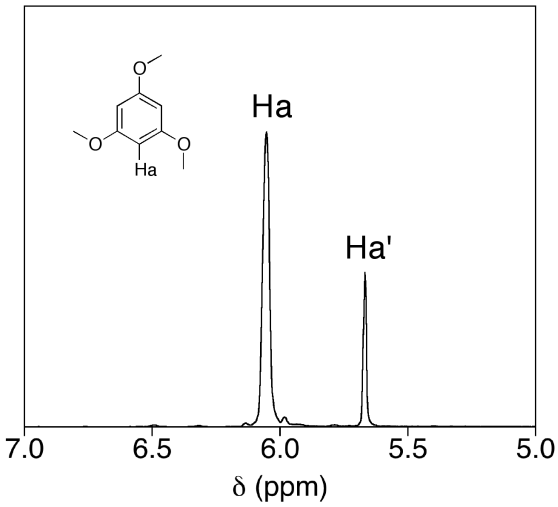

Figure 3.22. ^{1}H NMR spectrum of 1,3,5-trimethoxybenzene in d_8-THF at –80 °C in a coaxial NMR tube with one chamber containing the intermediate derived from the oxygenation of (^{Me2Hyd}Nac)Cu(NCCH$_3$). The peak labeled H$_a$ is assigned to the aryl-proton from the 1,3,5-trimethoxybenzene in solution with the intermediate and the peak labeled H$_{a'}$ originating from a solution of 1,3,5-trimethoxybenzene without the intermediate.

EPR spectroscopy was used to further characterize the electronic nature of the intermediate derived from the oxygenation of (^{Me2Hyd}Nac)Cu(NCCH$_3$). EPR spectra were measured in parallel mode to evaluate the S = 1 assignment from the Evans method data. The parallel mode EPR spectrum of the intermediate species is shown (Figure 3.23) with the g ~ 4 region enlarged and shown in the inset. The feature observed at ~ 1500 G is likely a $\Delta m_s = 2$ transition and the high field signal at ~ 3300 G is the $\Delta m_s = 1$ transition, consistent with what would be expected for a triplet ground state species.[123,125] Machonkin *et al*. reported the EPR spectrum for a triplet $[Cu_3O_2]^{2+}$ species that contained a strong derivative feature at 3525 G and a $\Delta m_s = 2$ transition at 1400 G.[123]These values are consistent with our assignment of the observed intermediate as a S = 1 triplet species.

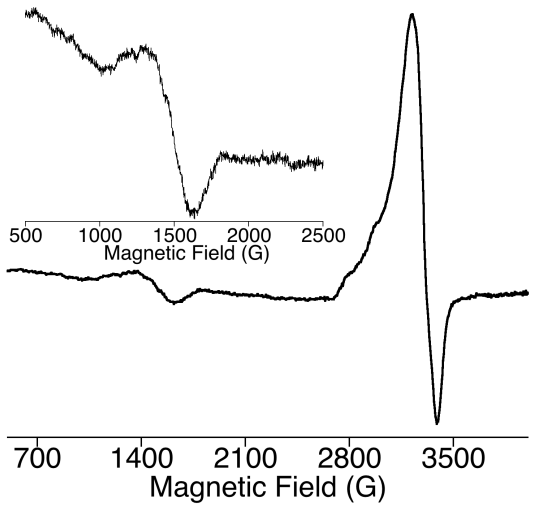

Figure 3.23. X-Band EPR spectrum of the oxygenation product of (^{Me2Hyd}Nac)Cu(NCCH$_3$) (60 mM) in THF in the parallel mode at 13 K. The inset displays an expand view of the $g \sim 4$ region.

Resonance Raman Spectroscopy. Resonance enhanced Raman spectroscopy was used to probe the structural nature of the oxygenated species. Samples of (^{Me2Hyd}Nac)Cu(NCCH$_3$) were oxygenated in THF, degassed, and frozen in liquid nitrogen for analysis. An exhaustive screening of excitation wavelengths and sample concentrations did not yield any non-solvent features with the exception of samples examined using λ_{ex} = 568.1 nm. These spectra displayed a non-solvent feature at 1000 cm^{-1} but this feature did not shift when the sample was prepared with $^{18}O_2$ (Figure 3.24). The lack of isotope sensitivity for the observed resonance Raman feature at 1000 cm^{-1} makes its assignment as originating from a copper-oxygen vibration unlikely. This feature falls between two regions that have been previously reported for copper-oxygen complex O–O stretches including Cu(II)-superoxo species (~1100 cm^{-1}) and Cu(III)-peroxo species (~970 cm^{-1}).[126,127] In contrast to species containing O–O bonds, the

reported $[Cu_3O_2]^{3+}$ species lacks an O–O bond so a vibration corresponding to an O–O stretching frequency in this or any region would be unexpected. To date, no resonance Raman spectroscopy characterization of a $[Cu_3O_2]^{3+}$ species has been reported.[113,114,115] We hypothesize that the feature at 1000 cm^{-1} shown in Figure 3.24 originates from a ligand based vibration and not from the postulated $[Cu_3O_2]^{3+}$ core.

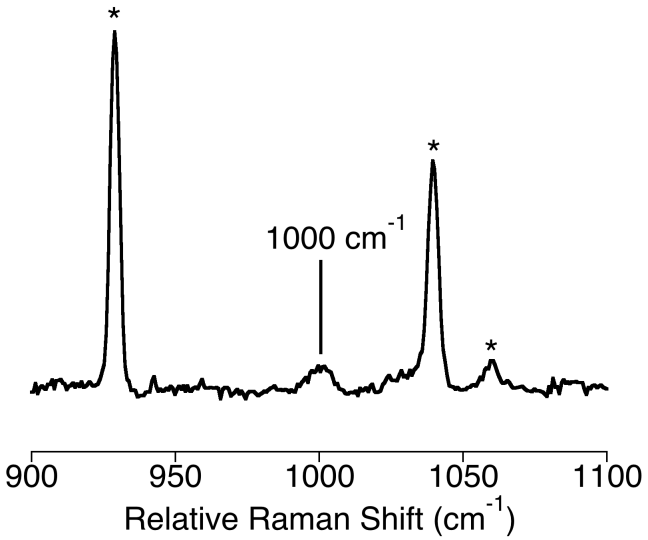

Figure 3.24. Resonance Raman spectrum of the oxygenated product of (^{Me2Hyd}Nac)Cu($NCCH_3$) in THF (10 mM) with λ_{ex} = 568.1 nm and peaks originating from solvent marked (*).

Attempts to Grow Crystals. Without clear resonance Raman data, a definitive structural assignment of the observed intermediate as (^{Me2Hyd}Nac)$_3Cu_3(O)_2$ is difficult to make. Attempts to grow crystals of the intermediate at –80 °C using numerous solvent systems and crystallization methods did not yield crystals suitable for X-ray analysis. Concentrated THF or acetone solutions of the oxygenated product of (^{Me2Hyd}Nac)Cu($NCCH_3$) retained their characteristic blue/green color indefinitely while stored at –80 °C, but no solid material was observed after several months. THF/pentane

solutions were examined at ratios up to a 1:5 THF/pentanes that also retained the characteristic color of the intermediate species for several weeks with no observed crystalline material. A fine amber solid/precipitate was observed in some samples but never in isolable amounts. Solvent layering and slow solvent diffusion were also attempted in efforts to grow crystals of the intermediate with THF/pentanes and THF/tetramethylsilane, but these methods only yielded micro-crystals that had sub-micron scale dimensions that were too small for crystallographic analysis.

The oxygenation reaction was examined in THF/toluene mixtures and sluggish oxygenation rates were observed at high toluene concentrations. Oxygenated solutions of (^{Me2Hyd}Nac)Cu($NCCH_3$) 3:7 toluene/THF yielded colorless crystals after several weeks at –80 °C. These crystals were treated and mounted as thermally sensitive crystals (See experimental section) and analyzed by X-ray crystallography. Unfortunately these crystals were found to be unreacted Cu(I) complex, (^{Me2Hyd}Nac)Cu($NCCH_3$) described in Section 3.2.3 (Figure 3.6, See Table 3.1 for full crystallographic details).

ESI-MS. With no crystallographic evidence to aid in a structural assignment of the intermediate species, we turned to ESI-MS analysis. Oxygenated solutions of (^{Me2Hyd}Nac)Cu($NCCH_3$) were first examined by ESI-MS in neat THF. The starting sample solution was kept at –78 °C and the sample transfer tube that is typically used to introduce an ESI-MS sample was removed to minimize sample warming/decomposition and maximize the peak intensities of the species of interest. Initial spectra did not display any signal in either the positive or negative ion detection modes, indicating that no easily ionizable species were present under these conditions. Oxygenated solutions of

(^{Me2Hyd}Nac)Cu(NCCH$_3$) in acetone also did not yield any observable species by ESI-MS analysis. Samples doped with methanol lost their characteristic blue/green color when warmed and displayed a strong peak envelope at m/z = 429.2640 in the ESI-MS spectrum (Figure 3.25, *left*). This feature was simulated with the formula [(^{Me2Hyd}Nac)$_2$Cu]$^+$ (Figure 3.25, *right*) and appears to be the final decomposed copper-containing product.

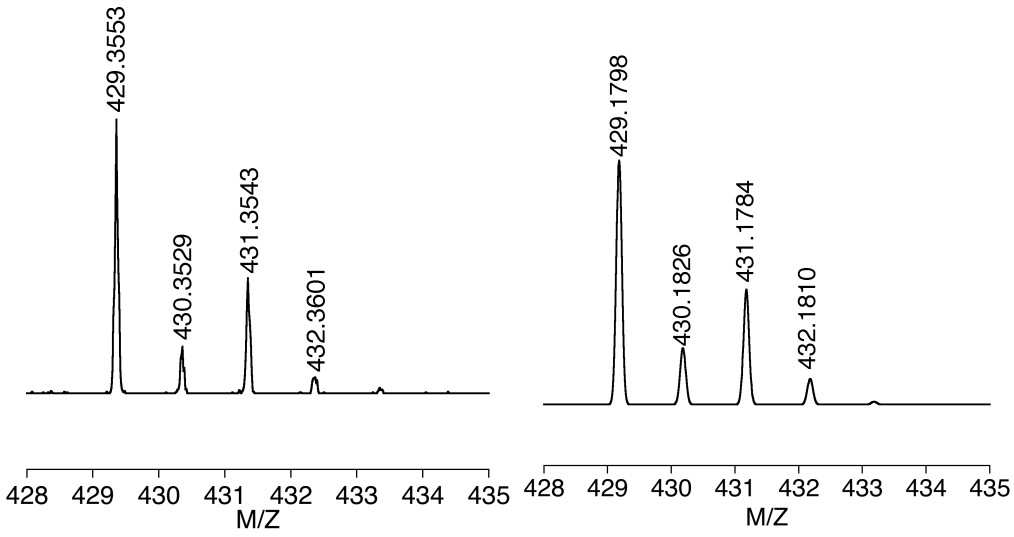

Figure 3.25. The experimentally obtained (*left*) and simulated (*right*) ESI-MS spectra showing the peak envelope assigned to the species of the formula [(^{Me2Hyd}Nac)$_2$Cu]$^+$.

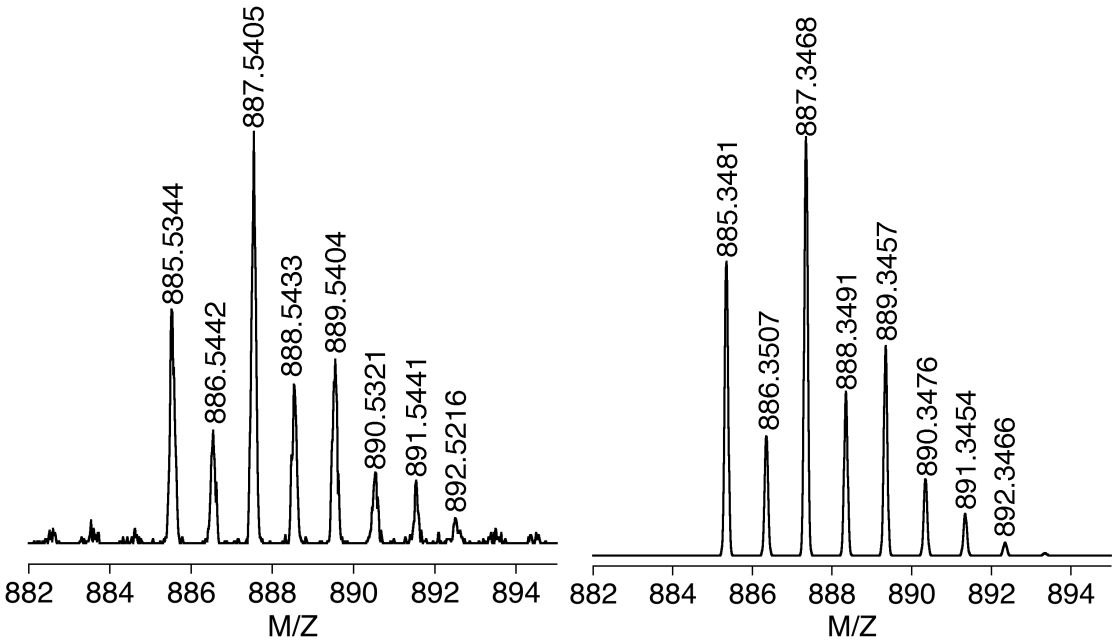

Figure 3.26. The experimentally obtained (*left*) and simulated (*right*) ESI-MS spectra showing the peak envelope assigned to the species of the formula $[(^{Me2Hyd}Nac)_3Cu_3(O)_2 + MeOH + (NCCH_3)_2 + H^+]^+$.

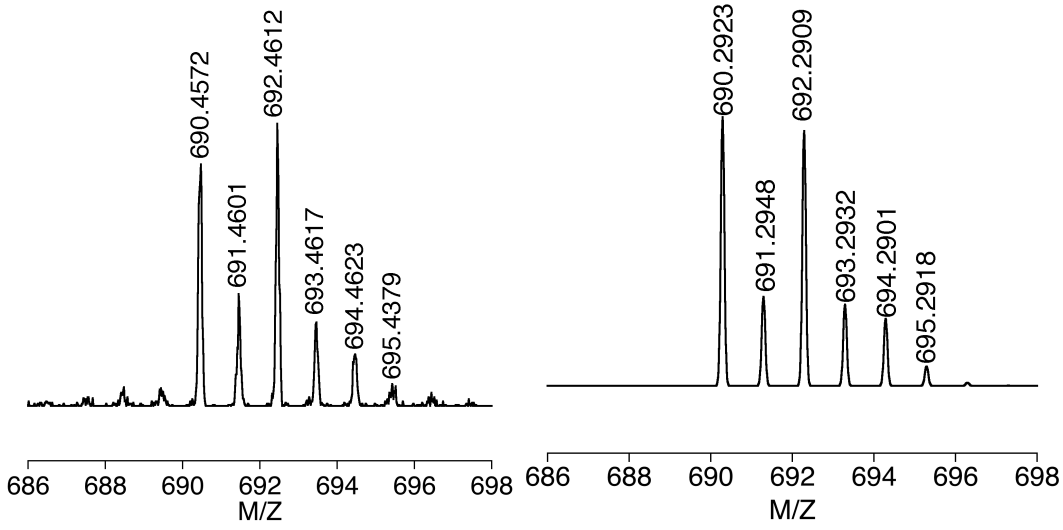

Figure 3.27. The experimentally obtained (*left*) and simulated (*right*) ESI-MS spectra showing the peak envelope assigned to a $[(^{Me2Hyd}Nac)_2Cu_2(OH)_2 + (NCCH_3)_4]^+$ species.

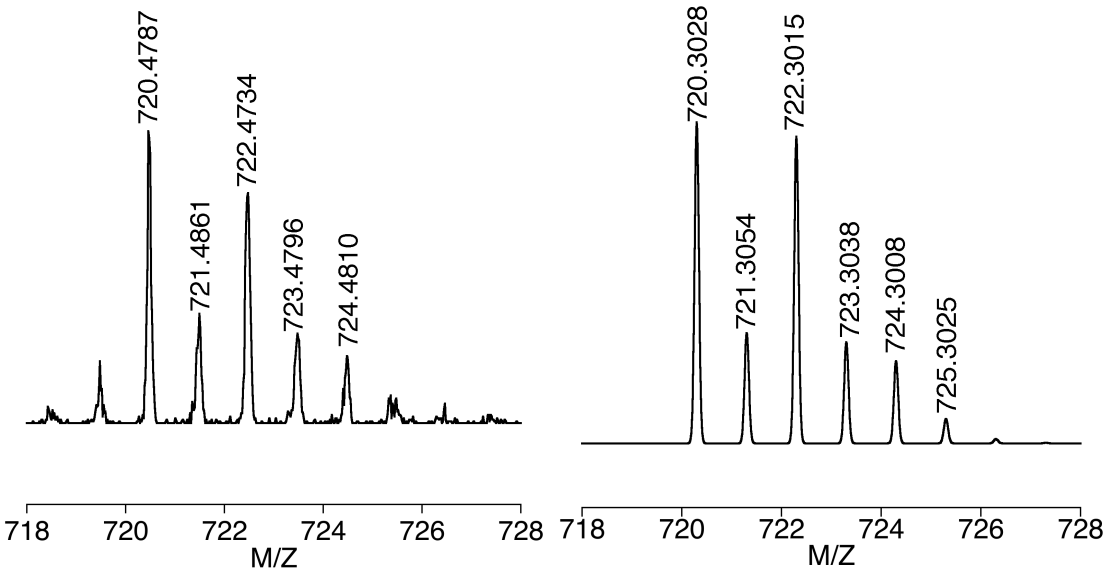

Figure 3.28. The experimentally obtained (*left*) and simulated (*right*) ESI-MS spectra showing the peak envelope assigned to the species of the formula $[(^{Me2Hyd}Nac)_2Cu_2(O)_2 + MeOH + (NCCH_3)_4]^+$.

An ESI-MS spectrum obtained by first loading a 100 μL sample syringe with 40 μL of an acetone solution of the intermediate species, followed by 60 μL MeOH, and rapidly injecting the solution into the spectrometer yielded several new copper containing peak envelopes at m/z = 690.4572, 720.4787, and 885.5344. These three peak envelopes displayed isotope patterns indicative of multiple copper atoms and their assignments based on simulations are discussed below.

The highest mass peak envelope at 885.5344 m/z displays an isotope pattern assigned to a tricopper species (Figure 3.26, *left*). The peak envelope was simulated with the formula $[(^{Me2Hyd}Nac)_3Cu_3(O)_2 + MeOH + (NCCH_3)_2 + H^+]^+$ with the MeOH molecule originating from the solvent and acetonitrile from the starting Cu(I) complex (Figure 3.26). Copper has two naturally occurring isotopes, ^{63}Cu and ^{65}Cu, that occur in 69.17 and 30.82% abundances, respectively. Copper complexes that are observed by mass

spectrometry techniques display peak envelopes that contain a peak for the exact mass $[M]^+$ and a $[M+2]^+$ in a ratio representative of the naturally occurring copper isotopes. When multiple copper atoms are present in a species, the relative intensities of the peaks in the peak envelope are indicative of the number of copper atoms present. The simulated spectrum in Figure 3.26 was generated from a species containing three copper atoms and the characteristic isotope pattern is identical to that observed in the experimental spectrum. To the best of our knowledge, this is the first example of the ESI-MS observation of a trinuclear $[Cu(III)Cu(II)_2]^{3+}$species. This result corroborates the conclusions based on UV-vis and ^{1}H NMR spectroscopy that the intermediate may be formulated as $(^{Me2Hyd}Nac)_3Cu_3(O)_2$.

Two additional copper-containing peak envelopes in the ESI-MS spectrum are likely due to the decomposition of $(^{Me2Hyd}Nac)_3Cu_3(O)_2$ in the instrument. Features at m/z = 690.4572 and 720.4787 both display isotope patterns characteristic of a dicopper species (Figures 3.27 and 3.28). The feature at m/z = 690.4572 was simulated with the formula $[(^{Me2Hyd}Nac)_2Cu_2(OH)_2 + (NCCH_3)_4]^+$ and the feature at m/z = 720.4787 was simulated with the formula $[(^{Me2Hyd}Nac)_2Cu_2(O)_2 + MeOH + (NCCH_3)_4]^+$. The $(^{Me2Hyd}Nac)_2Cu_2(O)_2$ species is likely derived from the loss of a Cu(I) fragment from the $[Cu_3O_2]^{3+}$ core and the $(^{Me2Hyd}Nac)_2Cu_2(OH)_2$ species resembles the H-atom abstraction product of $(^{Me2Hyd}Nac)_2Cu_2(O)_2$. No other experimental evidence for these two species has been obtained to date suggesting that the high temperatures required for ionization generated these two species.

The ESI-MS experiments presented above revealed a peak envelope assignable to

the trinuclear (^{Me2Hyd}Nac)$_3$Cu$_3$(O)$_2$ species. This strongly suggests that the oxygenation product of (^{Me2Hyd}Nac)Cu(NCCH$_3$) is (^{Me2Hyd}Nac)$_3$Cu$_3$(O)$_2$. This assignment is consistent with the UV-vis spectrum, photometric titration, magnetic susceptibility data, and EPR spectrum, and explains the difficulty in obtaining meaningful vibrational data by resonance Raman spectroscopy.

Hydrogen Peroxide Detection. Cole *et al.* reported a $[Cu_3O_2]^{3+}$ species that was characterized by X-ray crystallography that contained a long O–O distance of 2.37 Å confirming the full four electron reduction and bond cleavage of the O–O bond.[113] To support the identification and assignment of the copper-oxygen species derived from (^{Me2Hyd}Nac)Cu(NCCH$_3$) and O_2 as (^{Me2Hyd}Nac)$_3$Cu$_3$(O)$_2$, we sought to confirm the cleavage of the O–O bond and to rule out a Cu-peroxide species as the observed intermediate. To accomplish this we attempted to detect hydrogen peroxide upon the decay of the intermediate under controlled acidic conditions with Ti(IV)oxysulfate. If a peroxide species is present, its decay in the presence of a proton source results in the liberation of hydrogen peroxide, as previously demonstrated in the literature.[128] The free hydrogen peroxide is then photometrically detected by addition of Ti(IV)oxysulfate, which reacts with the hydrogen peroxide to form an intense chromophore (λ_{max} = 408 nm) that is detected and quantified by UV-vis spectroscopy.[128] The concentration of hydrogen peroxide is quantified using a standard curve generated by the serial dilution of known concentrations of hydrogen peroxide with Ti(IV)oxysulfate (Figure 3.29, *left*).

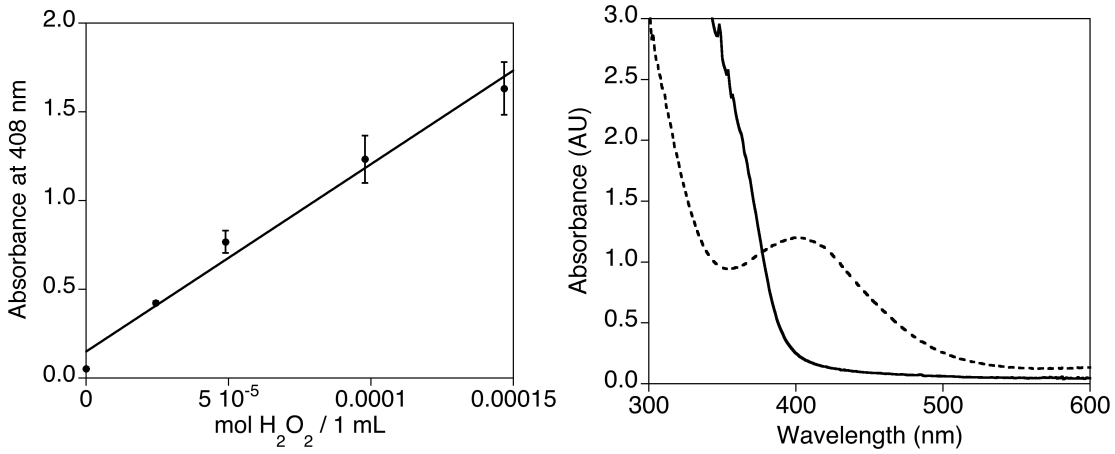

Figure 3.29. (*left*) Standard curve of a titration of Ti(IV)oxysulfate with H_2O_2 monitored by the intensity of a chromophore at λ_{max} = 408 nm. Each data point is the average intensity of three separate runs with the error bars representing the standard deviation. (*right*) UV-vis spectra of the decomposition products of trans-μ-1,2-peroxo-dicopper(II)$(TMPA)_2OTf_2$ (*dotted*) and $(^{Me2Hyd}Nac)_3Cu_3(O)_2$ (*solid*) after addition of Ti(IV)oxysulfate.

A control experiment was initially run to validate the experimental method for detection of H_2O_2 starting with a previously reported trans-μ-1,2-peroxo-dicopper(II) species supported by the TMPA ligand.[97b] Oxygenation of $(TMPA)Cu(NCCH_3)OTf$ in THF at –80 °C resulted in the formation of a characteristic purple solution confirming the formation of the desired trans-μ-1,2-peroxo-dicopper(II) species. Formic acid (2.4 equivalents per dicopper species) was added and the solution warmed to room temperature. Addition of Ti(IV)oxysulfate and quantification of the chromophore observed at λ_{max} = 408 nm (Figure 3.29, *right, dotted*) to a standard curve showed the recovery of 79% of the expected amount hydrogen peroxide, confirming the validity of the detection method. Extending this technique to the current intermediate supported by $^{Me2Hyd}Nac^-$ resulted in a final spectrum that did not display a chromophore at λ_{max} = 408 nm. Thus, the intermediate species apparently does not contain a peroxide ligand. The

lack of hydrogen peroxide generation is consistent with its assignment as $(^{Me2Hyd}Nac)_3Cu_3(O)_2$.

Formation of $(^{Me2Hyd}Nac)_3Cu_3(O)_2$ by Oxo-Transfer. The formation of $(^{Me2Hyd}Nac)_3Cu_3(O)_2$ was next explored by oxo-transfer rather than O_2 reduction and O–O bond cleavage. The formation of a copper-oxygen species by oxo-transfer was recently demonstrated by our group in the synthesis of a bis(μ-oxo)dicopper(III) species from a Cu(I) complex and trimethylamine oxide (TMAO).[51] The observed bis(μ-oxo)dicopper(III) species was spectroscopically identical to one formed from the Cu(I) complex and O_2. The observed and characterized bis(μ-oxo)dicopper(III) species was supported by a β-diketiminate ligand so we reasoned that we could form $(^{Me2Hyd}Nac)_3Cu_3(O)_2$ by oxo-transfer.

The reaction between $(^{Me2Hyd}Nac)Cu(NCCH_3)$ and TMAO was first examined.[51] Solutions of $(^{Me2Hyd}Nac)Cu(NCCH_3)$ in THF were cooled to –80 °C and TMAO was added by syringe in THF and the reaction monitored by UV-vis spectroscopy. No spectral changes were observed under these conditions suggesting no reaction had taken place. The reaction was warmed to room temperature while being continuously monitored by UV-vis spectroscopy. No observable spectral change other than baseline drifting was observed.

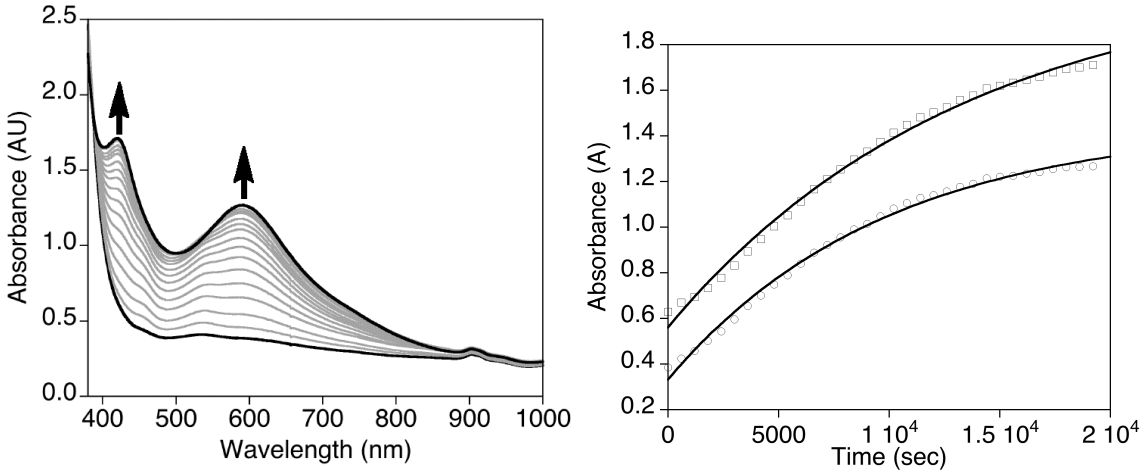

Figure 3.30. UV-vis spectra of a reaction of (^{Me2Hyd}Nac)Cu(NCCH$_3$) (1 mM, THF, –50 °C) with PhIO (*left*) with the kinetic trace of the growth of features at 420 and 590 nm (*left*). The growth of each feature was modeled as a 1st order exponential growth $A_1 + A_2$*exp(–*kt*) with A values corresponding to correction values, *t* representing time, and *k* the rate constant.

Table 3.3. Rate constants for the formation of (^{Me2Hyd}Nac)$_3$Cu$_3$(O)$_2$ from reactions between (^{Me2Hyd}Nac)Cu(NCCH$_3$) and PhIO.

Temperature (°C)	k_{obs} at 420 nm (s^{-1}) (R)	k_{obs} at 590 nm (s^{-1}) (R)
–40	9.05 x 10^{-5} (0.997)	1.17 x 10^{-4} (0.999)
–50	7.52 x 10^{-5} (0.997)	1.03 x 10^{-4} (0.997)
–60	4.12 x 10^{-5} (0.997)	7.28 x 10^{-5} (0.997)

A stronger oxidant, iodosobenzene, was reacted with (^{Me2Hyd}Nac)Cu(NCCH$_3$) at a range of low temperatures (–40 to –60 °C). The insolubility of iodosobenzene in nearly all solvents led to a minor experimental alteration with respect to the previously described oxygenation experiments. PhIO was measured and put directly into a quartz UV-vis cuvette, solvent added, and the cuvette sealed with a septum. This ensured the desired amount of PhIO was introduced into the reaction, albeit as a slurry, rather than residual reagent remaining in a transfer syringe. The mixture was cooled to the desired temperature under an argon purge and the Cu(I) complex added to the solution by syringe

to yield a final Cu(I) concentration in the cell of 1 mM. The reaction was monitored by UV-vis spectroscopy and revealed the formation of two spectroscopic features at λ_{max} = 420 and 590 nm over several hours (Figure 3.30, *left*). The growth of both features were monitored over time and a respective kinetic trace is shown in Figure 3.30 (*right*). The increase in intensity at both λ_{max} = 420 and 590 nm was modeled by a first-order exponential equation with the rate constants k = 7.55 x 10^{-5} and 1.03 x 10^{-4} s^{-1}, respectively, for the reaction at –50 °C. The rate constants for the growth of each feature at three reaction temperatures are shown in Table 3.3. The reaction of (^{Me2Hyd}Nac)Cu($NCCH_3$) with PhIO is sluggish with the representative reaction at –50 °C shown above taking over 5 h to near completion (Figure 3.30). The reaction rate of (^{Me2Hyd}Nac)Cu($NCCH_3$) with PhIO is in stark contrast with reactions of the complex with O_2, which occur almost instantaneously with trace amounts of O_2. The slow formation of (^{Me2Hyd}Nac)$_3$Cu$_3$(O)$_2$ from PhIO and (^{Me2Hyd}Nac)Cu($NCCH_3$), as indicated by small rate constants, is likely due to the poor solubility of PhIO in almost all solvents. The dissolution of PhIO is probably the rate limiting process and this process rather than the reaction of PhIO with the Cu(I) complex is likely represented by the rate constants obtained. The photometric titration of PhIO/Cu(I) was not done due to the experimental difficulties associated with the accurate measurement of the amount of PhIO added (poor solubility).

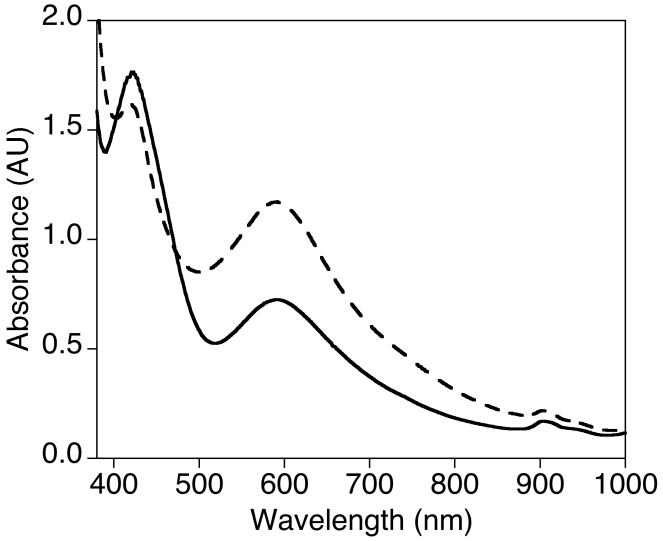

Figure 3.31. UV-vis spectra of the reaction products of (^{Me2Hyd}Nac)$_2$Cu(NCCH$_3$) with O_2 (*solid*) or PhIO (*dashed*) in THF at –80 °C (1 mM).

An overlay of the product formed from the reactions of (^{Me2Hyd}Nac)Cu(NCCH$_3$) with O_2 (Figure 3.31, *solid*) and with PhIO (Figure 3.31, *dotted*) shows that the energy of the features (λ_{max} = 420 and 590 nm) are identical although the relative intensities do vary somewhat (Figure 3.31). Remarkably, it appears that (^{Me2Hyd}Nac)$_3$Cu$_3$(O)$_2$ forms from the reaction of (^{Me2Hyd}Nac)Cu(NCCH$_3$) and PhIO. To the best of our knowledge, no isolable copper-oxygen intermediate species has been reported from the reaction of a Cu(I) complex and PhIO.[40,41,51,129] ESI-MS analysis was attempted on the intermediate derived from PhIO but has been unsuccessful and only decayed product, a peak envelope at m/z = 429 assigned to [(^{Me2Hyd}Nac)$_2$Cu]$^+$ (Section 3.3.4), was observed. We attribute this finding to technical difficulties. Samples analyzed by ESI-MS cannot contain precipitates, so filtration of the mixtures from reactions of (^{Me2Hyd}Nac)Cu(NCCH$_3$) with PhIO is required due to the presence of small amounts of insoluble PhIO. The warming that results from passing the reaction mixture over a filtration frit instantaneously causes

a color change from deep green, characteristic of (^{Me2Hyd}Nac)$_3$Cu$_3$(O)$_2$ described in previous sections, to a yellow brown color characteristic of the decomposed product solution.

3.4 Reactivity of (^{Me2Hyd}Nac)$_3$Cu$_3$(O)$_2$

In this section the reactivity of (^{Me2Hyd}Nac)$_3$Cu$_3$(O)$_2$ towards exogenous substrates will be presented. The reactivities of two $[Cu_3O_2]^{3+}$ species, reported by Cole *et al.* and Taki *et al.*, supported by either *N,N,N',N'*-(*1R,2R*)-cyclohexane-diamine (TMCD) or *N,N*-di(methyl)-2-(2-pyridyl)-ethylamine (^{H}Pyl^{Me,Me}) have only been examined towards a limited number of substrates.[113,114] The TMCD supported $[Cu_3O_2]^{3+}$ species was reduced by ferrocene at –80 °C and both TMCD and ^{H}Pyl^{Me,Me} supported species reacted with 2,4-di-*tert*-butylphenol via a radical pathway to form the coupled 3,3',5,5'-tetra-*tert*-butyl-2,2'-biphenol in high yield (> 97%).[113,114,115] We looked to expand on the known reactivity of $[Cu_3O_2]^{3+}$ cores and to determine if any differences in reactivity existed for a $[Cu_3O_2]^{3+}$ core supported by the anionic ^{Me2Hyd}Nac$^-$ versus the reported neutral TMCD and ^{H}Pyl^{Me,Me} ligands.

3.4.1 Reactivity of (^{Me2Hyd}Nac)$_3$Cu$_3$(O)$_2$ Towards Exogenous Substrates

Solutions of (^{Me2Hyd}Nac)$_3$Cu$_3$(O)$_2$ were generated by the oxygenation of (^{Me2Hyd}Nac)Cu(NCCH$_3$) in THF at –80 °C (1 mM) and monitored by UV-vis spectroscopy to ensure the complete formation of the desired intermediate. Upon formation of the intermediate the samples were purged with argon for approximately 20 min to remove excess O_2. Substrates were introduced at –80 °C and stirred for 2 h while

the reactions were monitored by UV-vis spectroscopy. Samples were then gradually warmed to room temperature and examined by GC-MS or ^{1}H NMR spectroscopy after an acidic workup to remove copper containing species. Samples examined by ^{31}P NMR were prepared in deuterated solvent and analyzed directly after samples were warmed to room temperature.

The H-atom abstraction ability of $(^{Me2Hyd}Nac)_3Cu_3(O)_2$ was first examined through studies of reactions with phenols and weak C–H bonds. Three phenols, 2,4-di-*tert*-butylphenol, 2,6-di-*tert*-butylphenol, and 2,4,6-tri-*tert*-butylphenol were examined. $(^{Me2Hyd}Nac)_3Cu_3(O)_2$ did not react with any of the selected phenols. No coupled products were observed for 2,4-di-*tert*-butylphenol and 2,6-di-*tert*-butylphenol, and no phenoxyl radical was seen for 2,4,6-tri-*tert*-butylphenol, the expected oxidation/H-atom abstraction products for these substrates. This reactivity is different than that reported for $[Cu_3O_2]^{3+}$ species supported by neutral N-donor ligands, which gave > 97% yields for the oxidation of 2,4-di-*tert*-butylphenol.[113,114] The lack of reactivity towards exogenous phenols suggests that $(^{Me2Hyd}Nac)_3Cu_3(O)_2$ is a poor hydrogen atom abstraction reagent. The phenols examined have O–H bond energies between 82–85 kcal/mol so a substrate with a weaker oxidizable bond, 9,10-dihydroanthracene was examined (C–H BDE = 78 kcal/mol).[130] The H-atom abstraction product of 9,10-dihydroanhracene is anthracene, which has characteristic UV-vis spectroscopy features at λ_{max} = 340, 360, and 375 nm.[131] Reactions of $(^{Me2Hyd}Nac)_3Cu_3(O)_2$ with 9,10-dihydroanthracene did not display any anthracene by UV-vis spectroscopy at –80 °C or GC-MS analysis after warming to room temperature.

We next examined the ability to reduce $(^{Me2Hyd}Nac)_3Cu_3(O)_2$ by one or more electrons with ferrocene or decamethylferrocene. Addition of excess ferrocene or decamethylferrocene to $(^{Me2Hyd}Nac)_3Cu_3(O)_2$ at –80 °C in THF did not result in the decay of its UV-vis spectral features. This result indicates the robustness of this species towards reduction and is consistent with its poor oxidation capability towards exogenous phenols or 9,10-dihydroanthracene. In contrast, the $[Cu_3O_2]^{3+}$ species reported by Cole *et al*. was reduced by ferrocene at –80 °C. We surmise that $(^{Me2Hyd}Nac)_3Cu_3(O)_2$ has an oxidation potential more negative than that of $(TMCD)_3Cu_3(O)_2OTf_3$, which was assigned to be between 0.48 and 0.79 V.[113]

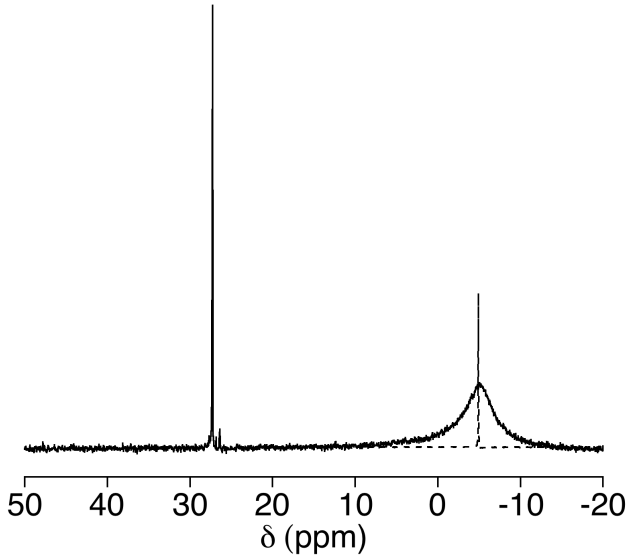

Figure 3.32. ^{31}P NMR spectra of PPh_3 (*dashed*) and of the reaction between $(^{Me2Hyd}Nac)_3Cu_3(O)_2$ and 1 equivalent of PPh_3 (per starting Cu(I) complex) in d_8-THF.

We next turned our focus towards O-atom transfer reactions and the reactivity of $(^{Me2Hyd}Nac)_3Cu_3(O)_2$ towards triphenylphosphine (PPh_3) and CO_2. Introduction of 5 equivalents of PPh_3 at –80 °C to solutions of $(^{Me2Hyd}Nac)_3Cu_3(O)_2$ did not result in any spectral changes as monitored by UV-vis spectroscopy. Samples were examined by ^{31}P

NMR spectroscopy after warming to room temperature and two distinct phosphorus species were observed as singlets at 27.25 and –5.03 ppm (Figure 3.32, solid). A PPh_3 reference sample displays a single peak at –5.03 ppm in d_8-THF (Figure 3.32, *dotted*). The feature at 27.25 ppm is assigned to triphenylphosphine-oxide ($OPPh_3$) based on literature assignments and its presence was confirmed by GC-MS analysis.[132] The yield of $OPPh_3$ was 40% per $(^{Me2Hyd}Nac)_3Cu_3(O)_2$ based on ^{31}P NMR peak integration of PPh_3 to $OPPh_3$. This indicates that although $(^{Me2Hyd}Nac)_3Cu_3(O)_2$ is a poor H-atom abstractor, it is capable of O-atom insertion/oxidation reactions. This was confirmed by reactions of $(^{Me2Hyd}Nac)_3Cu_3(O)_2$ in THF (1 mM) at –80 °C with CO_2. The starting UV-vis spectrum of these reactions displayed features at λ_{max} = 420 and 590 nm assigned to $(^{Me2Hyd}Nac)_3Cu_3(O)_2$ (Figure 3.33, left, dashed) that instantaneously changed to a spectrum with λ_{max} = 442, 614, and 720 nm with a weak shoulder at 486 nm when CO_2 was introduced (Figure 3.33, *left, solid*). This new species was thermally sensitive and decayed upon warming to room temperature (Figure 3.33, *right*, *solid→ dashed*). The UV-vis spectrum of the decayed product displays broad features between λ_{max} = 400–900 nm. The spectral changes and new UV-vis spectrum obtained when $(^{Me2Hyd}Nac)_3Cu_3(O)_2$ was reacted with CO_2 suggested a reaction had taken place so ESI-MS and FTIR spectroscopy were used to examine the reaction products.

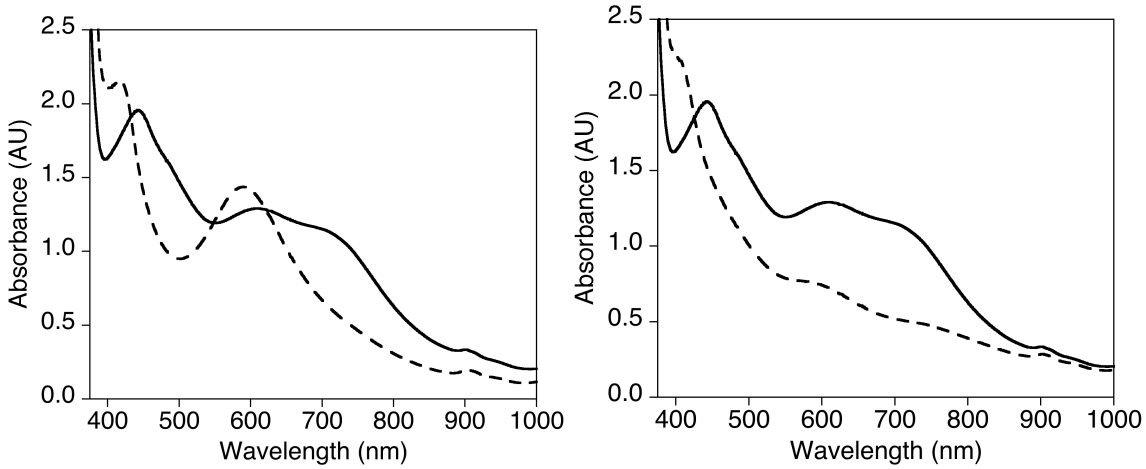

Figure 3.33. UV-vis spectra of the reaction of (^{Me2Hyd}Nac)$_3$Cu$_3$(O)$_2$ (*dashed*) with CO_2 to yield an intermediate species (*solid*) at 1 mM in THF at –80 °C (*left*) UV-Vis spectra of the thermal decomposition product upon warming the intermediate formed from a reaction between (^{Me2Hyd}Nac)$_3$Cu$_3$(O)$_2$ and CO_2 (*solid*) to room temperature (*dashed*) (*right*).

The ESI-MS spectrum of the product solution of (^{Me2Hyd}Nac)$_3$Cu$_3$(O)$_2$ with CO_2 displayed two copper containing peak envelopes along with a number of unidentifiable peaks that do not contain copper on the basis of isotope patterns. The peak envelope at m/z = 361.906 was simulated as a mononuclear [(^{Me2Hyd}Nac)Cu(CO_3) + MeOH + Na + H]$^+$ species (Figure 3.34). This species appears to contain a carbonate ligand $(CO_3)^{2-}$ that is most likely from the O-atom insertion product of CO_2. The peak envelope at m/z = 876.9525 was modeled as a dicopper species [(^{Me2Hyd}Nac)$_2$Cu$_2$(CO_3) + (NCCH3)$_5$ + (MeOH)$_3$ + Na + H]$^+$ (Figure 3.35). A number of solvent molecules are associated with the copper species, a characteristic also seen in the ESI-MS spectrum of (^{Me2Hyd}Nac)$_3$Cu$_3$(O)$_2$ (Section 3.4.4). The formation of a carbonate species in the mass spectrometer was a concern so we chose to supplement this observation with vibrational spectroscopy.

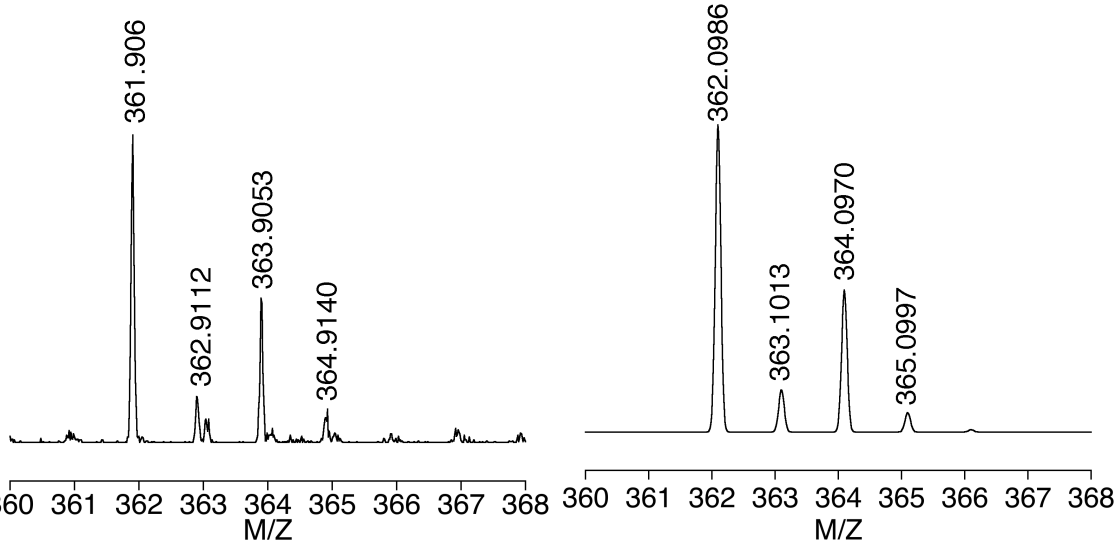

Figure 3.34. Experimental (*left*) and simulation (*right*) ESI-MS spectra displaying a peak envelope assigned to a $[(^{Me2Hyd}Nac)Cu(CO_3) + MeOH + Na + H]^+$ species.

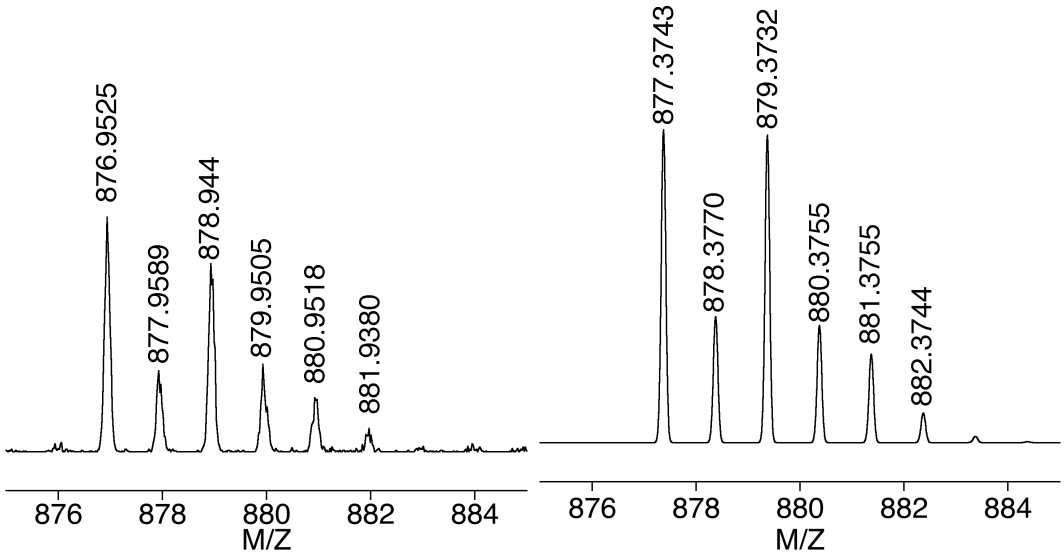

Figure 3.35. Experimental (*left*) and simulation (*right*) ESI-MS spectra displaying a peak envelope assigned to a $[(^{Me2Hyd}Nac)_2Cu_2(CO_3) + (NCCH3)_5 + (MeOH)_3 + Na + H]^+$ species.

FTIR spectroscopic analysis of the product of the reaction between $(^{Me2Hyd}Nac)_3Cu_3(O)_2$ and CO_2 further suggests the formation of carbonate. The FTIR spectrum of the product of the reaction of $(^{Me2Hyd}Nac)_3Cu_3(O)_2$ with CO_2 is overlaid with the FTIR spectrum of the starting Cu(I) complex (Figure 3.36). The product FTIR

spectrum contains a strong feature at 1775 cm^{-1} that was not observed in the starting Cu(I) complex. On the basis of literature precedent,[133] this feature is assigned to the ν_{asym} of a carbonate ligand bridging two metal centers. This assignment is consistent with the ESI-MS spectrum, discussed above, that includes a peak envelope that was assigned to a Cu_2/CO_3 species. Additional vibrations were observed between 1600–1350 cm^{-1} both in the starting Cu(I) complex and product FTIR spectra that are likely due to $^{Me2Hyd}Nac^-$ and acetonitrile ligand vibrations.

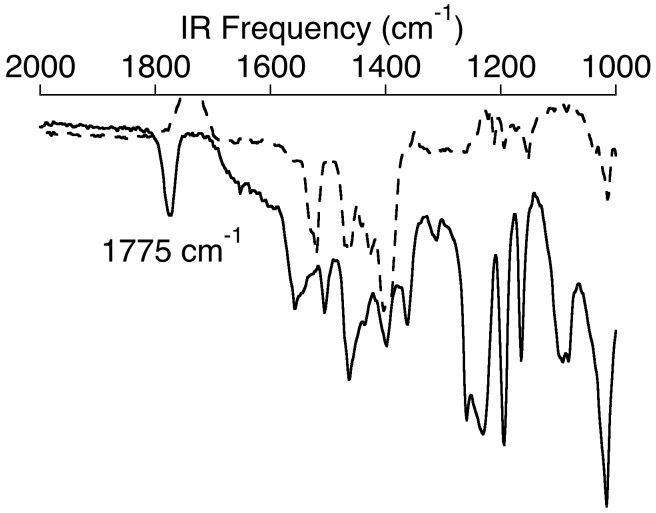

Figure 3.36. Solid state FTIR spectra of [(^{Me2Hyd}Nac)Cu($NCCH_3$) (*dashed*) and of the reaction product of (^{Me2Hyd}Nac)$_3Cu_3(O)_2$ with CO_2 (*solid*).

The lack of reactivity of (^{Me2Hyd}Nac)$_3Cu_3(O)_2$ towards weak C–H bonds, O–H bonds, and ferrocene is in direct contrast to the reported reactivities of $[Cu_3O_2]^{3+}$ cores supported by neutral N-donor ligands. This lack of reactivity may originate from the overall neutral charge of the $[Cu_3O_2]^{3+}$ species supported by the anionic $^{Me2Hyd}Nac^-$ ligand. It has been previously postulated by our group that the strong donating ability of

β-diketiminate ligands encourages the reactivity of Cu(I) complexes towards O_2.[134] That same donating ability effectively stabilizes the higher oxidation states observed in copper-oxygen intermediates and in turn makes them less reactive electrophiles towards exogenous substrates.[134] This explanation seems plausible in rationalizing the stability of $(^{Me2Hyd}Nac)_3Cu_3(O)_2$ in the presence of oxidizable bonds and electron donors. The strong electron donating potential of $^{Me2Hyd}Nac^-$ stabilizes the Cu(III) center in the proposed mixed valent $Cu(III)Cu(II)_2O_2$ species more than the previously reported neutral ligands. This additional stability diminishes the intermediates reactivity towards substrate oxidation.

3.4.2 Reaction of $(^{Me2Hyd}Nac)_3Cu_3(O)_2$ with H_2O_2, Benzoic Acid, and Benzoylformic Acid.

Preliminary reactions of $(^{Me2Hyd}Nac)_3Cu_3(O)_2$ with H_2O_2, benzoic acid, and benzoylformic acid were examined and the results are described below, although the findings are not fully understood at this time. All three of these substrates share the ability to act as proton donors, which may explain some of the observed reactivity with $(^{Me2Hyd}Nac)_3Cu_3(O)_2$.

Reactions of H_2O_2 (30% in H_2O) with $(^{Me2Hyd}Nac)_3Cu_3(O)_2$ at –80 °C in THF resulted in a rapid spectral change observable by UV-vis spectroscopy (Figure 3.37). Addition of water without H_2O_2 to $(^{Me2Hyd}Nac)_3Cu_3(O)_2$ did not result in any spectral changes at –80 °C confirming that the reaction involved H_2O_2. The features assigned to $(^{Me2Hyd}Nac)_3Cu_3(O)_2$ (λ_{max} = 328, 420, and 590 nm) give way to a new species with features at λ_{max} = 320, 353, 424, and 600 nm (Figure 3.37, *left, solid*). These features are

thermally sensitive and decay upon warming to yield a final spectrum that contains features at λ_{max} = 355 and 460 nm (Figure 3.37, *right*, *dashed*). The decay of the spectroscopic features was accompanied by formation of a dark precipitate that was insoluble in all examined solvents (THF, CH_2Cl_2, acetonitrile, *N,N*-di(methyl)formamide, toluene, acetone, methanol, H_2O, and hexanes). This precipitate was not observed when $(^{Me2Hyd}Nac)_3Cu_3(O)_2$ decayed in the absence of H_2O_2. Resonance enhanced Raman spectroscopy with λ_{ex} = 406.7 nm was performed on the products of reactions of $(^{Me2Hyd}Nac)_3Cu_3(O)_2$ with H_2O_2 and non-solvent peaks at 532, 695, and 824 cm^{-1} were observed (Figure 3.36). We have not yet used ^{18}O-labeled H_2O_2 to evaluate these peaks. Peaks between 700-900 cm^{-1} are typically assigned to copper-peroxo species with bands below 700 cm^{-1} being assigned either to Cu–O vibrations or the a_1 symmetric core breathing mode of a bis(μ-oxo)dicopper(III) species.[88a] A definitive assignment of the structure of this intermediate is beyond the scope of the current work.

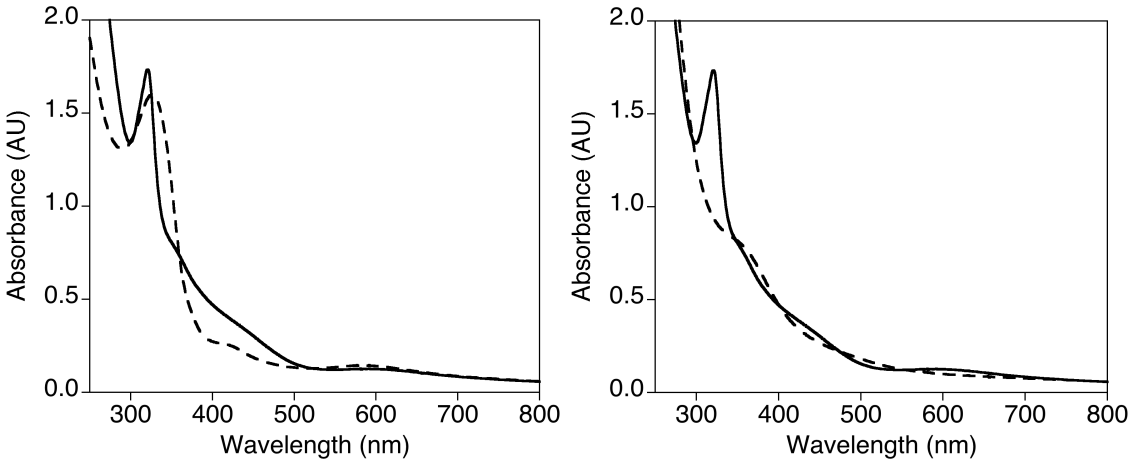

Figure 3.37. (*left*) UV-vis spectrum for a reaction between $(^{Me2Hyd}Nac)_3Cu_3(O)_2$ (*dashed*) (1 mM in THF at –80 °C in a 0.2 cm path length cuvette) and H_2O_2 (1 equivalent of a 30% H_2O_2 solution in water yielding the product spectrum (*solid*). (*right*) The thermal decomposition of the intermediate species derived from $(^{Me2Hyd}Nac)_3Cu_3(O)_2$ and H_2O_2 (*solid*) to the final product spectrum at room temperature (*dashed*).

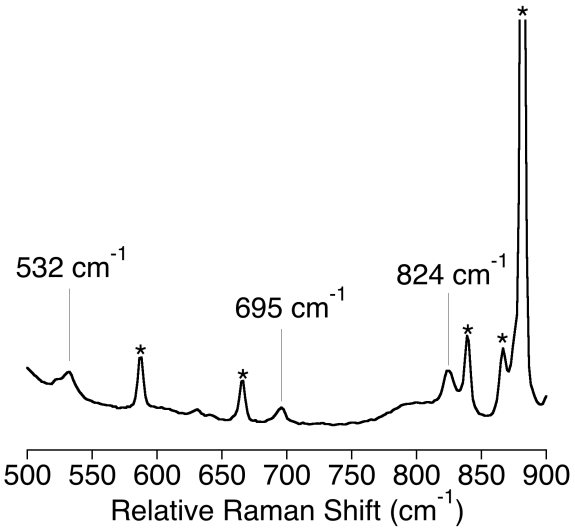

Figure 3.38. Resonance Raman spectrum of the reaction of $(^{Me2Hyd}Nac)_3Cu_3(O)_2$ with 1 equiv H_2O_2 in THF (10 mM) and a λ_{ex} = 406.7 nm. Peaks due to solvent are marked (*).

The reactivity of $(^{Me2Hyd}Nac)_3Cu_3(O)_2$ towards benzoylformic acid and benzoic acid were examined as an extension of the reactivity of $[Cu_2O_2]^{2+}$ species towards (α-keto)carboxylates described in Chapter 2. The reactions of TBA salts of both BF and BA with $(^{Me2Hyd}Nac)_3Cu_3(O)_2$ were first examined but the spectral changes as observed by UV-vis spectroscopy were irreproducible and further efforts to understand the intricacies of the reactions were not pursued. On the other hand, reproducible results were obtained in studies of the reactions of $(^{Me2Hyd}Nac)_3Cu_3(O)_2$ with commercially available benzoylformic acid and benzoic acid. One equivalent of benzoylformic acid in dry THF was added to solutions of $(^{Me2Hyd}Nac)_3Cu_3(O)_2$ in THF (1 mM) at –80 °C by syringe and the reaction monitored by UV-vis spectroscopy. Upon addition of the substrate, the feature at λ_{max} = 590 nm instantaneously gave way to a feature at λ_{max} = 640 nm (Figure 3.39, *left*, *dashed*) that decayed over approximately 100 s (Figure 3.39, *left, dotted*). The warmed reaction mixtures were demetallated by a mild acidic workup and the products

methylated and examined by GC-MS by a method identical to that described in Chapter 2. A peak for methylbenzoate was not observed; the only observable peak was assignable to the methyl ester of benzoylformate, indicating no decarboxylation chemistry had occurred. In a parallel experiment benzoic acid was introduced to a solution of $(^{Me2Hyd}Nac)_3Cu_3(O)_2$ in THF (1 mM) at –80 °C and the reaction monitored by UV-vis spectroscopy. Upon addition of benzoic acid to the reaction mixture, rapid spectral changes were observed with the initial feature at λ_{max} = 590 nm giving way to a feature at λ_{max} = 650 nm (Figure 3.39, *right, dashed*). This spectrum decayed further over 4-5 s and gave way to a feature at λ_{max} = 605 nm (Figure 3.39, *right*, *dash-dot*) that finally decayed to a spectrum after 100 s with a feature at λ_{max} = 650 nm (Figure 3.39, *right, dotted*). The structural assignments of these intermediate species have not been further explored. Additional experiments involving FTIR and resonance Raman spectroscopies are needed to determine the potential binding of an α-ketocarboxylate to the $(^{Me2Hyd}Nac)_3Cu_3(O)_2$ species, the protonation of $(^{Me2Hyd}Nac)_3Cu_3(O)_2$ by an (α-keto)carboxylic acid, or any number of complex combinations of both. It is clear that a reaction does occur between $(^{Me2Hyd}Nac)_3Cu_3(O)_2$ and (α-keto)carboxylic acids which may warrant additional exploration in the future.

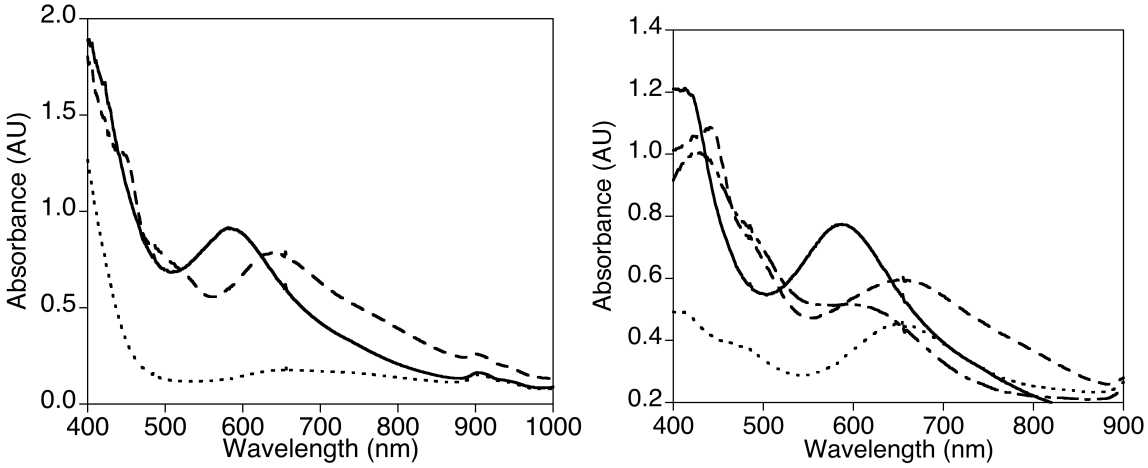

Figure 3.39. UV-vis spectra of reactions of (^{Me2Hyd}Nac)$_3$Cu$_3$(O)$_2$ (*solid*) with benzoylformic acid (*left*) and benzoic acid (*right*) with intermediate spectra shown leading to a final product (*dashed* to *dot-dashed*). Both reactions involved addition of 1 equivalent of substrate to (^{Me2Hyd}Nac)$_3$Cu$_3$(O)$_2$ (1 mM, THF, –80 °C).

3.5 Conclusion and Perspectives

The specific aims of the project described in this chapter were to synthesize a Cu(I) complex supported by an anionic bidentate ligand, react the Cu(I) complex with O_2 and oxo-transfer reagents, identify and characterize any copper-oxygen intermediates, and examine the reactivity of any isolable intermediates towards exogenous substrates. The ligand initially chosen was ^{Me2Hyd}NacH, a β-diketiminate derived from *N,N*-dimethylhydrazine.[92] Although the majority of work described in this chapter focused on ^{Me2Hyd}NacH, the simplest and initially chosen ligand, synthetic analogs of this ligand with various substituted alkyl groups on the hydrazine, ^{Et4Hyd}NacH, or the β-diketiminate backbone, ^{Et2Hyd}NacH and ^{Me2BzHyd}NacH, were synthesized according to literature procedures (^{Et4Hyd}NacH and ^{Et2Hyd}NacH)[92] or fully characterized by ^{1}H and ^{13}C NMR and HRESI-MS (^{Me2BzHyd}NacH). Synthesis of the Cu(I) complex supported by ^{Me2Hyd}Nac^{-} was accomplished and (^{Me2Hyd}Nac)Cu(NCCH$_3$) was fully characterized by a number of

techniques including X-ray crystallography. The complex contains an electron rich copper center, as suggested by by FTIR spectroscopy of (^{Me2Hyd}Nac)Cu(CO), similar to previously reported Cu(I) complexes that demonstrated reactivity towards O_2.[91] (^{Me2Hyd}Nac)Cu($NCCH_3$) displayed reactivity towards aryl-nitrosyl compounds and formed what is tentatively assigned as a mononuclear (^{Me2Hyd}Nac)Cu(ON-R) complex (R = aryl).

With (^{Me2Hyd}Nac)Cu($NCCH_3$) fully characterized, we sought to examine its reactivity towards O_2 and characterize any observed intermediates. Oxygenation of (^{Me2Hyd}Nac)Cu($NCCH_3$) at low temperature (–80 °C) in either acetone or THF resulted in the formation of an intermediate observed by UV-vis spectroscopy with λ_{max} (ε, M^{-1},cm^{-1}) = 328 (10700), 420 (1500), and 590 nm (835). These spectroscopic features are similar in energy to reported copper-oxygen intermediates assigned as $[Cu_3O_2]^{3+}$ species with the most intense absorption feature (λ_{max} = 300-380 nm) assigned to an oxo-ligand to Cu(III) charge transfer transition.[113,114,115] The photometric titration of (^{Me2Hyd}Nac)Cu($NCCH_3$) with an O_2-saturated solution of THF indicated a maximum intensity of spectroscopic features at 0.3 equivalents of O_2 per copper (Figure 3.30). This value is consistent with the assignment of the intermediate species as a trinuclear copper-oxygen species, particularly a $[Cu_3O_2]^{2+}$ species.

^{1}H NMR spectroscopy experiments were conducted that confirmed the intermediate species is paramagnetic in the solution state with only broad paramagnetically shifted peaks observed in the spectrum (Figure 3.21). The magnetic susceptibility of the intermediate species was determined by the Evans method and a μ_{eff}

= 2.8(1) was determined (Figure 3.22), consistent with a triplet (S = 1) ground state. This electronic assignment was corroborated by parallel mode EPR spectroscopy where a signal at g ~ 4 was observed (Figure 3.23) and can be assigned to the $\Delta m_s = 2$ transition with the $\Delta m_s = 1$ transition occurring in the g ~ 2 region.[123,125] The assignment of the species as a triplet ground state copper-oxygen species is consistent with a localized mixed-valent tricopper(II)(II)(III)-bis(μ-oxo) species.[135,136] Two separate triplet tricopper(II)(II)(III)-bis(μ-oxo) species that contain the copper sites in localized $Cu(II)_2Cu(III)$ oxidation states have been experimentally observed and thoroughly characterized.[113,115,123,124] In the first report of such a species, the magnetic susceptibility of the tricopper(II)(II)(III)-bis(μ-oxo) species was found to be $\mu_{eff} = 2.9$, consistent with a triplet ground state.[113] Additionally a crystal structure was obtained that contained one distinct copper center with shorter Cu–O distances (1.95 vs. 2.01) compared to other copper atoms. This distinct copper atom was assigned as the Cu(III) site.[113] Solid-state EPR spectroscopy confirmed the overall electronic assignment as a localized mixed valent trinuclear copper species.[123] Interestingly the previously reported $[Cu_3O_2]^{3+}$ species reported by Taki *et al.* claimed their species was EPR silent which seems to be in direct contradiction to their assignment, the literature precedent, and the results presented in this work.[114]

Further support for the assignment of the intermediate species as $[(^{Me2Hyd}Nac)_3Cu_3(O)_2$ came via ESI-MS. The intermediate species was formed by the oxygenation of $(^{Me2Hyd}Nac)Cu(NCCH_3)$ at –78 °C in acetone (1 mM) and injected directly into the ESI-MS instrument with methanol (see experimental for the full details). A peak

envelope for $[(^{Me2Hyd}Nac)_3Cu_3(O)_2 + H^+]^+$ along with associated solvent was observed and simulated with the distinctive three copper isotope pattern (Figure 3.26). The direct observation of $(^{Me2Hyd}Nac)_3Cu_3(O)_2$ by ESI-MS corroborates that the oxygenation product of $(^{Me2Hyd}Nac)Cu(NCCH_3)$ is a mixed valent tricopper(II)(II)(III)-bis(μ-oxo) species. This assignment is consistent with the presented UV-vis, NMR, EPR spectroscopic data along with a lack of observed vibrational data through attempted resonance Raman spectroscopy experiments. $(^{Me2Hyd}Nac)_3Cu_3(O)_2$ likely forms through a pathway similar to one previously reported by Cole *et al*. and shown in Figure 3.40.[113] In this pathway, the Cu(I) complex initially reacts with an equivalent of O_2 to form a Cu(II)-superoxo (Figure 3.40, ***b***). This species reacts with an additional equivalent of Cu(I) complex forming a dimeric $[Cu_2O_2]^{2+}$ species (Figure 3.40, ***c***). A final equivalent of Cu(I) complex reacts to complete the four electron reduction of O_2 to form the tricopper(II)(II)(III)-bis(μ-oxo) complex (Figure 3.40, ***d***)

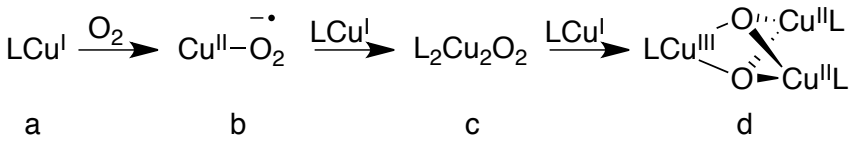

Figure 3.40. Proposed reaction pathway for the formation of $(^{Me2Hyd}Nac)_3Cu_3(O)_2$. L = $(^{Me2Hyd}Nac)$.

Unique to $(^{Me2Hyd}Nac)_3Cu_3(O)_2$, its formation is not limited to reactions between $(^{Me2Hyd}Nac)Cu(NCCH_3)$ and O_2. It was determined that the reaction between $(^{Me2Hyd}Nac)Cu(NCCH_3)$ and PhIO generates a spectroscopically similar species as observed by UV-vis spectroscopy. To the best of our knowledge this is the first example of the formation of a discrete copper-oxygen species from reactions with PhIO and only the second example of the formation of a copper-oxygen species from oxo-transfer.[51]

The reactivity of (^{Me2Hyd}Nac)$_3$Cu$_3$(O)$_2$ towards a number of substrates was next examined and presented. (^{Me2Hyd}Nac)$_3$Cu$_3$(O)$_2$ showed no reactivity towards either phenolic O–H bonds or weak C–H bonds at any temperature. All previously reported $[Cu_3O_2]^{3+}$ complexes supported by neutral *N*-donor ligands displayed high reactivity towards phenols, particularly 2,4-di-*tert*-butylphenol.[113,114] The anionic β-diketiminate supported (^{Me2Hyd}Nac)$_3$Cu$_3$(O)$_2$ species has a distinct reactivity, or lack thereof, compared to reported $[Cu_3O_2]^{3+}$ complexes with respect to H-atom abstraction. We next determined PPh_3 and CO_2 both act as O–atom acceptors when reacted with (^{Me2Hyd}Nac)$_3$Cu$_3$(O)$_2$. Addition of PPh_3 or CO_2 to solutions of (^{Me2Hyd}Nac)$_3$Cu$_3$(O)$_2$ resulted in the formation of $OPPh_3$ (40% by ^{31}P NMR) and carbonate (observed by FTIR spectroscopy and ESI-MS), respectively. There are no reports of either type of O-atom insertion reactions involving $[Cu_3O_2]^{3+}$ species supported by neutral N-donor ligands, making the reactivity of (^{Me2Hyd}Nac)$_3$Cu$_3$(O)$_2$ distinct.

The poor reactivity of (^{Me2Hyd}Nac)$_3$Cu$_3$(O)$_2$ towards exogenous substrates may be a result of the strong electron donating potential of the ^{Me2Hyd}Nac$^-$ ligand. A previously reported mononuclear Cu(III)-peroxo species reported by our group supported by a β-diketiminate ligand displayed poor reactivity towards exogenous substrates.[90a,c,d] This poor reactivity was attributed to the increased stabilization of the Cu(III) center by the anionic β-diketiminate supporting ligand.[134] The strong electron donation from the ligand increases the reactivity of the Cu(I) complex towards O_2 reduction but reduces the ability of the copper-oxygen species to oxidize substrates. These same effects can be extended to (^{Me2Hyd}Nac)$_3$Cu$_3$(O)$_2$ and previously reported $[Cu_3O_2]^{3+}$ species supported by neutral

diamine ligands. $^{Me2Hyd}Nac^-$ is anionic and on the basis of the characterization data for the Cu(I) complexes, seems to be significantly more electron donating than the TMCD or TMEN ligands reported to support $[Cu_3O_2]^{3+}$ species. The previously reported $[Cu_3O_2]^{3+}$ species were only capable of oxidizing weak O–H bonds or being reduced by ferrocene and no reactivity towards robust C–H or O–H bonds has been reported to date. This suggests that to increase the reactivity of a mixed valent $[Cu_3O_2]^{3+}$ species the electron donating ability of a bidentate *N*-donor ligand should be reduced with respect to peralkylated diamine ligands.

3.6 Experimental

General Considerations. All solvents and reagents were obtained from commercial sources unless otherwise noted. Solvents were thoroughly degassed via three cycles of freezing, evacuating, and thawing. THF and d_8-THF were dried over Na/benzophenone and distilled under vacuum. CH_2Cl_2 and acetonitrile were dried over CaH_2 and distilled under vacuum and acetonitrile was stored over molecular sieves. Tetramethylsilane was dried over $LiAlH_4$ and distilled under vacuum. Acetone was dried over 4 Å molecular sieves, distilled, and stored over sieves (4 Å) in the glove box. Et_2O, toluene, and pentanes were passed through solvent purification columns (Glass Contour, Laguna, CA) and stored over CaH_2 in the glove box. All metal complexes were prepared and stored in a Vacuum Atmospheres inert atmosphere glove box under dry nitrogen or were manipulated under argon or dry nitrogen using standard Schlenk techniques. Ligands $^{Me2Hyd}NacH$, $^{Et2Hyd}NacH$, and $^{Et4Hyd}NacH$ were prepared according to literature procedures,[92] dried over 4 Å molecular sieves, and distilled under vacuum prior to use.

Physical Methods. NMR spectra were recorded on either Varian VI-300, VXR-300, or VI-500 spectrometers at room temperature. Chemical shifts (δ) for ^{1}H and ^{13}C NMR spectra were referenced to residual protium in the deuterated solvent (^{1}H NMR experiments) or the characteristic solvent resonances of the solvent nuclei (^{13}C NMR experiments). Variable temperature ^{1}H NMR spectra were obtained on a Varian VI-300 spectrometer fitted with a liquid nitrogen cryostat. Stem coaxial inserts used for Evans method experiments were purchased from Wilmad Lab Glass. UV-vis spectra were collected on a HP8453 (190-1000 nm) diode array spectrophotometer. Low temperature UV-vis experiments were performed using an Unisoku low temperature UV-vis cell holder. UV-vis spectra that had drifting baselines due to minor frosting caused by the low-temperature device were corrected when necessary by subtracting the average of a region with no absorbance from the entire spectrum. Resonance Raman spectra were recorded on an Acton 506 spectrometer using a Princeton Instruments LN/CCD-11100-4 PB/UBAR detector and ST-1385 controller interfaced with Winspec software. The spectra were obtained at –196 °C using backscattering geometry. Excitation was provided by either a Spectra-Physics BeamLok 2060-KR-V Krypton or Argon ion laser. Raman shifts were externally referenced to liquid indene and internally referenced to solvent (THF). X-band electron paramagnetic resonance (EPR) spectra were recorded on a Bruker E-500 spectrometer with an Oxford Instruments EPR-10 liquid-helium cryostat (4-20 K, 9.61 GHz). Elemental analysis was performed by Robertson Microlit Lab (Madison, NJ). Electrospray ionization mass spectrometry (ESI-MS) was performed on a Bruker BioTOF II instrument with high-resolution data acquired by internally referencing

samples to a polyethylene glycol standard. All GC-MS experiments were conducted on an Agilent Technologies 7890A GC system and 5975C VL MSD. The GC column was a HP-5ms with dimensions 30 m x 0.250 mm. The standard method used for all runs involved an initial oven temperature of 60 °C (held for 4 min) followed by a 20 °C/min ramp to 230 °C that was held for 15 min. Infrared spectra were collected on a Nicolet Avatar 370 FT-IR equipped with an attenuated total reflectance attachment, using a CaF_2 solution cell (International Crystal Laboratories) or a Smart OMNI-Sampler for solid samples.

^{Me2BzHyd}NacH. A 25 mL Schlenk flask was charged with (^{Me2Hyd}Nac) (1.004 g, 5.45 mmol) in dry THF (15 mL) and cooled to –78 °C in a dry ice/acetone bath under dry N_2. *n*-BuLi in hexanes (2.2 mL of a 2.5 M solution) was slowly added via syringe and stirred for 1 h and gradually warmed to RT. Benzyl bromide (0.65 mL, 5.45 mmol) was added via syringe and a white precipitate was observed after several minutes. The reaction stirred overnight followed by removal of solvent *in vacuo*. The solid residue was extracted with hexanes and washed with water (4 x 20 mL). The organic layer was dried over $MgSO_4$, filtered, and solvent removed to yield a pale yellow oil that was distilled under vacuum to yield a colorless oil (650 mg, 43 % yield) ^{1}H NMR (CD_2Cl_2, 300 MHz): δ 7.61 (m, 5 H, *J* = 6 Hz), 3.35 (t, 1H, *J* = 7.8 Hz), 3.02 (d, 2H, *J* = 7.8 Hz) 2.32 (s, 12 H), 1.80 (s, 6H); ^{13}C{^{1}H} NMR (75.0 MHz, CD_2Cl_2): δ 164.74, 140.13, 129.08, 127.760, 125.61, 57.88, 46.45, 34.62, 14.76. HRESIMS $[M + H]^+$, m/z: Calcd for $C_{16}H_{27}N_4$, 275.2236. Found, 275.2274.

(^{Me2Hyd}Nac)Cu(NCCH$_3$) (^{Me2Hyd}Nac) (145 mg, 0.79 mmol) was dissolved in acetonitrile

(5 mL) and added to a slurry of Cu_4Mes_4 (142 mg, 0.19 mmol) in 5 mL of THF. The cloudy solution became clear over 20 min yielding a golden solution. The solution stirred for 2 hours and became dark brown with a brown precipitate. The solution was filtered and solvent removed *in vacuo* yielding a brown residue. The residue was dissolved in approximately 2 mL of fresh THF and cooled to –20 °C. Addition of pentanes to this solution resulted in the rapid formation of yellow needle crystals of (^{Me2Hyd}Nac)Cu($NCCH_3$) that were isolated by vacuum filtration (128 mg, 66%). ^{1}H NMR (d_8-THF, 300 MHz, –80 °C): δ 2.89 (s, 1H), 2.46 (s, 3H), 2.28 (s, 12 H), 1.91 (s, 6H). $^{13}C\{^1H\}$ NMR (75.0 MHz, d_8-THF): δ 165.1, 121.95, 86.37, 49.53, 21.84, 2.36. Anal. Calc. for $C_9H_{19}CuN_4$: C, 43.80; H, 7.76; N, 22.70. Found: C, 44.30; H, 6.82; N, 22.70.

FTIR Spectroscopy. A 5 mL Schlenk flask was charged with a 40 mM solution of (^{Me2Hyd}Nac)Cu($NCCH_3$) in THF and sealed by septum. CO was bubbled through the solution at RT until all solvent had evaporated leaving a solid residue. Samples examined in the solid-state were transferred by spatula to the FTIR spectrometer and infrared spectra collected on an attenuated total reflectance attachment. Samples to be examined in the solution state were transferred back into the glove box, fresh THF added to obtain a concentration of approximately 40 mM, and the solution loaded and sealed in a CaF_2 solution cell (International Crystal Laboratories) for analysis.

Low Temperature Oxygenations of (^{Me2Hyd}Nac)Cu($NCCH_3$). Anaerobically prepared solutions of (^{Me2Hyd}Nac)Cu($NCCH_3$) in THF or acetone (1 mM or 0.1 mM) were cooled to –80 °C in a septum sealed quartz cuvette under a constant argon purge. Dry O_2 was bubbled through the cooled solutions with the reaction monitored by UV-vis

spectroscopy. Spectral features at λ_{max} = 328, 420, and 590 nm developed rapidly and the reaction considered complete when these features stopped growing (~100 s).

Resonance Raman Spectroscopy. A Schlenk flask or NMR tube was charged with a 1 to 40 mM solution of (^{Me2Hyd}Nac)Cu($NCCH_3$) in THF in the glove box. Samples were cooled to –78 °C by submersion in a dry ice/acetone bath under an argon atmosphere. Dry O_2 was bubbled through the solutions for 10 min followed by 20 min of argon to remove excess O_2. Samples prepared in a NMR tube were rapidly frozen by immersion in liquid N_2 and stored for analysis. Samples prepared in a Schlenk flask were transferred by precooled pipette to a liquid N_2 cooled copper cup and frozen for analysis. Samples prepared with $^{18}O_2$ were prepared by pre-charging a 10 mL Schlenk flask with a stir bar and 1 to 40 mM solution of (^{Me2Hyd}Nac)Cu($NCCH_3$) in THF in the glove box. The sample was frozen in liquid N_2, the headspace evacuated under vacuum, and $^{18}O_2$ vacuum transferred into the flask. The sample was warmed to –78 °C in a dry ice/acetone bath and stirred for 20 min. The solution was either transferred to a precooled NMR tube and frozen by submersion in liquid N_2 or transferred to a liquid N_2 cooled copper cup and frozen for analysis.

Spectrophotometric Titrations. A 3.5 mL solution of (^{Me2Hyd}Nac)Cu($NCCH_3$) in THF (1 mM) was placed in a 1 cm path length cuvette and cooled to –80 °C under an argon atmosphere. An O_2 saturated THF solution was prepared by bubbling dry O_2 through argon saturated THF for 20 min.[116] Aliquots (20 μL) of the THF solution were transferred by gastight syringe to the cuvette and the sample allowed to equilibrate under stirring. The absorption band at 590 nm was monitored by UV-vis spectroscopy until no further

increase in absorbance was observed and the increase in intensity plotted against the equivalents of O_2 added per Cu (Figure 3.20).

EPR Spectroscopy. Solutions for examination by parallel X-band EPR spectroscopy were prepared by first charging a 5 mL Schlenk flask with (^{Me2Hyd}Nac)Cu(NCCH$_3$) in THF (60 mM) to obtain a 20 mM final concentration of (^{Me2Hyd}Nac)$_3$Cu$_3$(O)$_2$. The flask was sealed with a septum and cooled to –78 °C in a dry ice/acetone bath under argon. Dry O_2 was bubbled through the solution for 10 min followed by 45 min of an argon purge to remove excess O_2. Samples were transferred to precooled EPR tubes taking care to avoid any bubbles and rapidly frozen in liquid N_2 and stored for analysis.

ESI-MS of (^{Me2Hyd}Nac)$_3$Cu$_3$(O)$_2$. A 5 mL Schlenk flask was charged with a 1 mM solution of (^{Me2Hyd}Nac)Cu(NCCH$_3$) and cooled to –78 °C under argon in a dry ice/acetone bath. Dry O_2 was bubbled through the solution for 10 min followed by 20 min of an argon purge. An aliquot (40 μL) of the dark green solution was rapidly loaded into 100 μL gastight syringe followed by 40 μL of fresh methanol and the sample directly injected into the spectrometer while continuously collecting spectra in the positive ion detection mode. As the deep green portion entered the instrument the peaks of interest were observed and became more intense. Samples prepared from PhIO began with 1 equiv. PhIO being placed in a 5 mL Schlenk flask with THF and a stir bar and sealed by a septum. The heterogeneous mixture was cooled to –78 °C in a dry ice/acetone bath under argon. (^{Me2Hyd}Nac)Cu(NCCH$_3$) was added by gastight syringe in THF to yield a final copper concentration of 1 mM in the flask. The solution was stirred for 5 h at –78 °C. The insoluble solids were removed by rapidly passing the solution through a 0.45 μm

PTFE filter into a precooled 5 mL Schlenk flask. This process caused an instantaneous color change in the solution from deep green to a pale gold/green. Additionally this solution did not yield any peaks in the ESI-MS spectrum assignable to $(^{Me2Hyd}Nac)_3Cu_3(O)_2$ with only decomposition products observed.

Evans Method Determination of Magnetic Susceptibility. A stock solution of $(^{Me2Hyd}Nac)Cu(NCCH_3)$ (38.4 mg, 0.133 mmol) and 1,3,5-trimethoxybenzene (22.4 mg, 0.133 mmol) in d_8-THF (2.5 mL) was prepared in the glove box. An aliquot of the stock solution (0.6 mL) was sealed in an NMR tube by a septum and cooled to –78 °C in a dry ice/acetone bath under a positive argon atmosphere. The solution was oxygenated to form $(^{Me2Hyd}Nac)_3Cu_3(O)_2$ by bubbling dry O_2 through the solution for 5 min followed by an argon purge (15 min) to remove excess O_2. A separate stock solution of 1,3,5-trimethoxybenzene (22.5 mg, 0.134 mmol) in d_8-THF (2.5 mL) was prepared and loaded into a coaxial NMR insert and sealed in the glove box. The insert was placed into the NMR tube containing $(^{Me2Hyd}Nac)_3Cu_3(O)_2$ and the ^1H NMR spectrum obtained of the combined apparatus at –80 °C (Figure 3.22).

Photometric H_2O_2 Detection with Ti(IV)Oxysulfate. A stock H_2O_2 solution of 1.96 mM was prepared from a 30% H_2O_2 solution in H_2O serially diluted to known concentrations (0.899, 0.448, and 0.268 mM). Aliquots from the H_2O_2 (3 mL) were loaded into a UV-vis cuvette and 0.1 mL of Ti(IV)oxysulfate added (15% in dilute sulfuric acid). The UV-vis spectra of the solutions were recorded and the absorbance at λ_{max} = 408 nm recorded and plotted against the concentration of H_2O_2 (Figure 3.29). Detection of peroxide species originating from copper-oxygen intermediates followed a

procedure identical to those previously reported in the literature.[128]

Reactions of (^{Me2Hyd}Nac)Cu(NCCH$_3$) with Exogenous Substrates. Solutions of (^{Me2Hyd}Nac)$_3$Cu$_3$(O)$_2$ in 3.5 mL of THF (1 mM) were formed as described above. After complete formation of (^{Me2Hyd}Nac)$_3$Cu$_3$(O)$_2$ as determined by UV-vis spectroscopy, samples were purged for 20 min with argon. Substrates were introduced as THF solutions by syringe (9,10-dihydroanthracene, 2,6-di-*tert*-butylphenol, 2,4,6-tri-*tert*-butylphenol, 2,4-di-*tert*-butylphenol, ferrocene, triphenylphosphine, benzoylformic acid, benzoic acid, cyclohexene), added as a 30% by weight in water solution (H_2O_2), or bubbled as a gas (CO_2). Reactions were monitored by UV-vis spectroscopy for 2 h for any spectral changes and then warmed to room temperature. Samples for GC-MS analysis were demetallated by the following steps. Solvent was removed by vacuum and the remaining residue dissolved in CH_2Cl_2 (~ 5 mL). The solution was washed with dilute aqueous HCl (3 x 5 mL of 0.1 M HCl). The organic layer was dried over K_2CO_3, filtered, and examined by GC-MS.

CHAPTER 4. SYNTHESIS AND CHARACTERIZATION OF CU(I) COMPLEXES SUPPORTED BY *N*-HETEROCYCLIC CARBENE LIGANDS

4.1 Introduction

Since the first *N*-heterocyclic carbene (NHC) ligated metal complexes were reported in the late 1960s,[137] NHCs have been used as ligands in numerous metal complexes and catalysts.[138,139,140,141,142,143,144] The first account of a stable NHC, Ad (Figure 4.1), was reported by Arduengo *et al.*[145] This report led the way for synthetic inorganic chemists to use similar NHC ligands in the development of many catalyst systems including several generations of Grubb's catalysts (NHC-Ru complexes).[146] In addition to ruthenium, NHC-metal complexes have been reported with Pd,[147,148] Ni,[149] Rh,[150] Co,[151] Ir,[152] and many f-block elements.[140] The broad scope of existing NHC-metal chemistry led us to consider the potential for NHC-ligated copper complexes in copper mediated O_2-activation and the stabilization of copper-oxygen intermediates.

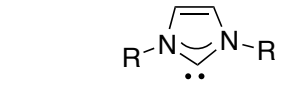

IPr: R = 2,6-di(isopropyl)phenyl
Mes: R = 2,4,6-tri(methyl)phenyl
Ad: R = adamantyl

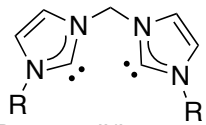

bis-IPr: R = 2,6-di(isopropyl)phenyl
bis-Mes: R = 2,4,6-tri(methyl)phenyl

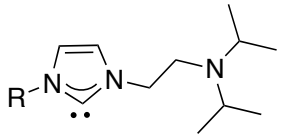

Mes-IPr$_2$N: R = 2,4,6-tri(methyl)phenyl

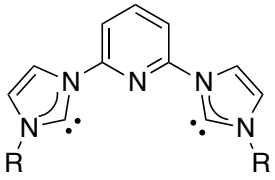

IPr$_2$Pyr: R = 2,6-di(isopropyl)phenyl
Mes$_2$Pyr: R = 2,4,6-tri(methyl)phenyl
Et$_2$Pyr: R = ethyl

Figure 4.1. *N*-heterocyclic carbene ligands used in the work reported in this chapter.

NHCs have been compared to phosphine ligands as they both coordinate metal centers with strong σ-bonds.[147] NHC ligands are known to have relatively inert metal-carbon bonds leading to robust ligand coordination and well-defined steric environments.[147,153,154] The strong donating ability of NHCs suggest that a Cu(I) complex ligated by one or more NHCs may be sufficiently activated to reduce O_2. The diversity of commercially available NHCs made this class of ligands attractive as a number of NHC-copper complexes could be rapidly synthesized and screened for reactivity with O_2. Additionally, most NHC syntheses are modular in nature allowing for the incorporation of additional functional groups including amines (Figure 4.1, Mes-IPr$_2$N) and pyridines (Figure 4.1, IPr$_2$Pyr, Mes$_2$Pyr, and Et$_2$Pyr) to form mixed-donor ligands.

Copper-NHC complexes have been reported in the literature and have found use as inexpensive catalysts both as discrete complexes[155,156] and through *in situ* formation.[139] One of the most common NHC-Cu complexes reported in the literature is (IPr)CuCl.[157] This complex has been used in the catalytic carboxylation of C–H bonds,[139] N–H bonds,[156] and organoboronic esters.[158] A number of NHC-Cu(I) complexes have been structurally characterized by single crystal X-ray crystallography. In reported structures the Cu(I) center is typically in a linear geometry ligated by one NHC and a strongly coordinating anion (Cl^-,[157f] $^-Cp^-$,[159] tBuO$^-$[160]) or in a linear geometry with two coordinating NHC ligands.[161,162,163] Only two examples of a Cu(I) atom coordinated by multiple NHC ligands with an open coordination site have been reported in the literature.[163,164] Hu *et al*. recently reported two Cu(I) complexes supported by tripodal tris(NHC)amine ligands (TIMEN$^{t\text{Bu}}$ and TIMEN$^{\text{Bz}}$) that contained open coordination sites

(Figure 4.2).[163,164] These ligands contain bulky protecting groups on the NHC heterocycles to shield the Cu(I) ion. It appears the larger protecting groups were necessary for the isolation of a mononuclear species as the use of the methyl substituted ligand, $TIMEN^{Me}$, resulted in the isolation of the trimeric species $[(TIMEN^{Me})_2Cu_3]^{3+}$. The trimeric complex contains three linear copper atoms with two coordinating NHC ligands bound to each copper ion. The mononuclear species $(TIMEN^{tBu})Cu(PF_6)$ and $(TIMEN^{Bz})Cu(Br)$ are of particular interest as they contain open coordination sites at the copper centers that may be useful in small molecule activation. While Hu *et al*. suggests that both $(TIMEN^{tBu})Cu(PF_6)$ and $(TIMEN^{Bz})Cu(Br)$ have potential utility for small molecule activation, the reactivities of these compounds towards small molecules have yet to be reported in the literature.[163,164]

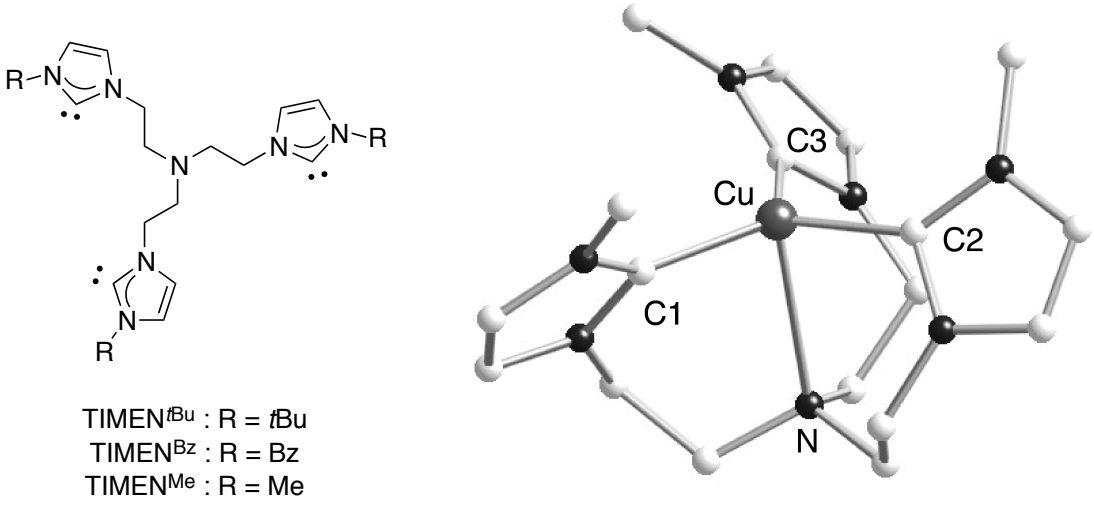

Figure 4.2. TIMEN ligand structure (*left*). Crystal structure of $(TIMEN^{tBu})Cu(PF_6)$ with *t*Bu groups, H-atoms, and PF_6 counteranion removed for clarity (*right*). The image was generated from the CIF file obtained from Ref [163].

The results presented in this chapter focus on the synthesis of NHC-Cu(I) complexes. A number of copper-complexes were synthesized with NHC ligands that

were envisioned to coordinate the metal centers in monodentate (mono-NHC) and bidentate (bis-NHC) modes. Additionally, copper-complexes supported by mixed donor systems that combined NHC groups along with either amine donors or pyridine donors in pincer type ligands were synthesized.

4.2 Ligand and Complex Synthesis

A number of NHC ligands were examined in this study to support Cu(I) complexes and are separated into three overall groups (Figure 4.1): (i) mono-NHCs that contain one NHC moiety (Figure 4.1, IPr, Mes, Ad); (ii) bis-NHCs that contain two NHC functionalities tethered together through an alkyl linker (Figure 4.1, bis-IPr, bis-Mes); (iii) and mixed-NHCs that contain at least one NHC group along with another ligating functionality such as a tertiary amine group (Figure 4.1, Mes-IPr_2N) or pyridine (Figure 4.1, IPr_2Pyr, Mes_2Pyr, Et_2Pyr). All NHC ligands were either purchased (IPr•HCl, Mes•HCl, Ad•HBF_4) or synthesized by reported procedures (bis-Mes,[165] bis-IPr,[166] Mes-IPr_2N,[167] IPr_2Pyr,[168] Mes_2Pyr,[168] and Mes_2Pyr[168]) as imidazolium salts.

4.2.1. Synthesis and Reactivity of Mono-NHC-Cu(I) complexes.

Mono-NHC ligands have found a number of applications in supporting metal-mediated catalysis as was introduced in Sections 4.1 and as such, several derivatives including IPr, Ad, and Mes are commercially available as air stable imidazolium salts. We envisioned a synthetic route that first involved the formation of NHC-copper complexes with either halide or BF_4^- counteranions, NHC-Cu(I)X (X = Cl^-, Br^-, BF_4^-) (Figure 4.3). These complexes would then be reacted with various silver salts in a

metathesis reaction to remove the coordinating halide and introduce a non-coordinating or weakly coordinating counteranion (Figure 5.3). We hypothesized this would yield NHC-Cu(I) complexes with labile metal coordination sites capable of O_2 coordination and activation by solvent displacement.

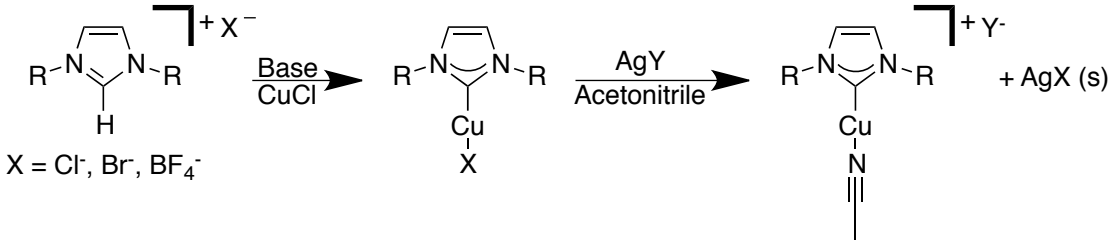

Figure 4.3. Proposed pathway for the synthesis of a mononuclear NHC-Cu(I) complex where R = 2,6-di(isopropyl)phenyl, 2,4,6-tri(methyl)phenyl, or adamantyl groups. X = Cl^-, Br^-, or BF_4^-. Y = $^-O_3SCF_3$, $^-SbF_6$, $^-PF_6$, or another non-coordinating or weakly coordinating counteranion.

We first examined Mes (Figure 4.1) as a supporting ligand. The imidazolium salt Mes•HCl was reacted with one equivalent of potassium *t*-butoxide (KO*t*Bu) in the presence of CuCl in dry THF. The colorless solution turned yellow and a grey precipitate formed within minutes. The solid was removed by filtration yielding a clear yellow solution. Removal of solvent *in vacuo*, dissolution in fresh THF, and slow addition of pentanes yielded colorless crystals of (Mes)CuCl that were analyzed by X-ray crystallography and found to be identical to the structure reported for the same compound by Díez-González *et al*. (Figure 4.4, See Table 4.1 for complete refinement details).[157d] The structure solved in the orthorhombic Fdd2 space group and displays the Cu(I) center in a linear geometry [C(1)-Cu-Cl = 180.000(1)] with C1 in a trigonal planar geometry (sum of bound atoms = 360°). A related structure reported by Díez-González *et al*. used an NHC derived from the 4,5-dihydro-imidazolium analog (4,5-dihydro-Mes) of Mes.[169]

This species contains an ethyl linker rather than an ethylene linker between N1 and N2 within the NHC heterocycle and was found to crystallize in the orthorhombic Pbca space group. The complex (4,5-dihydro-Mes)CuCl displays a nearly linear Cu(I) geometry [Cu(1)-Cu-Cl = 178.48(13)] and comparable Cu-C(1) (1.882 Å) and Cu-Cl (2.099 Å) distances to those found in (Mes)CuCl. Further reactions with (Mes)CuCl were not pursued because during the course of this work, two X-ray crystal structures of $[(Mes)_2Cu]X$ (X = $^-PF_6$ and $^-BF_4$) were reported.[161] In these structures, the replacement of the strongly coordinating chloride counteranion with either $^-PF_6$ or $^-BF_4$ led to the isolation of a linear Cu(I) complex with two NHC ligands. In the two reported structures, the mesityl side groups were not sterically bulky enough to prevent the formation of a linear $[(NHC)_2Cu(I)]^+$ species. We were therefore led to explore NHCs with larger side groups.

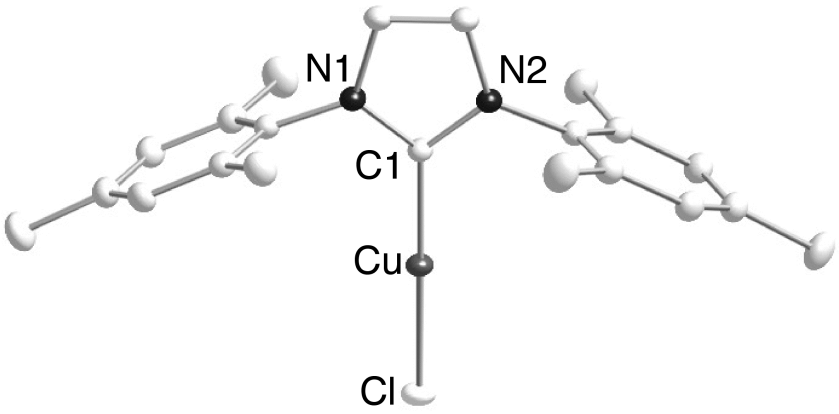

Figure 4.4 Representation of the X-ray structure of (Mes)CuCl with nonhydrogen atoms shown as 50% thermal ellipsoids. Selected interatomic distances (Å) and angles (deg): Cu-C(1), 1.893(8); Cu-Cl, 2.109(2); C(1)-N(1), 1.353(7);, C(1)-N(2), 1.354(7); C(1)-Cu-Cl, 180.000(1); N(1)-C(1)-N(2), 105.2(7), N(1)-C(1)-Cu,127.4(3); N(1)-C(1)-Cu(1), 127.4(3).

The bulkier mono-NHC Ad was examined next in an attempt to synthesize a

NHC-Cu(I) complex that would not adopt a linear $(NHC)_2Cu(I)$ structure. We hypothesized that the additional steric bulk produced by the adamantyl group would be sufficient to form an NHC-Cu(I) complex with an open metal coordination site capable of activating O_2 and stabilizing a copper-oxygen species. A solution of Ad•HBF_4 and KO*t*Bu in THF was added to a heterogeneous mixture of CuCl in THF. The mixture was stirred for 24 h and was filtered yielding a pale yellow solution. One equivalent of AgOTf was added resulting in the formation of a fine precipitate that was removed by filtration, which yielded a colorless solution. Concentration of the solution *in vacuo* yielded small crystals that were analyzed by X-ray crystallography, yielding the structure displayed in Figure 4.5. The crystals were small and provided poor quality data that only allowed for an isotropic final structural solution, but atom connectivity was nontheless established. The structure contains a copper atom ligated by two Ad ligands (Figure 4.5, *left*). The NHC heterocycle that should be planar displays a pronounced twisting that is likely an artifact of the poor resolution of the structure. The ring distortion is best observed when the structure is examined along the C1-Cu-C2 axis (Figure 4.5, *right*). Additionally, no counteranion was located due to the poor quality of data. Although no further structural information can be inferred, we can safely claim that the species is likely a linear Cu(I) complex with two ligating NHCs, $[(Ad)_2Cu]OTF$. It is clear that even with the large peripheral adamantyl groups on the NHC heterocycle, the steric bulk is directed too far away from the metal binding site to effectively protect the copper from forming a linear $L_2Cu(I)$ species. This led us to explore alternative NHC motifs including alkyl linked bis-NHCs and mixed-donor multidentate ligands that include at least one NHC group, which

will be discussed in Sections 4.2.2 and 4.2.3.

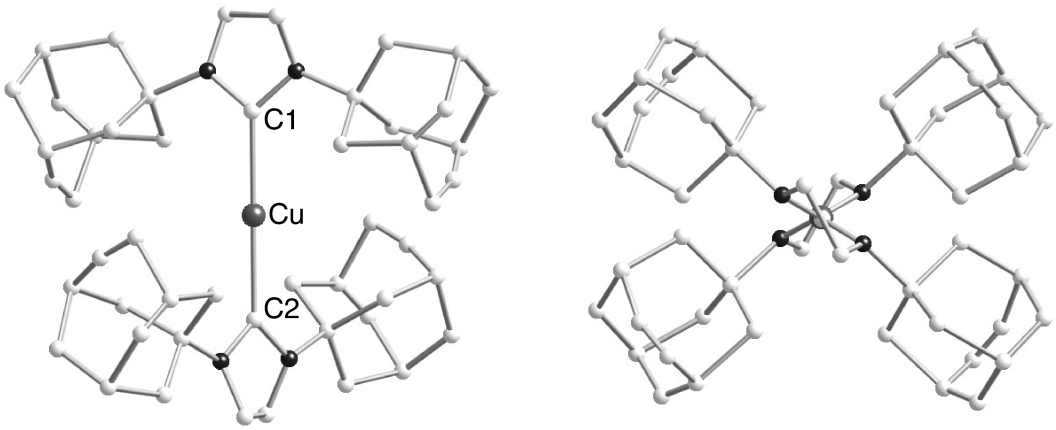

Figure 4.5. X-ray crystal structure of $[(Ad)_2Cu]OTF$ showing two views related by 90°.

Although a mononuclear NHC-copper complex with one NHC ligand and an open or labile coordination site on the copper atom was not isolated, reactions of $[(Ad)_2Cu]OTF$ with O_2 and iodosobenzene (PhIO) were examined. Solutions of $[(Ad)_2Cu]OTF$ (1 mM in CH_2Cl_2) were oxygenated at temperatures ranging from –80 °C to room temperature and monitored by UV-vis spectroscopy. No spectral changes were observed upon oxygenation at any temperature and solutions remained colorless suggesting that no reaction took place. Addition of 10 equivalents of PhIO to colorless solutions of $[(Ad)_2Cu]OTF$ (1 mM in CH_2Cl_2) at room temperature resulted in the observation of a transient feature by UV-vis spectroscopy at λ_{max} = 428 nm that formed instantaneously and decayed over 3 h (Figure 4.6, *left*). A feature at λ_{max} = 545 nm along with a less intense feature at λ_{max} = 420 nm formed and remained stable indefinitely under an atmosphere of argon, yielding a solution that displayed a red/pink color. Addition of a proton source such as methanol (MeOH) caused the decay of these features over several minutes via a transient species with a feature at λ_{max} = 400 nm, yielding a

final spectrum with a feature at λ_{max} = 430 nm.

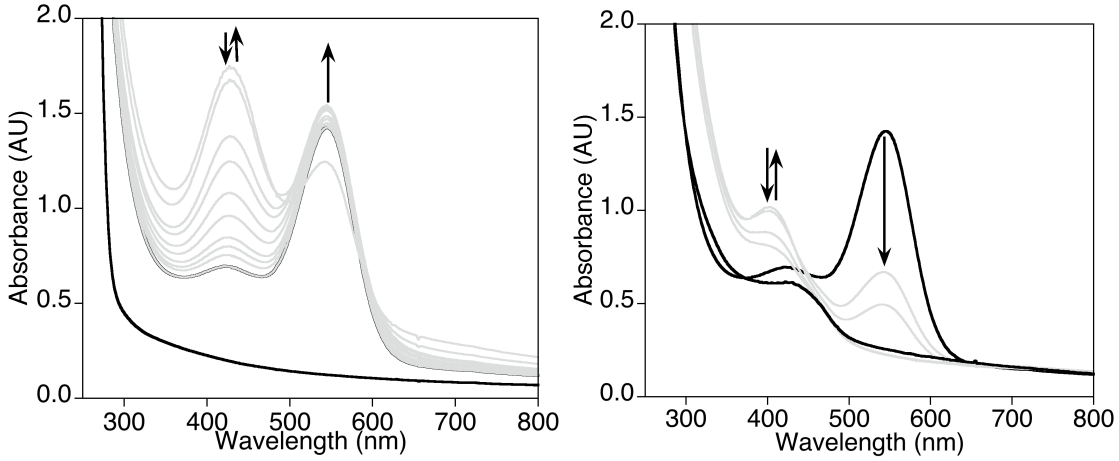

Figure 4.6. UV-vis spectra of the reaction of $[(Ad)_2Cu]OTF$ (1 mM in CH_2Cl_2) with 10 equivalents of PhIO at room temperature with spectra taken every 20 min for 3 hours (*left*). Addition of MeOH (10 equiv.) to the final product of a reaction of $[(Ad)_2Cu]OTF$ (1 mM in CH_2Cl_2) with 10 equivalents of PhIO with spectra taken every 1 min (*right*).

The feature at λ_{max} = 428 nm may be due to a copper-oxygen species resulting from O-atom transfer from PhIO to the Cu-complex (Figure 4.6). A feature at 428 nm is consistent with absorptions previously assigned to ligand-to-metal charge transfer transitions originating from dicopper(III)-bis(μ-oxo) intermediates. The formation of a dicopper(III)-bis(μ-oxo) species from $[(Ad)_2Cu]OTF$ would presumably require the loss of an Ad ligand to open a coordination site on the metal atom. ESI-MS analysis of the final reaction solution was dominated by a peak envelope assignable to $[AdH]^+$, the free imidizolium salt of the NHC ligand. A smaller peak envelope that corresponded to [Ad + 16 amu]$^+$ was observed. Based on literature precedent, the oxidized ligand is probably an imidazolidinone formed from the oxidation of the carbon atom that originally ligated the copper atom.[170] As mentioned in Section 4.1, NHC ligands are considered to be similar to phosphine ligands. A report by Kitajima *et* al. that was discussed at length in Section

1.2.3 reported the oxidation of a copper-bound phosphine ligand by PhIO.[50e] Upon subsequent dissociation, the copper atom reacted with an additional PhIO molecule leading to the formation of a copper-oxygen species. A similar pathway is proposed for the reactivity observed for $[(Ad)_2Cu]OTF$ with PhIO (Figure 4.7). The first equivalent of PhIO oxidizes and displaces one Ad ligand from $[(Ad)_2Cu]OTF$. A second equivalent of PhIO then reacts with [(Ad)Cu]OTf to form either an $[(Ad)Cu\text{-}PhIO]^+$ adduct or a Cu(II)-oxyl radical species that instantaneously dimerize to form the postulated dicopper(III)-bis(μ-oxo) species. Due to its transient nature, an accurate molar absorptivity for the feature at λ_{max} = 428 nm was not obtained to further corroborate the assignment as a dicopper(III)-bis(μ-oxo) species.

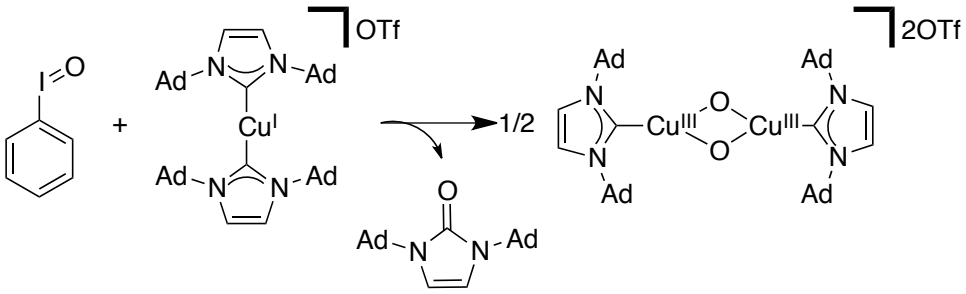

Figure 4.7. Proposed reaction between of $[(Ad)_2Cu]OTF$ and PhIO to form a dicopper(III)-bis(μ-oxo).

Further support for the formation of a dicopper(III)-bis(μ-oxo) species from the reaction between $[(Ad)_2Cu]OTF$ and PhIO came from resonance Raman spectroscopy. Reactions of $[(Ad)_2Cu]OTF$ and PhIO stirred for either 20 min or 5 h, were rapidly frozen in liquid N_2, and examined by resonance Raman spectroscopy (λ_{ex} = 406.7 nm). The sample frozen after 20 min displays a strong non-solvent feature at 622 cm^{-1} in the resonance Raman spectrum (Figure 4.8, *solid*). After the sample was stirred for 5 h, the

resonance Raman spectrum did not display this feature (Figure 4.8, *dashed*) suggesting that this feature is related to the transient absorption feature observed at λ_{max} = 428 nm by UV-vis spectroscopy. A resonance enhanced feature at 622 cm^{-1} in a Raman spectrum is consistent with our assignment of the transient species as a dicopper(III)-bis(μ-oxo) species, which have reported a_1 symmetric breathing mode vibrations from the $[Cu_2(O)_2]^{2+}$ core that are typically found near 600 cm^{-1}.[171] Spectroscopic analysis of the ^{18}O-labeled species would be required to confirm the isotope sensitivity of the feature observed at 622 cm^{-1} but to date that species has not been prepared.

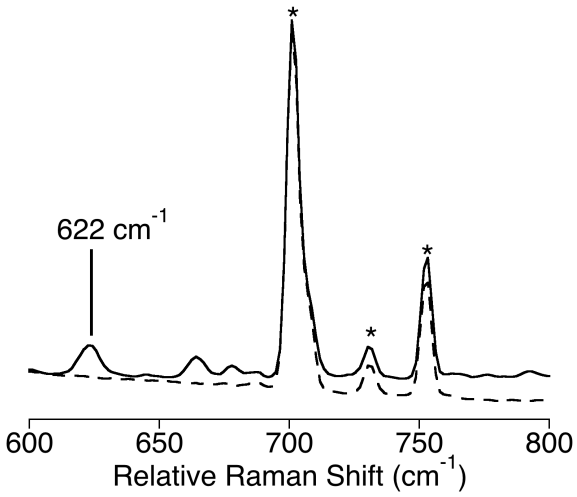

Figure 4.8. Resonance Raman spectra of reactions of $[(Ad)_2Cu]OTF$ (10 mM) and PhIO in CH_2Cl_2 after 20 min (*solid*) and 5 h (*dashed*) with an excitation wavelength of λ_{ex} = 406.7 nm. Peaks originating from the solvent, CH_2Cl_2, are marked (*).

The feature observed at λ_{max} = 545 nm in the UV-vis spectrum for the reaction between $[(Ad)_2Cu]OTF$ (10 mM) and PhIO (See Figure 4.6) is likely due to dissolved I_2, which has been reported to display absorption features near 550 nm.[172,173] Additionally, the absorption features of I_2 have been reported to be sensitive to solvent effects. More specifically, the observation that the addition of a protic solvent resulted in quenching of

the feature at λ_{max} = 545 nm would be consistent with the formation of hydrate cages.[173] The source of I_2 must be PhIO. Presumably after an equivalent of PhIO reacts with either Ad to form the imidazolidinone or with the Cu(I) complex to form a copper-oxygen species, iodobenzene, PhI, is formed. The insertion of copper atoms into the C–I bond of aryl-halides has been well documented in the literature, which may be a potential reaction pathway for the liberation of I^- or iodine radical that leads to the formation of the observed I_2.[174] Additionally, the photochemically induced homolytic cleavage of an aryl–I bond can lead to the release of I^- that can combine to form I_2.[175]

The reaction of $[(Ad)_2Cu]OTF$ with PhIO suggests that the formation of a copper-oxygen species supported by NHCs is possible. It has been proposed that the oxidation and dissociation of one NHC ligand from $[(Ad)_2Cu]OTF$ followed by an additional reaction with PhIO yields a transient dicopper(III)-bis(μ-oxo) species. The proposed reaction pathway presented in Figure 4.7 was supported by UV-vis and resonance Raman spectroscopies along with the observation of oxidized Ad ligand by ESI-MS. The work described in this section sought to synthesize a NHC-Cu(I) complex with a labile coordination site for O_2-binding and activation. It was determined that the propensity for NHC ligands to form linear $[(NHC)_2Cu]^+$ complexes is too strong, hindering direct reactions with O_2. Moreover, reactions with PhIO seemed to yield a dicopper(III)-bis(μ-oxo) species via the displacement of one NHC ligand. In the following sections, we expanded this research to include higher denticity NHC ligands (Section 4.2.2) and mixed donor ligands that include NHC ligation in addition to other *N*-donor functionalities (Section 4.2.3). We hypothesized that the chelation of the Cu(I) metal may allow for the

isolation of non-linear NHC-Cu(I) complexes.

4.2.2. Bidentate Alkyl coupled NHCs

As described in Section 4.2.1, attempts to synthesize monodentate NHC supported Cu(I) complexes led to the isolation of $[(Ad)_2Cu(I)]OTf$. The ligands bis-Mes and bis-IPr (Figure 4.1) were synthesized and used to attempt to make mononuclear Cu(I) complexes. One equivalent of (bis-Mes)•2HBr was reacted with two equivalents of KO*t*Bu in the presence of $Cu(I)(NCCH_3)_4PF_6$ in acetonitrile at room temperature for 24 h. Filtration of insoluble solids yielded a gold solution that upon concentration and addition of pentanes yielded a pale yellow crystalline material. Crystals were examined by X-ray crystallography and found to be $[(bis\text{-}Mes)_2Cu_2](PF_6)_2$ (Figure 4.9; see Table 4.1 for complete refinement details). The structure contains two bis-Mes ligands bridging two Cu(I) atoms. Both Cu(I) atoms are in distorted linear geometries [C-Cu(1)-C = 170° and C-Cu(2)-C = 169°]. The distortion from linear geometries at the metal sites are likely due to structural constraints caused by the ligand as the metal centers are separated by 3.2 Å, too far to consider the role of Cu–Cu bonding interactions that typically involve metal centers separated by approximately 2.5 Å or less.[176,177]

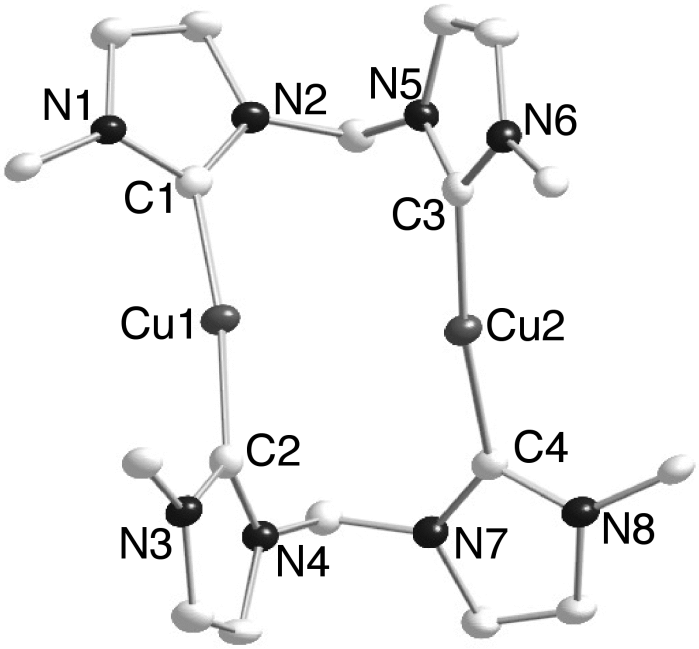

Figure 4.9. Representation of the X-ray structure of $[(\text{bis-Mes})_2\text{Cu}_2]2\text{PF}_6$ with nonhydrogen atoms shown as 50% thermal ellipsoids. Mesityl groups and counteranions have been omitted for clarity. Selected interatomic distances (Å) and angles (deg): Cu(1)-C(1), 1.904(5); Cu(1)-C(2), 1.897(5); Cu(2)-C(3), 1.902(5); Cu(2)-C(4), 1.895(5); C(1)-Cu(1)-C(2), 170.5(2); C(3)-Cu(2)-C(4), 169.5(2); N(1)-C(1)-N(2), 104.2(4); N(1)-C(1)-Cu(1), 126.2(4); N(2)-C(1)-Cu(1), 129.5(4); N(4)-C(2)-N(3), 104.0(4); N(4)-C(2)-Cu(1), 129.1(4); N(3)-C(2)-Cu(1), 126.3(4); N(6)-C(3)-N(5), 103.8(4); N(6)-C(3)-Cu(2), 130.2(4); N(5)-C(3)-Cu(2), 124.8(4); N(7)-C(4)-N(8), 103.5(4); N(7)-C(4)-Cu(2), 131.3(4); N(8)-C(4)-Cu(2), 125.2(4).

The dicopper complex $[(\text{bis-Mes})_2\text{Cu}_2]2\text{PF}_6$ did not display any appreciable reactivity towards O_2 as observed by the absence of spectral changes in the UV-vis spectrum upon oxygenation. After samples were oxygenated at room temperature for 30 min, crystalline material was isolated after removal of solvent *in vacuo*. This material was found to be $[(\text{bis-Mes})_2\text{Cu}_2]_2\text{PF}_6$ by X-ray crystallographic unit cell comparison to the structure shown in Figure 4.9. ESI-MS analysis of oxygenated solutions of $[(\text{bis-Mes})_2\text{Cu}_2]2\text{PF}_6$ demonstrated several copper-containing peak envelopes. A peak envelope at *m/z* = 1039.3 was observed and displays an isotope pattern indicative of a

dicopper species (Figure 4.10, *left*). The mass and isotope pattern were simulated successfully with the formula $\{[(\text{bis-Mes})_2\text{Cu}_2]\text{PF}_6\}^+$ (Figure 4.10, *right*). Additionally, a peak envelope for the dication $[(\text{bis-Mes})_2\text{Cu}_2]^{2+}$ was observed and simulated (Figure 4.11). Both the cation and dication contain the copper centers in the Cu(I) oxidation state. The observation of both peak envelopes in samples that had been oxygenated suggested that the dicopper(I) starting complexes did not react with O_2, which is consistent with no spectral changes in the UV-vis spectra upon O_2 introduction.

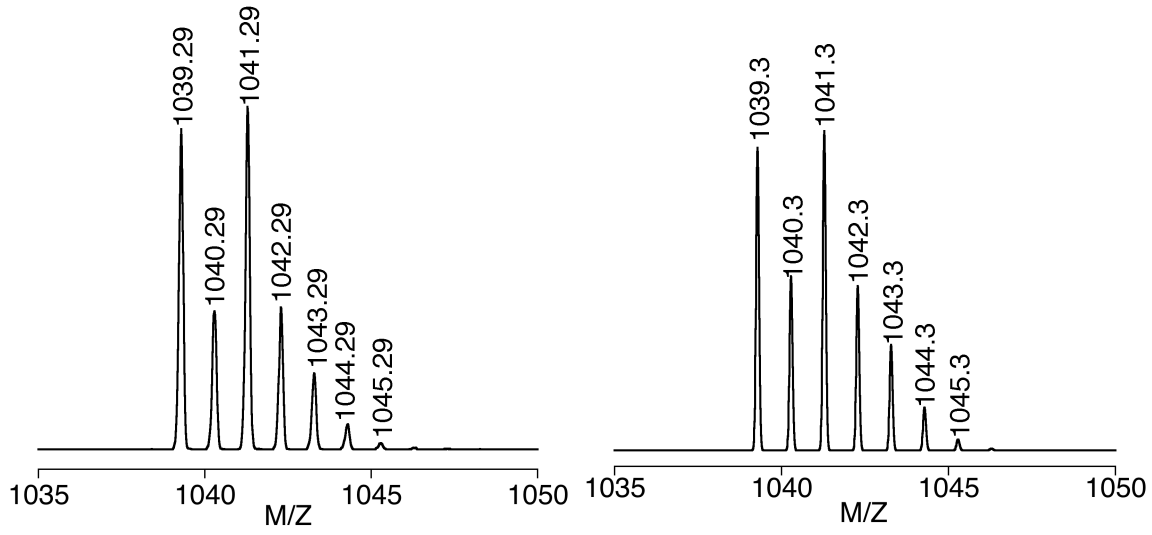

Figure 4.10. ESI-MS spectrum of the reaction products of the oxygenated solution of $[(\text{bis-Mes})_2\text{Cu}_2]2\text{PF}_6$ displaying the peak envelope assigned to $\{[(\text{bis-Mes})_2\text{Cu}_2]\text{PF}_6\}^+$ (*left*) and the simulated spectrum corresponding to the proposed ion formula (*right*).

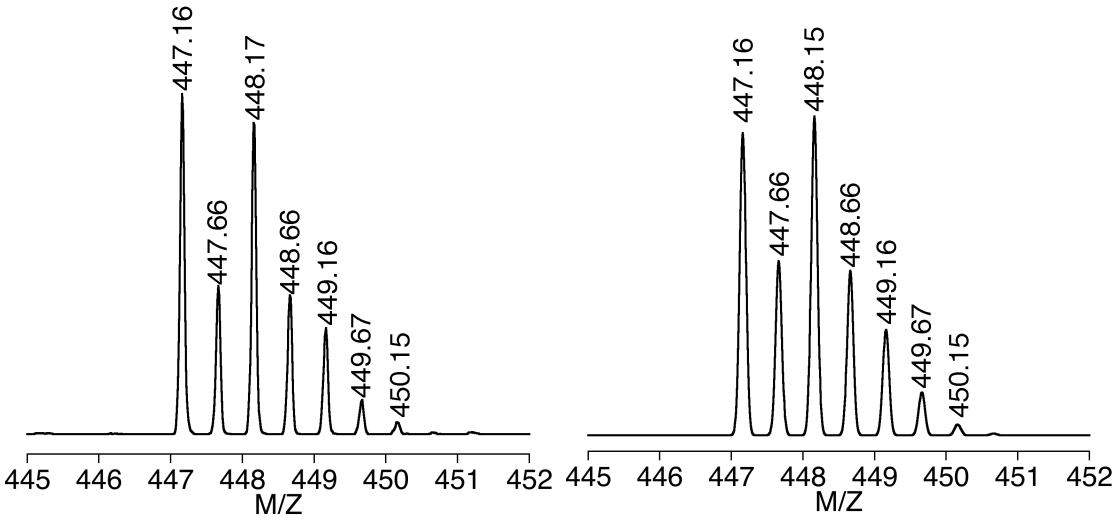

Figure 4.11. ESI-MS spectrum of the reaction products of the oxygenated solution of $[(\text{bis-Mes})_2\text{Cu}_2]2\text{PF}_6$ displaying the peak envelope assigned to $([(\text{bis-Mes})_2\text{Cu}_2])^{2+}$ (*left*) and the simulated spectrum corresponding to the proposed ion formula (*right*).

A third copper-containing peak envelope was observed in the ESI-MS spectrum for the oxygenated solution of $[(\text{bis-Mes})_2\text{Cu}_2]2\text{PF}_6$ at *m/z* = 863.4 that displays an isotope pattern indicative of a species containing one copper atom (Figure 4.12). The mass and isotope pattern were simulated successfully with the formula corresponding to $\{[(\text{bis-Mes})_2\text{Cu}(\text{O})_2]\}^+$ (Figure 4.12, *right*). This formula is generated by the loss of one Cu(I) atom and the introduction of two oxygen atoms into the starting $[(\text{bis-Mes})_2\text{Cu}_2]^{2+}$ species (Figure 4.13). It is likely that this species was formed in the ESI-MS instrument, as there is no other experimental observation of the oxidized ligand. This species likely formed by the decomposition of the parent $[(\text{bis-Mes})_2\text{Cu}_2]^{2+}$ complex by the loss of a Cu(I) atom and oxidation of the free NHC by O_2 (Figure 4.13).

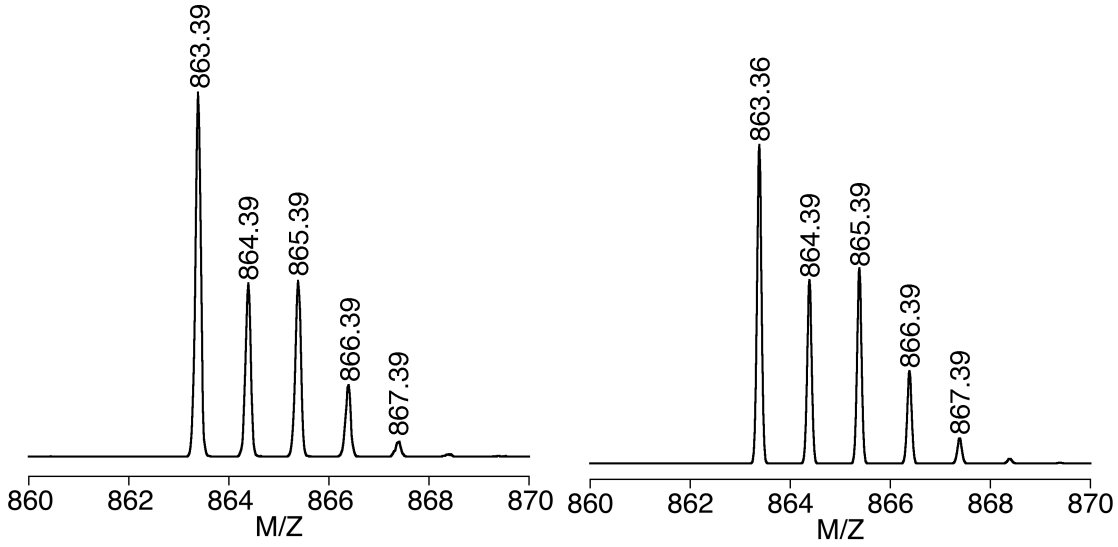

Figure 4.12. ESI-MS spectrum of the reaction products of the oxygenated solution of $[(\text{bis-Mes})_2\text{Cu}_2]2\text{PF}_6$ displaying the peak envelope assigned to $[(\text{bis-Mes})_2\text{Cu(O)}_2]^+$ (*left*) and the simulated spectrum corresponding to the proposed ion formula (*right*).

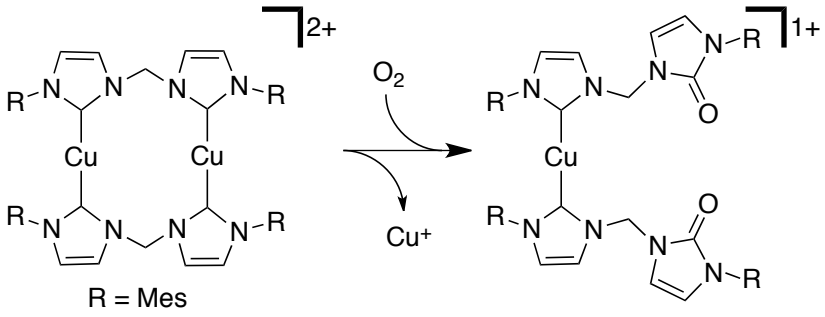

Figure 4.13. Proposed reaction resulting in the formation of $[(\text{bis-Mes})_2\text{Cu(O)}_2]^+$ involving the displacement of a Cu(I) atom and reaction of the NHC ligands with O_2.

4.2.3 Bidentate Mixed Donor NHCs

The difficulty in isolating non-linear NHC-Cu(I) complexes with mono- or bis-NHC ligands suggested that mixed donor ligands would potentially be better suited to form complexes for small molecule activation. The first ligand examined was Mes-IPr$_2$N, an asymmetric NHC with a bulky aryl group and a pendant amine group (See Figure 4.1). It was envisioned that Mes-IPr$_2$N would ligate a copper center with both the amine nitrogen and the NHC carbon atom. Reaction of Mes-IPr$_2$N with Ag_2O, to first form the

silver complex, resulted in the isolation of $[(Mes\text{-}IPr_2N)_2Ag]AgCl_2$ as large colorless crystals that were examined by X-ray crystallography and found to be identical to a previously reported structure (Figure 4.14).[178] As shown in Figure 4.14, the silver atom is ligated by two NHC carbon atoms, much like the linear $[(NHC)_2Cu]^+$ complexes described above. A second silver atom along with two coordinated chloride atoms were found in the unit cell acting as a counteranion. Ag(I) complexes typically demonstrate similar ligand coordination geometries with respect to analogous Cu(I) complexes.[179] With reported similarities in Ag(I) and Cu(I) coordination chemistry, this result was not encouraging in that the observed undesired linear $[(NHC)_2Ag]^+$ coordination would likely occur in a Cu(I) complex if $[(Mes\text{-}IPr_2N)_2Ag]AgCl_2$ was reacted with a Cu(I) salt in a metathesis/metal exchange reaction. Nonetheless, $[(Mes\text{-}IPr_2N)_2Ag]AgCl_2$ was reacted with CuCl in an attempt to access the mononuclear complex $[(Mes\text{-}IPr_2N)Cu]Cl$.

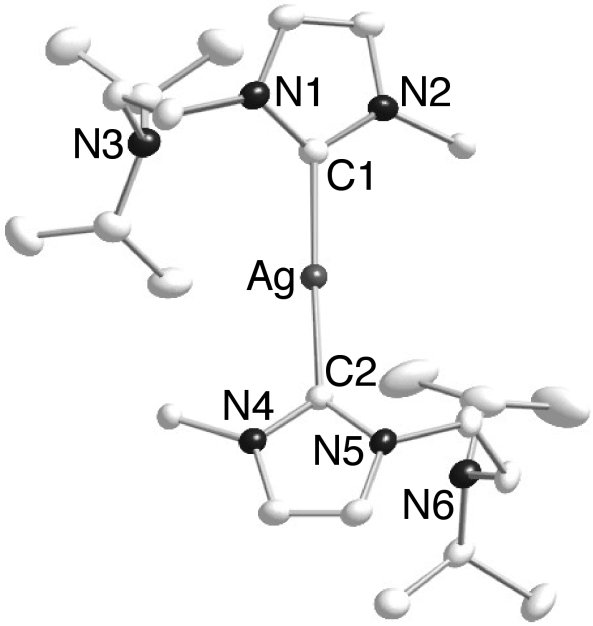

Figure 4.14. Representation of the X-ray structure of $[(\text{Mes-IPr}_2\text{N})_2\text{Ag}]\text{AgCl}_2$ with nonhydrogen atoms shown as 50% thermal ellipsoids and mesityl groups and counteranions omitted for clarity. Selected interatomic distances (Å) and angles (deg): Ag(1)-C(1), 2.071(3), Ag(1)-C(2), 2.069(3); C(1)-Ag(1)-C(2), 169.42(11); N(1)-C(1)-Ag(1), 132.1(2); N(1)-C(1)-N(2), 104.8(2); N(4)-C(2)-N(5), 104.5(2); N(2)-C(1)-Ag(1), 122.6(2); N(5)-C(2)-Ag(1), 130.5(2); N(4)-C(2)-Ag(1), 123.40(19).

Addition of one equivalent of CuCl to a solution of $[(\text{Mes-IPr}_2\text{N})_2\text{Ag}]\text{AgCl}_2$ resulted in the instantaneous formation of a grey precipitate. Filtration of the solid yielded a yellow solution that upon concentration yielded colorless crystalline material. The crystals were examined by X-ray crystallography and identified as an unexpected Cu(I)/Cl cluster (Figure 4.15). The cluster contained six copper atoms and ten bridging chloride atoms forming the tetranionic $[\text{Cu}_6\text{Cl}_{10}]^{4-}$ species. Additionally, four $[(\text{Mes-IPr}_2\text{N})\text{H}]^+$ cations were found in the unit cell. The protonation of the Mes-IPr_2N to yield the corresponding imidazolium cation cannot be explained except by invoking reaction with adventitious H_2O in the solvent used for the reaction and/or crystallization.

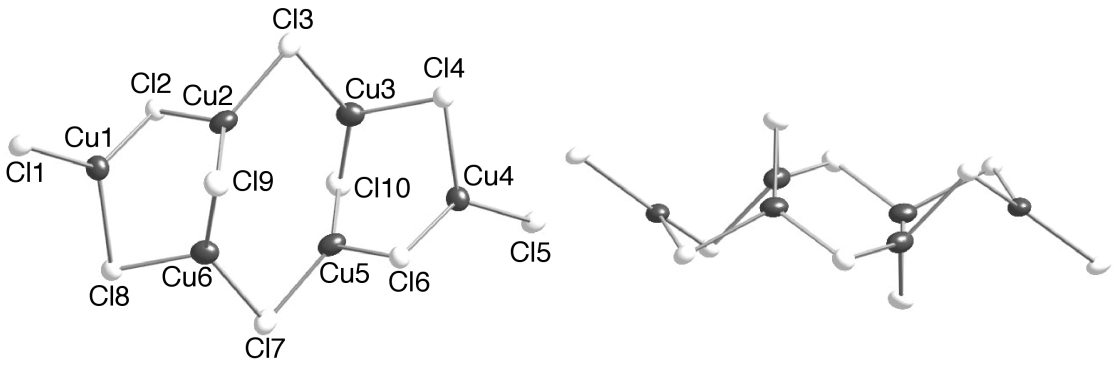

Figure 4.15. Representation of the X-ray structure of $[Cu_6Cl_{10}]^{4-}$ with nonhydrogen atoms shown as 50% thermal ellipsoids and with the imidazolium cations, 4[(Mes-IPr_2N)H]$^+$, removed for clarity. The two images are related to one another by a 90° rotation.

In a final attempt to synthesize a mononuclear NHC-Cu(I) complex with a labile coordination site on the copper atom, we turned towards pincer type ligands (Figure 4.1, IPr_2Pyr, Mes_2Pyr, and Et_2Pyr). We envisioned the central pyridine functionality would act to anchor the copper atom while the two peripheral NHC groups would bind the metal site to form a square planar metal complex along with a solvent derived fourth ligand. This methodology proved successful in the reports by Hu *et al*. that described the isolation of two Cu(I) complexes, (TIMEN$^{t\text{Bu}}$)Cu(PF_6) and (TIMEN$^{\text{Bz}}$)Cu(Br) (Figure 4.2).[163,164] In the reported complexes, an axial amine anchored the copper center with three NHC groups ligating the copper's equatorial positions. The first ligand examined, Et_2Pyr, was chosen due to the ease of its one step synthesis from commercially available starting materials. Et_2Pyr•2HBr was reacted with two equivalents KO*t*Bu in the presence of one equivalent of Cu(I)($NCCH_3)_4$OTf in acetonitrile. Removal of insoluble potassium salts by filtration, concentration of the reaction solution *in vacuo*, and addition of pentanes yielded a yellow crystalline solid that was isolated and analyzed by X-ray crystallography. The structure shown in Figure 4.16 revealed the metal complex was the

dicopper(I) complex, $(Et_2Pyr)_2Cu_2OTf_2$, with two bridging Et_2Pyr ligands coordinated via the NHC carbon atoms. The pyridine nitrogen atoms are not bound to the copper atoms as observed by long Cu–N_{pyr} distances (2.6–2.7 Å). The two copper centers are relatively close to one another at a distance of 2.87 Å, which is closer than the Cu–Cu distance observed in $[(bis\text{–}Mes)_2Cu_2]_2PF_6$ (3.2 Å) but still too long to indicate a Cu–Cu bond.[176]

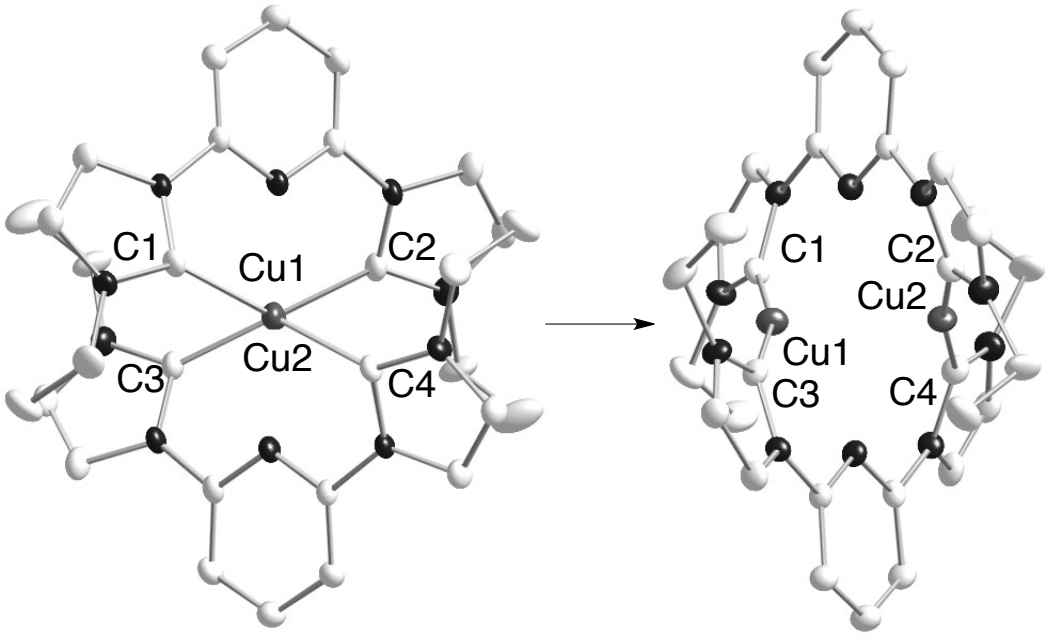

Figure 4.16. Representation of the X-ray structure of $(Et_2Pyr)_2Cu_2OTf_2$ with non-hydrogen atoms shown as 50% thermal ellipsoids with OTf counteranions and H-atoms omitted for clarity. The two structures are related by a 90° rotation. Selected interatomic distances (Å) and angles (deg): Cu(1)-C(1), 1.906(5); Cu(1)-C(3), 1.906(5); Cu(2)-C(2), 1.900(5); Cu(2)-C(4), 1.900(5); Cu(1)-Cu(2), 2.8650(14), C(1)-Cu(1)-C(3), 169.7(3), C(2)-Cu(2)-C(4), 163.4(3).

The structure of $(Et_2Pyr)_2Cu_2OTf_2$ shown in Figure 4.16 was discouraging as it demonstrated that the central pyridine linker in Et_2Pyr did not anchor the copper atom, resulting in the formation of a dicopper complex with linear Cu(I) atoms ligated by bridging Et_2Pyr ligands. A structure similar to $(Et_2Pyr)_2Cu_2OTf_2$ was reported by Caballero *et al.* with a benzyl-substituted NHC (Figure 4.17, Bz_2Pyr) and silver.[180] In the

silver analog, the bulkier Bz_2Pyr ligand was used and dimerization still occurred. The $(Bz_2Pyr)_2Ag_2OTf_2$ structure contains two silver atoms in a distorted linear geometry (C–Ag–C angle = 165.5°) similar to the copper atoms in $(Et_2Pyr)_2Cu_2OTf_2$ (C–Cu–C angles = 163–170°). Additionally, the ligating carbon atoms in $(Bz_2Pyr)_2Ag_2OTf_2$ display M–C bond lengths of 2.08 Å that are similar to those observed in the crystal structure of $(Et_2Pyr)_2Cu_2OTf_2$ (Figure 4.16). In the case of $(Bz_2Pyr)_2Ag_2OTf_2$, the pyridine moiety was ineffective at anchoring the metal center. A related report by Pugh *et al.* examined silver complexes with the extremely bulky IPr_2Pyr ligand (Figure 4.1) and found that dimerization occurs.[181] This led us to assume that the formation of a dicopper species would occur when using the significantly sterically hindered Mes_2Pyr or IPr_2Pyr ligands causing us to forgo further synthetic efforts to isolate mononuclear Cu(I) complexes with pincer type ligands. The propensity for pincer type ligands with NHC groups to form linear or distorted linear Cu(I) or Ag(I) complexes proved too great to isolate the desired complexes.

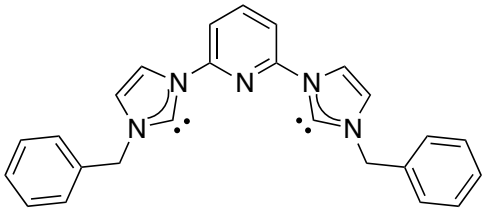

Figure 4.17. Structure of Bz_2Pyr ligand described in Ref [180].

4.3. Conclusion and Perspectives

The work presented in this chapter sought to synthesize and isolate Cu(I) complexes ligated by NHC ligands capable of coordinating and activating O_2 or reacting

with oxo-transfer reagents such as PhIO. The strong σ-donating ability of NHC ligands to metal centers suggested that they would be strong candidates to sufficiently activate Cu(I) towards O_2 reduction and additionally stabilize higher oxidation states, such as Cu(III), in reported copper-oxygen intermediates.[79] As introduced in Section 4.1, Hu *et al.* reported two tripodal ligands, $TIMEN^{tBu}$ and $TIMEN^{Bz}$, that were used to synthesize and isolate two Cu(I) complexes with coordination sites that may be used for small molecule activation (Figure 4.2).[163,164]

Attempted syntheses of Cu(I) or related Ag(I) complexes with Ad (Figure 4.5), bis-Mes (Figure 4.9), Mes-IPr_2N (Figure 4.14), and Et_2Pyr (Figure 4.16) ligands all resulted in the isolation and crystallographic conformation of linear metal complexes with two NHC ligands. These species were not ideal for O_2 reactivity in that an NHC ligand would need to be displaced in order for O_2 coordination and activation. Metal-NHC bonds, as previously mentioned, are robust[147,153,154] and as expected the linear $[(NHC)_2Cu]^+$ complexes $[(Ad)_2Cu]OTf$, $[(bis\text{-}Mes)_2Cu_2]2PF_6$, and $[(Et_2Pyr)_2Cu_2]OTf_2$ all appeared to be air stable. ESI-MS analysis of $[(bis\text{-}Mes)_2Cu_2]_2PF_6$ revealed the presence of O-atom inserted ligand, although this species likely formed via the loss of a Cu(I) atom followed by the reaction of a free NHC with O_2 inside the spectrometer (Section 4.2.2 and Figure 4.13).

One promising reaction between $[(Ad)_2Cu]OTf$ and PhIO was described in Section 4.2.1. It was found that $[(Ad)_2Cu]OTf$ reacts rapidly with PhIO at room temperature to form a transient species detected by UV-vis spectroscopy that was postulated to be a dicopper(III)-bis(μ-oxo) species (Figures 4.6). The O-atom inserted

NHC ligand, presumably an imidazolidinone, was detected by ESI-MS, leading us to propose the reaction pathway shown in Figure 4.7. $[(Ad)_2Cu]OTf$ first reacts with one equivalent of PhIO to form the oxidized NHC ligand that is displaced from the copper atom. A second PhIO then reacts with (Ad)CuOTf to form either a Cu(I)-PhIO adduct or Cu(II)-oxyl radical species that instantaneously dimerize to form the proposed dicopper(III)-bis(μ-oxo) species (Figure 4.7). Further evidence for the formation of a dicopper(III)-bis(μ-oxo) species came from resonance Raman spectroscopy that revealed a non-solvent feature at 622 cm^{-1} that is likely from the a_1 symmetric core breathing mode from a $[Cu_2(O)_2]^{2+}$ species (Figure 4.8).

4.4. Experimental

General Considerations. All solvents and reagents were obtained from commercial sources unless otherwise noted. Solvents were thoroughly degassed via three cycles of freezing, evacuating, and thawing. THF and d_8-THF were dried over Na/benzophenone and distilled under vacuum. CH_2Cl_2, CD_2Cl_2, and CH_3CN were dried over CaH_2 and distilled under vacuum and CH_3CN was stored over 4 Å molecular sieves. $CDCl_3$ was distilled under vacuum from $CaCl_2$. Pentanes were passed through solvent purification columns (Glass Contour, Laguna, CA) and stored over CaH_2 in a glove box. All metal complexes were prepared and stored in a Vacuum Atmospheres inert atmosphere glove box under dry nitrogen or were manipulated under argon or dry nitrogen using standard Schlenk techniques.

Physical Methods. NMR spectra were recorded on either Varian VI-300, VXR-300, or VI-500 spectrometers at room temperature. Chemical shifts (δ) for ^1H and ^{13}C NMR

spectra were referenced to residual protium in the deuterated solvent (^{1}H NMR experiments) or the characteristic solvent resonances of the solvent nuclei (^{13}C NMR experiments). UV-vis spectra were collected on a HP8453 (190-1000 nm) diode array spectrophotometer. Low temperature UV-vis experiments were performed using an Unisoku low temperature UV-vis cell holder. UV-vis spectra that had drifting baselines due to minor frosting caused by the low-temperature device were corrected when necessary by subtracting the average of a region with no absorbance from the entire spectrum. Elemental analysis was performed by Robertson Microlit Lab (Madison, NJ). Electrospray ionization mass spectrometry (ESI-MS) was performed on a Bruker BioTOF II instrument. All GC-MS experiments were conducted on an Agilent Technologies 7890A GC system and 5975C VL MSD. The GC column was a HP-5ms with dimensions 30 m x 0.250 mm. The standard method used for all runs involved an initial oven temperature of 60 °C (held for 4 min) followed by a 20 °C/min ramp to 230 °C that was held for 15 min. Resonance Raman spectra were recorded on an Acton 506 spectrometer using a Princeton Instruments LN/CCD-11100-4 PB/UBAR detector and ST-1385 controller interfaced with Winspec software. The spectra were obtained at –196 °C using backscattering geometry. Excitation at 406.7 nm was provided by a Spectra-Physics BeamLok 2060-KR-V Krypton ion laser. Raman shifts were externally referenced to liquid indene and internally referenced to solvent (CH_2Cl_2).

(Mes)CuCl. Mes•HCl (90.1 mg, 0.26 mmol) and CuCl (26.2 mg, 0.26 mmol) were combined in THF (10 mL) resulting in a heterogeneous slurry. NaH (6.3 mg, 0.26 mmol) was added in THF and the resulting mixture was stirred for 24 h at room temperature.

The solution was filtered yielding a clear yellow solution that upon concentration *in vacuo* and addition of pentanes yielded colorless crystalline solid of (Mes)CuCl (73.8 mg, 70 %). ^{1}H NMR (d_8-THF, 300 MHz): δ 8.10 (2H, s) 7.17 (4H, s), 2.37 (6H, s), 2.22 (12H, s).

[(Ad)$_2$Cu]OTf. Ad•HBF_4 (50 mg, 0.12 mmol) was added to a slurry of CuCl (11.7 mg, 0.12 mmol) and KO*t*Bu (13.2 mg, 0.12 mmol) in THF (5 mL). The reaction was stirred for 12 h, filtered, and the solvent removed *in vacuo*, yielding a white solid. This solid was dissolved in a 50:50 mixture of THF/acetonitrile (5 mL) and AgOTf (31 mg, 0.12 mmol) was added. The resulting off-white precipitate was removed by passing the reaction through a celite plug and this clear solution yielded a colorless crystalline solid upon concentration *in vacuo*. The crystalline solid was examined by X-ray crystallography and yielded the structure shown in Figure 4.5.

1-(Mesityl)imidazole. Concentrated H_3PO_4 (85 wt. % in H_2O) was added drop wise to a solution of mesitylamine (13.5 g, 0.1 mol) in H_2O (50 mL) until a pH of 2 was achieved. Ammonium chloride (5.35 g, 0.1 mol) in 20 mL of H_2O was added drop wise to this solution over a 30 min period. Paraformaldehyde (3.00 g, 0.1 mol) and glyoxal (11.5 mL, 0.1 mol) were added to the reaction as a mixture in H_2O (100 mL) and 1,4-dioxane (100 mL), and the reaction heated to 100 °C. The solution turned black and was stirred for an additional 1 h, and then cooled to 0 °C in an ice bath. An additional 100 mL of H_2O was added and the organic layer was extracted with hexanes (3 x 300 mL). The organic fractions were combined and dried over $MgSO_4$ overnight. The $MgSO_4$ was removed by filtration and the solvent removed *in vacuo* to yield a brown solid. The solid was

recrystallized from ethyl acetate to yield golden crystals (5.32 g, 29%). ^{1}H NMR ($CDCl_3$, 300 MHz): δ 7.44 (1H, s), 7.24 (1H, s), 6.98, (2H, s), 6.90 (1H, s), 2.35 (3H, s), 2.0 (6H, s).

Bis-Mes•2HBr. 1-(Mesityl)imidazole (1.5 g, 8.06 mmol) was added to CH_2Br_2 (1.4 g, 4.02 mmol) in toluene (10 mL) and the resulting mixture was refluxed for 48 h. The solution was cooled to room temperature and the white precipitate that formed was isolated by filtration. The solid was first washed with THF and then acetonitrile to yield a white powder (1.22 g, 42%). ^{1}H NMR ($CDCl_3$, 300 MHz): δ 11.44 (2H, s), 9.92 (2H, s), 7.98 (2H, s), 7.20 (2H, s), 7.05 (4H, s), 2.37 (6H, s), 2.06 (12H, s).

[(bis-Mes)$_2$Cu$_2$][PF$_6$]$_2$. Bis-Mes•2HBr (150 mg, 0.27 mmol) was added to a slurry of KO*t*Bu (62.9 mg, 0.56 mmol) and Cu(I)$(NCCH_3)_4PF_6$ (102.3 mg, 0.27 mmol) in 5 mL of acetonitrile at room temperature. After having been stirred for 24 h, the insoluble solids were removed by filtration to yield a golden brown solution. Concentration of the solution *in vacuo* and addition of pentanes yielded a white crystalline powder (41 mg, 25%). Anal. Calc for $C_{50}H_{56}Cu_2F_{12}N_8P_2$: C, 50.63; H, 4.76; N, 9.45. Found: C, 50.74; H, 4.62; N, 9.45. ESI-MS *m/z*: 448 $[M+2PF_6]^{2+}$, 1041 $[M+PF_6]^{1+}$.^{1}H NMR (CD_2Cl_2), 300 MHz): δ 7.69 (s, 2H), 7.00 (d, J = 13.8 Hz, 2H), 6.89 (s, 4H), 6.44 (d, J = 13.8 Hz, 2H), 2.45 (s, 6H), 1.63 (s, 6H), 1.34 (s, 6H), 1.17 (s, 3H), 1.14 (s, 3H), 0.07 (s, 12H).

[(Mes-IPr$_2$N)$_2$Ag]AgCl$_2$. Mes-IPr$_2$N•HCl (102.9 mg, 0.26 mmol) and Ag_2O (30.2 mg, 0.1 mmol) were combined in CH_2Cl_2 (10 mL) and refluxed over 4 Å molecular sieves for 24 h. The solution was filtered to remove the molecular sieves and the solvent removed *in vacuo* yielding a white solid. Addition of fresh CH_2Cl_2 (2 mL) and pentanes (2 mL)

yielded colorless crystalline blocks of [(Mes-IPr$_2$N)$_2$Ag]AgCl$_2$ that were characterized by X-ray crystallography (Figure 4.14). Calc. for $C_{40}H_{62}Ag_2Cl_2N_6$•(C_5H_{12})3•($NCCH_3$)$_2$: C, 58.46, H, 8.65; N, 9.24. Found: C, 58.44; H, 8.00; N, 9.66.

(Et$_2$Pyr)$_2$Cu$_2$OTf$_2$. Et$_2$Pyr•2HBr (67.4 mg, 0.16 mmol) was added to a solution of CuOTf($NCCH_3$)$_4$ (59.2 mg, 0.16 mmol) in acetonitrile (5 mL). KO*t*Bu (35.3 mg, 0.3 mmol) was added in acetonitrile (2 mL) and the solution was stirred for 12 h at room temperature. The cloudy heterogeneous mixture was filtered to yield a clear gold solution that upon concentration *in vacuo* yielded gold block shaped crystals. These crystals were analyzed by X-ray crystallography and were found to be the complex (Et$_2$Pyr)$_2$Cu$_2$OTf$_2$ (Figure 4.16). ^{1}H NMR (d_6-DMSO, 300 MHz): δ 8.63 (t, J = 7.8 Hz, 2H), 8.42 (s, 4H) 8.15 (d, J = 7.8 Hz, 4H), 7.76 (s, 4H), 3.73 (m, J = 7.2 Hz, 8H), 0.98 (t, J = 7.2 Hz, 6H). ^{13}C{^{1}H} NMR (75.0 MHz, d_8-DMSO): δ 178.1, 148.4, 144.5, 123.2, 118.7, 113.1, 54.9, 46.1, 15.57. IR (Neat): 1608, 1591, 1467, 1425, 1258, 1225, 1162, 1030 cm^{-1}. Calc. for $C_{32}H_{34}Cu_2F_6N_{10}O_6S_2$•($C_4H_8O$)•($NCCH_3$)$_4$: C, 44.18; H, 4.55; N, 16.39. Found: C, 43.84; H, 4.43; N, 16.60.

Reactions of [(Ad)$_2$Cu]OTf with PhIO. A quartz cuvette was charged with 3.5 mL of a 1 mM solution of [(Ad)$_2$Cu]OTf in CH_2Cl_2 and sealed with a rubber septum in a glove box. Additionally, PhIO (8 mg, 0.035 mmol) in 0.2 mL of CH_2Cl_2 and loaded into a syringe in the glove box. Under an atmosphere of argon, the PhIO was added to the quartz cuvette and monitored by UV-vis spectroscopy while constantly stirring. Reactions to be examined by resonance Raman spectroscopy were prepared in the glove box as 10 mM solutions of [(Ad)$_2$Cu]OTf in CH_2Cl_2 that were reacted with PhIO (10

equiv.) in the glove box. An aliquot (0.5 mL) was removed at 20 min via syringe and loaded into an NMR tube that was sealed by a septum. The tube was removed from the glove box and instantly frozen in liquid N_2 and stored for subsequent resonance Raman analysis. Similarly, an aliquot (0.5 mL) was removed from the reaction after 5 h and stored in an identical manner for subsequent analysis.

Table 4.1. Summary of X-Ray Crystallographic Data

	(Mes)CuCl	$(Ad)_2CuOTf$	$[(bis\text{–}Mes)_2Cu_2]2PF_6$	(Mes-$IPr_2N)_2Ag\bullet AgCl_2$	(Mes-$IPr_2N)_4Cu_6Cl_{10}$	$(Et_2Pyr)_2Cu_2OTf_2$
Empirical formula	$C_{21}H_{24}ClCuN_2$	$C_{47}H_{64}CuF_3N_4O_3S$	$C_{50}H_{60}Cl_2Cu_2F_6N_8P_2$	$C_{40}H_{62}AgClN_6$	$C_{20}H_{31}ClCuN_3$	$C_{16}H_{17}CuFN_5O_3S$
Formula weight	403.41	885.62	1146.98	770.28	412.47	441.95
Crystal system	Orthorhombic	Orthorhombic	Monoclinic	Triclinic	Monoclinic	Orthorhombic
Space group	Fdd2	Pnnn	$P2_1/n$	$P\bar{1}$	$P2_1/c$	Fddd
a (Å)	14.7587(11)	13.877(2)	12.5466(15)	11.3397(11)	14.240(2)	17.123(3)
b (Å)	29.157(2)	13.874(2)	15.8552(19)	13.6294(13)	11.0654(18)	24.036(4)
c (Å)	9.5273(7)	23.340(4)	32.373(4)	15.3667(16)	18.209(3)	44.618(7)
α (deg)	90	90	90	82.931(3)	90	90
β (deg)	90	90	94.993(4)	78.186(3)	113.02	90
γ (deg)	90	90	90	69.621(3)	90	90
Volume ($Å^3$)	4099.8(5)	4493.7(13)	6415.4(13)	2175.7(4)	2640.8(8)	18364(5)
Z	8	4	5	2	4	36
T(K)	173(2)	173(2)	173(2)	173(2)	173(2)	173(2)
ρ (calculated) (Mg/m^3)	1.307	1.309	1.484	1.176	1.037	1.439
θ range (deg)	2.64 to 24.97	1.71 to 25.24	1.26 to 25.08	1.36 to 25.12	1.55 to 25.06	1.53 to 25.02
μ (mm^{-1})	1.201	0.590	1.061	0.557	0.934	1.206
Reflections collected	9717	42284	60731	7751	23238	36600
Independent reflections	1801	4076	11374	7751	4670	4074
parameters	115	104	760	451	287	290
R1, wR2 (for $I > 2\sigma(I)$)	0.0421, 0.1100	0.4608, 0.8106	0.0753, 0.1791	0.0331, 0.0806	0.0285, 0.0624	0.0597, 0.1573
GOF	1.072	3.445	1.030	1.001	1.050	1.145
Largest Peak, Hole ($e.Å^{-3}$)	0.339 and -0.393	3.275 and -2.171	1.053 and -1.069	0.885 and -1.557	0.785 and -0.493	3.115 and -0.744
F(000)	1680	1880	2960	816	872	8136
Crystal color, morphology	Colorless, plate	Colorless, block	Yellow, plate	Colorless, prism	Colorless, plate	Gold, block
Crystal size	.4 x .2 x .2 mm^3	.2 x .1 x .1 mm^3	.5 x .3 x .3 mm^3	.3 x .2 x .2 mm^3	.3 x .2 x .2 mm^3	.5 x .4 x .4 mm^3
Index ranges	$-17 \le h \le 17$, $-34 \le k \le 34$, $-11 \le l \le 11$	$-16 \le h \le 16$, $-16 \le k \le 16$, $-27 \le l \le 27$	$-14 \le h \le 14$, $-18 \le k \le 18$, $-38 \le l \le 38$	$-13 \le h \le 13$, $-16 \le k \le 16$, $0 \le l \le 18$	$-16 \le h \le 16$, $-12 \le k \le 13$, $-21 \le l \le 21$	$-20 \le h \le 20$, $-28 \le k \le 28$, $-52 \le l \le 51$

Chapter 5. Collaborative Projects.

5.1. Collaborative Projects: Resonance Raman

During the course of the dissertation research described in the previous chapters, several collaborative projects were undertaken with all resonance Raman experiments done by myself in the laboratory of Prof. Lawrence Que Jr. A brief introduction for each project and the resonance Raman results that were completed for that project will be presented in the following sections.

5.1.1. A Mixed Valent $[Cu(III)Cu(II)_2S_2]^{2+}$ Species[182]

Nitrous oxide (N_2O) is an important greenhouse gas and component of the global nitrogen cycle.[183] The reduction of N_2O to N_2 is thermodynamically favorable ($E° = 1.76$ V) but contains a high kinetic barrier hindering its use as an environmentally friendly oxidant. Nature uses the metalloenzyme nitrous oxide reductase, N_2OR, to catalyze the reduction of N_2O to N_2 and H_2O at an active site μ-sulfido-tetracopper cluster.[184] A definitive mechanism for the copper-catalyzed reduction of N_2O has yet to be settled on in the scientific community leading to continued research both on the enzymatic system and synthetic Cu/S model complexes.

Dr. Itsik Bar-Nahum, a postdoctoral researcher in the Tolman group, found that reacting Na_2S_2 with the Cu(I) complexes $[LCu(CH_3CN)]X$ (L = 1,4,7-trimethyl-triazacyclononane, X = $O_3SCF_3^-$ or SbF_6^-) led to the formation of either **2a** or **2b** (Figure 5.1). These two species where identified as (μ-η^2:η^2-disulfido)dicopper(II) species that

were confirmed by resonance Raman spectroscopy (Figure 5.2 and 5.3). Samples of **2a** and **2b** were prepared as 4 mM solutions in CH_2Cl_2 in NMR tubes in the glove box and frozen in liquid N_2 prior to analysis. Compound **2a** displayed a strong visible feature at $\lambda_{max} \sim 400$ nm observable by UV-vis spectroscopy, so an excitation wavelength of $\lambda_{ex} = 406.7$ nm was chosen. The resonance Raman spectra of **2a** (both ^{32}S and ^{34}S) were acquired with samples frozen in liquid N_2 (–196 °C) with 30 sec frames, 256 spectra taken and averaged to yield the final spectra, and 100 mW laser power (Figure 5.2). The resonance Raman spectrum for **2a** was previously reported and the observed features in this study were identical (477 cm^{-1}, $\Delta^{34}S = 14$ cm^{-1}).[185] The resonance Raman spectrum for **2b** ($\lambda_{ex} = 457.0$ nm) displays three strong features at 434, 442, and 452 cm^{-1} that shift to 431 and 438 cm^{-1} upon isotope labeling (Figure 5.2). These values and isotope shifts are consistent with previously reported resonance Raman features from our laboratory for S–S vibrations in a (μ-η^2:η^2-disulfido)dicopper(II) species.[185]

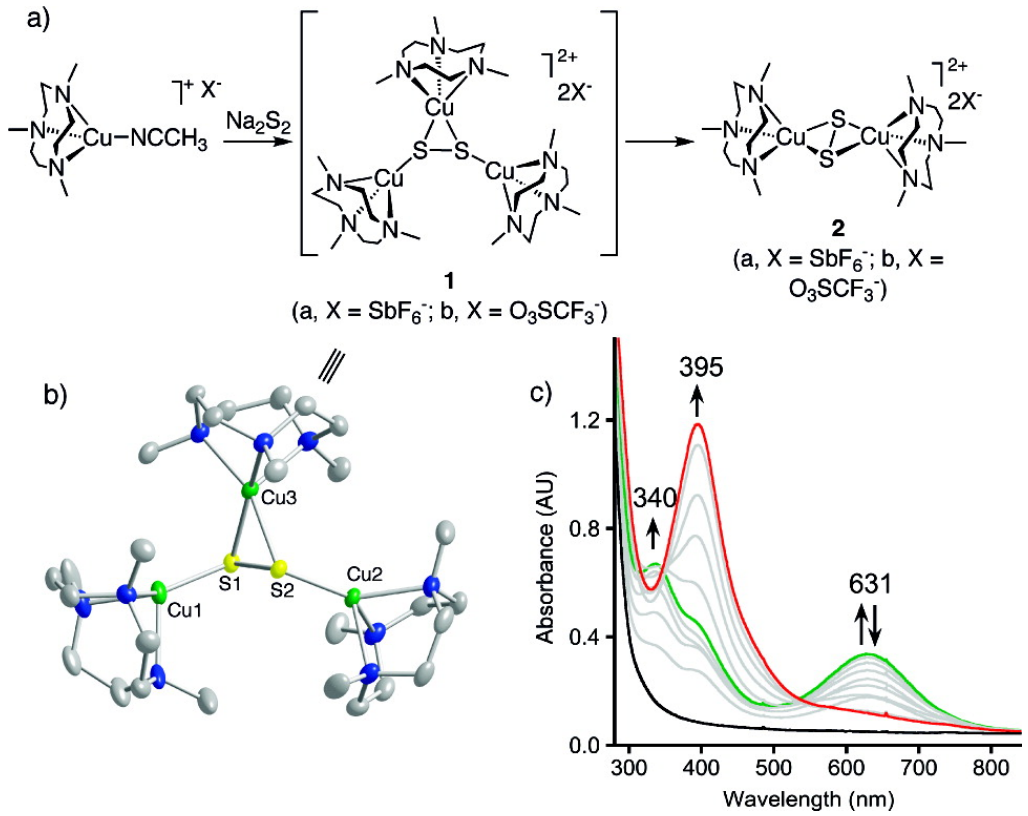

Figure 5.1. (a) Syntheses of disulfido complexes. (b) X-ray structure of cationic portion of **1b**, with all nonhydrogen atoms shown as 50% thermal ellipsoids. Selected bond distances: Cu1−S1, 2.1416(8) Å; Cu2−S2, 2.1367(8) Å; Cu3−S1, 2.2548(8) Å; Cu3−S2 = 2.2751(8) Å; S1−S2, 2.1267(10) Å. (c) UV-vis spectra of the reaction of [LCu(NCCH$_3$)]OTf (3.1 mM) with Na_2S_2 in THF with the intermediate species (λ_{max} = 340 and 631 nm) forming over 90 min at –20 °C. This species decays to a final spectrum (λ_{max} = 395 nm) when warmed to RT. Figure reproduced from Ref [185].

Dr. Bar-Nahum observed intermediate species, **1a** and **1b**, by UV-vis spectroscopy with λ_{max} ~ 630 nm ($t_{1/2}$ ~ 45 min) when Na_2S_2 was reacted with [LCu(CH$_3$CN)]X (L = 1,4,7-trimethyl-triazacyclononane, X = $O_3SCF_3^-$ or SbF_6^-) (Figure 5.1). The crystal structure of **1b** was obtained and revealed a novel $[L_3Cu_3S_2]^{2+}$ species that was assigned as a localized mixed valent Cu(II)Cu(I)$_2$ species with a bridging disulfide moiety (S_2^{2-}) based on crystallography, EPR spectroscopy, and TD-DFT calculations. Resonance Raman of **1b** in THF was obtained with a λ_{ex} = 647.1 nm (Figure

5.3). The resonance Raman spectrum obtained for **1b** derived from $Na_2{}^{32}S_2$ displays a strong feature at 453 cm^{-1} that shifts to 434 cm^{-1} upon ^{34}S labeling (Figure 5.3). The resonance Raman spectra for **1a** displays similar features and isotope sensitivity (Figure 5.4). The features observed in the resonance Raman spectra for **1a** and **1b** are consistent with the assignment of the visible chromophores with $\lambda_{max} \sim 630$ nm originating from a $Cu/S_2{}^{2-}$ charge-transfer transition and the primary vibration as a ν(S−S) stretching mode. The assignments of the resonance Raman features observed experimentally were supported by theory (TD-DFT) that predicted an S−S stretch at 406 cm^{-1} in the gas phase. The underestimate of the stretching frequency is likely due to an elongated S−S bond found in the gas phase optimized structure.

The resonance Raman results reported in this study were the first vibrational characterization of a (μ-η^2:η^1:η^1-disulfido)-tricopper(II)$(I)_2$ species and were consistent with all other experimental results and theoretical calculations presented in the report.[182]

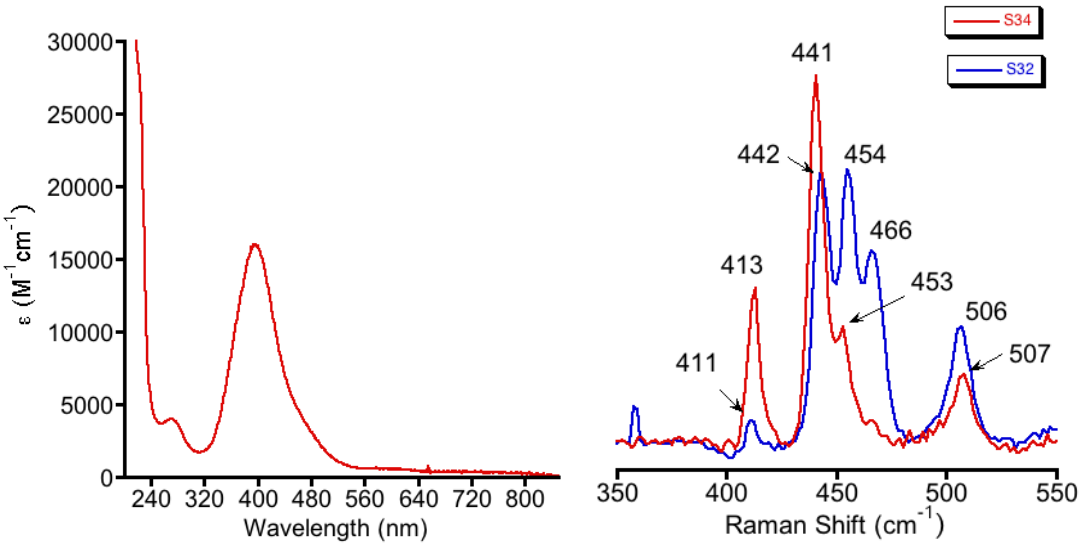

Figure 5.2. (left) UV-Vis spectrum of $[(Me_3tacn)_2Cu_2(\mu\text{-}S_2)](OTf)_2$ in CH_2Cl_2 at room temperature. (right) Resonance Raman spectrum obtained for $[(Me_3tacn)_2Cu_2(\mu\text{-}S_2)](OTf)_2$ (4 mM) in CH_2Cl_2 (1 mL). Recorded at –196 °C, λ_{ex} = 406.7 nm (^{32}S, blue line; ^{34}S, red line). Figure reproduced from Ref [182].

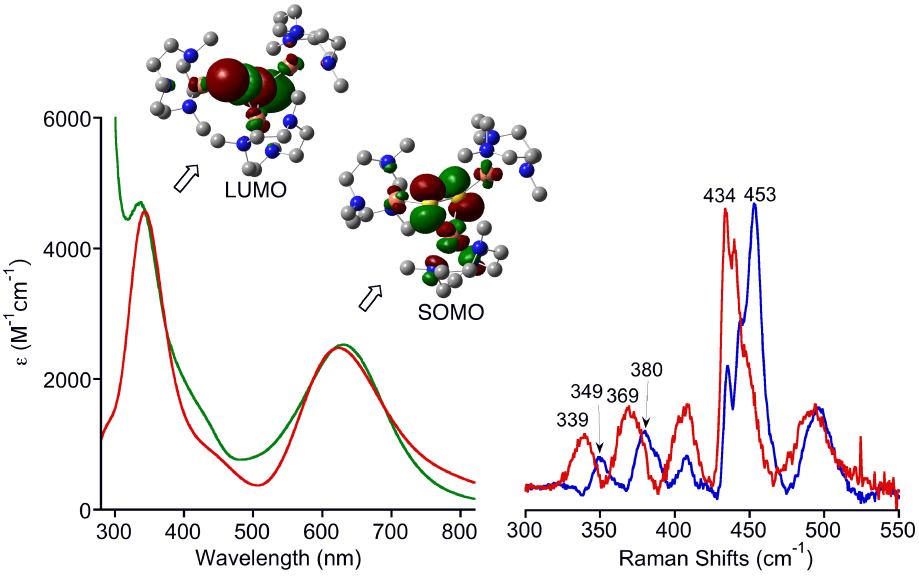

Figure 5.3. (left) Experimental absorption spectrum of the crude reaction solution containing 1b obtained upon slow addition of Na_2S_2 (0.5 eq) to $[LCu(MeCN)]O_3SCF_3$ in THF at –20 °C (green line) and TD-B98 calculated spectrum (red line), with drawings of the acceptor orbitals for the respective features shown. (right) Resonance Raman spectrum obtained from the reaction of $[LCu(MeCN)]O_3SCF_3$ with Na_2S_2 in THF (–196 °C, λ_{ex} = 647.1 nm; ^{32}S, blue line; ^{34}S, red line). Figure adapted from Ref [182].

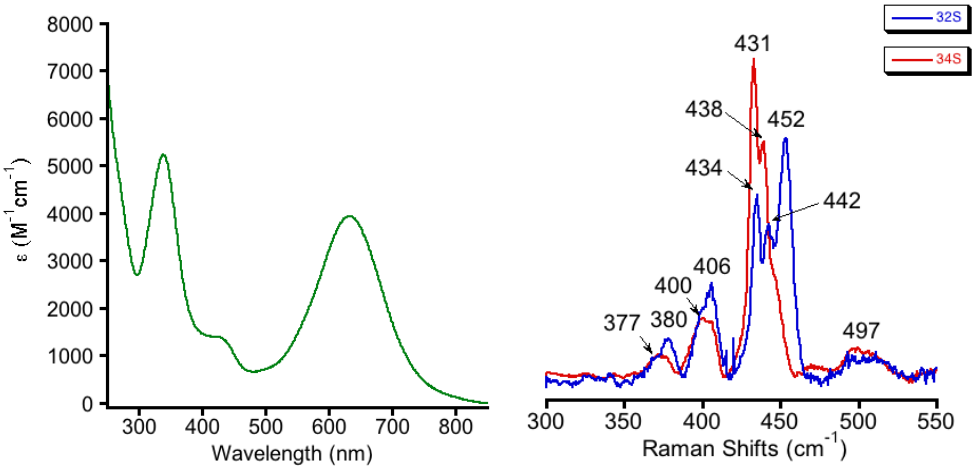

Figure 5.4. (left) UV-Vis spectrum of $[(Me_3tacn)_3Cu_3(\mu\text{-}S_2)](SbF_6)_2$ in CH_2Cl_2 at –80 °C. (right) Resonance Raman spectrum obtained for $[(Me_3tacn)_3Cu_2(\mu\text{-}S_2)](SbF_6)_2$ in CH_2Cl_2 (4 mM). Recorded at –196 °C, λ_{ex} = 647.1 nm (^{32}S, blue line; ^{34}S, red line). Figure reproduced from Ref [182].

5.1.2. A Tetragonal Copper(II)-Superoxo[186]

An important first step in copper-promoted aerobic oxidations in biology[187] and catalysis[87b,188] is the formation of a 1:1 copper-oxygen adduct, in which the O_2 molecule is activated for subsequent reactions either with substrate or to form different copper-oxygen species. One approach aimed at understanding such adducts targets synthetic 1:1 copper-oxygen complexes for detailed structural, spectroscopic, and reactivity studies.[189] To date, three types of 1:1 copper-oxygen species have been identified: (a) end-on, triplet Cu(II)-superoxos supported by tetradentate tripodal[190] or, in one case, tridentate N-donor ligands,[191] (b) side-on, singlet Cu(II)-superoxos supported by facially coordinating tris(pyrazolyl)hydroborates,[192] and (c) side-on, singlet Cu(III)-peroxos supported by strongly electron-donating, bidentate β-diketiminates or anilido-imines.[189,193] A key finding from reactivity studies of type (a) compounds is that they are electrophilic, with the ability to perform biologically relevant H-atom abstractions from phenols and weak

C-H bonds.[41,191] Investigations of the reactivity of type (b) compounds have not been reported and type (c) compounds are relatively unreactive with external organic substrates. The work presented in this section highlights a recent report that focuses on an end-on Cu(II)-superoxo complex that displays unique characteristics, including a tetragonal geometry and non-electrophilic reactivity.

Dr. Patrick J. Donoghue, a postdoctoral researcher in the Tolman laboratory, prepared complexes **1** and **2**, with the X-ray crystal structure of **2** having been solved by graduate student David W. Boyce (Figure 5.5). Complex **1** was found to react with a slurry of KO_2 and 18-crown-6 in DMF/THF to form the intermediate species **3**, an end-on triplet Cu(II)-superoxo species, at –80 °C. The UV-vis spectrum of **3** displays an absorption feature at λ_{max} = 627 nm ($\varepsilon \sim 1700\ M^{-1}cm^{-1}$) that was probed by resonance Raman spectroscopy. Excitation of a frozen sample (λ_{ex} = 647.1 nm) of **3** yielded a resonance Raman spectrum with an O-isotope sensitive feature at 1104 cm^{-1} ($\Delta^{18}O$ = 60 cm^{-1}) shown in Figure 5.6 as a difference spectrum ($^{16}O–^{18}O$). This value is lower than previously reported resonance Raman features for end-on triplet Cu(II)-superoxo species.[190,191] This feature is assigned to an O–O stretching vibration and based on literature precedent along with EPR spectroscopic data and theoretical calculations presented in the work by Donaghue *et al*. is consistent with an Cu(II)-superoxo species.

DFT calculations on the intermediate Cu(II)-superoxo species found an end-on triplet Cu(II)-superoxo species that yielded a ν(O–O) frequency of 1182 cm^{-1} to be the energetically favored species. The higher O–O stretching frequency in the calculated structure was attributed to a lack of counteranion or solvation in the calculations, which

reduces the likelihood for a negative charge to be found on the O_2 ligand thus increasing the stretching frequency. Attempts to acquire resonance Raman data on **3** derived from mixed isotope labeled O_2 ($^{16}O–^{18}O$) to identify Cu–^{16}O and Cu–^{18}O stretching vibrations and distinguish between either end-on or side-on O_2 coordination were not successful. No features assignable to Cu–O vibrations were observed for samples derived from $^{16}O_2$, $^{18}O_2$, or mixed isotope labeled O_2.

Further evidence that **3** is a Cu(II)-superoxo species came from trapping **3** with an additional equivalent of a Cu(I) complex, [(tmpa)Cu(NCCH$_3$)]OTf. It has been previously shown that such a reaction results in the formation of a (peroxo)dicopper species.[194] Reacting a solution of **3** with [(tmpa)Cu(NCCH$_3$)]OTf at –80 °C resulted in the formation of a bright purple intermediate, **4**, which exhibited features at λ_{max} = 624 and 550 nm in the UV-vis spectrum (Figures 5.5 and 5.6). The resonance Raman spectrum of **4** with λ_{ex} = 647.1 nm displays an isotope sensitive feature at 832 cm^{-1} ($\Delta^{18}O$ = 44 cm^{-1}) (Figure 5.6) that was assigned to the ν(O–O) for a (peroxo)dicopper species. The position of the observed resonance Raman feature is similar to those assigned as trans-1,2-peroxo-dicopper(II) complexes suggesting a similar geometry for **4**.[79] One concern was that the observed feature was originating from [(tmpa)$_2$Cu$_2$(O$_2$)]OTf$_2$ derived from [(tmpa)Cu(NCCH$_3$)]OTf and adventitious O_2. To rule out the possibility that the observed spectroscopic features were originating from this species, [(tmpa)$_2$Cu$_2$(O$_2$)]OTf$_2$ was intentionally synthesized by oxygenation of [(tmpa)Cu(NCCH$_3$)]OTf in 1:1 DMF/THF and the resonance Raman spectrum acquired (λ_{ex} = 647.1 nm) (Figure 5.6). A well resolved feature at 822 cm^{-1} was observed in the

spectrum that is similar to previously reported literature values[195] and more importantly, is distinct from the species derived from **3**.

In conclusion, this report highlighted a new tetragonal, anionic, end-on Cu(II)-superoxo species that was characterized by resonance Raman spectroscopy, along with other experimental techniques and theoretical methods. Additionally, the copper-oxygen intermediate derived from further reacting the Cu(II)-superoxo species with [(tmpa)Cu(NCCH$_3$)]OTf to form a trans-1,2-peroxo-dicopper(II) species was characterized by resonance Raman spectroscopy.

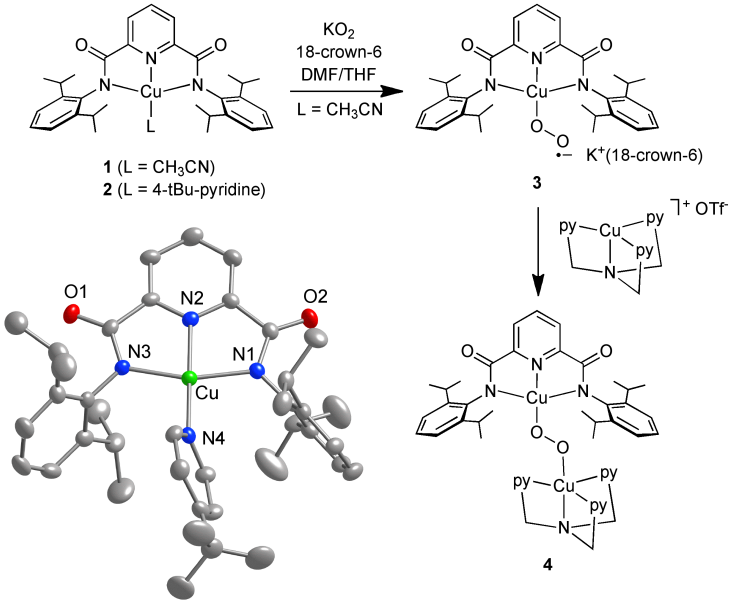

Figure 5.5. Compounds prepared in this work, and a representation of the X-ray crystal structure of **2** shown as 50% thermal ellipsoids. Hydrogen atoms omitted for clarity. Selected bond distances (Å) and angles (deg): Cu-N1, 2.004(2); Cu-N2, 1.920(2); Cu-N3, 1.994(2); Cu-N4, 1.973(2); N1-Cu-N2, 80.56(10); N1-Cu-N3, 161.19(9); N1-Cu-N4, 99.57(9); N2-Cu-N3, 80.84(10); N2-Cu-N4, 173.28(10); N3-Cu-N4, 99.23(10). Figure reproduced from Ref [186].

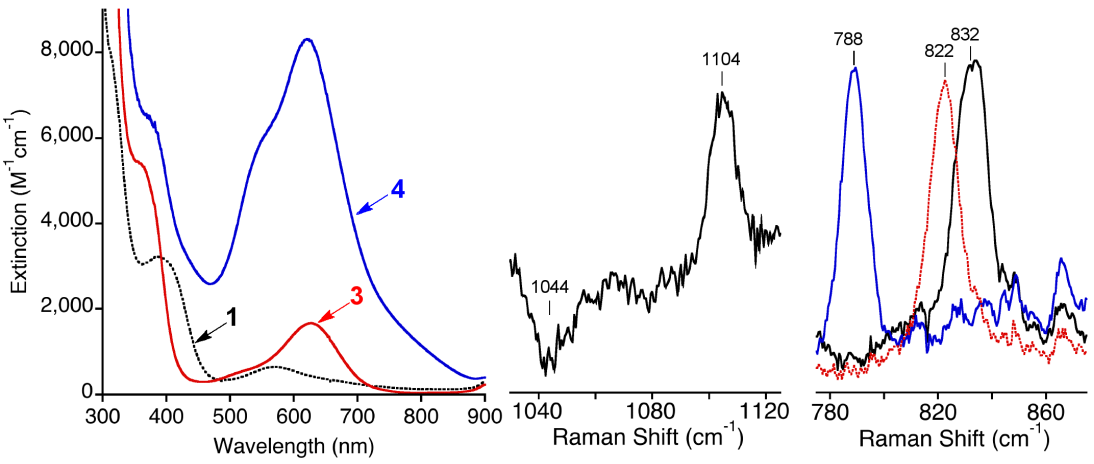

Figure 5.6. (left) UV-vis spectra of compounds **1**, **3**, and **4** (–80 °C, DMF/THF). (middle) Resonance Raman difference spectrum (^{16}O–^{18}O) for compound **3** prepared from $K^{16}O_2$ or $K^{18}O_2$ (–196 °C, λ_{ex} = 647.1 nm). (right) Resonance Raman spectra for compound 4 prepared from **3** (^{16}O) (black line) or **3** (^{18}O) (blue line), overlaid with spectrum of $[(tmpa)_2Cu_2(^{16}O_2)](OTf)_2$ (red dotted line) (–196 °C, λ_{ex} = 647.1 nm). Figure reproduced from Ref [186].

5.1.3 Electron Deficient Dicopper(III)-Bis(μ-oxo) Complexes[196]

The research described within this section highlights resonance Raman spectroscopy experiments performed as part of research reported by Hong *et al.* This work aimed to further explore bidentate ligand electronic and structural effects on Cu(I)/O_2 reactivity. The ligands used in the report are shown in Figure 5.7. It was hypothesized that while not observed, a 1:1 copper-oxygen adduct from oxygenation of (**2**)Cu(NCMe) might be present at a low equilibrium concentration. To test this idea, we sought to trap a similar 1:1 copper-oxygen adduct supported by **4**,[197] which we proposed would have similar electronic/redox properties to **2**, but by virtue of its decreased steric bulk could enable irreversible formation of a bis(μ-oxo)dicopper(III) complex like that known for **3**.[198] A complimentary set of experiments using **5** as a supporting ligand were also reported.[199,200] The synthesis and characterization of Cu(I) complexes of electron poor ligands **4** and **5** (relative to β-diketiminates like **3**), along with the results of their low temperature oxygenation reactions were reported. Spectroscopic evidence, including

results obtained from resonance Raman spectroscopy and theoretical studies support formation of bis(μ-oxo)dicopper(III) complexes in both cases, implicating the intermediacy of 1:1 copper-oxygen adducts as transient intermediates.

Oxygenation of LCu(CH_3CN) (L = **4** or **5**) at –80 °C in THF resulted in the growth of new features in the UV-vis spectra that were unperturbed upon removal of excess O_2 but which bleached upon warming (Figure 5.8). New features below 400 nm (**4**) (not shown) or 500 nm (**5**) are likely to arise in large part from ligand-based π-π* transitions, and a weak band at 780 nm (ε = 200 $cm^{-1}M^{-1}$) was also observed for the system supported by **4**. Most importantly, oxygenation resulted in intense new bands at 470 nm (ε ~ 15,000 $M^{-1}cm^{-1}$; **4**) or 525 nm (ε ~ 23,000 $M^{-1}cm^{-1}$; **5**) that are suggestive of CT transitions associated with bis(μ-oxo)dicopper cores.[84,201] Spectrophotometric titration results confirmed the requisite 2:1 Cu:O_2 stoichiometry (insets to plots in Figure 5.8). However, the spectroscopic features are shifted to longer wavelengths relative to typical $[Cu_2(\mu\text{-}O)_2]^{2+}$ core electronic transitions that occur in the ranges 300–330 nm (ε ~ 10,000–20,000 $M^{-1}cm^{-1}$) and 400–450 nm (ε ~ 10,000–30,000 $M^{-1}cm^{-1}$). The 525 nm band for the complex supported by **5** is a particularly notable outlier at significantly different energy from typical bis(μ-oxo)dicopper core transitions. A low energy feature at 550 nm with an extinction much lower than what we observe (1300 $M^{-1}cm^{-1}$) was reported for a bis(μ-oxo)dicopper complex supported by a guanidine ligand and assigned as a guanidine → $[Cu_2(\mu\text{-}O)_2]^{2+}$ CT transition.[202]

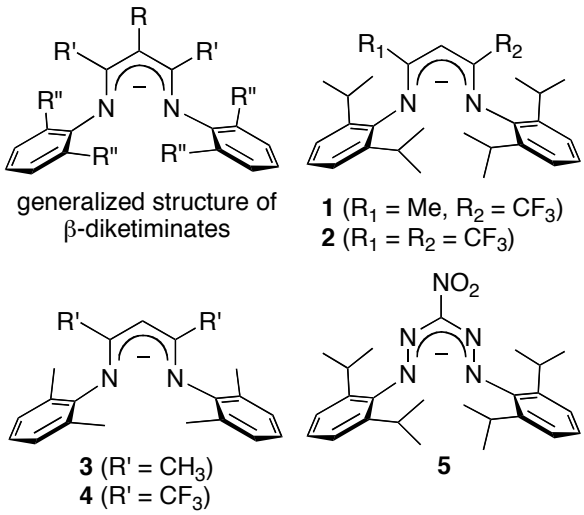

Figure 5.7. β-Diketiminate and formazan (**5**) ligands used in the work described in this section. Figure reproduced from Ref [196].

To confirm the assignments that the intermediate species contain $[Cu_2(\mu\text{-}O)_2]^{2+}$ cores, we performed resonance Raman spectroscopy experiments on samples prepared using $^{16}O_2$ or $^{18}O_2$ with excitation wavelengths of 457.9 nm (**4**) or 514.5 nm (**5**). The spectrum for the oxygenated product of (**4**)Cu(CH_3CN) (Figure 5.9a) contains two peaks at 598 cm^{-1} and 610 cm^{-1} that are replaced by a single peak at 566 cm^{-1} upon ^{18}O-labeling. This pattern has been seen previously for bis(μ-oxo)dicopper complexes,[201,203] and is usually attributed to a symmetric Cu_2O_2 core vibration that appears as a Fermi doublet with $^{16}O_2$ but converts to a single peak with $^{18}O_2$. For the case of the reaction with (**5**)Cu(CH_3CN) (Figure 5.9b), a peak at 581 cm^{-1} appears to shift to 558 cm^{-1} upon use of $^{18}O_2$, although an overlapping additional peak at 581 cm^{-1} complicates the analysis. As shown in the inset to Figure 5.9b, frequency doubled overtone peaks are observed at 1160 cm^{-1} ($^{16}O_2$) and 1112 cm^{-1} ($^{18}O_2$). The combined data for both cases **4** and **5** are consistent with assignment of the 470 and 525 nm transitions, respectively, as CT transitions involving bis(μ-oxo)dicopper cores. Also consistent with these formulations, the intermediates are EPR silent (X-band, 4 K). In conclusion, resonance

Raman experiments confirmed the assignments that the oxygenation products of (**4**)Cu(CH_3CN) and (**5**)Cu(CH_3CN) are in fact bis(μ-oxo)dicopper(III) species.

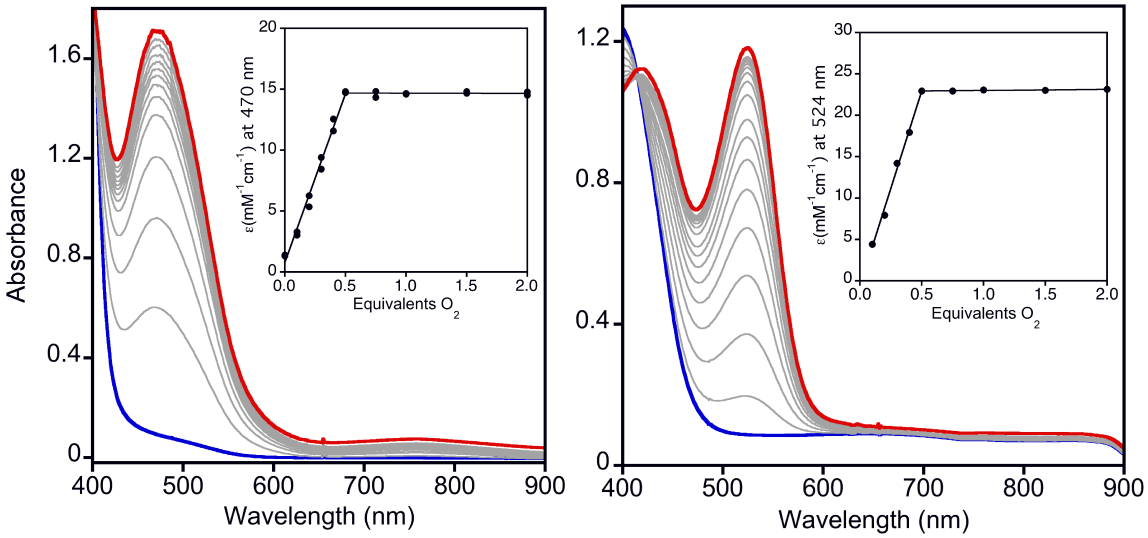

Figure 5.8. UV-vis changes accompanying oxygenation of (left) (**4**)Cu(CH_3CN) and (right) (**5**)Cu(CH_3CN) at –80 °C in THF, using starting concentrations of 0.2 mM or 0.1 mM, respectively. The initial and final spectra are in blue and red, respectively. The insets show the results of spectrophotometric titrations of the complexes with O_2 as linear fits to (left) data for two replicate runs or (right) average data from three replicate runs. Figure reproduced from Ref [196].

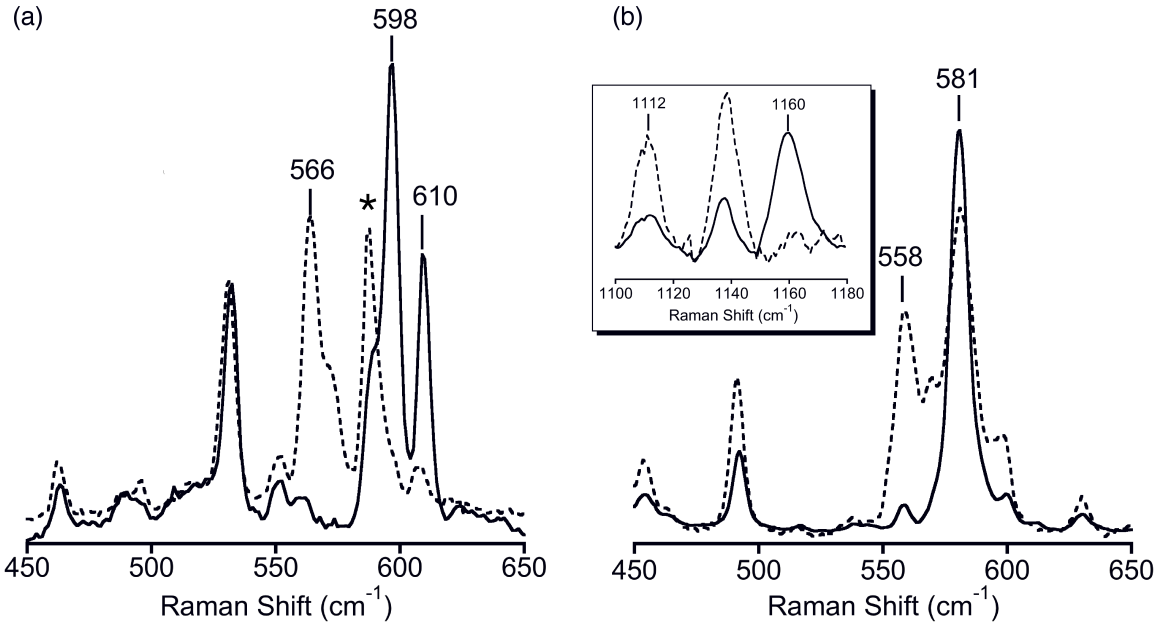

Figure 5.9. Resonance Raman spectra of the frozen solutions resulting from oxygenations of (a) (**4**)Cu(CH_3CN) (40 mM) and (b) (**5**)Cu(CH_3CN) (10 mM) in THF at –80 °C, using $^{16}O_2$ (solid line) or $^{18}O_2$ (dashed line). The inset to plot (b) shows overtone bands. Excitation wavelengths were 457.9 nm and 514.5 nm, respectively. The asterisk (*) indicates a solvent peak. Figure reproduced from Ref [196].

5.1.4 Bis(μ-oxo)Dicopper(III) Complex Derived from Oxo-Transfer[204]

Copper-promoted oxidation reactions play important roles in biology and catalysis so great effort has been expended to uncover mechanistic information and, in particular, to identify possible copper-oxygen intermediates. Of notable interest are $[CuO]^+$ species (Cu(III)-O^{2-} ↔ Cu(II)-O^{-}·), which have been invoked in catalysis by enzymes and synthetic systems and characterized by theory and in the gas phase as discussed in Chapter 1.

Research headed by Dr. Sungjun Hong sought to investigate the reactions of pyridine- and tri(alkyl)amine-*N*-oxides with Cu(I) complexes. A range of supporting ligands with variable electronic and steric profiles that have been previously used in O_2

reactivity investigations were examined. The work highlighted in this section focuses on the reaction of trimethylamine oxide (TMAO) with a Cu(I) complex supported by an anionic β-diketiminate ligand (Figure 5.7, **3**) resulting in the formation of a bis(μ-oxo)dicopper(III) species that was spectroscopically identical to a bis(μ-oxo)dicopper(III) species derived from O_2.

(**3**)Cu($NCCH_3$) reacted rapidly with TMAO at room temperature to give a brown solution, from which a few crystals of the known complex [(**3**)$_2$$Cu_2$(μ-$OH)_2$] were obtained;[205] no Cu(I)-TMAO adduct was observed. When the reaction was performed at –78 °C, smooth conversion to an intermediate occurred over approximately 1 h that was identified as the bis(μ-oxo)dicopper complex [(**3**)$_2$$Cu_2$(μ-$O)_2$] (**6**) on the basis of comparison of its UV-vis (λ_{max} = 423 nm, ε ~ 16,000 $cm^{-1}M^{-1}$) and resonance Raman (ν(Cu_2O_2) = 608 cm^{-1}, λ_{ex} = 457.9 nm) spectroscopic properties to a sample prepared independently from O_2 and to data in the literature[206] (Figure 5.10). To our knowledge, this is the first report of a bis(μ-oxo)dicopper complex derived from an oxo transfer reagent.[50e,207] In conclusion, this is the first copper-oxygen species derived by oxo-transfer to be characterized by resonance Raman spectroscopy and its identity was confirmed by independently synthesizing the species from O_2 and comparing their resonance Raman spectra.

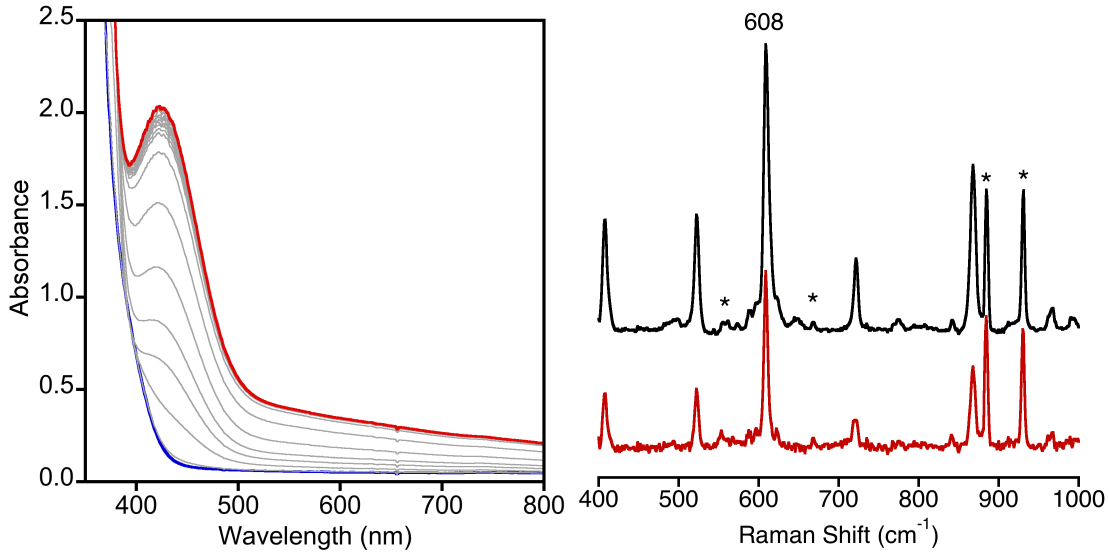

Figure 5.10. (left) UV-vis spectra obtained during the reaction of (**3**)Cu(CH_3CN) (0.25 mM) with TMAO (10 equiv) in THF at –80 °C over 1 h (starting spectrum in blue, final spectrum in red). (right) Resonance Raman spectra obtained on samples obtained from the reaction of (**3**)Cu(CH_3CN) in THF at –80 °C with TMAO (*bottom*) or O_2 (*top*). The spectra were obtained using λ_{ex} = 457.9 nm at –196 °C; solvent peaks are marked with asterisks and the peak assigned as the Cu_2O_2 core vibration is indicated at 608 cm^{-1}. Figure reproduced from Ref [204].

5.2. Collaborative Projects: X-ray Crystallography

During the course of the dissertation research described in the previous chapters, one collaborative project was undertaken with the X-ray crystallography components of the research done by myself in the X-Ray Crystallographic Laboratory at the University of Minnesota. A brief introduction for the project and the crystallographic results that were completed for that project will be presented in the following section.

5.2.1. [$InCl_3$(3-diethylamino-1-propanol)(H_2O)]$_2$[208]

Developing biodegradable materials from biorenewable resources is a crucial step in future sustainable polymer technologies.[209] Of particular interest is polylactide (PLA), a biodegradable and biocompatible polyester,[210] which due to its mechanical and physical

properties is suitable for a variety of applications such as product packaging,[211,212] sutures,[213,214] and artificial tissue matrices.[215,216] A recent report from our group by Pietrangelo *et al.* revealed a catalyst system prepared *in situ* from $InCl_3$, NEt_3, and BnOH that stereoselectively polymerizes *D,L*-lactide to form heterotactic PLA.[217] The stereocontrol observed is unusual as there was no need for the introduction of a directing ligand on the catalytic metal site. We therefore aimed to determine the structure of the active catalyst to obtain mechanistic details on the polymerization of lactide.

Initial attempts to grow crystals from solutions of $InCl_3$, NEt_3, and BnOH only led to repeated isolation of colorless needle crystals that were identified as the ammonium salt $[HNEt_3]Cl$ by unit cell determination obtained from X-ray crystallography. Substituting pyridine for NEt_3 resulted in the isolation of colorless block-like crystals that were identified as the known compound $(Pyr)_3InCl_3$ (Pyr = pyridine) by X-ray crystallography.[218] In an alternative strategy, 3-diethylamino-1-propanol (deapH) was used in lieu of BnOH and NEt_3 to exploit the propensity of ammonium salts to crystallize. In a typical experiment, deapH (1 eq.) was added to a stirring suspension of $InCl_3$ in CH_2Cl_2. After stirring overnight, an amorphous solid was precipitated upon drop wise addition of the reaction solution to vigorously stirring pentane. Crystals were grown over a period of two months by slow diffusion of pentane vapor into a solution of the product of a reaction between $InCl_3$ and deapH in CH_2Cl_2.

X-ray crystallographic analysis revealed the product to be a dinuclear indium complex with the structural formula $[InCl_3(deapH)(H_2O)]_2$ (Figure 5.11, See Table A.1 for complete refinement details). The indium(III) ions are bridged by two alkoxides

forming a planar In_2O_2 ring-motif similar to that found in various organoindium alkoxides and aryloxides.[219] The coordination sphere of each indium(III) ion is completed by three chloride ligands and a water molecule (presumably introduced during the crystallization process) to yield a six-coordinate distorted octahedral geometry, with *cis*- and *trans*-angles about the metal centers ranging from *ca*. 76-99° and 164-172°, respectively. The coordinated water molecules participate in hydrogen bonds, one intramolecular (to Cl3 and Cl3', Figure 5.11a) and the other to Cl1/Cl1' in an adjacent molecule in the unit cell (Figure 5.11b). The ammonium proton is also hydrogen bonded to a chloride in the adjacent molecule (Cl2/Cl2').

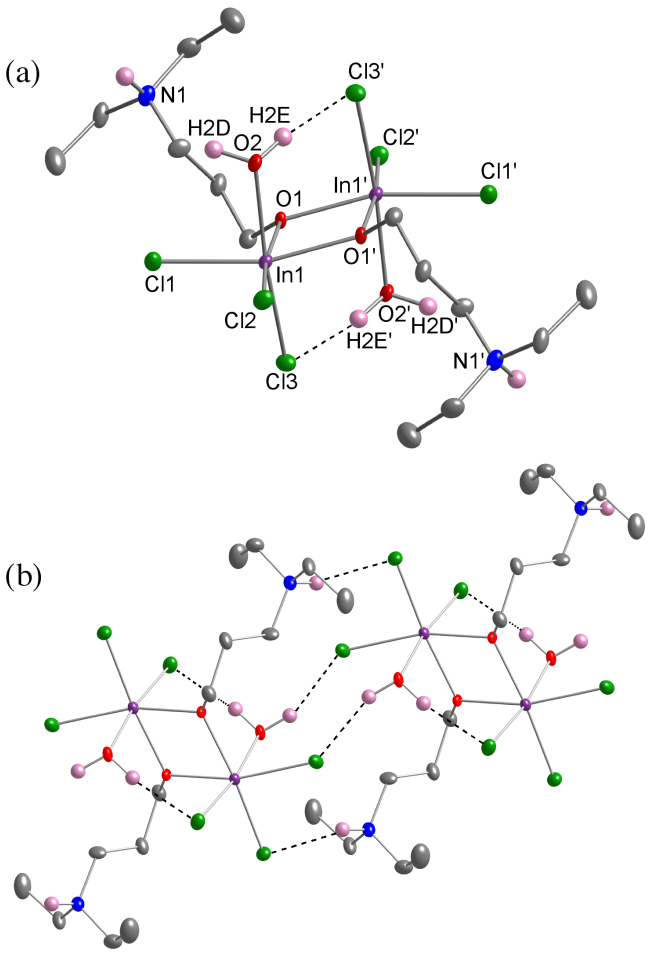

Figure 5.11. Representations of the X-ray crystal structure of $[InCl_3(deapH)(H_2O)]_2$ as 50% thermal ellipsoids (except hydrogen atoms). (a) A single molecule is shown with selected nonhydrogen atoms labeled and hydrogen atoms on C atoms omitted for clarity. (b) View showing adjacent molecules and hydrogen bonds (dashed lines), without atom labels and hydrogen atoms on C atoms omitted for clarity. Key: In = purple, Cl = green, C = gray, N = blue, O = red, H = pink spheres. Selected bond distances (Å) and angles (deg): In1-O1, 2.158(3); In1-O1′, 2.160(3); In1-O2, 2.290(4); O1-In1-O1′, 74.77(14); In1-O-In1′, 104.23(14). Figure reproduced from Ref [208].

Table 5.1. Crystallographic details for $[InCl_3(deapH)(H_2O)]_2$.

	$[InCl_3(deapH)(H_2O)]_2$
Empirical formula	$C_{14}\ H_{38}\ Cl_6\ In_2\ N_2\ O_4$
Formula weight	740.80
Crystal system	Monoclinic
Space group	$P2_1/n$
a (Å)	8.2451(14)
b (Å)	19.209(3)
c (Å)	8.7380(15)
α (deg)	90
β (deg)	103.634(2)
γ (deg)	90
Volume ($Å^3$)	1344.9(4)
Z	2
T(K)	123(2)
ρ (calculated) (Mg/m^3)	1.829
θ range (deg)	2.12 to 25.06
μ (mm^{-1})	2.332
Reflections collected	10788
Independent reflections	2376
parameters	129
R1, wR2 (for $I > 2\sigma(I)$)	0.0343, 0.0655
GOF	1.105
Largest Peak, Hole ($e.Å^{-3}$)	0.551 and -0.778
F(000)	736
Crystal color, morphology	Colorless, plate
Crystal size	0.2 x 0.1 x 0.1 mm^3
Index ranges	$-9 \le h \le 9$, $-22 \le k \le 22$, $-10 \le l \le 10$

It was confirmed that $[InCl_3(deapH)(H_2O)]_2$ is catalytically active and displayed a similar degree of stereocontrol with respect to the original $InCl_3/NEt_3$/BnOH catalyst system. Additionally, pulsed gradient spin-echo NMR spectroscopy experiments were done and suggest that the structure obtained in the solid state X-ray crystal structure was retained in solution.[208] With the experimental evidence presented in the full report along with the structure determined and presented above, a postulated mechanism for the polymerization of lactide was reported (Figure 5.12). As shown, LA polymerization occurs via a coordination-insertion mechanism that employs an $[InCl_{(3-n)}(OR)_n]_m$

propagating species (with R_3NH^+ as the counter ion), drawn as a dinuclear complex (m = 2) in Figure 5.12 by analogy to the X-ray structure of the model $[InCl_3(deapH)(H_2O)]_2$. We hypothesize that a lactide molecule coordinates to the Lewis acidic indium center via a carbonyl oxygen, perhaps at the site where water binds in $[InCl_3(deapH)(H_2O)]_2$. Subsequent insertion into the indium-alkoxide bond would occur via nucleophilic attack of the alkoxide on the LA carbonyl carbon (step i) and cleavage of the acyl-oxygen bond (step ii). Rationalizing the stereocontrol exhibited in this system is challenging, and at this juncture we can only speculate on the basis of precedent provided by theoretical analysis of the stereoselective polymerization of *D,L*-LA to heterotactic PLA by (BDI)MgOMe (BDI = β-diketiminate).[220] As proposed for that system, we hypothesize that energy differences in the environment created by a combination of steric and electronic effects imparted by the halide(s) and multiple stereocenters of the growing polymer chain-end during propagation dictate the rate of monomer insertion and stereocontrol. Evidently, the steric effects are substantial despite the absence of a hindered ancillary supporting ligand that is typically required for stereocontrol in polymerizations catalyzed by metal-alkoxide complexes.

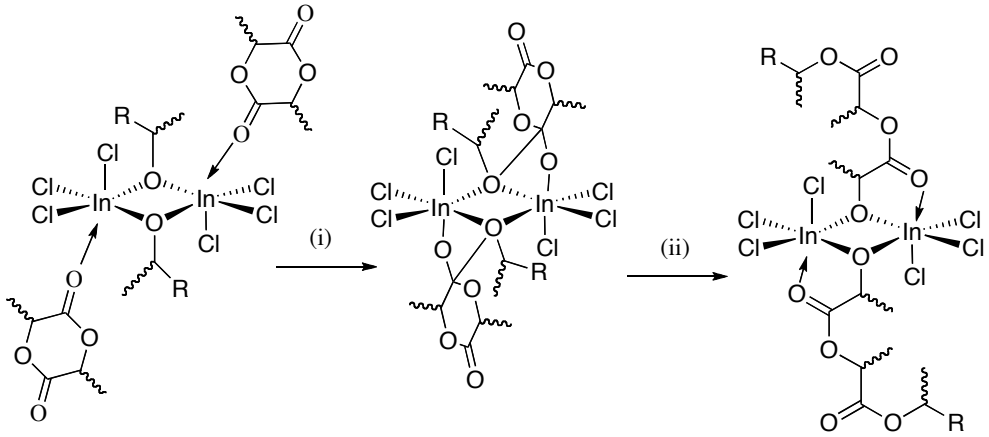

Figure 5.12. Postulated mechanism for the polymerization of lactide. Figure reproduced from Ref [208].

Bibliography

(1) Atkins, P. W. Physical Chemistry, 6th Edition; W.H. Freeman and Company: New York, 1998.

(2) Anderson, A. B.; Roques, J.; Mukerjee, S.; Murthi, V. S.; Markovic, N. M.; Stamenkovic, V. "Activation Energies for Oxygen Reduction on Platinum Alloys: Theory and Experiment." *J. Phys. Chem. B* **2005**, *109*, 1198-1203.

(3) Tolman, W. B.; Editor Activation of Small Molecules: Organometallic and Bioinorganic Perspectives; Wiley-VCH: Weinheim, 2006; Vol. 1.

(4) Bertini, I.; Gray, H. B.; Stiefel, E. I.; Valentine, J. S. Biological Inorganic Chemistry Structure and Reactivity; University Science Books: Sausalito, 2007; Vol. 1.

(5) Jin, N.; Lahaye, D. E.; Groves, J. T. "A "Push-Pull" Mechanism for Heterolytic O-O Bond Cleavage in Hydroperoxo Manganese Porphyrins." *Inorg. Chem.*, *49*, 11516-11524.

(6) (a) de Visser, S. P.; Valentine, J. S.; Nam, W. "A Biomimetic Ferric Hydroperoxo Porphyrin Intermediate." *Angew. Chem., Int. Ed.* **2010**, *49*, 2099-2101. (b) Fujii, T.; Ozawa, T.; Funahashi, Y.; Jitsukawa, K.; Masuda, H. "Synthesis of mononuclear non-heme iron(III)-hydroperoxo complex as an oxidative catalyst." *Adv. Mater. Res.* **2006**, *11-12*, 331-334. (c) Park, M. J.; Lee, J.; Suh, Y.; Kim, J.; Nam, W. "Reactivities of Mononuclear Non-Heme Iron Intermediates Including Evidence that Iron(III)-Hydroperoxo Species Is a Sluggish Oxidant." *J. Am. Chem. Soc.* **2006**, *128*, 2630-2634. (d) Lehnert, N.; Neese, F.; Ho, R. Y. N.; Que, L., Jr.; Solomon, E. I. "Electronic Structure and Reactivity of Low-Spin Fe(III)-Hydroperoxo Complexes: Comparison to Activated Bleomycin." *J. Am. Chem. Soc.* **2002**, *124*, 10810-10822. (e) Wada, A.; Ogo, S.; Nagatomo, S.; Kitagawa, T.; Watanabe, Y.; Jitsukawa, K.; Masuda, H. "Reactivity of Hydroperoxo Bound to a Mononuclear Non-Heme Iron Site." *Inorg. Chem.* **2002**, *41*, 616-618. (f) Simaan, A. J.; Dopner, S.; Banse, F.; Bourcier, S.; Bouchoux, G.; Boussac, A.; Hildebrandt, P.; Girerd, J.-J. "Fe(III)-hydroperoxo and peroxo complexes with aminopyridyl ligands and the resonance Raman spectroscopic identification of the Fe-O and O-O stretching modes." *Eur. J. Inorg. Chem.* **2000**, 1627-1633. (g) Bach, R. D.; Su, M. D.; Andres, J. L.; Schlegel, H. B. "Structure and reactivity of diamidoiron(III) hydroperoxo. The mechanism of oxygen-atom transfer to ammonia." *J. Am. Chem. Soc.* **1993**, *115*, 8763-8769.

(7) Yamaguchi, S.; Masuda, H. "Basic approach to development of environment-friendly oxidation catalyst materials. Mononuclear hydroperoxo copper(II)

complexes." *Science and Technology of Advanced Materials.* **2005**, *6*, 34-47.

(8) Recent examples of manganese-oxo species: (a) Latifi, R.; Tahsini, L.; Karamzadeh, B.; Safari, N.; Nam, W.; de Visser, S. P. "Manganese substituted Compound I of cytochrome P450 biomimetics: A comparative reactivity study of Mn^{V}-oxo versus Mn^{IV}-oxo species." *Arch. Biochem. Biophys.* **2011**, *507*, 4-13. (b) Fukuzumi, S.; Kotani, H.; Prokop, K. A.; Goldberg, D. P. "Electron- and Hydride-Transfer Reactivity of an Isolable Manganese(V)-Oxo Complex." *J. Am. Chem. Soc.* **2011**, *133*, 1859-1869. (c) Han, Y.; Lee, Y.-M.; Mariappan, M.; Fukuzumi, S.; Nam, W. "Manganese(V)-oxo corroles in hydride-transfer reactions." *Chem. Commun.* **2010**, *46*, 8160-8162. (d) Sawant, S. C.; Wu, X.; Cho, J.; Cho, K.-B.; Kim, S. H.; Seo, M. S.; Lee, Y.-M.; Kubo, M.; Ogura, T.; Shaik, S.; Nam, W. "Water as an Oxygen Source: synthesis, Characterization, and Reactivity Studies of a Mononuclear Nonheme Manganese(IV) Oxo Complex." *Angew. Chem., Int. Ed.* **2010**, *49*, 8190-8194, S8190/8191-S8190/8124. (e) Prokop, K. A.; de Visser, S. P.; Goldberg, D. P. "Unprecedented Rate Enhancements of Hydrogen-Atom Transfer to a Manganese(V)-Oxo Corrolazine Complex." *Angew. Chem., Int. Ed.* **2010**, *49*, 5091-5095, S5091/5091-S5091/5058.

(9) (a) Lacy, D. C.; Gupta, R.; Stone, K. L.; Greaves, J.; Ziller, J. W.; Hendrich, M. P.; Borovik, A. S. "Formation, Structure, and EPR Detection of a High Spin FeIV-Oxo Species Derived from Either an Fe^{III}-Oxo or Fe^{III}-OH Complex." *J. Am. Chem. Soc.* **2010**, *132*, 12188-12190. (b) Geng, C.; Ye, S.; Neese, F. "Analysis of Reaction Channels for Alkane Hydroxylation by Nonheme Iron(IV)-Oxo Complexes." *Angew. Chem., Int. Ed.* **2010**, *49*, 5717-5720, S5717/5711-S5717/5713. (c) Yin, G. "Active transition metal oxo and hydroxo moieties in nature's redox, enzymes and their synthetic models: Structure and reactivity relationships." *Coord. Chem. Rev.* **2010**, *254*, 1826-1842.

(10) Klinman, J. P. "Mechanisms Whereby Mononuclear Copper Proteins Functionalize Organic Substrates." *Chem. Rev.* **1996**, *96*, 2541-2561.

(11) Tian, G.; Berry, J. A.; Klinman, J. P. "Oxygen-18 kinetic isotope effects in the dopamine β-monooxygenase reaction: evidence for a new chemical mechanism in non-heme metallomonooxygenases." *Biochemistry.* **1994**, *33*, 226-234.

(12) Wimalasena, K.; May, S. W. "Mechanistic studies on dopamine β-monooxygenase catalysis: *N*-dealkylation and mechanism-based inhibition by benzylic-nitrogen-containing compounds. Evidence for a single-electron-transfer mechanism." *J. Am. Chem. Soc.* **1987**, *109*, 4036-4046.

(13) Meunier, B.; de Visser, S. P.; Shaik, S. "Mechanism of Oxidation Reactions Catalyzed by Cytochrome P450 Enzymes." *Chem. Rev.* **2004**, *104*, 3947-3980.

(14) Francisco, W. A.; Blackburn, N. J.; Klinman, J. P. "Oxygen and Hydrogen Isotope Effects in an Active Site Tyrosine to Phenylalanine Mutant of Peptidylglycine α-Hydroxylating Monooxygenase: Mechanistic Implications." *Biochemistry.* **2003**, *42*, 1813-1819.

(15) Chen, P.; Solomon, E. I. "Oxygen Activation by the Noncoupled Binuclear Copper Site in Peptidylglycine α-Hydroxylating Monooxygenase. Reaction Mechanism and Role of the Noncoupled Nature of the Active Site." *J. Am. Chem. Soc.* **2004**, *126*, 4991-5000.

(16) Evans, J. P.; Ahn, K.; Klinman, J. P. "Evidence that dioxygen and substrate activation are tightly coupled in dopamine β-monooxygenase: Implications for the reactive oxygen species." *J. Biol. Chem.* **2003**, *278*, 49691-49698.

(17) Miller, S. M.; Klinman, J. P. "Secondary isotope effects and structure-reactivity correlations in the dopamine β-monooxygenase reaction: evidence for a chemical mechanism." *Biochemistry.* **1985**, *24*, 2114-2127.

(18) Decker, A.; Solomon, E. I. "Dioxygen activation by copper, heme and non-heme iron enzymes: comparison of electronic structures and reactivities." *Current Opinion in Chemical Biology* **2005**, *9*, 152-163.

(19) Chen, P.; Bell, J.; Eipper, B.A.; Solomon, E.I. "Oxygen activation by the noncoupled binuclear copper site in peptidylglycine α-hydroxylating monooxygenase. Spectroscopic definition of the resting sites and the putative Cu(II)M-OOH intermediate." *Biochemistry*, **2004**, *43*, 5735-5747.

(20) Solomon, E. I.; Decker, A.; Lehnert, N. "Non-heme iron enzymes: contrasts to heme catalysis.." *Proc. Natl. Acad. Sci.* **2003**, *100*, 3589-3594.

(21) Shiota, Y.; Yoshizawa, K. "Methane-to-Methanol Conversion by First-Row Transition-Metal Oxide Ions: ScO^+, TiO^+, VO^+, CrO^+, MnO^+, FeO^+, CoO^+, NiO^+, and CuO^+." *J. Am. Chem. Soc.* **2000**, *122*, 12317-12326.

(22) Schroeder, D.; Schwarz, H. "C-H and C-C bond activation by bare transition-metal oxide cations in the gas phase." *Angew. Chem., Int. Ed. Engl.* **1995**, *34*, 1973-1995.

(23) Clemmer, D. E.; Aristov, N.; Armentrout, P. B. "Reactions of scandium oxide (ScO^+), titanium oxide (TiO^+) and vanadyl (VO^+) with deuterium: M+-OH bond energies and effects of spin conservation." *J. Phys. Chem.* **1993**, *97*, 544-552.

(24) Kamachi, T.; Kihara, N.; Shiota, Y.; Yoshizawa, K. "Computational Exploration of the Catalytic Mechanism of Dopamine β-Monooxygenase: Modeling of Its Mononuclear Copper Active Sites." *Inorg. Chem.* **2005**, *44*, 4226-4236.

(25) Yoshizawa, K.; Kihara, N.; Kamachi, T.; Shiota, Y. "Catalytic Mechanism of Dopamine β-Monooxygenase Mediated by Cu(III)-Oxo." *Inorg. Chem.* **2006**, *45*, 3034-3041.

(26) Yoshizawa, K.; Shiota, Y. "Conversion of Methane to Methanol at the Mononuclear and Dinuclear Copper Sites of Particulate Methane Monooxygenase (pMMO): A DFT and QM/MM Study." *J. Am. Chem. Soc.* **2006**, *128*, 9873-9881.

(27) Chen, P.; Fujisawa, K.; Solomon, E. I. "Spectroscopic and Theoretical Studies of Mononuclear Copper(II) Alkyl- and Hydroperoxo Complexes: Electronic Structure Contributions to Reactivity." *J. Am. Chem. Soc.* **2000**, *122*, 10177-10193.

(28) (a) Solomon, E. I.; Brunold, T. C.; Davis, M. I.; Kemsley, J. N.; Lee, S.-K.; Lehnert, N.; Neese, F.; Skulan, A. J.; Yang, Y.-S.; Zhou, J. "Geometric and Electronic Structure/Function Correlations in Non-Heme Iron Enzymes." *Chem. Rev.* **2000**, *100*, 235-349. (b) Harris, D. L.; Loew, G. H. "Theoretical investigation of the proton assisted pathway to formation of cytochrome P450 compound I." *J. Am. Chem. Soc.* **1998**, *120*, 8941-8948.

(29) Crespo, A.; Marti, M. A.; Roitberg, A. E.; Amzel, L. M.; Estrin, D. A. "The catalytic mechanism of peptidylglycine α-hydroxylating monooxygenase investigated by computer simulation." *J. Am. Chem. Soc.* **2006**, *128*, 12817-12828.

(30) Anzenbacher, P.; Editor Advances in the Inorganic Biochemistry of Cytochrome P450, Nitric Oxide Synthase and Related Systems. *J. Inorg. Biochem.* **2004**, 98(7)]; Elsevier: Amsterdam.

(31) Sülzle, D.; Schwarz, H.; Moock, K. H.; Terlouw, J. K. "On the existence of novel nitrides and oxides of copper: copper mononitride, copper dioxide and copper-nitrogen-oxygen compound (CuNO)." *Int. J. Mass Spectrom. Ion Processes* **1991**, *108*, 269-272.

(32) Rodgers, M. T.; Walker, B.; Armentrout, P. B. "Reactions of Cu^+(^1S and ^3D) with O_2, CO, CO_2, N_2, NO, N_2O, and NO_2 studied by guided ion beam mass spectrometry." *Int. J. Mass Spectrom.* **1999**, *182/183*, 99-120.

(33) Fisher, E. R.; Elkind, J. L.; Clemmer, D. E.; Georgiadis, R.; Loh, S. K.; Aristov, N.; Sunderlin, L. S.; Armentrout, P. B. "Reactions of fourth-period metal ions

(calcium(1+)-zinc(1+)) with oxygen: metal-oxide ion bond energies." *J. Chem. Phys.* **1990**, *93*, 2676-2691.

(34) Schroeder, D.; Holthausen, M. C.; Schwarz, H. "Radical-Like Activation of Alkanes by the Ligated Copper Oxide Cation (Phenanthroline)CuO^+." *J. Phys. Chem. B* **2004**, *108*, 14407-14416.

(35) Dietl, N.; van der Linde, C.; Schlangen, M.; Beyer, M. K.; Schwarz, H. "Diatomic $[CuO]^+$ and Its Role in the Spin-Selective Hydrogen- and Oxygen-Atom Transfers in the Thermal Activation of Methane." *Angew. Chem., Int. Ed.* **2011**, *50*, 4966-4969.

(36) Schroeder, D.; Schwarz, H. "C-H and C-C bond activation by bare transition-metal oxide cations in the gas phase." *Angew. Chem., Int. Ed. Engl.* **1995**, *34*, 1973-1995.

(37) Capdevielle, P.; Maumy, M. "Selective *ortho*-hydroxylation of phenols. II. A new preparative catalytic system." *Tetrahedron Lett.* **1982**, *23*, 1577-1580.

(38) Capdevielle, P.; Sparfel, D.; Baranne-Lafont, J.; Nguyen Kim, C.; Maumy, M. "Copper(I) and copper(II) mediated two-electron oxidations of benzylic alcohols and diaryl acetic acids by trimethylamine *N*-oxide." *J. Chem. Soc., Chem. Commun.* **1990**, 565-566.

(39) Reinaud, O.; Capdevielle, P.; Maumy, M. "Copper(II) mediated aromatic hydroxylation by trimethylamine *N*-oxide." *J. Chem. Soc., Chem. Commun,* **1990**, 566-568.

(40) Maiti, D.; Narducci Sarjeant, A. A.; Karlin, K. D. "Copper-Hydroperoxo-Mediated *N*-Debenzylation Chemistry Mimicking Aspects of Copper Monooxygenases." *Inorg. Chem.* **2008**, *47*, 8736-8747.

(41) Maiti, D.; Lee, D.-H.; Gaoutchenova, K.; Wuertele, C.; Holthausen, M. C.; Narducci Sarjeant, A. A.; Sundermeyer, J.; Schindler, S.; Karlin, K. D. "Reactions of a copper(II) superoxo complex lead to C-H and O-H substrate oxygenation: modeling copper-monooxygenase C-H hydroxylation." *Angew. Chem., Int. Ed.* **2008**, *47*, 82-85.

(42) Capdevielle, P.; Audebert, P.; Maumy, M. "Reaction of oxygen with copper(I) alkoxides." *Tetrahedron Lett.* **1984**, *25*, 4397-4400.

(43) Capdevielle, P.; Baranne-Lafont, J.; Sparfel, D.; Nguyen Kim, C.; Maumy, M. "Synthesis of salicylaldehydes by copper- or iron-catalyzed selective dehydrogenation of saligenols." *J. Mol. Catal.* **1988**, *47*, 59-66.

(44) Toussaint, O.; Capdevielle, P.; Maumy, M. "Oxidative decarboxylation of aliphatic carboxylic acids by the copper(I)/oxygen system." *Tetrahedron Lett.* **1984**, *25*, 3819-3822.

(45) Hong, S.; Huber, S. M.; Gagliardi, L.; Cramer, C. C.; Tolman, W. B. "Copper(I)-α-Ketocarboxylate Complexes: Characterization and O_2 Reactions That Yield Copper-Oxygen Intermediates Capable of Hydroxylating Arenes." *J. Am. Chem. Soc.* **2007**, *129*, 14190-14192.

(46) Costas, M.; Mehn, M. P.; Jensen, M. P.; Que, L., Jr. "Dioxygen Activation at Mononuclear Nonheme Iron Active Sites: Enzymes, Models, and Intermediates." *Chem. Rev.* **2004**, *104*, 939-986.

(47) Huber, S. M.; Ertem, M. Z.; Aquilante, F.; Gagliardi, L.; Tolman, W. B.; Cramer, C. J. "Generating Cu(II)-Oxyl/Cu(III)-Oxo Species from Cu(I)-α-Ketocarboxylate Complexes and O2: In Silico Studies on Ligand Effects and C-H-Activation Reactivity." *Chem.--Eur. J.* **2009**, *15*, 4886-4895, S4886/4881-S4886/4334.

(48) Samsel, E. G.; Srinivasan, K.; Kochi, J. K. "Mechanism of the chromium-catalyzed epoxidation of olefins. Role of oxochromium(V) cations." *J. Am. Chem. Soc.* **1985**, *107*, 7606-7617.

(49) (a) Goldberg, D. P. "Corrolazines: New Frontiers in High-Valent Metalloporphyrinoid Stability and Reactivity." *Acc. Chem. Res.* **2007**, *40*, 626-634. (b) Shaik, S.; Hirao, H.; Kumar, D. "Reactivity of High-Valent Iron-Oxo Species in Enzymes and Synthetic Reagents: A Tale of Many States." *Acc. Chem. Res.* **2007**, *40*, 532-542. (c) Costas, M.; Mehn, M., P.; Jensen, M., P.; Que, L., Jr. "Dioxygen activation at mononuclear nonheme iron active sites: enzymes, models, and intermediates." *Chem. Rev.* **2004**, *104*, 939-986. (d) Askari, M. S.; Ottenwaelder, X. "Oxygen-atom transfer to a nucleophilic molybdenum complex." *Dalton Trans.* **2010**, *39*, 2644-2650. (e) Bryliakov, K. P.; Babushkin, D. E.; Talsi, E. P. "^{1}H NMR and EPR spectroscopic monitoring of the reactive intermediates of (Salen)Mn(III) catalyzed olefin epoxidation." *J. Mol. Catal. A: Chem.* **2000**, *158*, 19-35. (f) Che, C. M.; Yam, V. W. W.; Mak, T. C. W. "A novel monooxoruthenium(V) complex containing a polydentate pyridyl amine ligand. Syntheses, reactivities, and x-ray crystal structure of $[Ru(III)(N_4O)(H_2O)](ClO_4)_2$." *J. Am. Chem. Soc.* **1990**, *112*, 2284-2291. (g) Groves, J. T.; Nemo, T. E. "Epoxidation reactions catalyzed by iron porphyrins. Oxygen transfer from iodosylbenzene." *J. Am. Chem. Soc.* **1983**, *105*, 5786-5791.

(50) (a) Lee, D.-H.; Murthy, N. N.; Karlin, K. D. "Copper(I)/Dioxygen Reactivity with Dinuclear Compounds: Catalytic Oxygenation and Oxo-Transfer to a Ketone."

Inorg. Chem. **1996**, *35*, 804-805. (b) Sanyal, I.; Mahroof-Tahir, M.; Nasir, M. S.; Ghosh, P.; Cohen, B. I.; Gultneh, Y.; Cruse, R. W.; Farooq, A.; Karlin, K. D.; et al. "Reactions of dioxygen (O_2) with mononuclear copper(I) complexes: temperature-dependent formation of peroxo- or oxo- (and dihydroxo-) bridged dicopper(II) complexes." *Inorg. Chem.* **1992**, *31*, 4322-4332. (c) Maiti, D.; Narducci Sarjeant, A. A.; Karlin, K. D. "Copper-Hydroperoxo-Mediated *N*-Debenzylation Chemistry Mimicking Aspects of Copper Monooxygenases." *Inorg. Chem.* **2008**, *47*, 8736-8747. (d) Kitajima, N.; Koda, T.; Hashimoto, S.; Kitagawa, T.; Morooka, Y. "Synthesis and characterization of the dinuclear copper(II) complexes [Cu(HB(3,5-Me_2pz)$_3$)]2X (X = O^{2-}, $(OH)_2^{2-}$, CO_2^{2-}, O_2^{2-})." *J. Am. Chem. Soc.* **1991**, *113*, 5664-5671.

(51) Hong, S.; Gupta, A. K.; Tolman, W. B. "Intermediates in Reactions of Copper(I) Complexes with *N*-Oxides: From the Formation of Stable Adducts to Oxo Transfer." *Inorg. Chem.* **2009**, *48*, 6323-6325.

(52) Spencer, D. J. E.; Reynolds, A. M.; Holland, P. L.; Jazdzewski, B. A.; Duboc-Toia, C.; Le Pape, L.; Yokota, S.; Tachi, Y.; Itoh, S.; Tolman, W. B. "Copper Chemistry of β-Diketiminate Ligands: Monomer/Dimer Equilibria and a New Class of Bis(μ-oxo)dicopper Compounds." *Inorg. Chem.* **2002**, *41*, 6307-6321.

(53) Yoshizawa, K.; Shiota, Y. "Conversion of Methane to Methanol at the Mononuclear and Dinuclear Copper Sites of Particulate Methane Monooxygenase (pMMO): A DFT and QM/MM Study." *J. Am. Chem. Soc.* **2006**, *128*, 9873-9881.

(54) Kamachi, T.; Kihara, N.; Shiota, Y.; Yoshizawa, K. "Computational Exploration of the Catalytic Mechanism of Dopamine β-Monooxygenase: Modeling of Its Mononuclear Copper Active Sites." *Inorg. Chem.* **2005**, *44*, 4226-4236.

(55) Reglier, M.; Amadei, E.; Tadayoni, R.; Waegell, B. "Pyridine Nucleus Hydroxylation with Copper Oxygenase Models." *J. Chem. Soc., Chem. Commun.* **1989**, 447-450.

(56) Capdevielle, P.; Sparfel, D.; Baranne-Lafont, J.; Nguyen Kim, C.; Maumy, M. "Copper(I) and Copper(II) Mediated Two-Electron Oxidations of Benzylic Alcohols and Diaryl Acetic Acids by Trimethylamine N-oxide." *J. Chem. Soc., Chem. Commun.* **1990**, 565-566.

(57) Schroeder, D.; Holthausen, M. C.; Schwarz, H. "Radical-Like Activation of Alkanes by the Ligated Copper Oxide Cation (Phenanthroline)CuO^+." *J. Phys. Chem. B.* **2004**, *108*, 14407-14416.

(58) Suelzle, D.; Schwarz, H.; Moock, K. H.; Terlouw, J. K. "On the Existence of

Novel Nitrides and Oxides of Copper: Copper Mononitride, Copper Dioxide and Copper-Nitrogen-Oxygen Compound (CuNO)." *Int. J. Mass Spectrom. Ion Processes.* **1991**, *108*, 269-272.

(59) (a) Price, J. C.; Barr, E. W.; Tirupati, B.; Bollinger, J. M., Jr.; Krebs, C. "The First Direct Characterization of a High-Valent Iron Intermediate in the Reaction of an α-Ketoglutarate-Dependent Dioxygenase: A High-Spin Fe(IV) Complex in Taurine/α-Ketoglutarate Dioxygenase (TauD) from Escherichia coli." *Biochemistry.* **2003**, *42*, 7497-7508. (b) Ortiz de Montellano, P. R.; Editor Cytochrome P450: Structure, Mechanism, and Biochemistry, Second Edition, 1995. (c) Krebs, C.; Fujimori, D. G.; Walsh, C. T.; Bollinger, J. M., Jr. "Non-Heme Fe(IV)-Oxo Intermediates." *Acc. Chem. Res.* **2007**, *40*, 484-492. (d) Que, L. "The Road to Non-Heme Oxoferryls and Beyond." *Acc. Chem. Res.* **2007**, *40*, 493-500.

(60) (a) Que, L., Jr.; Ho, R. Y. N. "Dioxygen Activation by Enzymes with Mononuclear Non-Heme Iron Active Sites." *Chem. Rev.* **1996**, *96*, 2607-2624. (b) Solomon, E. I.; Brunold, T. C.; Davis, M. I.; Kemsley, J. N.; Lee, S.-K.; Lehnert, N.; Neese, F.; Skulan, A. J.; Yang, Y.-S.; Zhou, J. "Geometric and Electronic Structure/Function Correlations in Non-Heme Iron Enzymes." *Chem. Rev.* **2000**, *100*, 235-349. (c) Hanauske-Abel, H. M.; Popowicz, A. M. "The HAG Mechanism: A Molecular Rationale for the Therapeutic Application of Iron Chelators in Human Diseases Involving the 2-Oxoacid Utilizing Dioxygenases." *Curr. Med. Chem.* **2003**, *10*, 1005-1019. (d) Hanauske-Abel, H. M.; Guenzler, V. "A Stereochemical Concept for the Catalytic Mechanism of Prolylhydroxylase. Applicability to Classification and Design of Inhibitors." *J. Theor. Biol.* **1982**, *94*, 421-455.

(61) Mahadevan, V.; Henson, M. J.; Solomon, E. I.; Stack, T. D. P. "Differential Reactivity between Interconvertible Side-On Peroxo and Bis-μ-oxodicopper Isomers Using Peralkylated Diamine Ligands." *J. Am. Chem. Soc.* **2000**, *122*, 10249-10250.

(62) (a) Mahadevan, V.; DuBois, J. L.; Hedman, B.; Hodgson, K. O.; Stack, T. D. P. "Exogenous Substrate Reactivity with a $[Cu(III)_2O_2]^{2+}$ Core: Structural Implications." *J. Am. Chem. Soc.* **1999**, *121*, 5583-5584. (b) Mahadevan, V.; Hou, Z.; Cole, A. P.; Root, D. E.; Solomon, E. I.; Stack, T. D. P. "Irreversible Reduction of Dioxygen by Simple Peralkylated Diamine-Copper(I) Complexes: Characterization and Thermal Stability of a $[Cu_2(\mu\text{-}O)_2]^{2+}$ Core." *J. Am. Chem. Soc.* **1997**, *119*, 11996-11997.

(63) Reproduced in part with permission from Gupta, A. K.; Tolman, W. B. "Copper/α-Ketocarboxylate Chemistry With Supporting Peralkylated Diamines:

Reactivity of Copper(I) Complexes and Dicopper-Dioxygen Intermediates." *Inorg. Chem.* **2010**, *49*, 3531-3539. Copyright 2010 American Chemical Society.

(64) El-Sayed, M. A.; El-Toukhy, A.; Davies, G. "Stoichiometry and Kinetics of Oxidation of Dimeric bis(μ-halo)-bis-((diamine)copper(I)) Complexes $L_2Cu_2X_2$ by Dioxygen in Aprotic Solvents." *Inorg. Chem.* **1985**, *24*, 3387-3390.

(65) Friese, S. J.; Kucera, B. E.; Young, V. G.; Que, L.; Tolman, W. B. "Iron(II) Complexes of Sterically Bulky α-Ketocarboxylates. Structural Models for α-Ketoacid-Dependent Nonheme Iron Halogenases." *Inorg. Chem.* **2008**, *47*, 1324-1331.

(66) Handley, D. A.; Hitchcock, P. B.; Lee, T. H.; Leigh, G. J. "Complexes of Metal(II) Halides of the First Transition Series with *N,N,N′,N′*-Tetramethylmethane-diamine,-Ethane-1,2-diamine and -Propane-1,3-diamine." *Inorg. Chim. Acta* **2001**, *314*, 14-21.

(67) Chaudhuri, P.; Wieghardt, K. "The Chemistry of 1,4,7-Triazacyclononane and Related Tridentate Macrocyclic Compounds." *Prog. Inorg. Chem.* **1987**, *35*, 329-436.

(68) Selected Fe(II) complexes: (a) Mehn, M. P.; Fujisawa, K.; Hegg, E. L.; Que, L., Jr. "Oxygen Activation by Nonheme Iron(II) Complexes: α-Ketocarboxylate Versus Carboxylate." *J. Am. Chem. Soc.* **2003**, *125*, 7828-7842. (b) Paine, T. K.; Zheng, H.; Que, L., Jr. "Iron Coordination Chemistry of Phenylpyruvate: An Unexpected κ_3-Bridging Mode That Leads to Oxidative Cleavage of the C2-C3 Bond." *Inorg. Chem.* **2005**, *44*, 474-476. (c) Chiou, Y. M.; Que, L., Jr. "Model Complexes for α-Ketoacid-Dependent Enzymes. Structure and Reactivity of $\{Fe^{II}$[tris[(6-methyl-2-pyridyl)methyl]amine](benzoylformate)$\}(ClO_4)$." *J. Am. Chem. Soc.* **1992**, *114*, 7567-7568. (d) Hegg, E. L.; Whiting, A. K.; Saari, R. E.; McCracken, J.; Hausinger, R. P.; Que, L., Jr. "Herbicide-Degrading α-Keto Acid-Dependent Enzyme TfdA: Metal Coordination Environment and Mechanistic Insights." *Biochemistry.* **1999**, *38*, 16714-16726. (e) Hikichi, S.; Ogihara, T.; Fujisawa, K.; Kitajima, N.; Akita, M.; Moro-oka, Y. "Synthesis and Characterization of the Benzoylformato Ferrous Complexes with Hindered Tris(pyrazolyl)borate Ligand as a Structural Model for Mononuclear Non-Heme Iron Enzymes." *Inorg. Chem.* **1997**, *36*, 4539-4547.

(69) Deacon, G. B.; Phillips, R. J. "Relationships Between the Carbon-Oxygen Stretching Frequencies of Carboxylato Complexes and the Type of Carboxylate Coordination." *Coord. Chem. Rev.* **1980**, *33*, 227-250.

(70) Pretsch, E.; Buehlmann, P.; Affolter, C. Structure Determination of Organic

Compounds: Tables of Spectral Data, 2003.

(71) Geary, W. J. "Use of Conductivity Measurements in Organic Solvents for the Characterization of Coordination Compounds." *Coord. Chem. Rev.* **1971**, *7*, 81-122.

(72) Casella, L.; Ibers, J. A. "Synthesis, Characterization, and Reactivity of Copper(I) and Copper(II) Complexes of *N,N′*-bis(3-(2-thenylideneimino)propyl)piperazine (tipp) and *N,N′*-bis(3-(2-thenylamino)propyl)piperazine (tapp). Crystal Structure of $[Cu(tapp)][ClO_4]_2$" *Inorg. Chem.* **1981**, *20*, 2438-2448.

(73) Yang, L.; Powell, D. R.; Houser, R. P. "Structural Variation in Copper(I) Complexes with Pyridylmethylamide Ligands: Structural Analysis with a New Four-Coordinate Geometry Index, τ_4." *Dalton Trans.* **2007**, 955-964.

(74) Selected Cu(II) complexes: (a) Arnaud, C.; Faure, R.; Loiseleur, H. "Bis[2-(2-thienyl)glyoxylato]copper(II) and diaquabis[2-(2-thienyl)glyoxylato]copper(II)." *Acta Crystallogr., Sect. C: Cryst. Struct. Commun.* **1986**, *C42*, 814-816. (b) Nakasa, K.; Nakagawa, H.; Kani, Y.; Tsuchimoto, M.; Ohba, S. "Copper(II) 2-Thiopheneglyoxylate Adducts with Pyridine Derivatives" *Acta Crystallogr., Sect. C: Cryst. Struct. Commun.* **1999**, *C55*, 513-517. (c) Ovcharenko, V. I.; Vostrikova, K. E.; Podoplelov, A. V.; Romanenko, G. V.; Ikorskii, V. N.; Reznikov, V. A. "Synthesis and Structure of Mono- and Binuclear Copper(II) Complexes with Polyfunctional Nitroxide 4-(1'-carboxy-2'-oxopropylidene)-2,2,5,5-tetramethyl-3-imidazolidine-1-oxyl, $[Cu(LH)_2(H_2O)_2]$ and $[Cu_2L_2(H_2O)_5]$. Caterpillar-like Reaction." *Polyhedron* **1997**, *16*, 1279-1289. (d) Kaizer, J.; Csonka, R.; Speier, G.; Giorgi, M.; Reglier, M. "Synthesis, Structure and Catalase-like Activity of New Dicopper(II) Complexes with Phenylglyoxylate and Benzoate Ligands." *J. Mol. Catal. A: Chem.* **2005**, *236*, 12-17. (e) Lippai, I.; Speier, G.; Huttner, G.; Zsolnai, L. "Crystal and Molecular Structure of α-Ketocarboxylatocopper(II) Intermediate in the Oxygenation of a Copper(I) Flavonolate Complex." *Chem. Commun.* **1997**, 741-742. (f) Zheng, H.; Que, L., Jr. "Cu(II) α-Ketoacid Complexes as Structural Models of α-Ketoacid-Dependent Enzymes: Syntheses, Crystal Structure and Properties of [Cu(L)(benzoylformate)]X." *Inorg. Chim. Acta* **1997**, *263*, 301-307.

(75) Selected examples of complexes other than Cu and Fe: (a) Law, G.-L.; Wong, K.-L.; Lau, K.-K.; Tam, H.-L.; Cheah, K.-W.; Wong, W.-T. "Synthesis, Crystal Structures, and Photophysical Properties of Lanthanide Complexes Containing Pyrrole-Derivatized Carboxylate Ligands." *Eur. J. Inorg. Chem.* **2007**, 5419-5425. (b) Mueller, R.; Huebner, E.; Burzlaff, N. "Ruthenium(II) Complexes Bearing Carboxylato and 2-oxocarboxylato Ligands." *Eur. J. Inorg. Chem.* **2004**, 2151-2159. (c) Ruman, T.; Ciunik, Z.; Szklanny, E.; Wolowiec, S. "Complexes of

Heteroscorpionate Trispyrazolylborate Ligands. Part VI. Carboxylate Induced Conversion of Mono-ligand Tp'M(L) into bis-ligand Tp'2M complexes (M = Co(II) and Cu(II)).” *Polyhedron* **2002**, *21*, 2743-2753. (d) Tekeste, T.; Vahrenkamp, H. ""Inhibition" of the Enzyme Model TpPh,MeZn-OH by Diketo Compounds.” *Eur. J. Inorg. Chem.* **2006**, 5158-5164. (e) Teoh, S.-G.; Looi, E.-S.; Teo, S.-B.; Ng, S.-W. "Synthesis and Crystal Structure of the Tetrabutylbis(thiophene glyoxylato)distannoxane dimer, $\{[(C_4H_9)_2SnO_2CC(O)C_4H_3S]_2O\}_2$.” *J. Organomet. Chem.* **1996**, *509*, 57-61. (f) Sharutin, V. V.; Sharutina, O. K.; Bondar, E. A.; Pakusina, A. P.; Krivolapov, D. B.; Gubaidullin, A. T.; Litvinov, I. A. "Tetraphenylantimony Phenylglyoxylate: Synthesis and Structure.” *Russ. J. Gen. Chem.* **2002**, *72*, 226-228. (g) Krogmann, K.; Hausen, H. D. "Structures with Platinum Chains. I. "Violet" Potassium Tetracyanoplatinate, $K_2[Pt(CN)_4]X0.3.2.5H_2O$ (X = chlorine, bromine).” *Z. Anorg. Allg. Chem.* **1968**, *358*, 67-81. (h) Ng, S. W. "Crystal structure of a-oxobenzeneacetatotris(triphenylphosphine)silver(I), $[(C_8H_5O_3)(C_{18}H_{15}P)_3Ag]$.” *Z. Kristallogr. - New Cryst. Struct.* **1997**, *212*, 279-281.

(76) Griffiths, V. S.; Socrates, G. "N.M.R. Study of the Hydration of Pyruvic Acid.” *Trans. Faraday Soc.* **1967**, *63*, 673-677.

(77) (a) Hagadorn, J. R.; Zahn, T. I.; Que, L., Jr.; Tolman, W. B. "Dicopper(I,I) and Delocalized Mixed-Valent Dicopper(I,II) Complexes of a Sterically Hindered Carboxylate Ligand.” *Dalton Trans.* **2003**, 1790-1794. (b) LeCloux, D. D.; Davydov, R.; Lippard, S. J. "Synthesis and Characterization of Spin-Delocalized Carboxylate-Bridged Cu(I)-Cu(II) Mixed-Valence Complexes Having Only Oxygen Donor Ligands.” *J. Am. Chem. Soc.* **1998**, *120*, 6810-6811. (c) LeCloux, D. D.; Davydov, R.; Lippard, S. J. "Mixed-Valence Cu(I)-Cu(II) and Heterodimetallic Cu(I)-M(II) Bis(carboxylate-bridged) Complexes: Structural, Electrochemical, and Spectroscopic Investigations.” *Inorg. Chem.* **1998**, *37*, 6814-6826. (d) Kriz, O.; Rheingold, A. L.; Shang, M.; Fehlner, T. P. "Clusters as Substituents. Synthesis and Thermal Decomposition of Metal Carboranecarboxylates.” *Inorg. Chem.* **1994**, *33*, 3777-3783. (e) Morgan, Y. R.; Turner, P.; Kennedy, B. J.; Hambley, T. W.; Lay, P. A.; Ray Biffin, J.; Regtop, H. L.; Warwick, B. "Preparation and Characterization of Dinuclear Copper-Indomethacin Anti-Inflammatory drugs.” *Inorg. Chim. Acta* **2001**, *324*, 150-161. (f) Calderazzo, F.; Donati, N.; Englert, U.; Marchetti, F.; Pampaloni, G.; Passarelli, V. "Synthesis, Reactivity and Structures of Mono- and Dihaloacetato Complexes of Copper(I) and Copper(II).” *Inorg. Chim. Acta* **2003**, *346*, 100-110. (g) Sevryugina, Y.; Rogachev, A. Y.; Petrukhina, M. A. "The First Hexanuclear Copper(I) Carboxylate: X-ray Crystal Structure and Reactivity in Solution and Gas-Phase Reactions.” *Inorg. Chem.* **2007**, *46*, 7870-7879.

(78) Henson, M. J.; Mukherjee, P.; Root, D. E.; Stack, T. D. P.; Solomon, E. I.

"Spectroscopic and Electronic Structural Studies of the $Cu(III)_2$ Bis-μ-oxo Core and Its Relation to the Side-On Peroxo-Bridged Dimer." *J. Am. Chem. Soc.* **1999**, *121*, 10332-10345.

(79) Mirica, L. M.; Ottenwaelder, X.; Stack, T. D. P. "Structure and Spectroscopy of Copper-Dioxygen Complexes." *Chem. Rev.* **2004**, *104*, 1013-1045.

(80) Funahashi, Y.; Nishikawa, T.; Wasada-Tsutsui, Y.; Kajita, Y.; Yamaguchi, S.; Arii, H.; Ozawa, T.; Jitsukawa, K.; Tosha, T.; Hirota, S.; Kitagawa, T.; Masuda, H. "Formation of a Bridged Butterfly-Type μ-η^2:η^2-Peroxo Dicopper Core Structure with a Carboxylate Group." *J. Am. Chem. Soc.* **2008**, *130*, 16444-16445.

(81) Ottenwaelder, X.; Rudd, D. J.; Corbett, M. C.; Hodgson, K. O.; Hedman, B.; Stack, T. D. P. "Reversible O-O Bond Cleavage in Copper-Dioxygen Isomers: Impact of Anion Basicity." *J. Am. Chem. Soc.* **2006**, *128*, 9268-9269.

(82) Pidcock, E.; Obias, H. V.; Abe, M.; Liang, H.-C.; Karlin, K. D.; Solomon, E. I. "Spectroscopic and Theoretical Studies of Oxygenated Dicopper(I) Complexes Containing Hydrocarbon-Linked Bis[2-(2-pyridyl)ethyl]amine Units: Investigation of a Butterfly $[Cu_2(\mu\text{-}\eta^2\text{:}\eta^2)(O_2)]^{2+}$ Core." *J. Am. Chem. Soc.* **1999**, *121*, 1299-1308.

(83) Solomon, E. I.; Tuczek, F.; Root, D. E.; Brown, C. A. "Spectroscopy of Binuclear Dioxygen Complexes." *Chem. Rev.* **1994**, *94*, 827-856.

(84) Lewis, E. A.; Tolman, W. B. "Reactivity of Dioxygen-Copper Systems." *Chem. Rev.* **2004**, *104*, 1047-1076.

(85) Tsuda, T.; Yazawa, T.; Watanabe, K.; Fujii, T.; Saegusa, T. "Preparation of Thermally Stable and Soluble Mesitylcopper(I) and its Application in Organic Synthesis." *J. Org. Chem.* **1981**, *46*, 192-194.

(86) Hayoz, P.; Ilg, S.; (Ciba Specialty Chemicals Holding Inc., Switz.). WO Patent 2006067061. 2006, 92.

(87) (a) Rosenzweig, A. C.; Sazinsky, M. H. "Structural insights into dioxygen-activating copper enzymes." *Curr. Opin. Struct. Biol.* **2006**, *16*, 729-735. (b) Woertink, J. S.; Smeets, P. J.; Groothaert, M. H.; Vance, M. A.; Sels, B. F.; Schoonheydt, R. A.; Solomon, E. I. "A $[Cu_2O]^{2+}$ core in Cu-ZSM-5, the active site in the oxidation of methane to methanol." *Proc. Natl. Acad. Sci. U. S. A.* **2009**, *106*, 18908-18913, S18908/18901-S18908/18913. (c) Que, L., Jr.; Tolman, W. B. "Biologically inspired oxidation catalysis." *Nature* **2008**, *455*, 333-340.

(88) Cramer, C. J.; Tolman, W. B. "Mononuclear Cu-O_2 Complexes: Geometries, Spectroscopic Properties, Electronic Structures, and Reactivity." *Acc. Chem. Res.* **2007**, *40*, 601-608.

(89) Smeets, P. J.; Hadt, R. G.; Woertink, J. S.; Vanelderen, P.; Schoonheydt, R. A.; Sels, B. F.; Solomon, E. I. "Oxygen Precursor to the Reactive Intermediate in Methanol Synthesis by Cu-ZSM-5." *J. Am. Chem. Soc.* **2010**, *132*, 14736-14738.

(90) (a) Aboelella, N. W.; Kryatov, S. V.; Gherman, B. F.; Brennessel, W. W.; Young, V. G., Jr.; Sarangi, R.; Rybak-Akimova, E. V.; Hodgson, K. O.; Hedman, B.; Solomon, E. I.; Cramer, C. J.; Tolman, W. B. "Dioxygen Activation at a Single Copper Site: Structure, Bonding, and Mechanism of Formation of 1:1 Cu-O_2 Adducts." *J. Am. Chem. Soc.* **2004**, *126*, 16896-16911. (b) Aboelella, N. W.; York, J. T.; Reynolds, A. M.; Fujita, K.; Kinsinger, C. R.; Cramer, C. J.; Riordan, C. G.; Tolman, W. B. "Mixed metal bis(μ-oxo) complexes with $[CuM(\mu\text{-}O)_2]^{n+}$ (M = Ni(III) or Pd(II)) cores." *Chem. Commun.* **2004**, 1716-1717. (c) Aboelella, N. W.; Lewis, E. A.; Reynolds, A. M.; Brennessel, W. W.; Cramer, C. J.; Tolman, W. B. "Snapshots of Dioxygen Activation by Copper: The Structure of a 1:1 Cu/O_2 Adduct and Its Use in Syntheses of Asymmetric Bis(μ-oxo) Complexes." *J. Am. Chem. Soc.* **2002**, *124*, 10660-10661. (d) Spencer, D. J. E.; Aboelella, N. W.; Reynolds, A. M.; Holland, P. L.; Tolman, W. B. "β-Diketiminate Ligand Backbone Structural Effects on Cu(I)/O_2 Reactivity: Unique Copper-Superoxo and Bis(μ-oxo) Complexes." *J. Am. Chem. Soc.* **2002**, *124*, 2108-2109.

(91) (a) Hill, L. M. R.; Gherman, B. F.; Aboelella, N. W.; Cramer, C. J.; Tolman, W. B. "Electronic Tuning of β-diketiminate Ligands with Fluorinated Substituents: Effects on the O_2-Reactivity of Mononuclear Cu(I) Complexes." *Dalton Trans.* **2006**, 4944-4953. (b) Hong, S.; Hill, L. M. R.; Gupta, A. K.; Naab, B. D.; Gilroy, J. B.; Hicks, R. G.; Cramer, C. J.; Tolman, W. B. "Effects of Electron-Deficient β-Diketiminate and Formazan Supporting Ligands on Copper(I)-Mediated Dioxygen Activation." *Inorg. Chem.* **2009**, *48*, 4514-4523.

(92) (a) Domnin, N. A.; Yakimovich, S. I. "Reaction of β-Dicarbonyl Compounds with Hydrazines. I. Reaction of Aliphatic β-Diketones with *N,N*-dialkylhydrazines." *Zh. Organ. Khim.* **1965**, *1*, 658-666. (b) Sedai, B.; Heeg, M. J.; Winter, C. H. "Volatility Enhancement in Calcium, Strontium, and Barium Complexes Containing β-Diketiminate Ligands with Dimethylamino Groups on the Ligand Core Nitrogen Atoms." *Organometallics* **2009**, *28*, 1032-1038. (c) Sedai, B.; Heeg, M. J.; Winter, C. H. "Magnesium complexes containing β-ketiminate and β-diketiminate ligands with dimethylamino substituents on the ligand core nitrogen atoms." *J. Organomet. Chem.* **2008**, *693*, 3495-3503.

(93) Lide, D. R. CRC Handbook of Chemistry and Physics, 2009-2010, 90th ed.

Editor-in-Chief, 2009; Vol. 131.

(94) Souma, Y.; Iyoda, J.; Sano, H. "Formation and properties of Group IB metal carbonyl cations." *Osaka Kogyo Gijutsu Shikensho Kiho* **1976**, *27*, 277-281.

(95) Liao, M.-S.; Scheiner, S. "Electronic structure and bonding in unligated and ligated Fe(II) porphyrins." *J. Chem. Phys.* **2002**, *116*, 3635-3645.

(96) Liao, M.-S.; Scheiner, S. "Electronic structure and bonding in metal porphyrins, metal = Fe, Co, Ni, Cu, Zn." *J. Chem. Phys.* **2002**, *117*, 205-219.

(97) (a) Papish, E. T.; Donahue, T. M.; Wells, K. R.; Yap, G. P. A. "How are Tris(triazolyl)borate Ligands Electronically Different from Tris(pyrazolyl)borate Ligands? A Study of (TztBu,Me)CuCO [TztBu,Me = tris(3-t-butyl-5-methyl-1,2,4-triazolyl)borate]." *Dalton Trans.* **2008**, 2923-2925. (b) Fry, H. C.; Lucas Heather, R.; Sarjeant, A. A. N.; Karlin K. D.; Meyer, G. J. "Carbon Monoxide Coordination and Reversible Photodissociation in Copper(I) Pyridylalkylamine Compounds." *Inorg. Chem.* **2008**, *47*, 241-256. (c) Pasquali, M.; Floriani, C.; Venturi, G.; Gaetani-Manfredotti, A.; Chiesi-Villa, A. "Copper(I)-Carbon Monoxide Chemistry: Genesis and Chemical and Structural Properties of Copper(I) Terminal and Bridging Carbonyls." *J. Am. Chem. Soc.* **1982**, *104*, 4092-4099. (d) Li, Q.; Liu, Y.; Xie, Y.; King, R. B.; Schaefer, H. F., 3rd "Binuclear Homoleptic Copper Carbonyls $Cu_2(CO)(x)$ (x = 1-6): Remarkable Structures Contrasting Metal-Metal Multiple Bonding with Low-Dimensional Copper Bonding Manifolds." *Inorg. Chem.* **2001**, *40*, 5842-5850. (e) Kou, X.; Wu, J.; Cundari, T. R.; Dias, H. V. R. "Sandwiched Sodium and Half-Sandwiched Copper Carbonyl Complexes Featuring Polyfluorinated Tris(triazolyl)borate [$HB(3,5\text{-}(CF_3)_2Tz)_3$]." *Dalton Trans.* **2009**, 915-917. (f) Perez, J.; Morales, D.; Garcia-Escudero, L. A.; Martinez-Garcia, H.; Miguel, D.; Bernad, P. "Synthesis of New Copper(I) Complexes with Tris(2-pyridyl) Ligands. Applications to Carbene and Nitrene Transfer Reactions." *Dalton Trans.* **2009**, 375-382. (g) Souma, Y.; Iyoda, J.; Sano, H. "Formation and Properties of Group 1B Metal Carbonyl Cations." *Inorg. Chem.* **1976**, *15*, 968-970.

(98) Kitajima, N.; Fujisawa, K.; Fujimoto, C.; Morooka, Y.; Hashimoto, S.; Kitagawa, T.; Toriumi, K.; Tatsumi, K.; Nakamura, A. "A New Model for Dioxygen Binding in Hemocyanin. Synthesis, Characterization, and Molecular Structure of the $\mu\text{-}\eta^2\text{:}\eta^2$-Peroxo Dinuclear Copper(II) Complexes, $[Cu(HB(3,5\text{-}R_2pz)_3)]_2(O_2)$ (R = isopropyl and Ph)." *J. Am. Chem. Soc.* **1992**, *114*, 1277-1291.

(99) Ivanova, S. M.; Ivanov, S. V.; Miller, b. S. M.; Anderson, O. P.; Solntsev, K. A.; Strauss, S. H. "Mono-, Di-, Tri-, and Tetracarbonyls of Copper(I), Including the Structures of Cu(CO)2(1-Bn-$CB_{11}F_{11}$) and $[Cu(CO)_4][1\text{-Et-}CB_{11}F_{11}]$." *Inorg. Chem.* **1999**, *38*, 3756-3757.

(100) Polyakov, O. G.; Ivanova, S. M.; Gaudinski, C. M.; Miller, S. M.; Anderson, O. P.; Strauss, S. H. "$Cu(CO)_2(N(SO_2CF_3)_2)$. The First Structurally Characterized Copper(I) Polycarbonyl." *Organometallics* **1999**, *18*, 3769-3771.

(101) Rack, J. J.; Webb, J. D.; Strauss, S. H. "$[Cu(CO)_n]^+$ Complex Ions in the Solid State (n = 1, 2, 3)." *Inorg. Chem.* **1996**, *35*, 277-278.

(102) Zecchina, A.; Bordiga, S.; Salvalaggio, M.; Spoto, G.; Scarano, D.; Lamberti, C. "Formation of nonplanar $CuI(CO)_3$ tricarbonyls on CuI-ZSM-5: an FTIR study at 80 K." *J. Catal.* **1998**, *173*, 540-542.

(103) Iwamoto, M.; Hoshino, Y. "Assignment of Nonclassical $[Cu(CO)_n]^+$ (n = 1, 2) Complex Ions in Zeolite Cages." *Inorg. Chem.* **1996**, *35*, 6918-6921.

(104) Borovkov, V. Y.; Karge, H. G. "Use of Combination Modes and Overtones of Metal Carbonyls for the IR Study of Cation States in Zeolites: Copper(I) Carbonyls in Reduced CuNaY Zeolites." *J. Chem. Soc., Faraday Trans.* **1995**, *91*, 2035-2039.

(105) Ivanova, S. M.; Ivanov, S. V.; Miller, b. S. M.; Anderson, O. P.; Solntsev, K. A.; Strauss, S. H. "Mono-, Di-, Tri-, and Tetracarbonyls of Copper(I), Including the Structures of $Cu(CO)_2(1\text{-Bn-}CB_{11}F_{11})$ and $[Cu(CO)_4]$[1-Et-CB11F11]." *Inorg. Chem.* **1999**, *38*, 3756-3757.

(106) Polyakov, O. G.; Ivanova, S. M.; Gaudinski, C. M.; Miller, S. M.; Anderson, O. P.; Strauss, S. H. "$Cu(CO)_2(N(SO_2CF_3)_2)$. The First Structurally Characterized Copper(I) Polycarbonyl." *Organometallics* **1999**, *18*, 3769-3771.

(107) Rack, J. J.; Webb, J. D.; Strauss, S. H. "$[Cu(CO)_n]^+$ Complex Ions in the Solid State (n = 1, 2, 3)." *Inorg. Chem.* **1996**, *35*, 277-278.

(108) Zecchina, A.; Bordiga, S.; Salvalaggio, M.; Spoto, G.; Scarano, D.; Lamberti, C. "Formation of Nonplanar $CuI(CO)_3$ Tricarbonyls on CuI-ZSM-5: an FTIR Study at 80 K." *J. Catal.* **1998**, *173*, 540-542.

(109) Iwamoto, M.; Hoshino, Y. "Assignment of Nonclassical $[Cu(CO)_n]^+$ (n = 1, 2) Complex Ions in Zeolite Cages." *Inorg. Chem.* **1996**, *35*, 6918-6921.

(110) Borovkov, V. Y.; Karge, H. G. "Use of Combination Modes and Overtones of Metal Carbonyls for the IR Study of Cation States in Zeolites: Copper(I) Carbonyls in Reduced CuNaY Zeolites." *J. Chem. Soc., Faraday Trans.* **1995**, *91*, 2035-2039.

(111) Wiese, S.; Kapoor, P.; Williams, K. D.; Warren, T. H. "Nitric Oxide Oxidatively Nitrosylates Ni(I) and Cu(I) C-Organonitroso Adducts." *J. Am. Chem. Soc.* **2009**, *131*, 18105-18111.

(112) Gottlieb, H. E.; Kotlyar, V.; Nudelman, A. "NMR chemical shifts of common laboratory solvents as trace impurities." *J. Org. Chem.* **1997**, *62*, 7512-7515.

(113) Cole, A. P.; Root, D. E.; Mukherjee, P.; Solomon, E. I.; Stack, T. D. P. "A Trinuclear Intermediate in the Copper-Mediated Reduction of O_2: Four Electrons from Three Coppers." *Science.* **1996**, *273*, 1848-1850.

(114) Taki, M.; Teramae, S.; Nagatomo, S.; Tachi, Y.; Kitagawa, T.; Itoh, S.; Fukuzumi, S. "Fine-Tuning of Copper(I)-Dioxygen Reactivity by 2-(2-Pyridyl)ethylamine Bidentate Ligands." *J. Am. Chem. Soc.* **2002**, *124*, 6367-6377.

(115) Kang, P.; Bobyr, E.; Dustman, J.; Hodgson, K. O.; Hedman, B.; Solomon, E. I.; Stack, T. D. P. "Bis(μ-oxo) Dicopper(III) Species of the Simplest Peralkylated Diamine: Enhanced Reactivity toward Exogenous Substrates." *Inorg. Chem.* **2010**, *49*, 11030-11038.

(116) Battino, R.; Editor Solubility Data Series, Vol. 7: Oxygen and Ozone, 1981.

(117) Piguet, C. "Paramagnetic susceptibility by NMR: the "solvent correction" removed for large paramagnetic molecules." *J. Chem. Educ.* **1997**, *74*, 815-816.

(118) Sur, S. K. "Measurement of magnetic susceptibility and magnetic moment of paramagnetic molecules in solution by high-field Fourier transform NMR spectroscopy." *J. Magn. Reson.* **1989**, *82*, 169-173.

(119) Evans, D. F. "The determination of the paramagnetic susceptibility of substances in solution by nuclear magnetic resonance." *J. Chem. Soc.* **1959**, 2003-2005.

(120) Taktak, S.; Ye, W.; Herrera, A. M.; Rybak-Akimova, E. V. "Synthesis and Catalytic Properties in Olefin Epoxidation of Novel Iron(II) Complexes with Pyridine-Containing Macrocycles Bearing an Aminopropyl Pendant Arm." *Inorg. Chem.* **2007**, *46*, 2929-2942.

(121) Drago, R. S. Physical Methods in Chemistry, Vol. 1, 1981.

(122) Girerd, J.-J.; Journaux, Y. "Molecular magnetism in bioinorganic chemistry." *Phys. Methods Bioinorg.* **2000**, 321-374.

(123) Machonkin, T. E.; Mukherjee, P.; Henson, M. J.; Stack, T. D. P.; Solomon, E. I. "The EPR spectrum of a Cu(II/II/III) cluster: anisotropic exchange in a bent $Cu(II)_2O_2$ core." *Inorg. Chim. Acta* **2002**, *341*, 39-44.

(124) Root, D. E.; Henson, M. J.; Machonkin, T.; Mukherjee, P.; Stack, T. D. P.; Solomon, E. I. "Electronic and Geometric Structure of a Trinuclear Mixed-Valence Copper(II,II,III) Cluster." *J. Am. Chem. Soc.* **1998**, *120*, 4982-4990.

(125) Yang, F.-A.; Guo, C.-W.; Chen, Y.-J.; Chen, J.-H.; Wang, S.-S.; Tung, J.-Y.; Hwang, L.-P.; Elango, S. "ESR, Zero-Field Splitting, and Magnetic Exchange of Exchange-Coupled Copper(II)-Copper(II) Pairs in Copper(II) Tetraphenylporphyrin N-Oxide." *Inorg. Chem.* **2007**, *46*, 578-585.

(126) Donoghue, P. J.; Gupta, A. K.; Boyce, D. W.; Cramer, C. J.; Tolman, W. B. "An Anionic, Tetragonal Copper(II) Superoxide Complex." *J. Am. Chem. Soc.* **2010**, *132*, 15869-15871.

(127) Wuertele, C.; Gaoutchenova, E.; Harms, K.; Holthausen, M. C.; Sundermeyer, J.; Schindler, S. "Crystallographic characterization of a synthetic 1:1 end-on copper dioxygen adduct complex." *Angew. Chem. Int. Ed.* **2006**, *45*, 3867-3869.

(128) (a) Halime, Z.; Kieber-Emmons, M. T.; Qayyum, M. F.; Mondal, B.; Gandhi, T.; Puiu, S. C.; Chufan, E. E.; Sarjeant, A. A. N.; Hodgson, K. O.; Hedman, B.; Solomon, E. I.; Karlin, K. D. "Heme-Copper-Dioxygen Complexes: Toward Understanding Ligand-Environmental Effects on the Coordination Geometry, Electronic Structure, and Reactivity." *Inorg. Chem.*, *49*, 3629-3645. (b) Sanyal, I.; Strange, R. W.; Blackburn, N. J.; Karlin, K. D. "Formation of a copper-dioxygen complex (Cu_2-O_2) using simple imidazole ligands." *J. Am. Chem. Soc.* **1991**, *113*, 4692-4693. (c) Chaudhuri, P.; Hess, M.; Mueller, J.; Hildenbrand, K.; Bill, E.; Weyhermueller, T.; Wieghardt, K. "Aerobic Oxidation of Primary Alcohols (Including Methanol) by Copper(II)- and Zinc(II)-Phenoxyl Radical Catalysts." *J. Am. Chem. Soc.* **1999**, *121*, 9599-9610. (d) Eisenberg, G. M. "Colorimetric determination of hydrogen peroxide." *Ind. Eng. Chem., Anal. Ed.* **1943**, *15*, 327-328.

(129) Reglier, M.; Amadei, E.; Tadayoni, R.; Waegell, B. "Pyridine nucleus hydroxylation with copper oxygenase models." *J. Chem. Soc., Chem. Commun.* **1989**, 447-450.

(130) Luo, Y.-R. Handbook of Bond Dissociation Energies in Organic Compounds; CRC Press LLC: Boca Raton, FL, 2002.

(131) Fan, B.; Qu, L.; Shi, G. "Electrochemical Polymerization of Anthracene in Boron

Trifluoride Diethyl Etherate." *J. Electroanal. Chem.* **2005**, *575*, 287-292.

(132) Zeldin, M.; Mehta, P.; Vernon, W. D. "Phosphorus-31 NMR of Triphenylphosphine Oxide Complexes with Compounds of Silicon, Germanium, and Tin." *Inorg. Chem.* **1979**, *18*, 463-466.

(133) Du, H.; Williams, C. T.; Ebner, A. D.; Ritter, J. A. "In Situ FTIR Spectroscopic Analysis of Carbonate Transformations during Adsorption and Desorption of CO_2 in K-Promoted HTlc." *Chem. Mater.* **2010**, *22*, 3519-3526.

(134) Cramer, C. J.; Tolman, W. B. "Mononuclear Cu-O_2 Complexes: Geometries, Spectroscopic Properties, Electronic Structures, and Reactivity." *Acc. Chem. Res.* **2007**, *40*, 601-608.

(135) DuBois, J. L.; Mukherjee, P.; Collier, A. M.; Mayer, J. M.; Solomon, E. I.; Hedman, B.; Stack, T. D. P.; Hodgson, K. O. "Cu K-Edge XAS Study of the $[Cu_2(\mu\text{-}O)_2]$ Core: Direct Experimental Evidence for the Presence of Cu(III)." *J. Am. Chem. Soc.* **1997**, *119*, 8578-8579.

(136) DuBois, J. L.; Mukherjee, P.; Stack, T. D. P.; Hedman, B.; Solomon, E. I.; Hodgson, K. O. "A Systematic K-edge x-ray Absorption Spectroscopic Study of Cu(III) Sites." *J. Am. Chem. Soc.* **2000**, *122*, 5775-5787.

(137) (a) Wanzlick, H. W.; Schoenherr, H. J. "Chemistry of nucleophilic carbenes. XIV. Direct synthesis of a mercury salt-carbene complex." *Angew. Chem., Int. Ed. Engl.* **1968**, *7*, 141-142. (b) Oefele, K. "1,3-Dimethyl-4-imidazoline-2-pentacarbonylchromium, a new transition metal-carbene complex." *J. Organometal. Chem.* **1968**, *12*, P42-P43.

(138) Crudden, C. M.; Allen, D. P. "Stability and reactivity of N-heterocyclic carbene complexes." *Coord. Chem. Rev.* **2004**, *248*, 2247-2273.

(139) Ackermann, L. "Transition-Metal-Catalyzed Carboxylation of C-H Bonds." *Angew. Chem., Int. Ed.* **2011**, *50*, 3842-3844.

(140) Arnold, P. L.; Casely, I. J. "F-Block N-Heterocyclic Carbene Complexes." *Chem. Rev.* **2009**, *109*, 3599-3611.

(141) Mata, J. A.; Poyatos, M.; Peris, E. ."Structural and catalytic properties of chelating bis- and tris-*N*-heterocyclic carbenes" *Coord. Chem. Rev.* **2007**, *251*, 841-859.

(142) Sommer, W. J.; Weck, M. ."Supported *N*-heterocyclic carbene complexes in

catalysis." *Coord. Chem. Rev.* **2007**, *251*, 860-873.

(143) Marion, N.; Nolan, S. P. "Well-Defined N-Heterocyclic Carbenes-Palladium(II) Precatalysts for Cross-Coupling Reactions." *Acc. Chem. Res.* **2008**, *41*, 1440-1449.

(144) Nolan, S. P. "The Development and Catalytic Uses of *N*-Heterocyclic Carbene Gold Complexes." *Acc. Chem. Res.* **2011**, *44*, 91-100.

(145) Arduengo, A. J., III; Harlow, R. L.; Kline, M. "A stable crystalline carbene." *J. Am. Chem. Soc.* **1991**, *113*, 361-363.

(146) Sanford, M. S.; Love, J. A.; Grubbs, R. H. "Mechanism and activity of ruthenium olefin metathesis catalysts." *J. Am. Chem. Soc.* **2001**, *123*, 6543-6554.

(147) Herrmann, W. A. "*N*-Heterocyclic carbenes. Part 31. N-heterocyclic carbenes: A new concept in organometallic catalysis." *Angew. Chem., Int. Ed.* **2002**, *41*, 1290-1309.

(148) McGuinness, D. S.; Green, M. J.; Cavell, K. J.; Skelton, B. W.; White, A. H. "Synthesis and reaction chemistry of mixed ligand methylpalladium-carbene complexes." *J. Organomet. Chem.* **1998**, *565*, 165-178.

(149) McGuinness, D. S.; Cavell, K. J.; Skelton, B. W.; White, A. H. "Zerovalent Palladium and Nickel Complexes of Heterocyclic Carbenes: Oxidative Addition of Organic Halides, Carbon-Carbon Coupling Processes, and the Heck Reaction." *Organometallics* **1999**, *18*, 1596-1605.

(150) Martin, H. C.; James, N. H.; Aitken, J.; Gaunt, J. A.; Adams, H.; Haynes, A. "Oxidative Addition of MeI to a Rhodium(I) *N*-Heterocyclic Carbene Complex. A Kinetic Study." *Organometallics* **2003**, *22*, 4451-4458.

(151) Simms, R. W.; Drewitt, M. J.; Baird, M. C. "Equilibration between a Phosphine-Cobalt Complex and an Analogous Complex Containing an *N*-Heterocyclic Carbene: The Thermodynamics of a Phosphine-Carbene Exchange Reaction." *Organometallics* **2002**, *21*, 2958-2963.

(152) Prinz, M.; Grosche, M.; Herdtweck, E.; Herrmann, W. A. "Unsymmetrically Substituted Iridium(III)-Carbene Complexes by a CH-Activation Process." *Organometallics* **2000**, *19*, 1692-1694.

(153) Bourissou, D.; Guerret, O.; Gabbaie, F. P.; Bertrand, G. "Stable Carbenes." *Chem. Rev.* **2000**, *100*, 39-91.

(154) Nolan, S. P.; Editor N-Heterocyclic Carbenes in Synthesis; Wiley-VCH: Weinheim, 2006.

(155) Zhang, L.; Cheng, J.; Ohishi, T.; Hou, Z. "Copper-Catalyzed Direct Carboxylation of C-H Bonds with Carbon Dioxide." *Angew. Chem., Int. Ed.* **2010**, *49*, 8670-8673, S8670/8671-S8670/8648.

(156) Boogaerts, I. I. F.; Fortman, G. C.; Furst, M. R. L.; Cazin, C. S. J.; Nolan, S. P. "Carboxylation of N-H/C-H Bonds Using N-Heterocyclic Carbene Copper(I) Complexes." *Angew. Chem., Int. Ed.* **2011** , *49*, 8674-8677, S8674/8671-S8674/8620.

(157) Recent examples of (IPr)CuCl: (a) Chun, J.; Lee, H. S.; Jung, I. G.; Lee, S. W.; Kim, H. J.; Son, S. U. "Cu_2O: A Versatile Reagent for Base-Free Direct Synthesis of NHC-Copper Complexes and Decoration of 3D-MOF with Coordinatively Unsaturated NHC-Copper Species." *Organometallics* **2010**, *29*, 1518-1521. (b) Cisnetti, F.; Lemoine, P.; El-Ghozzi, M.; Avignant, D.; Gautier, A. "Copper(I) thiophenolate in copper N-heterocyclic carbene preparation." *Tetrahedron Lett.* **2010**, *51*, 5226-5229. (c) Citadelle, C. A.; Le Nouy, E.; Bisaro, F.; Slawin, A. M. Z.; Cazin, C. S. J. "Simple and versatile synthesis of copper and silver N-heterocyclic carbene complexes in water or organic solvents." *Dalton Trans.* **2010**, *39*, 4489-4491. (d) Diez-Gonzalez, S.; Escudero-Adan, E. C.; Benet-Buchholz, J.; Stevens, E. D.; Slawin, A. M. Z.; Nolan, S. P. "[(NHC)CuX] complexes: Synthesis, characterization and catalytic activities in reduction reactions and Click Chemistry. On the advantage of using well-defined catalytic systems." *Dalton Trans.* **2010**, *39*, 7595-7606. (e) Jurkauskas, V.; Sadighi, J. P.; Buchwald, S. L. "Conjugate Reduction of α,β-Unsaturated Carbonyl Compounds Catalyzed by a Copper Carbene Complex." *Org. Lett.* **2003**, *5*, 2417-2420. (f) Kaur, H.; Zinn, F. K.; Stevens, E. D.; Nolan, S. P. "(NHC)CuI (NHC = N-Heterocyclic Carbene) Complexes as Efficient Catalysts for the Reduction of Carbonyl Compounds." *Organometallics* **2004**, *23*, 1157-1160. (g) Tominaga, S.; Oi, Y.; Kato, T.; An, D. K.; Okamoto, S. "γ-Selective allylic substitution reaction with Grignard reagents catalyzed by copper N-heterocyclic carbene complexes and its application to enantioselective synthesis." *Tetrahedron Lett.* **2004**, *45*, 5585-5588. (h) Tsuji, T.; Yamamoto, Y.; Yasuda, S.; (Ube Industries, Ltd., Japan). Application: US, 2005, p 5. (i) Liu, R.; Herron, S. R.; Fleming, S. A. "Copper-Catalyzed Tethered Aziridination of Unsaturated N-Tosyloxy Carbamates." *J. Org. Chem.* **2007**, *72*, 5587-5591. (j) Chun, J.; Jung, I. G.; Kim, H. J.; Park, M.; Lah, M. S.; Son, S. U. "Concomitant Formation of N-Heterocyclic Carbene-Copper Complexes within a Supramolecular Network in the Self-Assembly of Imidazolium Dicarboxylate with Metal Ions." *Inorg. Chem.* **2009**, *48*, 6353-6355. (k) Liu, J.; Zhang, R.; Wang, S.; Sun, W.; Xia, C. "A General and Efficient Copper Catalyst for the Double Carbonylation Reaction." *Org. Lett.*

2009, *11*, 1321-1324. (l) Nolan, S. P.; Diez-Gonzalez, S.; (Institut Catala D'Investigacio Quimica, Spain; Institucio Catalana de Recerca I Estudis Avancats). Application:US, 2009, p 12.

(158) Ohishi, T.; Nishiura, M.; Hou, Z. "Carboxylation of organoboronic esters catalyzed by N-heterocyclic carbene copper(I) complexes." *Angew. Chem., Int. Ed.* **2008**, *47*, 5792-5795.

(159) Ren, H.; Zhao, X.; Xu, S.; Song, H.; Wang, B. "Synthesis and structures of cyclopentadienyl N-heterocyclic carbene copper(I) complexes." *J. Organomet. Chem.* **2006**, *691*, 4109-4113.

(160) Mankad, N. P.; Laitar, D. S.; Sadighi, J. P. "Synthesis, Structure, and Alkyne Reactivity of a Dimeric (Carbene)copper(I) Hydride." *Organometallics* **2004**, *23*, 3369-3371.

(161) Diez-Gonzalez, S.; Stevens, E. D.; Scott, N. M.; Petersen, J. L.; Nolan, S. P. "Synthesis and characterization of $[Cu(NHC)_2]X$ complexes: catalytic and mechanistic studies of hydrosilylation reactions." *Chem.--Eur. J.* **2008**, *14*, 158-168.

(162) Biffis, A.; Tubaro, C.; Scattolin, E.; Basato, M.; Papini, G.; Santini, C.; Alvarez, E.; Conejero, S. "Trinuclear copper(I) complexes with triscarbene ligands: catalysis of C-N and C-C coupling reactions." *Dalton Trans.* **2009**, 7223-7229.

(163) Hu, X.; Castro-Rodriguez, I.; Meyer, K. "Copper complexes of nitrogen-anchored tripodal *N*-heterocyclic carbene ligands." *J. Am. Chem. Soc.* **2003**, *125*, 12237-12245.

(164) Hu, X.; Castro-Rodriguez, I.; Meyer, K. "A Bis-Carbenealkenyl Copper(I) Complex from a Tripodal Tris-Carbene Ligand." *Organometallics.* **2003**, *22*, 3016-3018.

(165) Gardiner, M. G.; Herrmann, W. A.; Reisinger, C.-P.; Schwarz, J.; Spiegler, M. "Dicationic chelating *N*-heterocyclic carbene complexes of palladium: new catalysts for the copolymerization of C_2H_4 and CO." *J. Organomet. Chem.* **1999**, *572*, 239-247.

(166) Kreisel, K. A.; Yap, G. P. A.; Theopold, K. H. "A Chelating *N*-Heterocyclic Carbene Ligand in Organochromium Chemistry." *Organometallics* **2006**, *25*, 4670-4679.

(167) (a) Warsink, S.; de Boer, S. Y.; Jongens, L. M.; Fu, C.-F.; Liu, S.-T.; Chen, J.-T.;

Lutz, M.; Spek, A. L.; Elsevier, C. J. "Synthesis and characterization of Pd(II)-methyl complexes with N-heterocyclic carbene-amine ligands." *Dalton Trans.* **2009**, 7080-7086. (b) Warsink, S.; Hauwert, P.; Siegler, M. A.; Spek, A. L.; Elsevier, C. J. "Palladium(0) pre-catalysts with heteroditopic NHC-amine ligands by transmetallation from their silver(I) complexes." *Appl. Organomet. Chem.* **2009**, *23*, 225-228.

(168) (a) Serra, D.; Cao, P.; Cabrera, J.; Padilla, R.; Rominger, F.; Limbach, M. "Development of platinum(II) and -(IV) CNC pincer complexes and their application in a hydrovinylation reaction." *Organometallics* **2011**, *30*, 1885-1895. (b) Nielsen, D. J.; Cavell, K. J.; Skelton, B. W.; White, A. H. "Methyl-palladium(II) complexes of pyridine-bridged bis(nucleophilic heterocyclic carbene) ligands: Substituent effects on structure, stability, and catalytic performance." *Inorg. Chim. Acta* **2006**, *359*, 1855-1869. (c) Danopoulos, A. A.; Tulloch, A. A. D.; Winston, S.; Eastham, G.; Hursthouse, M. B. "Chelating and 'pincer' dicarbene complexes of palladium; synthesis and structural studies." *Dalton Trans.* **2003**, 1009-1015.

(169) Diez-Gonzalez, S.; Kaur, H.; Zinn, F. K.; Stevens, E. D.; Nolan, S. P. "A simple and efficient copper-catalyzed procedure for the hydrosilylation of hindered and functionalized ketones." *J. Org. Chem.* **2005**, *70*, 4784-4796.

(170) (a) Al Nashef, I. M.; Hashim, M. A.; Mjalli, F. S.; Ali, M. Q. A.-h.; Hayyan, M. "A novel method for the synthesis of 2-imidazolones." *Tetrahedron Lett.* **2010**, *51*, 1976-1978. (b) Khramov, D. M.; Boydston, A. J.; Bielawski, C. W. "Synthesis and study of Janus bis(carbene)s and their transition-metal complexes." *Angew. Chem., Int. Ed.* **2006**, *45*, 6186-6189. (c) Begtrup, M. "Azolium anions and their reaction with electrophilic reagents." *J. Chem. Soc., Chem. Commun.* **1975**, 334-335.

(171) Henson, M. J.; Mukherjee, P.; Root, D. E.; Stack, T. D. P.; Solomon, E. I. "Spectroscopic and Electronic Structural Studies of the $Cu(III)_2$ Bis-μ-oxo Core and Its Relation to the Side-On Peroxo-Bridged Dimer." *J. Am. Chem. Soc.* **1999**, *121*, 10332-10345.

(172) Saiz-Lopez, A.; Saunders, R. W.; Joseph, D. M.; Ashworth, S. H.; Plane, J. M. C. "Absolute absorption cross-section and photolysis rate of I_2." *Atmos. Chem. Phys.* **2004**, *4*, 1443-1450.

(173) Kerenskaya, G.; Goldschleger, I. U.; Apkarian, V. A.; Fleischer, E.; Janda, K. C. "Spectroscopic Signatures of Halogens in Clathrate Hydrate Cages. 2. Iodine." *J. Phys. Chem. A* **2007**, *111*, 10969-10976.

(174) (a) Allred, G. D.; Liebeskind, L. S. "Copper-Mediated Cross-Coupling of Organostannanes with Organic Iodides at or below Room Temperature." *J. Am. Chem. Soc.* **1996**, *118*, 2748-2749. (b) Whitesides, G. M.; Fischer, W. F., Jr.; San Filippo, J., Jr.; Bashe, R. W.; House, H. O. "Reaction of lithium dialkyl- and diarylcuprates with organic halides." *J. Am. Chem. Soc.* **1969**, *91*, 4871-4882. (c) Maze, F.; Purpura, M.; Bernaud, F.; Mangeney, P.; Alexakis, A. "Regio- and diastereoselective SN2' or SN2" reactions on chiral acetals of cyclic aldehydes promoted by PhCu, BF_3." *Tetrahedron: Asymmetry* **2001**, *12*, 1957-1960. (d) Spanenberg, W. J.; Snell, B. E.; Su, M. C. "Kinetic study of aryl substitutions with lithium organocopper reagents." *Microchem. J.* **1993**, *47*, 79-89. (e) Ebert, G.; Rieke, R. D. "Direct formation of organocopper compounds by oxidative addition of zerovalent copper to organic halides." *J. Org. Chem.* **1984**, *49*, 5280-5282. (f) Whitesides, G. M.; San Filippo, J., Jr.; Stredronsky, E. R.; Casey, C. P. "Reaction of copper(I) hydride with organocopper(I) compounds." *J. Am. Chem. Soc.* **1969**, *91*, 6542-6544. (g) Corey, E. J.; Jautelat, M. "Construction of ring systems containing the gemdimethylcyclopropane unit using diphenylsulfonium isopropylide." *J. Am. Chem. Soc.* **1967**, *89*, 3912-3914.

(175) Rahn, R. O. "Photochemistry of halogen pyrimidines: iodine release studies." *Photochem. Photobiol.* **1992**, *56*, 9-15.

(176) Hagadorn, J. R.; Zahn, T. I.; Que, L., Jr.; Tolman, W. B. "Dicopper(I,I) and Delocalized Mixed-Valent Dicopper(I,II) Complexes of a Sterically Hindered Carboxylate Ligand." *Dalton Trans.* **2003**, 1790-1794.

(177) Fairuz, Z. A.; Aiyub, Z.; Abdullah, Z.; Ng, S. W.; Tiekink, E. R. T. "Tetra-μ-acetato-κ^8O:O'-bis{[*N*-(4-chlorophenyl)-4-methylpyridin-2-amine-κN^1]copper(II)}." *Acta Crystallogr., Sect. E: Struct. Rep. Online E66*, m1049-m1050.

(178) Warsink, S.; de Boer, S. Y.; Jongens, L. M.; Fu, C.-F.; Liu, S.-T.; Chen, J.-T.; Lutz, M.; Spek, A. L.; Elsevier, C. J. "Synthesis and characterization of Pd^{II}-methyl complexes with N-heterocyclic carbene-amine ligands" *Dalton Trans.* **2009**, 7080-7086.

(179) Arduengo, A. J., III; Dias, H. V. R.; Calabrese, J. C.; Davidson, F. "Homoleptic carbene-silver(I) and carbene-copper(I) complexes." *Organometallics* **1993**, *12*, 3405-3409.

(180) (a) Caballero, A.; Diez-Barra, E.; Jalon, F. A.; Merino, S.; Rodriguez, A. M.; Tejeda, J. "Corrigendum to: "1,1'-(Pyridine-2,6-diyl)bis(3-benzyl-2,3-dihydro-1H-imidazol-2-ylidene), a new multidentate *N*-heterocyclic biscarbene and its silver(I) complex derivative." [J. Organomet. Chem. 617-618 (2000) 395]." *J.*

Organomet. Chem. **2001**, *627*, 263-264. (b) Caballero, A.; Diez-Barra, E.; Jalon, F. A.; Merino, S.; Tejeda, J. "1,1'-(Pyridine-2,6-diyl)bis(3-benzyl-2,3-dihydro-1H-imidazol-2-ylidene), a new multidentate *N*-heterocyclic biscarbene and its silver(I) complex derivative." *J. Organomet. Chem.* **2001**, *617-618*, 395-398.

(181) Pugh, D.; Boyle, A.; Danopoulos, A. A. "'Pincer' pyridine dicarbene complexes of nickel and their derivatives. Unusual ring opening of a coordinated imidazol-2-ylidene." *Dalton Trans.* **2008**, 1087-1094.

(182) Reproduced in part with permission from Bar-Nahum, I.; Gupta, A. K.; Huber, S. M.; Ertem, M. Z.; Cramer, C. J.; Tolman, W. B. "Reduction of nitrous oxide to dinitrogen by a mixed valent tricopper-disulfido cluster." *J. Am. Chem. Soc.* **2009**, *131*, 2812-2814. Copyright 2009 American Chemical Society.

(183) (a) Trogler, W. C. "Physical properties and mechanisms of formation of nitrous oxide." *Coord. Chem. Rev.* **1999**, *187*, 303-327.(b) Duce, R. A.; LaRoche, J.; Altieri, K.; Arrigo, K. R.; Baker, A. R.; Capone, D. G.; Cornell, S.; Dentener, F.; Galloway, J.; Ganeshram, R. S.; Geider, R. J.; Jickells, T.; Kuypers, M. M.; Langlois, R.; Liss, P. S.; Liu, S. M.; Middelburg, J. J.; Moore, C. M.; Nickovic, S.; Oschlies, A.; Pedersen, T.; Prospero, J.; Schlitzer, R.; Seitzinger, S.; Sorensen, L. L.; Uematsu, M.; Ulloa, O.; Voss, M.; Ward, B.; Zamora, L. "Impacts of atmospheric anthropogenic nitrogen on the open ocean." *Science.* **2008**, *320*, 893-897.

(184) (a) Zumft, W. G.; Kroneck, P. M. H. "Respiratory transformation of nitrous oxide (N_2O) to dinitrogen by Bacteria and Archaea." *Adv. Microb. Physiol.* **2007**, *52*, 107-227. (b) Brown, K.; Tegoni, M.; Prudencio, M.; Pereira, A. S.; Besson, S.; Moura, J. J.; Moura, I.; Cambillau, C. "A novel type of catalytic copper cluster in nitrous oxide reductase." *Nat Struct Biol* . **2000**, *7*, 191-195. (c) Brown, K.; Djinovic-Carugo, K.; Haltia, T.; Cabrito, I.; Saraste, M.; Moura, J. J. G.; Moura, I.; Tegoni, M.; Cambillau, C. "Revisiting the catalytic CuZ cluster of nitrous oxide (N_2O) reductase. Evidence of a bridging inorganic sulfur." *J. Biol. Chem.* **2000**, *275*, 41133-41136. (d) Paraskevopoulos, K.; Antonyuk, S. V.; Sawers, R. G.; Eady, R. R.; Hasnain, S. S. "Insight into Catalysis of Nitrous Oxide Reductase from High-resolution Structures of Resting and Inhibitor-bound Enzyme from Achromobacter cycloclastes." *J. Mol. Biol.* **2006**, *362*, 55-65. (e) Rasmussen, T.; Berks, B. C.; Sanders-Loehr, J.; Dooley, D. M.; Zumft, W. G.; Thomson, A. J. "The catalytic center in nitrous oxide reductase, CuZ, is a copper-sulfide cluster." *Biochemistry.* **2000**, *39*, 12753-12756. (f) Chen, P.; Cabrito, I.; Moura, J. J. G.; Moura, I.; Solomon, E. I. "Spectroscopic and Electronic Structure Studies of the micro 4-Sulfide Bridged Tetranuclear CuZ Cluster in N_2O Reductase: Molecular Insight into the Catalytic Mechanism." *J. Am. Chem. Soc.* **2002**, *124*, 10497-10507. (g) Alvarez, M. L.; Ai, J.; Zumft, W.; Sanders-Loehr, J.; Dooley, D. M.

"Characterization of the copper-sulfur chromophores in nitrous oxide reductase by resonance Raman spectroscopy: evidence for sulfur coordination in the catalytic cluster." *J. Am. Chem. Soc.* **2001**, *123*, 576-587. (h) Ghosh, S.; Gorelsky, S. I.; DeBeer George, S.; Chan, J. M.; Cabrito, I.; Dooley, D. M.; Moura, J. J. G.; Moura, I.; Solomon, E. I. "Spectroscopic, Computational, and Kinetic Studies of the micro 4-Sulfide-Bridged Tetranuclear CuZ Cluster in N_2O Reductase: pH Effect on the Edge Ligand and Its Contribution to Reactivity." *J. Am. Chem. Soc.* **2007**, *129*, 3955-3965. (i) Oganesyan, V. S.; Rasmussen, T.; Fairhurst, S.; Thomson, A. J. "Characterisation of [Cu_4S], the catalytic site in nitrous oxide reductase, by EPR spectroscopy." *Dalton Trans.* **2004**, 996-1002. (j) Solomon, E. I.; Sarangi, R.; Woertink, J. S.; Augustine, A. J.; Yoon, J.; Ghosh, S. "O_2 and N_2O Activation by Bi-, Tri-, and Tetranuclear Cu Clusters in Biology." *Acc. Chem. Res.* **2007**, *40*, 581-591.

(185) Bar-Nahum, I.; York, J. T.; Young, V. G., Jr.; Tolman, W. B. "Novel reactivity of side-on (disulfido)dicopper complexes supported by Bi- and tridentate nitrogen donors: impact of axial coordination." *Angew. Chem., Int.* **2008**, *47*, 533-536.

(186) Reproduced in part with permission from Donoghue, P. J.; Gupta, A. K.; Boyce, D. W.; Cramer, C. J.; Tolman, W. B. "An Anionic, Tetragonal Copper(II) Superoxide Complex." *J. Am. Chem. Soc.* **2010**, *132*, 15869-15871. Copyright 2010 American Chemical Society.

(187) (a) Himes, R. A.; Karlin, K. D. "Copper-dioxygen complex mediated C-H bond oxygenation: relevance for particulate methane monooxygenase (pMMO)." *Curr. Opin. Chem. Biol.* **2009**, *13*, 119-131. (b) Rolff, M.; Tuczek, F. "How do copper enzymes hydroxylate aliphatic substrates? Recent insights from the chemistry of model systems." *Angew. Chem., Int. Ed.* **2008**, *47*, 2344-2347. (c) Solomon, E. I.; Sarangi, R.; Woertink, J. S.; Augustine, A. J.; Yoon, J.; Ghosh, S. "O_2 and N_2O Activation by Bi-, Tri-, and Tetranuclear Cu Clusters in Biology." *Acc. Chem. Res.* **2007**, *40*, 581-591. (d) Klinman, J. P. "The copper-enzyme family of dopamine β-monooxygenase and peptidylglycine α-hydroxylating monooxygenase: Resolving the chemical pathway for substrate hydroxylation." *J. Biol. Chem.* **2006**, *281*, 3013-3016. (e) Solomon, E. I.; Sundaram, U. M.; Machonkin, T. E. "Multicopper Oxidases and Oxygenases." *Chem. Rev.* **1996**, *96*, 2563-2605.

(188) Que, L., Jr.; Tolman, W. B. "Biologically inspired oxidation catalysis." **2008**, *455*, 333-340. , and references cited therein.

(189) (a) Cramer, C. J.; Tolman, W. B. "Mononuclear Cu-O_2 Complexes: Geometries, Spectroscopic Properties, Electronic Structures, and Reactivity." *Acc. Chem. Res.* **2007**, *40*, 601-608. (b) Itoh, S. "Mononuclear copper active-oxygen complexes." *Curr. Opin. Chem. Biol.* **2006**, *10*, 115-122.

(190) (a) Wuertele, C.; Gaoutchenova, E.; Harms, K.; Holthausen, M. C.; Sundermeyer, J.; Schindler, S. "Crystallographic characterization of a synthetic 1:1 end-on copper dioxygen adduct complex." *Angew. Chem. Int. Ed.* **2006**, *45*, 3867-3869. (b) Maiti, D.; Fry, H. C.; Woertink, J. S.; Vance, M. A.; Solomon, E. I.; Karlin, K. D. "A 1:1 Copper-Dioxygen Adduct is an End-on Bound Superoxo Copper(II) Complex which Undergoes Oxygenation Reactions with Phenols." *J. Am. Chem. Soc.* **2007**, *129*, 264-265. (c) Komiyama, K.; Furutachi, H.; Nagatomo, S.; Hashimoto, A.; Hayashi, H.; Fujinami, S.; Suzuki, M.; Kitagawa, T. "Dioxygen reactivity of copper(I) complexes with tetradentate tripodal ligands having aliphatic nitrogen donors: Synthesis, structures, and properties of peroxo and superoxo complexes." *Bull. Chem. Soc. Jpn.* **2004**, *77*, 59-72. (d) Jazdzewski, B. A.; Reynolds, A. M.; Holland, P. L.; Young, V. G.; Kaderli, S.; Zuberbuehler, A. D.; Tolman, W. B. "Copper(I)-phenolate complexes as models of the reduced active site of galactose oxidase: synthesis, characterization, and O_2 reactivity." *J. Biol. Inorg. Chem.* **2003**, *8*, 381-393.

(191) Kunishita, A.; Kubo, M.; Sugimoto, H.; Ogura, T.; Sato, K.; Takui, T.; Itoh, S. "Mononuclear Copper(II)-Superoxo Complexes that Mimic the Structure and Reactivity of the Active Centers of PHM and DβM." *J. Am. Chem. Soc.* **2009**, *131*, 2788-2789.

(192) (a) Chen, P.; Root, D. E.; Campochiaro, C.; Fujisawa, K.; Solomon, E. I. "Spectroscopic and Electronic Structure Studies of the Diamagnetic Side-On Cu(II)-Superoxo Complex $Cu(O_2)[HB(3\text{-}R\text{-}5\text{-}iPrpz)_3]$: Antiferromagnetic Coupling versus Covalent Delocalization." *J. Am. Chem. Soc.* **2003**, *125*, 466-474. (b) Fujisawa, K.; Tanaka, M.; Moro-oka, Y.; Kitajima, N. "A Monomeric Side-On Superoxocopper(II) Complex: $Cu(O_2)(HB(3\text{-}tBu\text{-}5\text{-}iPrpz)_3)$." *J. Am. Chem. Soc.* **1994**, *116*, 12079-12080.

(193) (a) Aboelella, N. W.; Lewis, E. A.; Reynolds, A. M.; Brennessel, W. W.; Cramer, C. J.; Tolman, W. B. "Snapshots of Dioxygen Activation by Copper: The Structure of a 1:1 Cu/O_2 Adduct and Its Use in Syntheses of Asymmetric Bis(μ-oxo) Complexes." *J. Am. Chem. Soc.* **2002**, *124*, 10660-10661. (b) Spencer, D. J. E.; Aboelella, N. W.; Reynolds, A. M.; Holland, P. L.; Tolman, W. B. "β-Diketiminate Ligand Backbone Structural Effects on $Cu(I)/O_2$ Reactivity: Unique Copper-Superoxo and Bis(μ-oxo) Complexes." *J. Am. Chem. Soc.* **2002**, *124*, 2108-2109. (c) Aboelella, N. W.; Kryatov, S. V.; Gherman, B. F.; Brennessel, W. W.; Young, V. G., Jr.; Sarangi, R.; Rybak-Akimova, E. V.; Hodgson, K. O.; Hedman, B.; Solomon, E. I.; Cramer, C. J.; Tolman, W. B. "Dioxygen Activation at a Single Copper Site: Structure, Bonding, and Mechanism of Formation of 1:1 $Cu\text{-}O_2$ Adducts." *J. Am. Chem. Soc.* **2004**, *126*, 16896-16911. (d) Reynolds, A. M.; Gherman, B. F.; Cramer, C. J.; Tolman, W. B. "Characterization of a 1:1 Cu-

O_2 Adduct Supported by an Anilido Imine Ligand." *Inorg. Chem.* **2005**, *44*, 6989-6997.

(194) Tyeklar, Z.; Jacobson, R. R.; Wei, N.; Murthy, N. N.; Zubieta, J.; Karlin, K. D. "Reversible reaction of dioxygen (and carbon monoxide) with a copper(I) complex. X-ray structures of relevant mononuclear Cu(I) precursor adducts and the trans-(μ-1,2-peroxo)dicopper(II) product." *J. Am. Chem. Soc.* **1993**, *115*, 2677-2689.

(195) (a) Baldwin, M. J.; Ross, P. K.; Pate, J. E.; Tyeklar, Z.; Karlin, K. D.; Solomon, E. I. "Spectroscopic and theoretical studies of an end-on peroxide-bridged coupled binuclear copper(II) model complex of relevance to the active sites in hemocyanin and tyrosinase." *J. Am. Chem. Soc.* **1991**, *113*, 8671-8679. (b) Henson, M. J.; Vance, M. A.; Zhang, C. X.; Liang, H.-C.; Karlin, K. D.; Solomon, E. I. "Resonance Raman Investigation of Equatorial Ligand Donor Effects on the $Cu_2O_2^{2+}$ Core in End-On and Side-On μ-Peroxo-Dicopper(II) and Bis-μ-oxo-Dicopper(III) Complexes." *J. Am. Chem. Soc.* **2003**, *125*, 5186-5192.

(196) Reproduced in part with permission from Hong, S.; Hill, L. M. R.; Gupta, A. K.; Naab, B. D.; Gilroy, J. B.; Hicks, R. G.; Cramer, C. J.; Tolman, W. B. "Effects of Electron-Deficient β-Diketiminate and Formazan Supporting Ligands on Copper(I)-Mediated Dioxygen Activation." *Inorg. Chem.* **2009**, *48*, 4514-4523. Copyright 2010 American Chemical Society.

(197) Carey, D. T.; Cope-Eatough, E. K.; Vilaplana-Mafe, E.; Mair, F. S.; Pritchard, R. G.; Warren, J. E.; Woods, R. J. "Structures and reactions of monomeric and dimeric lithium diazapentadienyl complexes with electrophiles: synthesis of α-C,C'-dialkyl-beta -diimines, and dissolution-reversible synthesis of an α-alkoxylithium-β-diimine." *Dalton Trans.* **2003**, 1083-1093.

(198) Spencer, D. J. E.; Reynolds, A. M.; Holland, P. L.; Jazdzewski, B. A.; Duboc-Toia, C.; Le Pape, L.; Yokota, S.; Tachi, Y.; Itoh, S.; Tolman, W. B. "Copper Chemistry of β-Diketiminate Ligands: Monomer/Dimer Equilibria and a New Class of Bis(μ-oxo)dicopper Compounds." *Inorg. Chem.* **2002**, *41*, 6307-6321.

(199) Gilroy, J. B.; Otieno, P. O.; Ferguson, M. J.; McDonald, R.; Hicks, R. G. "Synthesis and Characterization of 3-Cyano- and 3-Nitroformazans, Nitrogen-Rich Analogues of β-Diketimine Ligands." *Inorg. Chem.* **2008**, *47*, 1279-1286.

(200) Gilroy, J. B.; Patrick, B. O.; McDonald, R.; Hicks, R. G. "Transition Metal Complexes of 3-Cyano- and 3-Nitroformazans." *Inorg. Chem.* **2008**, *47*, 1287-1294.

(201) Henson, M. J.; Mukherjee, P.; Root, D. E.; Stack, T. D. P.; Solomon, E. I. "Spectroscopic and Electronic Structural Studies of the $Cu(III)_2$ Bis-μ-oxo Core and Its Relation to the Side-On Peroxo-Bridged Dimer." *J. Am. Chem. Soc.* **1999**, *121*, 10332-10345.

(202) Herres-Pawlis, S.; Verma, P.; Haase, R.; Kang, P.; Lyons, C. T.; Wasinger, E. C.; Floerke, U.; Henkel, G.; Stack, T. D. P. "Phenolate Hydroxylation in a Bis(μ-oxo)dicopper(III) Complex: Lessons from the Guanidine/Amine Series." *J. Am. Chem. Soc.* **2009**, *131*, 1154-1169.

(203) Holland, P. L.; Cramer, C. J.; Wilkinson, E. C.; Mahapatra, S.; Rodgers, K. R.; Itoh, S.; Taki, M.; Fukuzumi, S.; Que, L., Jr.; Tolman, W. B. "Resonance Raman spectroscopy as a probe of the bis(μ-oxo)dicopper core." *J. Am. Chem. Soc.* **2000**, *122*, 792-802.

(204) Reproduced in part with permission from Hong, S.; Gupta, A. K.; Tolman, W. B. "Intermediates in Reactions of Copper(I) Complexes with N-Oxides: From the Formation of Stable Adducts to Oxo Transfer." *Inorg. Chem.* **2009**, *48*, 6323-6325. Copyright 2009 American Chemical Society.

(205) Dai, X.; Warren, T. H. "Dioxygen activation by a neutral β-diketiminato copper(I) ethylene complex." *Chem Commun.* **2001**, 1998-1999.

(206) Spencer, D. J. E.; Reynolds, A. M.; Holland, P. L.; Jazdzewski, B. A.; Duboc-Toia, C.; Le Pape, L.; Yokota, S.; Tachi, Y.; Itoh, S.; Tolman, W. B. "Copper Chemistry of β-Diketiminate Ligands: Monomer/Dimer Equilibria and a New Class of Bis(μ-oxo)dicopper Compounds." *Inorg. Chem.* **2002**, *41*, 6307-6321.

(207) Reactions of PhIO with Cu(I) complexes that yield other types of products have been reported: (a) Obias, H. V.; Lin, Y.; Murthy, N. N.; Pidcock, E.; Solomon, E. I.; Ralle, M.; Blackburn, N. J.; Neuhold, Y.-M.; Zuberbuehler, A. D.; Karlin, K. D. "Peroxo-, Oxo-, and Hydroxo-Bridged Dicopper Complexes: Observation of Exogenous Hydrocarbon Substrate Oxidation." *J. Am. Chem. Soc.* **1998**, *120*, 12960-12961. (b) Franklin, C. C.; VanAtta, R. B.; Tai, A. F.; Valentine, J. S. "Copper ion mediated epoxidation of olefins by iodosylbenzene." *J. Am. Chem. Soc.* **1984**, *106*, 814-816.

(208) Reproduced in part with permission from Pietrangelo, A.; Knight, S. C.; Gupta, A. K.; Yao, L. J.; Hillmyer, M. A.; Tolman, W. B. "Mechanistic Study of the Stereoselective Polymerization of *d,l*-Lactide Using Indium(III) Halides." *J. Am. Chem. Soc.* **2010**, *132*, 11649-11657. Copyright 2009 American Chemical Society.

(209) Drumright, R. E.; Gruber, P. R.; Henton, D. E. "Polylactic acid technology." *Adv. Mater.* **2000**, *12*, 1841-1846.

(210) Gupta, A. P.; Kumar, V. "New emerging trends in synthetic biodegradable polymers - Polylactide: A critique." *Eur. Polym.* **2007**, *43*, 4053-4074.

(211) Auras, R.; Harte, B.; Selke, S. "An overview of polylactides as packaging materials." *Macromol. Biosci.* **2004**, *4*, 835-864.

(212) Sinclair, R. G. "The case for polylactic acid as a commodity packaging plastic." *J. Macromol. Sci., Pure Appl. Chem.* **1996**, *A33*, 585-597.

(213) Mainil-Varlet, P.; Rahn, B.; Gogolewski, S. "Long-term in vivo degradation and bone reaction to various polylactides. 1. One-year results." *Biomaterials.* **1997**, *18*, 257-266.

(214) Vert, M.; Li, S. M.; Spenlehauer, G.; Guerin, P. "Bioresorbability and biocompatibility of aliphatic polyesters." *J. Mater. Sci.: Mater. Med.* **1992**, *3*, 432-446.

(215) Hubbell, J. A.; Langer, R. "Tissue engineering." *Chem. Eng. News* **1995**, *73*, 42-54.

(216) Langer, R.; Vacanti, J. P. "Tissue engineering." *Science.* **1993**, *260*, 920-926.

(217) Pietrangelo, A.; Hillmyer, M. A.; Tolman, W. B. "Stereoselective and controlled polymerization of *D,L*-lactide using indium(iii) trichloride" *Chem. Commun. (Cambridge, U. K.)* **2009**, 2736-2737.

(218) Jeffs, S. E.; Small, R. W. H.; Worrall, I. J. "Structure of the 4:1 complexes formed by pyridine and the Group III halides $InCl_3$ and $TlCl_3$: *mer*-trichlorotris(pyridine)indium(III)-pyridine (1/1), $[InCl_3(C_5H_5N)_3].C_5H_5N$, and *mer*-trichlorotris(pyridine)thallium(III)-pyridine (1/1), $[TlCl_3(C_5H_5N)_3].C_5H_5N$." *Acta Crystallogr., Sect. C: Cryst. Struct. Commun.* **1984**, *C40*, 1329-1331.

(219) (a) Carmalt, C. J.; King, S. J. "Gallium(III) and indium(III) alkoxides and aryloxides." *Coord. Chem. Rev.* **2006**, *250*, 682-709. (b) Trentler, T. J.; Goel, S. C.; Hickman, K. M.; Viano, A. M.; Chiang, M. Y.; Beatty, A. M.; Gibbons, P. C.; Buhro, W. E. "Solution-Liquid-Solid Growth of Indium Phosphide Fibers from Organometallic Precursors: Elucidation of Molecular and Nonmolecular Components of the Pathway." *J. Am. Chem. Soc.* **1997**, *119*, 2172-2181. (c) Veith, M.; Hill, S.; Huch, V. "Synthesis and single-crystal x-ray diffraction studies on new methylindium(III) alkoxides." *Eur. J. Inorg. Chem.* **1999**, 1343-1350. (d)

Alcock, N. W.; Degnan, I. A.; Roe, S. M.; Wallbridge, M. G. H. "Preparation and characterization of novel organoindium derivatives; x-ray crystal structure of dimethyl(salicylaldehyde)indium." *J. Organomet. Chem.* **1991**, *414*, 285-293. (e) Beachley, O. T., Jr.; MacRae, D. J.; Kovalevsky, A. Y. "Chemistry of Indium(III) Tris(cyclopentadienide). Reactions with Diphenylphosphine, tert-Butyl Alcohol, and Acetylacetone. Cyclopentadiene and Reductive Elimination Reactions." *Organometallics*. **2003**, *22*, 1690-1695. (f) Shen, Y.; Pan, Y.; Jin, X.; Xu, X.; Sun, X.; Huang, X. "Synthesis and characterization of dialkylaluminum, -gallium or -indium [2-(2-pyridyl)]ethoxides. Crystal structure of $[Me_2In\{\mu\text{-}O\text{-}CH_2CH_2(2\text{-}C_5H_4N)\}]_2$." *Polyhedron.* **1999**, *18*, 2423-2426.

(220) Marshall, E. L.; Gibson, V. C.; Rzepa, H. S. "A computational analysis of the ring-opening polymerization of *rac*-lactide initiated by single-site β-diketiminate metal complexes: defining the mechanistic pathway and the origin of stereocontrol." *J. Am. Chem. Soc.* **2005**, *127*, 6048-6051.